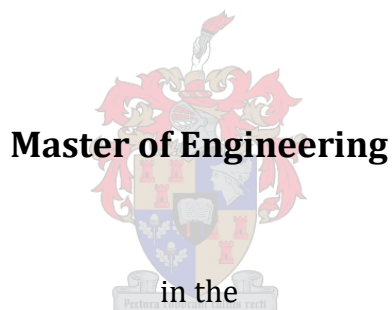


**PROTECTION OF RIVER EMBANKMENTS DOWNSTREAM OF
LOW-LEVEL RIVER CROSSINGS USING STEPPED CHUTE
ENERGY DISSIPATION STRUCTURES**

By

Pierre Lourens Cloete

Thesis presented in fulfilment of the requirements for the degree of



Department of Civil Engineering

Faculty of Engineering

University of Stellenbosch

Supervisor: Mrs Adèle Bosman (Neé Vos)

APRIL 2019



PLAGIAATVERKLARING / PLAGIARISM DECLARATION

1. Plagiaat is die oorneem en gebruik van die idees, materiaal en ander intellektuele eiendom van ander persone asof dit jou eie werk is.

Plagiarism is the use of ideas, material and other intellectual property of another's work and to present is as my own.

2. Ek erken dat die pleeg van plagiaat 'n strafbare oortreding is aangesien dit 'n vorm van diefstal is.

I agree that plagiarism is a punishable offence because it constitutes theft.

3. Ek verstaan ook dat direkte vertalings plagiaat is.

I also understand that direct translations are plagiarism.

4. Dienooreenkomsdig is alle aanhalings en bydraes vanuit enige bron (ingesluit die internet) volledig verwys (erken). Ek erken dat die woordelikse aanhaal van teks sonder aanhalingsstekens (selfs al word die bron volledig erken) plagiaat is.

Accordingly, all quotations and contributions from any source whatsoever (including the internet) have been cited fully. I understand that the reproduction of text without quotation marks (even when the source is cited) is plagiarism.

5. Ek verklaar dat die werk in hierdie skryfstuk vervat, behalwe waar anders aangedui, my eie oorspronklike werk is en dat ek dit nie vantevore in die geheel of gedeeltelik ingehandig het vir bepunting in hierdie module/werkstuk of 'n ander module/werkstuk nie.

I declare that the work contained in this assignment, except where otherwise stated, is my original work and that I have not previously (in its entirety or in part) submitted it for grading in this module/assignment or another module/assignment.

Studentenommer / Student number	Handtekening / Signature
P.L. Cloete	
Voorletters en van / Initials and surname	Datum / Date

Copyright © 2019 Stellenbosch University

All rights reserved



ABSTRACT

Low-level river crossings (LLRCs) have been used as an economic means of access for lower order roads. LLRCs typically provide openings underneath the prepared surface to allow for passing flow but additionally allow for overtopping flow. However, when the LLRC overflows, the portion of flow on the approach roads tends to accelerate and discharges on the embankment directly downstream of it. This causes erosion of the downstream embankment, exposing the approach road foundations and damaging the structure.

Following such a case where ten LLRCs in the Eastern Cape sustained tremendous damage, the use of a stepped chute energy dissipator (rather than the traditional means of erosion protection with riprap) was considered to protect the downstream embankments. No formal design guidelines for the use of a stepped chute energy dissipator downstream of a LLRC were available.

A 1:15 scale hydraulic model of an LLRC with a stepped chute energy dissipator was designed and constructed at the Hydraulic Laboratory of Stellenbosch University to verify anticipated hydraulic operation and to identify unforeseen potential phenomena. Two model configurations were considered.

The first configuration included a chute sidewall to contain approach road overflow on the stepped chute. Flow from the road formed a nappe that impinged on the chute steps and formed a hydraulic jump on each step. Flow was then diverted down the chute, and steps in the direction of the chute further dissipated energy while returning the flow to the main channel.

The second model configuration omitted the chute sidewall and discharged approach road overflow onto riprap, placed directly downstream of the chute. Flow from the approach road formed a nappe that impinged on the chute steps. The formation of hydraulic jumps on each step was, however, not as effective as with the first model configuration and instances of supercritical discharge onto the riprap were noted.

Pressures of the nappe cavity (forming from the approach road onto the chute steps) were found to be sub atmospheric. However, the magnitude of the sub-atmospheric conditions (less than 1 m below atmosphere) was not enough to cause a collapsed/clinging nappe and was also found to be within the cavitation threshold (7 m below atmosphere). Ventilation of the nappe due to negative pressure indicated that an increase in overflow discharge caused an increase in the air requirement. The addition of air vents however, did not have a marked effect on the nappe pressure or the flow profiles on the stepped chute in either one of the model configurations.

The use of a stepped chute energy dissipator to prevent erosion of downstream LLRC embankments is a viable option, particularly in cases where large rock for riprap revetments are not available. The first model configuration (stepped chute with sidewall) is a more favourable option as the approach road overflow is contained on the stepped chute and diverted back to the main channel in a controlled manner. A regression analysis was performed on the model variables of model setup 1 and the relationships can be used to determine the width, height and length of the chute steps.

OPSOMMING

Laagwaterbrûe is 'n ekonomies haalbare manier om toegang te verseker vir laer orde paaie. Laagwaterbrûe het normaalweg openinge vir deurstroming onderdeur die padvlak, maar word ook ontwerp om vloeい bo-oor die padvlak toe te laat. Wanneer oorstroming van 'n laagwater-brug plaasvind, is die vloeい oor die aankomspaaie geneig om te versnel en op die grondwalle stroomaf van die brug te val. Dit veroorsaak verspoeling van die grondwalle wat die brug se fondament ontbloot en skade aan die struktuur veroorsaak.

Tien sulke gevalle is in die Oos-Kaap aangemeld waar groot skade aan die laagwaterbrûe veroorsaak was. Die gebruik van trap-geleidingstrukture (Engl.: stepped chute) is voorgestel in plaas van die normale erosie-bekampingsmetode van stortklip beskermingsmatrassen. Daar was geen formele ontwerpsriglyne beskikbaar vir die ontwerp van so 'n trap-geleidingstruktuur nie.

'n Een tot 15 geskaalde hidrouliese model van 'n trap-geleidingstruktuur is ontwerp en gebou in die Hidrouliese Laboratorium van die Universiteit van Stellenbosch, met die doel om hidrouliese verskynsels te bevestig en te identifiseer. Twee modelle is oorweeg tydens die studie.

Die eerste modelsamestelling het 'n kantmuur ingesluit wat pad-oorloop-water vanaf die brug padvlak op die trap-geleidingstruktuur behou het. Vloeい vanaf die padvlak het 'n uitloopstraalprofiel gevorm wat op die trappe geval het en daarna 'n hidrouliese sprong op elke trap gevorm het. Die vloeい is toe gelei met behulp van die kantmuur in die rigting van die verstappings waar nog energie-dissipasie plaasgevind het en het uiteindelik weer aangesluit by die hoofstroom.

Die tweede modelsamestelling het die kantmuur uitgesluit, maar het 'n stortklip beskermingsmatras, stroom-af van die trap geleidingstruktuur, ingesluit. Vloeい vanaf die padvlak het weereens 'n uitloopstraalprofiel gevorm waarna dit op die trappe geval en 'n hidrouliese sprong op elke trap gevorm het. Vloeい na die hidrouliese sprong het eenvoudig net voortgegaan om oor die kant van die trap-geleidingstruktuur te vloeい en uiteindelik op die stortklip beskermingsmatras te val. Die afwesigheid van die kantmuur het veroorsaak dat die hidrouliese spronge nie so prominent gevorm het soos in die eerste modelsamestelling nie en het laer vlakke van energie-dissipasie tot gevolg gehad. Daar was ook waargeneem dat die vloeい vanaf die trappe tot op die stortklip beskermingsmatras superkrities was.

Sub-atmosferiese drukke in die uitloopstraalprofiel holte (wat gevorm het vanaf die aankomspad tot op die trappe) is waargeneem, maar die grootte van die drukke was nie genoeg om die uitloopstraalprofiel te laat inval en aan die brug vas te laat klou nie. Daar was

ook bevind dat die sub-atmosferiese drukke binne die kavitasie drumpel van 7 m sub-atmosferies was. Toelating vir belugting van die uitloopstraalprofiel holte, as gevolg van die negatiewe drukke, het aangedui dat 'n toename in oorloop vanaf die padvlak, 'n toename in die belugtings-behoefte gehad het. Die byvoeging van belugtings-pype het wel geen noemenswaardige verskil gemaak in die drukke van beide modelle nie.

Die gebruik van 'n trap-geleidingstruktuur om verspoeling van die grondwalle stroomaf van 'n laagwaterbrug te voorkom blyk 'n haalbare alternatief te wees, veral wanneer groot genoeg rotse vir 'n stortklip beskermingsmatras nie beskikbaar is nie. Die eerste model-samestelling (met die kantmuur ingesluit) was meer gunstig omdat die pad-oorloop-water tot die trap-geleidingstruktuur beperk is en onder beheerde toestande terug na die hoofstroom geleei was. 'n Regressie analise is ook uitgevoer met die eerste model samestelling se ontwerpveranderlikes. Die formules wat afgelei is, kan gebruik word om die traphoogte, lengte en wydte van die geleidingstruktuur te bepaal.

ACKNOWLEDGEMENTS

I would like to extend my deepest appreciation toward the following persons without whom this thesis would not have been realised:

- ☛ My supervisor, Mrs Adèle Bosman, for her patience, knowledge, guidance, and especially her commitment and dedication during the months leading up to her accouchement;
- ☛ Mr. Johan Nieuwoudt, Mr. Iliyaaz Williams and Mr. Marvin Lindoor at the University of Stellenbosch's Hydraulic Laboratory, for their efforts and hard work constructing the model and continued assistance during the testing phases;
- ☛ Mr. Ning Ma for accommodating my unique laboratory scheduling requirements;
- ☛ The University of Stellenbosch for granting me the opportunity to continue my studies and providing a conducive environment for students to receive a high-quality education;
- ☛ My loving wife, Antoinette Cloete, for all your support, care and encouragement. For taking on the extra responsibilities to afford me more time to work. For your motivation when I needed it the most. For believing in me and for loving me;
- ☛ My mother, Magda Cloete, for always supporting me and inspiring me to constantly strive towards realising my full potential. For always trying your best to give us the opportunities you never had. Your love, care and sacrifices did not go unnoticed;
- ☛ To my friends and family for your continued support and words of encouragement during this period; and
- ☛ Lastly, I would like to thank our saviour, God, for graciously giving me the gift of knowledge, health and endurance to complete this thesis.

TABLE OF CONTENT

Plagiaatverklaring / Plagiarism Declaration.....	i
Abstract	ii
Opsomming.....	iv
Acknowledgements	vi
Table of Content.....	vii
List of Figures	xiii
List of Tables	xix
List of Acronyms and Abbreviations.....	xxii
Nomenclature	xxiii
Chapter 1: Introduction	1
1.1. Motivation for the Thesis	3
1.2. Problem Statement and Study Objectives.....	5
1.3. Limitations and Delineation of the Study.....	6
1.4. Thesis Structure.....	6
Chapter 2: Literature Review	7
2.1. Introduction.....	7
2.2. Low Level River Crossings.....	7
2.2.1. Upstream (Inlet) Control	7
2.2.2. Downstream (Outlet) Control.....	8
2.2.3. Downstream Riprap.....	11
2.3. Hydraulic Jump.....	13
2.3.1. Hydraulic Jump Length (L_j).....	14
2.3.2. Energy Loss from a Hydraulic Jump.....	15
2.3.3. Hydraulic Jump Types.....	16
2.4. Stepped Chute Spillways	17
2.4.1. Nappe Flow.....	17
2.4.1.1. Nappe Flow with Hydraulic Jump (sub-regimes NA1 and NA2)	18
2.4.1.2. Nappe Flow without Hydraulic Jump (sub-regime NA3)	20

2.4.1.3. Ventilation of the Nappe.....	20
2.4.2. Transition Flow	21
2.4.3. Skimming Flow	22
2.4.3.1. Flow Regions in Skimming Flow.....	23
2.4.3.2. Air Entrainment.....	24
2.4.3.3. Pressures Profiles on the Steps	25
2.4.4. Guidelines for the Design of Stepped Chute Spillways.....	26
2.5. Model Scaling	26
2.5.1. Hydraulic Similarity.....	27
2.5.1.1. Geometric Similarity	27
2.5.1.2. Kinematic Similarity.....	27
2.5.1.3. Dynamic Similarity	27
2.5.2. Laws of Hydraulic Similarity.....	28
2.5.2.1. Froude's Law.....	28
2.5.2.2. Reynolds' Law.....	29
2.5.2.3. Weber's Law	29
2.5.2.4. Euler's Law.....	30
2.5.3. Summary of Hydraulic Model Scaling	31
2.6. Conclusion of Literature Review.....	31
Chapter 3: Hydraulic Design of the Prototype and Model.....	33
3.1. Introduction.....	33
3.2. Scope of The Hydraulic Model Tests	34
3.2.1. Model Scale.....	34
3.2.2. Laboratory Limitations.....	34
3.2.3. Model Layout	34
3.3. Test Conditions and Schedule	36
3.4. Model Design.....	37
3.4.1. Determining of Design Flow	38
3.4.2. Low-Level River Crossing.....	38

3.4.2.1. Overflow Depth	38
3.4.2.2. Approach Road	39
3.4.2.3. Culvert Openings	40
3.4.3. Stepped Chute	41
3.4.3.1. Nappe Flow from the Approach Road onto the Stepped Chute	42
3.4.3.2. Nappe Flow from One Chute Step to the Next	44
3.4.3.3. Ventilation of the Nappe	46
3.4.4. Riprap Design	47
3.5. Model Construction	48
3.5.1. Low-Level River Crossing	48
3.5.2. Stepped Chute	49
3.5.3. Nappe Ventilation	50
3.5.4. Riprap	50
3.6. Data Collection	51
3.6.1. Discharge	51
3.6.1.1. Instrumentation	51
3.6.1.2. Position	53
3.6.2. Water Level	53
3.6.2.1. Instrumentation	53
3.6.2.2. Position	54
3.6.3. Pressures Behind Nappes	54
3.6.3.1. Instrumentation	54
3.6.3.2. Position	55
3.6.3.3. Duration and Frequency	55
3.6.3.4. Data Conversion	55
3.6.4. Flow Profiles on Chute Steps	58
3.6.4.1. Instrumentation	58
3.6.4.2. Position	58
3.6.5. Nappe Ventilation	58

3.6.5.1. Instrumentation.....	58
3.6.5.2. Position.....	59
Chapter 4: Test Results	60
4.1. Introduction.....	60
4.2. Results of Model Setup 1 (Stepped Chute with Wall Intact).....	60
4.2.1. Flow Profiles	61
4.2.2. Pressure Behind the Nappe	63
4.2.3. Nappe Ventilation.....	68
4.2.4. Brief Discussion of Stepped Chute with Wall Intact.....	70
4.3. Results of Model Setup 2 (Stepped Chute Wall Omitted, and Downstream Riprap Added).....	70
4.3.1. Flow Profiles	71
4.3.2. Pressure Behind the Nappe	74
4.3.3. Nappe Ventilation.....	77
4.3.4. Displacement of Riprap.....	79
4.3.5. Brief Discussion of Stepped Chute with Chute Wall Removed, and Downstream Riprap Added.....	79
4.4. Repeatability of Tests	79
4.4.1. Flow Profiles on Stepped Chute Steps.....	80
4.4.2. Pressure Behind the Nappe	81
4.5. Analysis and Discussion	82
4.5.1. Comparison Between Vented and Unvented Hydraulic Models	82
4.5.2. Comparison Between Two Different Hydraulic Models	82
4.5.3. Notable Observations.....	83
4.5.3.1. Flow behind the nappe.....	83
4.5.3.2. Hydraulic ventilation of the nappe.....	84
4.5.4. Discussion on the Hydraulic Model Performance with One Open Culvert	85
4.5.5. Discussion on the Hydraulic Model Performance with All Culverts Open (2.5)	86
Chapter 5: Regression Analysis	87
5.1. Introduction.....	87



5.2. Dimensional Analysis	87
5.2.1. LLRC Dimension of Interest.....	87
5.2.1.1. Height of the steps (h_{S-S})	88
5.2.1.2. Width of the steps (W_{Step}).....	89
5.2.1.3. Length of the steps (L_{Step}).....	89
5.2.1.4. Physical Quantities Affecting the Length of the Steps.....	89
5.3. Multi-Linear Regression Analysis.....	90
5.3.1. Regression Models	91
5.3.2. Variables Dataset	91
5.3.3. Results of Regression Analysis.....	92
5.3.3.1. Linear Regression Model.....	92
5.3.3.2. Logarithmic Transformed Linear Regression Model.....	94
5.3.3.3. Linear-Logarithmic Regression Model.....	96
5.4. Conclusion of Regression Analysis.....	98
Chapter 6: Conclusions.....	100
6.1. Findings from the Literature Review	100
6.2. Findings from the Hydraulic Model Tests.....	101
6.3. Summary of the Hydraulic Model Study	102
Chapter 7: Recommendations	104
7.1. Recommendations on the use Of a Stepped Chute in Combination with a LLRC.....	104
7.2. Future Research.....	105
References	106
APPENDICES.....	I
APPENDIX A: Prototype Design Procedure	II
A.1. Prototype Design Procedure	III
A.2. Design Steps of the Prototype Low-Level River Crossing	III
A.3. Steps for the Design of the Prototype Stepped Chute	VII
APPENDIX B: Model Design	XI
B.1. Model Design.....	XII

B.2. Design of the Low-Level River Crossing.....	XIII
B.3. Design of the Stepped Chute.....	XVI
B.4. Application of the Regression Analysis Equation for the Stepped Chute Length.....	XX
APPENDIX C: Design Drawings of the Model.....	XXIV
APPENDIX D: Complete Testing Schedule.....	XXVIII
APPENDIX E: Pressure Data	XXXI
APPENDIX F: Flow Profiles.....	XXXVI
APPENDIX G: Photographs of Model Tests.....	LXIII

LIST OF FIGURES

Figure 1.1: Downstream Photograph of Low-Level River Crossing (R223 crossing the Pienaars River, Pretoria, South Africa)	2
Figure 1.2: Plan view and Downstream Elevation of Low-Level River Crossing	2
Figure 1.3: Erosion Downstream of LLRC Approach Road (R223 crossing the Pienaars River, Pretoria, South Africa)	3
Figure 1.4: Orange-Fish-Sundays Transfer Scheme (dwa.gov.za, 2018).....	4
Figure 1.5: Embankment Scour Downstream of LLRC Approach Road (Photograph Courtesy of Hennie Maas, BVi Consulting Engineers).....	5
Figure 2.1: Flow Through a Culvert Under Inlet Control Conditions.....	8
Figure 2.2: Conservation of mass.....	9
Figure 2.3: Flow Through a Culvert Under Outlet Control Conditions.....	10
Figure 2.4: Recommended Grading for Riprap (adapted from CSRA, 1994:2-4).....	13
Figure 2.5: Hydraulic Jump on Horizontal Surface	13
Figure 2.6: Hydraulic Jump Length in terms of conjugate depth in horizontal channels (adapted from USBR, 1987)	15
Figure 2.7: Hydraulic Jump Length in terms of sequent depth in horizontal channels (adapted from Thompson and Kilgore, 2006).....	15
Figure 2.8: Hydraulic Jump Types	16
Figure 2.9: Nappe Flow with a Fully- and Partially Developed Hydraulic Jump	17
Figure 2.10: Nappe Geometry of Flow at a Drop Structure.....	18
Figure 2.11: Comparison of Hydraulic Length Relationships	19
Figure 2.12: Nappe Flow with No Developed Hydraulic Jump (NA3) Down a Stepped Chute.....	20
Figure 2.13: Transition Flow Down a Stepped Chute	21
Figure 2.14: Flow Regimes on Stepped Spillways (adapted from Khatsuria:2005).....	22
Figure 2.15: Skimming Flow with a Pseudo Bottom Down a Stepped Chute	23
Figure 2.16: Flow Regions for Skimming Flow Stepped Chute Spillway	24
Figure 3.1: Model Setup Variations: (a) Model Setup 1: Chute Wall Intact; (b) Model Setup 2: Chute Wall Removed and Riprap Added	33
Figure 3.2: General Layout of Hydraulic Model Setup (Not to Scale)	35
Figure 3.3: Enlargement of the V-notch Weir Layout (Not to Scale).....	36
Figure 3.4: Isometric View of the Model with its Main Components Indicated.....	37
Figure 3.5: Full Prototype Elevations (Not to Scale).....	38
Figure 3.6: Prototype Step Chute Dimensions (Not to Scale).....	42
Figure 3.7: Positions for Overflow Depth ($y_{over road}$) and Nappe Fall Height (h_{R-S}).....	43
Figure 3.8: Nappe Geometry for Flow from the Approach Road	44

Figure 3.9: Cross-sectional View for Determining Stepped Chute Width	45
Figure 3.10: Illustration of ventilation pipe installation	47
Figure 3.11: Upstream Elevation of the Left Bank Approach Road and River Crossing	48
Figure 3.12: Installation of the Nappe Ventilation Pipes and Pressure Sensors	49
Figure 3.13: Installation of the Clear Perspex Chute Wall.....	49
Figure 3.14: Installation of the Nappe Ventilation Pipes	50
Figure 3.15: Reading Gauge of Flowmetrix Magflow DN100 Flow Meter.....	51
Figure 3.16: Coefficient of Discharge for $\theta=90^\circ$ V-Notch Weir.....	52
Figure 3.17: Flow Meter, Gate Valve and V-Notch Weir Setup	53
Figure 3.18: Flow Depth Water Measurement Needles: (a) LLRC Overflow Depth Measurements; (b) V-notch Weir Flow Depth Measurements	54
Figure 3.19: Wika S-10 High-Quality Pressure Transmitter.....	55
Figure 3.20: Pressure Transmitter Readings for Atmospheric Conditions.....	57
Figure 3.21: Stanley 9 mm x 3 m PowerLock Retractable Tape Rule	58
Figure 3.22: Lutron Hot-Wire Anemometer.....	58
Figure 3.23: Airflow Measurement Positions	59
Figure 4.1: Hydraulic Model with Stepped Chute Wall Intact.....	61
Figure 4.2: Hydraulic Model Flow Profiles – Test Run No.: 1.1.1. E ($y_{over road} = 20$ mm)	62
Figure 4.3: Hydraulic Model Flow Profiles – Test Run No.: 1.1.2. E ($y_{over road} = 20$ mm)	62
Figure 4.4: Hydraulic Model Flow Profiles – Test Run No.: 1.2.1. E ($y_{over road} = 20$ mm)	62
Figure 4.5: Hydraulic Model Flow Profiles – Test Run No.: 1.2.2. E ($y_{over road} = 20$ mm)	62
Figure 4.6: Hydraulic Model Photo – Test Run No.: 1.1.2. E ($y_{over road} = 20$ mm)	63
Figure 4.7: Hydraulic Model Photo – Test Run No.: 1.2.2. E ($y_{over road} = 20$ mm)	63
Figure 4.8: Prototype Pressure for Unvented Model Without Culvert Flow.....	65
Figure 4.9: Prototype Pressure for Vented Model Without Culvert Flow	65
Figure 4.10: Prototype Pressure for Unvented Model with Culvert Flow	65
Figure 4.11: Prototype Pressure for Vented Model with Culvert Flow	65
Figure 4.12: Downstream View of the Nappe Formation from the Approach Road onto the Stepped Chute	65
Figure 4.13: Summarised Prototype Nappe Cavity Pressures – Without Vents or Culvert Flow.	66
Figure 4.14: Summarised Prototype Nappe Cavity Pressures – With Vents, Without Culvert Flow	66
Figure 4.15: Summarised Prototype Nappe Cavity Pressures – Without Vents, With Culvert Flow	66
Figure 4.16: Summarised Prototype Nappe Cavity Pressures – With Vents and Culvert Flow	67
Figure 4.17: Nappe Deformation: (a) Low Tailwater Conditions; (b) High Tailwater Conditions	68

Figure 4.18: Total Prototype Nappe Ventilation Airflows – Model with Chute Wall.....	69
Figure 4.19: Hydraulic Model Without Stepped Chute Wall, and with Downstream Riprap Added	71
Figure 4.20: Hydraulic Model Flow Profiles – Test Run No.: 2.1.1. E ($y_{over road} = 20$ mm).....	72
Figure 4.21: Hydraulic Model Flow Profiles – Test Run No.: 2.1.2. E ($y_{over road} = 20$ mm).....	72
Figure 4.22: Hydraulic Model Flow Profiles – Test Run No.: 2.2.1. E ($y_{over road} = 20$ mm).....	72
Figure 4.23: Hydraulic Model Flow Profiles – Test Run No.: 2.2.2. E ($y_{over road} = 20$ mm).....	72
Figure 4.24: Hydraulic Model Photo – Test Run No.: 2.1.2. E ($y_{over road} = 20$ mm).....	73
Figure 4.25: Hydraulic Model Photo – Test Run No.: 2.2.2. E ($y_{over road} = 20$ mm).....	73
Figure 4.26: Prototype Pressure for Unvented Model Without Culvert Flow	75
Figure 4.27: Prototype Pressure for Vented Model Without Culvert Flow	75
Figure 4.28: Prototype Pressure for Unvented Model with Culvert Flow	75
Figure 4.29: Prototype Pressure for Vented Model with Culvert Flow	75
Figure 4.30: Summarised Prototype Nappe Cavity Pressures – Without Vents or Culvert Flow.	76
Figure 4.31: Summarised Prototype Nappe Cavity Pressures – With Vents, Without Culvert Flow	76
Figure 4.32: Summarised Prototype Nappe Cavity Pressures – Without Vents, With Culvert Flow	76
Figure 4.33: Summarised Prototype Nappe Cavity Pressures – With Vents and Culvert Flow	77
Figure 4.34: Prototype Nappe Ventilation Airflows – Model without Chute Wall.....	78
Figure 4.35: Hydraulic Model Flow Profiles – Test Run No.: 1.1.3 ($y_{over road} = 20$ mm)	80
Figure 4.36: Hydraulic Model Flow Profiles – Test Run No.: 1.2.3 ($y_{over road} = 20$ mm)	80
Figure 4.37: Hydraulic Model Flow Profiles – Test Run No.: 2.1.3 ($y_{over road} = 20$ mm)	81
Figure 4.38: Hydraulic Model Flow Profiles – Test Run No.: 2.2.3 ($y_{over road} = 20$ mm)	81
Figure 4.39: Prototype Pressure for Repeatability Tests.....	81
Figure 4.40: Downstream view of step 3 and culvert – Test Run No.: 1.1.2. E ($y_{over road} = 20$ mm)	83
Figure 4.41: Downstream view of step 3 and culvert – Test Run No.: 1.2.2. E ($y_{over road} = 20$ mm)	83
Figure 4.42: Downstream view of step 3 and culvert – Test Run No.: 2.1.2. E ($y_{over road} = 20$ mm)	83
Figure 4.43: Downstream view of step 3 and culvert – Test Run No.: 2.2.2. E ($y_{over road} = 20$ mm)	83
Figure 4.44: Flow Down the Chute Steps Behind the Nappe	84
Figure 4.45: Nappe Impingement without Culvert Flow ($y_{over road} = 20$ mm)	84
Figure 4.46: Nappe Intersection with Culvert Ouflow ($y_{over road} = 20$ mm)	84
Figure 4.47: Downstream View of Step 1 with Culvert Tailwater and Riprap.....	86
Figure 5.1: Definition sketch of physical quantities and dimensions (not to scale)	88
Figure 5.2: Linear Regression Model Predicted Q_0 vs. Actual Q_0	94
Figure 5.3: Logarithmic Transformed Linear Regression Model Predicted Q_0 vs. Actual Q_0	96
Figure 5.4: Linear-Logarithmic Regression Model Predicted Q_0 vs. Actual Q_0	98

Figure A.1: Culvert Geometry (not to scale)	IV
Figure A.2: Nappe Geometry from Approach Road onto Chute Steps	VII
Figure A.3: Flow Accumulation Down the Stepped Chute.....	VIII
Figure A.4: Effective Chute Step Overflow Width.....	IX
Figure A.5: Flow Regimes on Stepped Spillways (adapted from Khatsuria:2005)	X
Figure B.1: Flow Regimes on Stepped Chute (adapted from Khatsuria:2005).....	XIX
Figure E.1: Prototype Pressures – Test Run No.: 1.1.1.....	XXXII
Figure E.2: Prototype Pressures – Test Run No.: 1.1.2.....	XXXII
Figure E.3: Prototype Pressures – Test Run No.: 1.2.1.....	XXXIII
Figure E.4: Prototype Pressures – Test Run No.: 1.2.2.....	XXXIII
Figure E.5: Prototype Pressures – Test Run No.: 2.1.1.....	XXXIV
Figure E.6: Prototype Pressures – Test Run No.: 2.1.2.....	XXXIV
Figure E.7: Hydraulic Model Pressures – Test Run No.: 2.2.1.....	XXXV
Figure E.8: Hydraulic Model Pressures – Test Run No.: 2.2.2.....	XXXV
Figure F.1: Hydraulic Model Flow Profiles – Test Run No.: 1.1.1.A.....	XXXVII
Figure F.2: Hydraulic Model Flow Profiles – Test Run No.: 1.1.1.B.....	XXXVII
Figure F.3: Hydraulic Model Flow Profiles – Test Run No.: 1.1.1.C.....	XXXVIII
Figure F.4: Hydraulic Model Flow Profiles – Test Run No.: 1.1.1.D	XXXVIII
Figure F.5: Hydraulic Model Flow Profiles – Test Run No.: 1.1.1.E.....	XXXIX
Figure F.6: Hydraulic Model Flow Profiles – Test Run No.: 1.1.2.A.....	XL
Figure F.7: Hydraulic Model Flow Profiles – Test Run No.: 1.1.2.B.....	XL
Figure F.8: Hydraulic Model Flow Profiles – Test Run No.: 1.1.2.C.....	XLI
Figure F.9: Hydraulic Model Flow Profiles – Test Run No.: 1.1.2.D	XLI
Figure F.10: Hydraulic Model Flow Profiles – Test Run No.: 1.1.2.E	XLII
Figure F.11: Hydraulic Model Flow Profiles – Test Run No.: 1.2.1.A.....	XLIII
Figure F.12: Hydraulic Model Flow Profiles – Test Run No.: 1.2.1.B	XLIII
Figure F.13: Hydraulic Model Flow Profiles – Test Run No.: 1.2.1.C	XLIV
Figure F.14: Hydraulic Model Flow Profiles – Test Run No.: 1.2.1.D	XLIV
Figure F.15: Hydraulic Model Flow Profiles – Test Run No.: 1.2.1.E	XLV
Figure F.16: Hydraulic Model Flow Profiles – Test Run No.: 1.2.2.A	XLVI
Figure F.17: Hydraulic Model Flow Profiles – Test Run No.: 1.2.2.B	XLVI
Figure F.18: Hydraulic Model Flow Profiles – Test Run No.: 1.2.2.C	XLVII
Figure F.19: Hydraulic Model Flow Profiles – Test Run No.: 1.2.2.D	XLVII
Figure F.20: Hydraulic Model Flow Profiles – Test Run No.: 1.2.2.E	XLVIII
Figure F.21: Hydraulic Model Flow Profiles – Test Run No.: 2.1.1.A	XLIX
Figure F.22: Hydraulic Model Flow Profiles – Test Run No.: 2.1.1.B	XLIX
Figure F.23: Hydraulic Model Flow Profiles – Test Run No.: 2.1.1.C	L

Figure F.24: Hydraulic Model Flow Profiles – Test Run No.: 2.1.1.D	L
Figure F.25: Hydraulic Model Flow Profiles – Test Run No.: 2.1.1.E	LI
Figure F.26: Hydraulic Model Flow Profiles – Test Run No.: 2.1.2.A	LII
Figure F.27: Hydraulic Model Flow Profiles – Test Run No.: 2.1.2.B	LII
Figure F.28: Hydraulic Model Flow Profiles – Test Run No.: 2.1.2.C	LIII
Figure F.29: Hydraulic Model Flow Profiles – Test Run No.: 2.1.2.D	LIII
Figure F.30: Hydraulic Model Flow Profiles – Test Run No.: 2.1.2.E	LIV
Figure F.31: Hydraulic Model Flow Profiles – Test Run No.: 2.2.1.A	LV
Figure F.32: Hydraulic Model Flow Profiles – Test Run No.: 2.2.1.B	LV
Figure F.33: Hydraulic Model Flow Profiles – Test Run No.: 2.2.1.C	LVI
Figure F.34: Hydraulic Model Flow Profiles – Test Run No.: 2.2.1.D	LVI
Figure F.35: Hydraulic Model Flow Profiles – Test Run No.: 2.2.1.E	LVII
Figure F.36: Hydraulic Model Flow Profiles – Test Run No.: 2.2.2.A	LVIII
Figure F.37: Hydraulic Model Flow Profiles – Test Run No.: 2.2.2.B	LVIII
Figure F.38: Hydraulic Model Flow Profiles – Test Run No.: 2.2.2.C	LIX
Figure F.39: Hydraulic Model Flow Profiles – Test Run No.: 2.2.2.D	LIX
Figure F.40: Hydraulic Model Flow Profiles – Test Run No.: 2.2.2.E	LX
Figure F.41: Hydraulic Model Flow Profiles – Test Run No.: 1.1.3.....	LXI
Figure F.42: Hydraulic Model Flow Profiles – Test Run No.: 1.2.3.....	LXI
Figure F.43: Hydraulic Model Flow Profiles – Test Run No.: 2.1.3.....	LXII
Figure F.44: Hydraulic Model Flow Profiles – Test Run No.: 2.2.3.....	LXII
Figure G.1: Hydraulic Model Photograph – Test Run No.: 1.1.1. A ($y_{over road} = 4 \text{ mm}$)	LXIV
Figure G.2: Hydraulic Model Photograph – Test Run No.: 1.1.2. A ($y_{over road} = 4 \text{ mm}$)	LXIV
Figure G.3: Hydraulic Model Photograph – Test Run No.: 1.2.1. A ($y_{over road} = 4 \text{ mm}$)	LXIV
Figure G.4: Hydraulic Model Photograph – Test Run No.: 1.2.2. A ($y_{over road} = 4 \text{ mm}$)	LXIV
Figure G.5: Hydraulic Model Photograph – Test Run No.: 1.1.1. B ($y_{over road} = 8 \text{ mm}$)	LXV
Figure G.6: Hydraulic Model Photograph – Test Run No.: 1.1.2. B ($y_{over road} = 8 \text{ mm}$)	LXV
Figure G.7: Hydraulic Model Photograph – Test Run No.: 1.2.1. B ($y_{over road} = 8 \text{ mm}$)	LXV
Figure G.8: Hydraulic Model Photograph – Test Run No.: 1.2.2. B ($y_{over road} = 8 \text{ mm}$)	LXV
Figure G.9: Hydraulic Model Photograph – Test Run No.: 1.1.1. C ($y_{over road} = 12 \text{ mm}$)	LXVI
Figure G.10: Hydraulic Model Photograph – Test Run No.: 1.1.2. C ($y_{over road} = 12 \text{ mm}$)	LXVI
Figure G.11: Hydraulic Model Photograph – Test Run No.: 1.2.1. C ($y_{over road} = 12 \text{ mm}$)	LXVI
Figure G.12: Hydraulic Model Photograph – Test Run No.: 1.2.2. C ($y_{over road} = 12 \text{ mm}$)	LXVI
Figure G.13: Hydraulic Model Photograph – Test Run No.: 1.1.1. D ($y_{over road} = 16 \text{ mm}$).....	LXVII
Figure G.14: Hydraulic Model Photograph – Test Run No.: 1.1.2. D ($y_{over road} = 16 \text{ mm}$).....	LXVII
Figure G.15: Hydraulic Model Photograph – Test Run No.: 1.2.1. D ($y_{over road} = 16 \text{ mm}$).....	LXVII
Figure G.16: Hydraulic Model Photograph – Test Run No.: 1.2.2. D ($y_{over road} = 16 \text{ mm}$).....	LXVII

Figure G.17: Hydraulic Model Photograph – Test Run No.: 1.1.1. E ($y_{over road} = 20$ mm)	LXVIII
Figure G.18: Hydraulic Model Photograph – Test Run No.: 1.1.2. E ($y_{over road} = 20$ mm)	LXVIII
Figure G.19: Hydraulic Model Photograph – Test Run No.: 1.2.1. E ($y_{over road} = 20$ mm)	LXVIII
Figure G.20: Hydraulic Model Photograph – Test Run No.: 1.2.2. E ($y_{over road} = 20$ mm)	LXVIII
Figure G.21: Hydraulic Model Photograph – Test Run No.: 2.1.1. A ($y_{over road} = 4$ mm).....	LXIX
Figure G.22: Hydraulic Model Photograph – Test Run No.: 2.1.2. A ($y_{over road} = 4$ mm).....	LXIX
Figure G.23: Hydraulic Model Photograph – Test Run No.: 2.2.1. A ($y_{over road} = 4$ mm).....	LXIX
Figure G.24: Hydraulic Model Photograph – Test Run No.: 2.2.2. A ($y_{over road} = 4$ mm).....	LXIX
Figure G.25: Hydraulic Model Photograph – Test Run No.: 2.1.1. B ($y_{over road} = 8$ mm).....	LXX
Figure G.26: Hydraulic Model Photograph – Test Run No.: 2.1.2. B ($y_{over road} = 8$ mm).....	LXX
Figure G.27: Hydraulic Model Photograph – Test Run No.: 2.2.1. B ($y_{over road} = 8$ mm).....	LXX
Figure G.28: Hydraulic Model Photograph – Test Run No.: 2.2.2. B ($y_{over road} = 8$ mm).....	LXX
Figure G.29: Hydraulic Model Photograph – Test Run No.: 2.1.1. C ($y_{over road} = 12$ mm)	LXXI
Figure G.30: Hydraulic Model Photograph – Test Run No.: 2.1.2. C ($y_{over road} = 12$ mm)	LXXI
Figure G.31: Hydraulic Model Photograph – Test Run No.: 2.2.1. C ($y_{over road} = 12$ mm)	LXXI
Figure G.32: Hydraulic Model Photograph – Test Run No.: 2.2.2. C ($y_{over road} = 12$ mm)	LXXI
Figure G.33: Hydraulic Model Photograph – Test Run No.: 2.1.1. D ($y_{over road} = 16$ mm).....	LXXII
Figure G.34: Hydraulic Model Photograph – Test Run No.: 2.1.2. D ($y_{over road} = 16$ mm).....	LXXII
Figure G.35: Hydraulic Model Photograph – Test Run No.: 2.2.1. D ($y_{over road} = 16$ mm).....	LXXII
Figure G.36: Hydraulic Model Photograph – Test Run No.: 2.2.2. D ($y_{over road} = 16$ mm).....	LXXII
Figure G.37: Hydraulic Model Photograph – Test Run No.: 2.1.1. E ($y_{over road} = 20$ mm)	LXXIII
Figure G.38: Hydraulic Model Photograph – Test Run No.: 2.1.2. E ($y_{over road} = 20$ mm)	LXXIII
Figure G.39: Hydraulic Model Photograph – Test Run No.: 2.2.1. E ($y_{over road} = 20$ mm)	LXXIII
Figure G.40: Hydraulic Model Photograph – Test Run No.: 2.2.2. E ($y_{over road} = 20$ mm)	LXXIII
Figure G.41: Hydraulic Model Photograph – Test Run No.: 1.1.3. ($y_{over road} = 20$ mm)	LXXIV
Figure G.42: Hydraulic Model Photograph – Test Run No.: 1.2.3. ($y_{over road} = 20$ mm)	LXXIV
Figure G.43: Hydraulic Model Photograph – Test Run No.: 2.1.3. ($y_{over road} = 20$ mm)	LXXIV
Figure G.44: Hydraulic Model Photograph – Test Run No.: 2.2.3. ($y_{over road} = 20$ mm)	LXXIV

LIST OF TABLES

Table 2-1: Froude's Law Scale Ratios.....	31
Table 3-1: Summarised Test Conditions.....	36
Table 3-2: Hydraulic Model Design Recommendations and Procedures	37
Table 3-3: Recommended Maximum Approach Road Gradients.....	39
Table 3-4: Flow Over the Crossing for the Different Overflow Test Depths	40
Table 3-5: Flow Through the Culvert for the Different Overflow Test Depths	40
Table 3-6: Approach Road Overflows Impinging on Each Step.....	43
Table 3-7: Nappe Drop-lengths and Hydraulic Jump Roller Lengths from Road to Steps	44
Table 3-8: Nappe Drop-lengths and Hydraulic Jump Roller Lengths from One Step to the Next	45
Table 3-9: Prototype Nappe Ventilation Requirement Variables.....	46
Table 3-10: Nappe Ventilation Requirement.....	46
Table 3-11: Riprap Design Parameters	48
Table 3-12: Hydraulic Model Riprap Grading Requirement.....	50
Table 3-13: Flowmetrix Magflow DN100: Recommended and Actual Minimum Up- and Downstream Straight Pipe Lengths.....	53
Table 3-14: Wika S-10 Pressure Transmitter Operating Ranges and Parameters.....	55
Table 3-15: Averaged Pressure Transmitter Readings and Standard Deviations	57
Table 3-16: Lutron Hot-Wire Anemometer Operating Parameters	59
Table 4-1: Test Number Convention	60
Table 4-2: Prototype Pressure heads for the Test Runs 1.1.1. to 1.2.2.	63
Table 4-3: Model Setup 1 – Prototype Nappe Pressure Heads	67
Table 4-4: Prototype Nappe Ventilation Airflows.....	69
Table 4-5: Prototype Pressure heads for the Test Runs 2.1.1. and 2.2.2.....	74
Table 4-6: Model Setup 2 - Prototype Nappe Pressure Heads.....	77
Table 4-7: Prototype Nappe Ventilation Airflows – Model without Chute Wall	78
Table 4-8: Hydraulic Model Test Runs with Corresponding Repeatability Tests.....	80
Table 4-9: Prototype Pressure heads for Repeatability Tests	82
Table 5-1: Data Set Used for Regression Analyses.....	92
Table 5-2: Variables Used for Linear Regression Model.....	93
Table 5-3: Linear Regression Model Statistics	93
Table 5-4: Linear Regression Model Statistics	93
Table 5-5: Variables Used for Logarithmic Transformed Linear Regression Model.....	95
Table 5-6: Logarithmic Transformed Linear Regression Model Statistics	95
Table 5-7: Logarithmic Transformed Linear Regression Model Statistics	95
Table 5-8: Variables Used for Linear-Logarithmic Regression Model.....	97

Table 5-9: Linear-Logarithmic Regression Model Statistics.....	97
Table 5-10: Linear-Logarithmic Regression Model Statistics	97
Table A-1: Dimensions Used for Low-Level River Crossing Design	III
Table A-2: Nappe Geometry from Approach Road onto Chute Steps	VII
Table A-3: Nappe Geometry from One Chute Step onto the Next.....	IX
Table B-1: Froude's Law Scale Ratios	XII
Table B-2: Dimensions Used for Low-Level River Crossing	XIII
Table B-3: Flow Over the Low-Level River Crossing	XIII
Table B-4: Upstream Energy Levels.....	XIV
Table B-5: H_1/D Ratios.....	XIV
Table B-6: Culvert Flow Input Parameters	XV
Table B-7: Culvert Flow Results	XV
Table B-8: Total Prototype and Hydraulic Model Flows	XV
Table B-9: Preliminary Prototype Chute Dimensions	XVI
Table B-10: Preliminary Hydraulic Model Chute Dimensions.....	XVI
Table B-11: Flow Distribution over the Left Bank ($y_{over road} = 60$ mm)	XVI
Table B-12: Flow Distribution over the Left Bank ($y_{over road} = 120$ mm).....	XVI
Table B-13: Flow Distribution over the Left Bank ($y_{over road} = 180$ mm).....	XVI
Table B-14: Flow Distribution over the Left Bank ($y_{over road} = 240$ mm).....	XVII
Table B-15: Flow Distribution over the Left Bank ($y_{over road} = 300$ mm).....	XVII
Table B-16: Drop Height from Approach Road onto Each Step	XVII
Table B-17: Nappe Geometry from Approach Road onto Each Chute Step ($y_{over road} = 300$ mm)	XVII
Table B-18: Nappe Cavity Ventilation Requirement from Approach Road onto Each Chute Step ($y_{over road} = 300$ mm)	XVIII
Table B-19: Flow Accumulation Down the Chute ($y_{over road} = 300$ mm)	XVIII
Table B-20: Flow Accumulation Down the Chute ($y_{over road} = 300$ mm)	XVIII
Table B-21: Nappe Geometry from One Chute Step onto the Next ($y_{over road} = 300$ mm).....	XVIII
Table B-22: Nappe Cavity Ventilation Requirement from One Chute Step onto the Next ($y_{over road} = 300$ mm)	XIX
Table B-23: Comparison of Drop Length ($L_{dS-S(ns)}$) Plus Hj Roller Length ($L_{rS-S(ns)}$) with Step Length in Direction of Flow ($y_{over road} = 300$ mm)	XIX
Table B-24: Dimensions Determined for a Low-Level River Crossing.....	XX
Table B-25: Flow Over the Low-Level River Crossing.....	XX
Table B-26: Preliminary Chute Dimensions	XXI
Table B-27: Flow distribution over Both the Left and Right Bank ($y_{over road} = 150$ mm).....	XXI
Table B-28: Drop Height from Approach Road onto Each Step	XXI

Table B-29: Calculated Chute Step Lengths	XXI
Table B-30: Altered Chute Step Lengths	XXII
Table B-31: Nappe Geometry from Approach Road onto Each Chute Step ($y_{over road} = 150$ mm)	XXII
Table B-32: Nappe Geometry from One Chute Step onto the Next ($y_{over road} = 150$ mm)	XXII
Table B-33: Comparison of Drop Length ($L_{d S-S(ns)}$) Plus Hj Roller Length ($L_{r S-S(ns)}$) with Step Length in Direction of Flow ($y_{over road} = 150$ mm)	XXIII
Table D-1: Test Run Details	XXIX
Table D-2: Test Run Details (cont.)	XXX

LIST OF ACRONYMS AND ABBREVIATIONS

A	Ampere
BSI	British Standards Institution
CSRA	Committee of State Road Authorities (South Africa)
DN	Nominal diameter of a pipe, usually followed by a dimension in millimetres
DWS	Department of Water and Sanitation (South Africa)
Eq.	Equation
HGL	Hydraulic Grade Line
HJ	Hydraulic Jump
Hz	Hertz (The SI unit of frequency; 1 Hz is equal to 1 cycle per second)
LB	Left Bank (of approach road)
LLRC	Low Level River Crossing
ms	Milliseconds (A fraction of a second; 1 ms is equal to 1×10^{-3} seconds)
NA1	Nappe Flow with Fully Developed Hydraulic Jump
NA2	Nappe Flow with Partially Developed Hydraulic Jump
NA3	Nappe Flow Without Hydraulic Jump
NH	Nappe Flow with Fully Developed Hydraulic Jump
NP	Nappe Flow with Partially Developed or No Hydraulic Jump
RB	Right Bank (of approach road)
RCC	Roller Compacted Concrete
SANRAL	South African National Roads Agency SOC Limited
SCED	Stepped Chute Energy Dissipator
SK	Skimming Flow Regime
TEL	Total Energy Line
TR	Transition Flow Regime

NOMENCLATURE

Symbol	Description	Units
\bar{v}_1	Average flow velocity at section 1	m/s
\bar{v}_2	Average flow velocity at section 2	m/s
$h_{f_{1-2}}$	Friction loss between section 1 and 2	m
$h_{l_{1-2}}$	Secondary head losses between section 1 and 2	m
A	Cross-sectional flow area	m^2
B	Channel width	m
C	Coefficient for specific gravity and stability	<i>dimensionless</i>
C_b	Coefficient expressing the effect of width contraction in the flow	<i>dimensionless</i>
C_e	Coefficient of discharge	<i>dimensionless</i>
C_h	Coefficient of contraction in the vertical plane	<i>dimensionless</i>
D	Height of the culvert opening	m
D_{50}	Nominal 50% stone size	m
F_r	Froude number	<i>dimensionless</i>
Fr_1	Froude number at section 1	<i>dimensionless</i>
g	Gravitational acceleration constant taken as 9.81 m/s^2	m/s^2
h	<ul style="list-style-type: none"> • Stepped chute: spillway step height • V-notch weir: upstream head measured from the vertex of the V-notch 	m
H_1	Energy level at section 1	m
H_2	Energy level at section 2	m
$H_{d,u}$	Vertical distance below the crest required for uniform flow to be reached	m
h_{deck}	Height of the culvert measured from the culvert invert to the top of the deck	m
h_e	Effective head	m
H_{nappe}	Nappe cavity pressure head	m
h_{R-S}	Nappe drop height from the LLRC approach road onto the chute step	m
h_{S-S}	Chute step height	m
K_1	Dimensionless factor	<i>dimensionless</i>
k_h	Experimentally determined constant°	m
K_u	Dimensionless unit conversion constant	<i>dimensionless</i>
L_d	Horizontal length of a nappe drop, measured from the face of the drop to the impingement point	m

L_{dR-S}	Horizontal length of the nappe drop formed from the LLRC approach road onto the chute step	m
L_{dR-S}	Horizontal length of the nappe drop formed from one chute step onto the next	m
L_j	Length of the hydraulic jump	m
L_r	Length of the hydraulic jump roller taken to the point where the flow velocity at the top reverses and the jet continues (Chaudhry 2008:216)	m
L_{rR-S}	Horizontal length of the hydraulic jump, formed from the approach road, on the chute step	m
L_{rR-S}	Horizontal length of the hydraulic jump formed from one chute step onto the next	m
$L_{Step(ns)}$	Length of chute step number ns	m
ns	The number of the chute step in question	dimensionless
n_{steps}	Number of chute steps	dimensionless
p	Height of the vertex of the V-notch with respect to the floor of the approach channel	m
Q	Discharge	m^3/s
q	unit discharge	$m^3/s/m$
Q_{air}	Air-flow rate required to ventilate the nappe cavity	m^3/s
$Q_{R-S(ns)}$	Flow from the approach road onto chute step number ns	m^3/s
$Q_{S-S(ns+1)}$	Flow from the previous chute step ($ns+1$) onto step number ns	m^3/s
Q_{under}	Flow rate through the LLRC culverts	m^3/s
Q_w	Discharge of the nappe	m^3/s
r^2	Coefficient of determination	dimensionless
Re	Reynolds number describing the ratio of inertial forces to viscous forces	dimensionless
$S_{approach}$	Approach road slope	m/m
S_F	Safety factor	dimensionless
S_s	Specific gravity of riprap	kg/l
T_w	Width of the top water surface	m
v	Flow velocity	m/s
$w_{culvert}$	Width of the culvert opening	m
W_{Step}	Width of the chute steps	m
y_1	Flow depth at section 1	m
y_2	Flow depth at section 2	m
$y_{90,u}$	Uniform flow depth corresponding to 90% air concentration	m
y_{avg}	Average flow depth	m
y_b	Overflow depth at the brink of a step	m

y_c	Critical flow depth	<i>m</i>
$y_{c,\text{onset}}$	Characteristic critical depth where skimming flow would occur	<i>m</i>
$y_{\text{over road}}$	Flow depth on top of the LLRC deck	<i>m</i>
y_p	Pool depth beneath the nappe	<i>m</i>
y_{top}	Flow depth from the step above the receiving step	<i>m</i>
Z_1	Inlet invert level of the culvert measured relative to a datum level	<i>m</i>
Z_2	Outlet invert level of the culvert measured relative to a datum level	<i>m</i>
ΔE	Energy dissipated from a hydraulic jump	<i>m</i>
θ	<ul style="list-style-type: none"> • Riprap: revetment bank angle with the horizontal • V-notch weir: notch opening angle 	°
θ_{chute}	Stepped chute spillway angle of inclination	°
φ	Riprap angle of repose	°
ℓ	Stepped chute spillway step length	<i>m</i>

CHAPTER 1: INTRODUCTION

A low-level river crossing (LLRC) is a road structure that crosses either a river or stream and could be submerged under flood conditions. Low-level river crossings are normally provided when lower order roads need to cross a river and/or stream in a cost-effective manner with the least amount of disruption to natural flow conditions and are designed in such a way to limit damage when overtopped. (Pienaar and Kruger, 2013)

LLRCs can be classified as either a drift or a causeway, with the main aspects being:

- **Drift** – A drift is a river crossing where the travelled surface can be constructed from materials consisting of concrete or grouted stone. The main identifying characteristic of a drift is the fact that it only allows water flow to traverse the travelled surface.
- **Causeway** – A causeway, similar to a drift, has a prepared surface for vehicles to travel on when crossing a river but also provides openings underneath the prepared surface to allow for the passing of flow. This is also referred to as a vented causeway or vented fords (Johannessen, 2008). Pipes, portal culverts or short decks can typically be used for the openings.

The study focused on vented causeways and any mention of low-level river crossings refer to vented causeways, unless stated otherwise.

LLRCs consist of a main deck, approach roads and any number of openings under the deck. The height from the river bed to the deck is typically less than 2 m (Pienaar & Kruger, 2013). LLRCs are designed to overflow during lower recurrence intervals (typically 1:2 to 1:10 year return periods). The roads they serve are lower order roads and are normally not the primary access roads between communities, i.e. other higher order access roads would still provide access to a community during flooding but would lead to longer travel routes. The higher order access roads would typically be either a bridged crossing or a culvert crossing designed for higher return periods.

Constructing a bridged crossing at each access point to a community is normally expensive. Reducing the number of bridges and rather opting for LLRCs at lower order roads, maintains increased access during periods of no flooding, and may prove to be economically viable. Factors such as acceptability of reduced access during flooding, the risk of road users who might still attempt to cross the LLRC during inundation and be washed away, and the required maintenance and repairs after floods also need to be considered. Figure 1.1 illustrates the downstream view of a typical vented causeway.



Figure 1.1: Downstream Photograph of Low-Level River Crossing (R223 crossing the Pienaars River, Pretoria, South Africa)

During flooding, the approaches to the main deck of the LLRC would cause flow to accelerate and when reaching the end of the approach road (in the direction of the flow), would erode the downstream embankment as illustrated in Figure 1.2 and Figure 1.3. This phenomenon can be countered by constructing a layer of riprap on the downstream end of the approach roads. Obtaining rock suitable for riprap may, however, be expensive if no sources of rock are in close proximity to the LLRC.

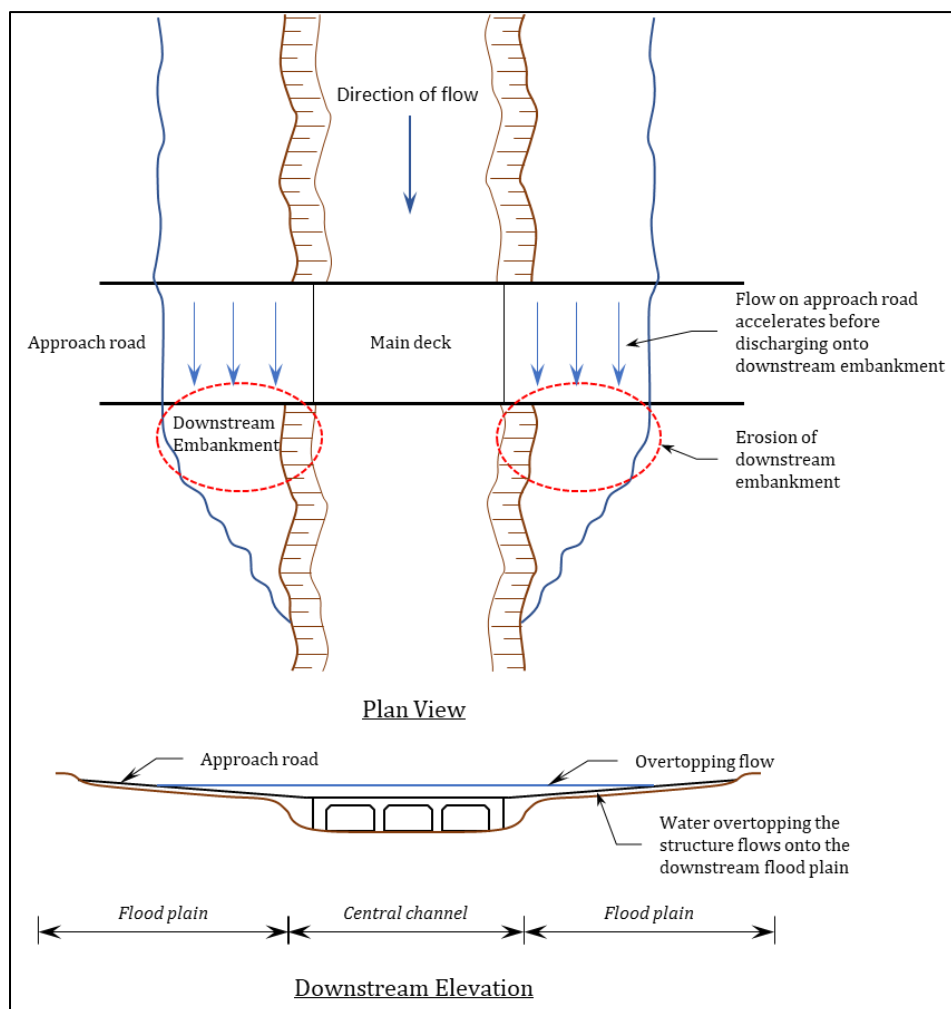


Figure 1.2: Plan view and Downstream Elevation of Low-Level River Crossing

A possible mitigating measure against downstream bank erosion at LLRCs is the use of stepped chutes. Stepped chutes increase energy dissipation by means of vertical drops and hydraulic jumps on each step. Should it prove to be hydraulically effective, this type of structure could be used to replace the traditional means of downstream erosion protection, which consisted of placing considerably large riprap mattresses (>1m dia boulders) directly downstream of the LLRC approaches.

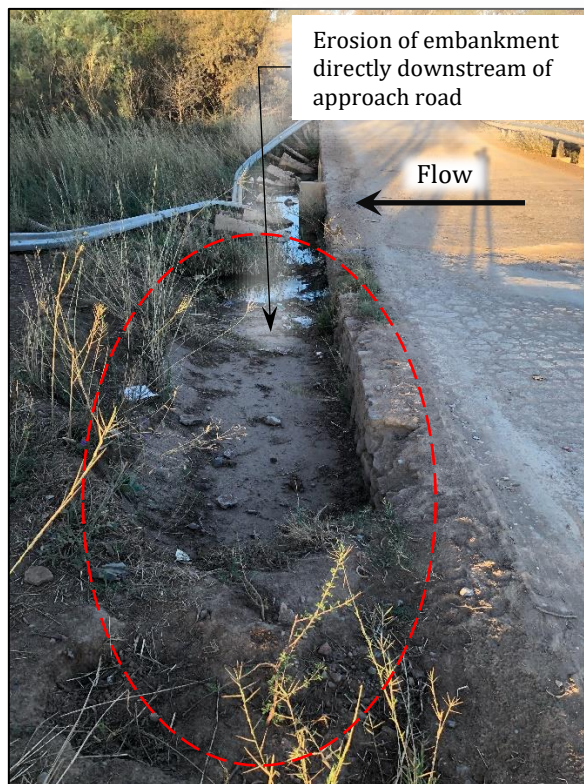


Figure 1.3: Erosion Downstream of LLRC Approach Road (R223 crossing the Pienaars River, Pretoria, South Africa)

1.1. MOTIVATION FOR THE THESIS

The focus of this thesis was based on a Department of Water and Sanitation (DWS) project named “The Rehabilitation of Skoenmakers River (2016)” and is located in the Karoo region of the Eastern Cape, South Africa.

The Skoenmakers River is used as a transfer route for water transferred by the Orange-Fish-Sundays River Interbasin Transfer Scheme. Water from the Gariep Dam is transferred via the Orange-Fish gravity tunnel to the Teebusspruit. The Teebusspruit flows into the Grassridge Dam which ultimately discharges into the Great Fish river. Water is then diverted from the Great Fish River at the Elandsdrift Weir, using tunnels and canals to the Small Fish River for a short distance which then flows into the De Mistkraal Weir. Water is then discharged into the Skoenmakers River via a canal from the De Mistkraal Weir. The Skoenmakers River finally discharges into the Darlington Dam. This transfer system is intended to supplement the

existing water supply to the Sundays River Valley in the Eastern Cape. The schematic layout of the transfer system is depicted in Figure 1.4.

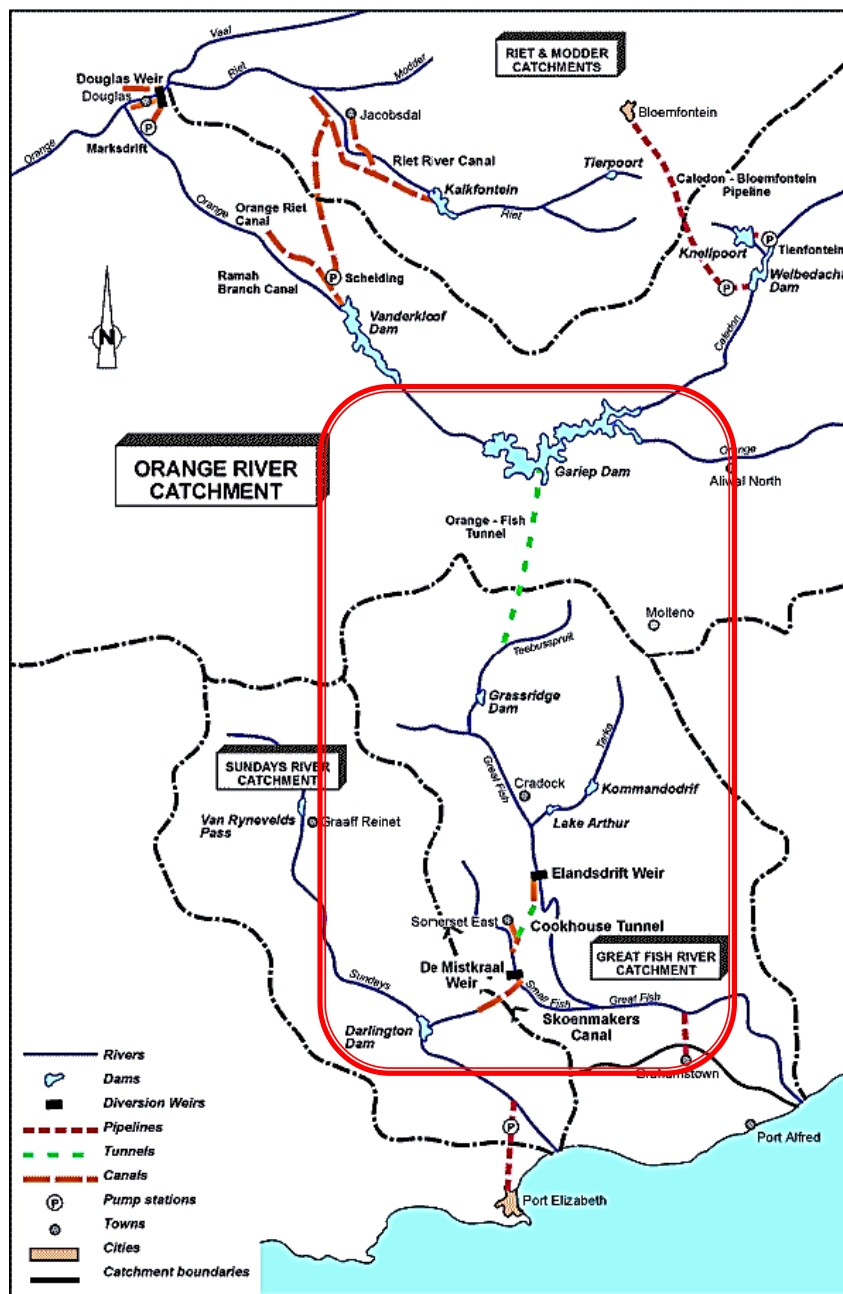


Figure 1.4: Orange-Fish-Sundays Transfer Scheme (dwa.gov.za, 2018)

The development of the Orange-Fish-Sundays River Interbasin Transfer Scheme in the 1970s to early 1980s caused hazardous access conditions for farmers who had to cross the Skoenmakers River to get to their farms. To overcome the inaccessibility, ten river crossings were constructed. However, due to the change in the hydrological regime from a once ephemeral stream to a bigger perennial river, changes to both the physical structure and riparian vegetation structure of the river resulted in erosion of river embankments and damage to infrastructure such as road crossings and water extraction weirs.

This continual change led to the deterioration of the ten river crossings. The DWS project envisaged the restoring and/or upgrading of the crossings. BVi Consulting Engineers were appointed to perform a feasibility study and one of their proposed erosion prevention measures included the construction of a concrete stepped chute structure downstream of the approaches of the causeway. Figure 1.5 indicates the severity of the erosion that was encountered at one of the ten sites.



Figure 1.5: Embankment Scour Downstream of LLRC Approach Road (Photograph Courtesy of Hennie Maas, BVi Consulting Engineers)

1.2. PROBLEM STATEMENT AND STUDY OBJECTIVES

No formal guidelines for the design of a stepped chute energy dissipation structure to protect embankments downstream of low-level river crossings were available. The objective of this study was, therefore, to:

- design a prototype model using literature describing the anticipated hydraulics;
- construct a scaled model to be tested in the Hydraulic Laboratory of Stellenbosch University;
- test the scale model to verify initial hydraulic operations and identify unforeseen phenomena; and
- to provide practical recommendation on the application of such a stepped chute.

1.3. LIMITATIONS AND DELINEATION OF THE STUDY

This study was confined to the stepped chute that included flow accepted from the approach road and culvert tailwater during upstream control conditions. The main objective was to verify anticipated flow conditions which existed on the stepped chute and the influence that culvert tailwater had on the model operation. The influence of the stepped chute structure on downstream flow conditions was not considered, nor was the financial implication of a stepped chute when compared to the more traditional method of using riprap as erosion protection. The addition of guide blocks along the river crossing travelled way was omitted to simplify the design and construction of the hydraulic model.

1.4. THESIS STRUCTURE

This thesis consists of seven chapters including this introductory chapter, as well as relevant appendices. The first chapter motivates the need for the study. The second chapter illustrates the knowledge gained during the literature study. The third chapter discusses the application of the knowledge, from the previous chapter, to design of the hydraulic model and describes the tests which were performed. The fourth chapter includes the results and brief discussion thereof. The fifth chapter includes the regression analysis of the test variable to obtain dimensionless relationships for the design of a LLRC stepped chute. The sixth and seventh chapters include the conclusions and recommendations for the use of stepped chutes in practice.

The appendices at the end of this thesis include the prototype and model design (Appendix A and B), while Appendix C contains the model construction drawings. The complete model testing schedule is contained in Appendix D. Appendix E and F contain the pressure data results and the flow profile plots following testing of the hydraulic model. Appendix G concludes the document with photographs of the separate tests.

CHAPTER 2: LITERATURE REVIEW

2.1. INTRODUCTION

The purpose of this chapter is to provide the reader with the necessary background and knowledge which were used for the prototype design discussed in Section 3.

Section 2.2 contains the two different operating conditions (upstream- and downstream control) encountered with culvert flow and the corresponding design procedures used to determine the discharge capacity.

Section 2.3 provides the reader with information on hydraulic jumps and their ability to dissipate excessive amounts of energy. Section 2.4 discusses the three different flow regimes encountered on stepped chute spillways.

Section 2.5 contains information on hydraulic similarity which was adhered to during the design of the hydraulic model. Section 2.5 also discusses the different forces acting on a fluid and how maintaining prototype and hydraulic model similarity between gravitational- and viscous forces, surface tension and elasticity is not always possible.

2.2. LOW LEVEL RIVER CROSSINGS

Low-level river crossings have the same hydraulic design calculations as that of lesser culverts with the exception of a low-level river crossing being designed to also allow for water to flow over the structure and not only underneath it.

When designing a lesser culvert, distinction must be made between upstream-, or downstream control. These two controls are discussed in more detail in Sections 2.2.1 and 2.2.2. The addition and sizing requirements of riprap, to protect downstream embankments from erosion due to the overtopping flow, is discussed in Section 2.2.3.

2.2.1. Upstream (Inlet) Control

Inlet control conditions occur when critical flow conditions occur (Froude number=1) at the inlet due to the entrance flow capacity being less than the flow capacity through the culvert. Henderson (1966) reported that the water surface does not come into contact with the soffit of the culvert at the entry for $H/D < 1.2$, but for H/D values greater than 1.2, the water surface does come into contact with the soffit at the inlet and would therefore essentially act as a sluice gate.

Figure 2.1 illustrates flow through a culvert under inlet conditions.

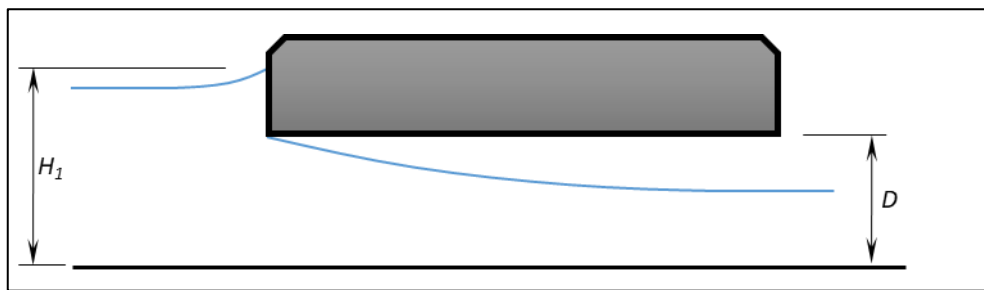


Figure 2.1: Flow Through a Culvert Under Inlet Control Conditions

Rooseboom and Van Vuuren (2013) recommend using Eq. 2.1 and Eq. 2.2 to calculate the discharge for square/rectangular culverts:

For: $0 < H_1/D < 1.2$

$$Q = \frac{2}{3} C_b w_{culvert} H_1 \sqrt{\frac{2}{3} g H_1} \quad \text{Eq. 2.1}$$

For: $H_1/D > 1.2$

$$Q = C_h w_{culvert} D \sqrt{2g(H_1 - C_h D)} \quad \text{Eq. 2.2}$$

where:

Q is the discharge through the culvert (m^3/s);

C_b is the coefficient expressing the effect of width contraction in the flow (dimensionless). $C_b = 0.9$ for square inlets and $C_b = 1.0$ for rounded inlets where $r > 0.1 w_{culvert}$;

r is the radius of the rounding at the inlet (m);

C_h is the coefficient of contraction in the vertical plane (dimensionless). $C_h = 0.6$ for square inlets and $C_h = 0.8$ for rounded inlets;

$w_{culvert}$ is the width of the culvert opening (m);

D is the height of the culvert opening (m);

H_1 is the upstream energy level of the culvert (m); and

g is the gravitational acceleration constant taken as 9.81 m/s^2 .

2.2.2. Downstream (Outlet) Control

Outlet control conditions occur when tailwater (water levels downstream of the LLRC) influences upstream conditions at the LLRC. Even though a culvert might initially be found to operate only under inlet conditions at first, a downstream (of the LLRC) obstruction might

cause a flow regime change leading to backwater effects that could partially- or fully submerge the outlet of the LLRC and thereby change the operation to outlet control.

The design of outlet controlled low-level river crossings is based on the two fundamental laws: conservation of mass and conservation of energy. These are briefly discussed below.

Conservation of mass:

Although reference is made to mass, conservation of mass refers to the conservation of flow seeing that the mass of a fluid can be computed by multiplying the fluid volume with the fluid density. Assuming the fluid is homogeneous and incompressible (i.e. density remains the same), the conservation of mass, and therefore volume, is obtained between two points for a control volume as shown in Figure 2.2.

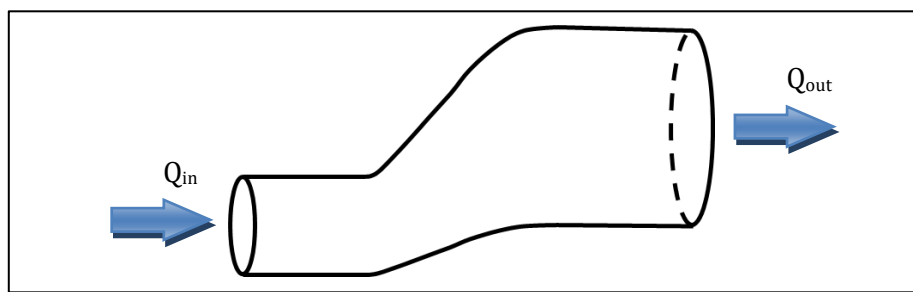


Figure 2.2: Conservation of mass

$$Vol_{in} \times \rho = Vol_{out} \times \rho \quad \text{Eq. 2.3}$$

Assuming a constant density (ρ), Eq. 2.3 becomes:

$$Vol_{in} = Vol_{out} \quad \text{Eq. 2.4}$$

Assuming flow rate (Q) (m^3/s) as a time increment for a volumetric change ($\frac{\Delta Vol}{\Delta t}$), Eq. 2.4 becomes:

$$Q_{in} = Q_{out} \quad \text{Eq. 2.5}$$

Conservation of energy:

Conservation of energy, also known as Bernoulli's equation, is based on the summation of the potential energy (flow depth and elevation change between two control sections) and kinetic energy (flow velocity converted to energy head) components of a system.

Figure 2.3 illustrates the upstream and downstream components for applying conservation of energy to outlet control.

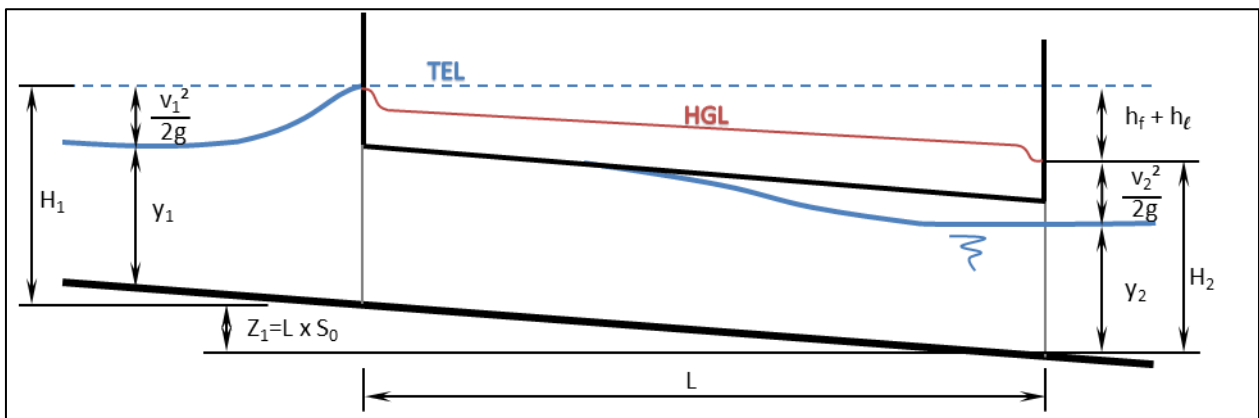


Figure 2.3: Flow Through a Culvert Under Outlet Control Conditions

Rooseboom and Van Vuuren (2013) provided the following relationship for the conservation of energy:

$$y_1 + \frac{\bar{v}_1^2}{2g} + Z_1 = y_2 + \frac{\bar{v}_2^2}{2g} + Z_2 + h_{f_{1-2}} + \sum h_{l_{1-2}} \quad \text{Eq. 2.6}$$

where:

HGL is the Hydraulic Grade Line measured relative to the invert (m);

TEL is the Total Energy Line measured from a specific datum (m);

y₁ and *y₂* are the respective upstream and downstream water depths (m);

Z₁ and *Z₂* are the respective upstream and downstream invert levels (m) which can be simplified (assuming *Z₂* as the datum and setting it equal to zero) to *Z₁=LS₀* (culvert length and bed slope);

v̄₁ and *v̄₂* are the respective upstream and downstream average flow velocities (m/s);

h_{f₁₋₂} is the friction loss between cross-section 1 (upstream) and 2 (downstream) (m); and

$\sum h_{l_{1-2}}$ is the sum of all the secondary transition losses between cross-section 1 and 2 (m).

H₁ and *H₂* are the upstream and downstream energy levels (in metres) measured relative to the inlet and outlet invert levels. For outlet control to apply, at least part of the culvert should be full flowing. However, to simplify design calculation, the entire length of the culvert is normally assumed to be full flowing.

The energy equation (Eq. 2.6) for outlet control can therefore be rewritten as follows:

$$H_1 - H_2 = h_{f_{1-2}} + \sum h_{l_{1-2}} - z_1 \quad \text{Eq. 2.7}$$

2.2.3. Downstream Riprap

Riprap can be used for protection of erodible river banks, road embankments from overtopping flow and pier foundations. Protection from road overtopping flow can be attained with the placement of a riprap layer on the downstream face of a road embankment (CSRA, 1994:2-4).

The CSRA¹ (1994) defines riprap as a term given to loose rock armour that has the following protection advantages:

- Ease of construction even when placed under water with proper control;
- Flexibility of placement, use and operation;
- Increase hydraulic roughness which assists with the attenuation of currents and waves; and
- High degree of durability with low maintenance and ease of repair.

The design of riprap is based on multiple factors such as channel velocity, flow depth and embankment slope and can be determined as follows (Jansen van Vuuren *et al*, 2013):

Protection of revetments:

$$D_{50} = \frac{K_u C v^3}{y_{avg}^{0.5} K_1^{1.5}} \quad \text{Eq. 2.8}$$

Coefficient for specific gravity and stability:

$$C = \frac{1.61(S_F)^{1.5}}{(S_S - 1)^{1.5}} \quad \text{Eq. 2.9}$$

Dimensionless factor K_1 :

$$K_1 = \left[1 - \frac{(\sin\theta)^2}{(\sin\varphi)^2} \right]^{0.5} \quad \text{Eq. 2.10}$$

where:

D_{50} is the nominal 50% angular shaped stone size (m);

¹ Committee of State Road Authorities

y_{avg} is the average flow depth (m);

K_u is 0.0059 (SI unit conversion);

C is the coefficient for specific gravity and stability (dimensionless);

v is the average flow velocity (m/s);

K_1 is a dimensionless factor as per Eq. 2.10;

θ is the bank angle with the horizontal taken as 45° ($^\circ$);

φ is the riprap angle of repose taken as $\pm 42^\circ$ for highly angular riprap with a particle size exceeding 400 mm ($^\circ$);

S_F is the recommended safety factor (taken as 2 for rapidly varied flow with high turbulence) (dimensionless); and

S_s is the specific gravity of riprap (taken as 2.5 kg/l) (kg/l).

The Public Safety Section (2000:7) notes that riprap rocks should be blocky and angular, with sharp clean edges and individual rocks should be as close to eqi-dimensional as possible (recommended average ratio of the long axis to the thickness should be less than 2). However, should rounded rocks be used, oversizing of approximately 40% is recommended to provide equivalent protection compared to angular riprap (CSRA, 1994:2-4).

CSRA (1994:2-4) mentions that there is no definite grading for riprap stones but recommends using the grading as shown in Figure 2.4.

The Public Safety Section (2000:8) recommends a riprap layer thickness thick enough to include all the rocks in the specified grading and that oversize rocks protruding from the layer be avoided as this may cause turbulence and lead to failure. The following criteria is proposed:

- Layer thickness exceeding 350 mm;
- Layer thickness exceeding $1.5 \times D_{50}$; and
- Layer thickness exceeding D_{100} .

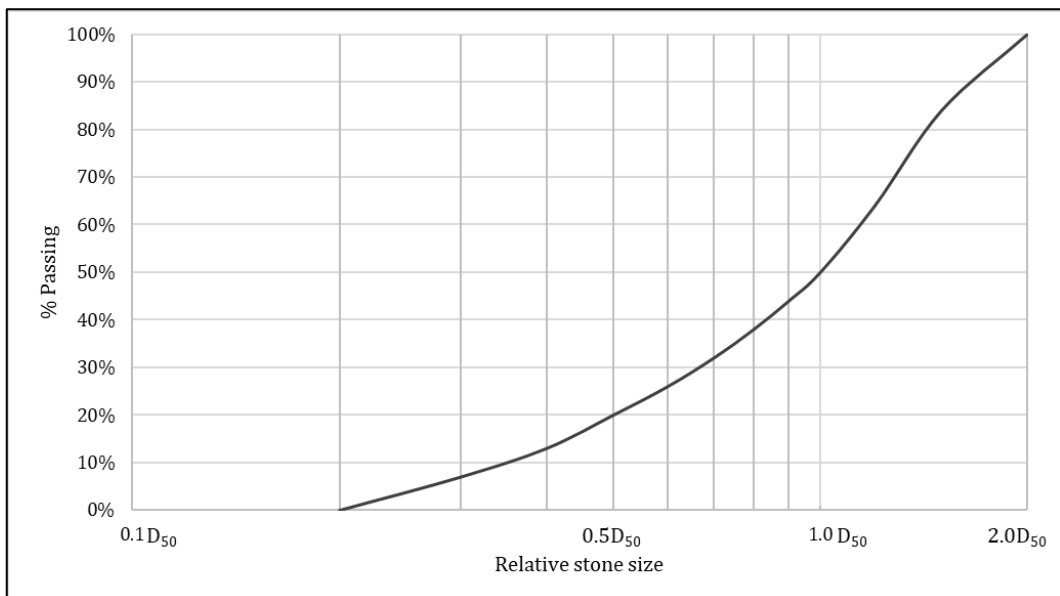


Figure 2.4: Recommended Grading for Riprap (adapted from CSRA, 1994:2-4)

2.3. HYDRAULIC JUMP

A hydraulic jump is an example of a stationary surge wave that occurs when supercritical flow ($F_r > 1$) meets subcritical flow ($F_r < 1$). A large energy loss is associated with the rapid flow transition (Chadwick *et al.* 2004:150).

The Froude number can be calculated as follows (Chadwick *et al.* 2004:164):

$$F_r^2 = \frac{Q^2 T_w}{g A^3} \quad \text{Eq. 2.11}$$

where:

F_r is the Froude number (dimensionless);

Q is the flow rate (m^3/s);

T_w is the width of the top water surface (m); and

A is the cross-sectional flow area (m^2).

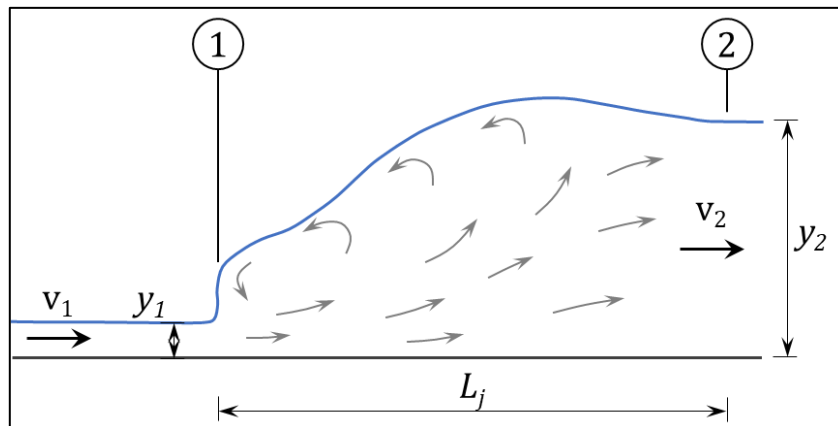


Figure 2.5: Hydraulic Jump on Horizontal Surface

The upstream (section 1 in Figure 2.5) and downstream depth (section 2) of a hydraulic jump is normally referred to as the *sequent depth* and *conjugate depth* respectively.

The conjugate flow depth (y_2) can be determined if the sequent depth (y_1) and Froude number (Fr_1) are known using Eq. 2.12, provided the channel is rectangular and has a horizontal floor (USBR 1987:590):

$$y_2 = \frac{y_1}{2} \left(\sqrt{8Fr_1^2 + 1} - 1 \right) \quad \text{Eq. 2.12}$$

2.3.1. Hydraulic Jump Length (L_j)

Chadwick *et al.* (2013) asserted that the length of a hydraulic jump is of practical importance when designing hydraulic structures or analysing situations in which the jump may occur.

Chaudhry (2008:216) listed the following three equations that can be used to calculate the length of the roller and hydraulic jump for a rectangular channel:

$$L_r = y_1 \left[160 \tanh \left(\frac{Fr_1}{20} \right) - 1.2 \right] \quad (\text{for } \frac{y_1}{B} < 0.1) \dots \quad (\text{Hager, 1991a}) \quad \text{Eq. 2.13}$$

$$L_j = 220y_1 \tanh \left(\frac{Fr_1 - 1}{22} \right) \dots \quad (\text{Hager, 1991a}) \quad \text{Eq. 2.14}$$

$$L_j = 6y_2 \quad (\text{for } 4 < Fr_1 < 12) \quad \text{Eq. 2.15}$$

where:

Fr_1 is the Froude number for the sequent depth (dimensionless), calculated with

Eq. 2.11;

B is channel width (m);

L_r is the length of the hydraulic jump roller (m);

L_j is the length of the hydraulic jump (m); and

y_2 is the conjugate depth (m).

Chaudhry (2008:216) mentions that the length of the roller may be taken to the point where the flow velocity at the top reverses and the jet continues.

The US Bureau of Reclamation (1987:591) proposed the use of Figure 2.6 for the determination of the jump length which requires the conjugate depth (y_2) and the sequent depth Froude number (Fr_1). It can be seen from Figure 2.6 that a steady hydraulic jump with the most energy dissipation occurs for an upstream Froude number between $4.5 \leq Fr_1 \leq 9$.

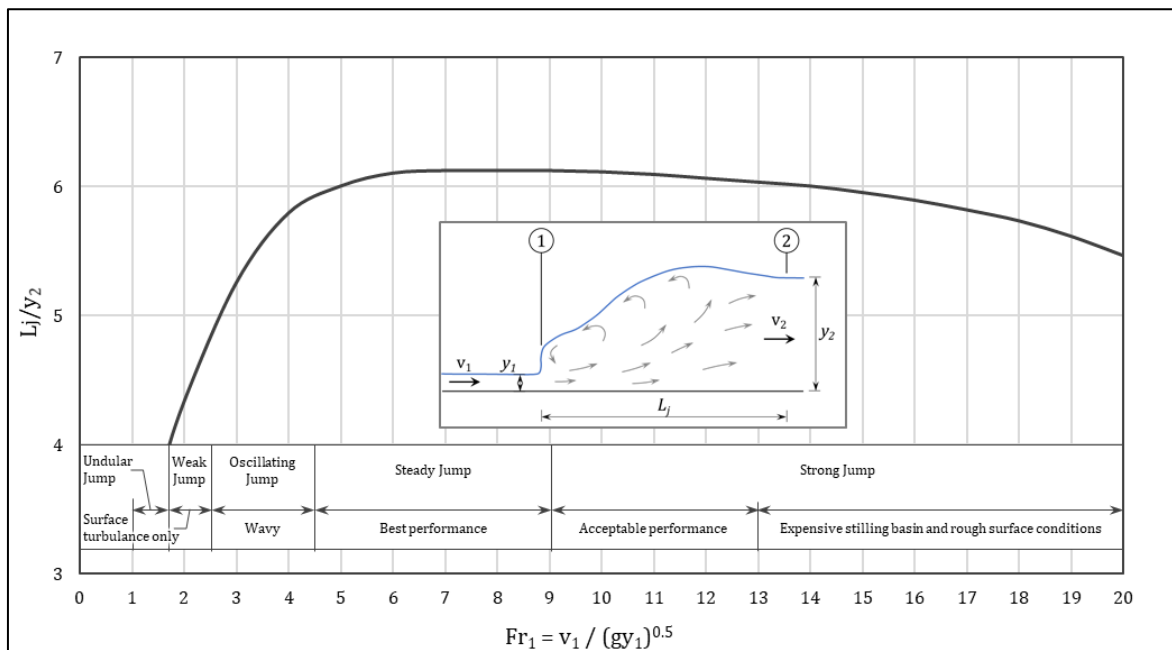


Figure 2.6: Hydraulic Jump Length in terms of conjugate depth in horizontal channels (adapted from USBR, 1987)

Thompson and Kilgore (2006) proposed the use of Figure 2.7 for the determination of the jump length which requires the sequent depth (y_1) and Froude number (Fr_1).

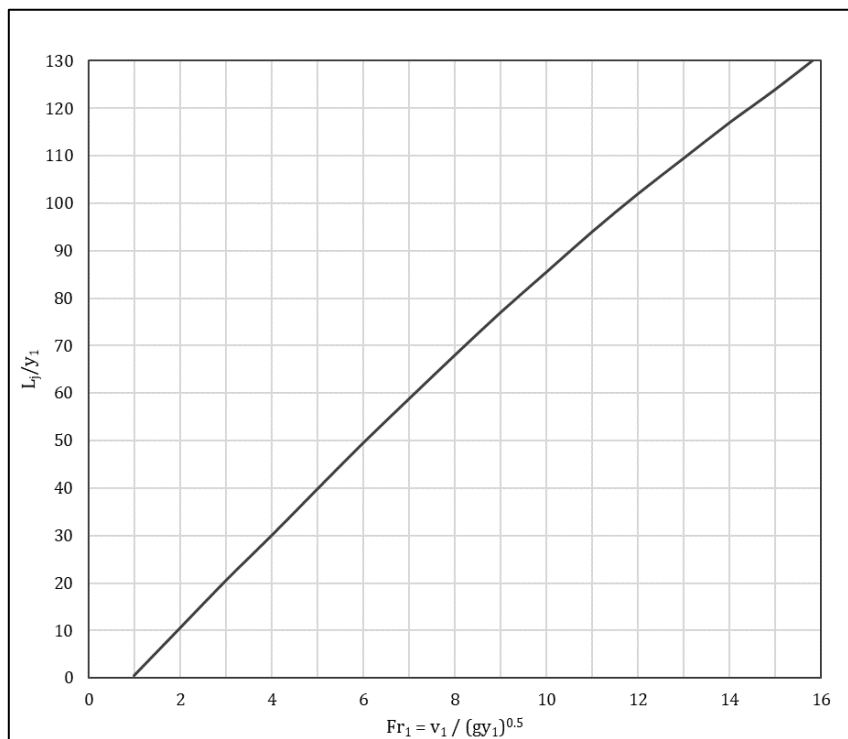


Figure 2.7: Hydraulic Jump Length in terms of sequent depth in horizontal channels (adapted from Thompson and Kilgore, 2006)

2.3.2. Energy Loss from a Hydraulic Jump

Chadwick *et al.* (2004) stated that hydraulic jumps can only form if the upstream flow is supercritical. Energy loss from a hydraulic jump occurs due to high levels of turbulence caused

from the sudden transition in flow conditions. Chadwick *et al.* (2004) concluded that a higher upstream Froude number (Fr_1) would cause a greater jump height resulting in a higher rate of energy dissipation.

The energy loss from a hydraulic jump can be calculated using Eq. 2.16 (Chadwick *et al.* 2004:154):

$$\Delta E = \frac{(y_2 - y_1)^3}{4y_1 y_2} \quad \text{Eq. 2.16}$$

where:

y_1 is the sequent depth (m);

y_2 is the conjugate depth (m); and

ΔE is the energy dissipated from the hydraulic jump (m);

2.3.3. Hydraulic Jump Types

Hydraulic jumps occur in four distinct forms, depending on the sequent Froude number (Fr_1), with their own unique flow pattern, formation of rollers and eddies (Chaudhry 2008:216). Figure 2.8 (a) to (d) explain the four different hydraulic jump types and give the corresponding sequent Froude number.

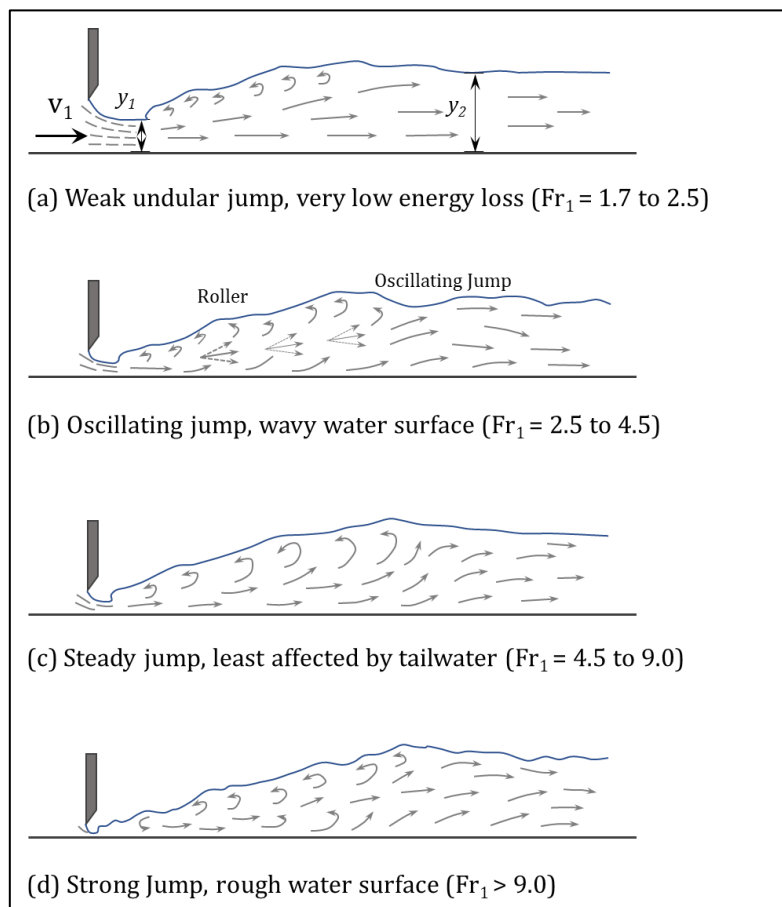


Figure 2.8: Hydraulic Jump Types

2.4. STEPPED CHUTE SPILLWAYS

An increased interest has been shown in stepped spillways around the world due to the technical advantages in the construction of Roller Compacted Concrete (RCC) dams and the considerable amount of energy dissipation that leads to reduced stilling basin sizes (Khatsuria 2005:95).

Flow down stepped chutes can generally be divided into three distinct flow regimes. Flow can either be nappe flow, skimming flow or transition flow. These different flow types are discussed in Sections 2.4.1 to 2.4.3.

2.4.1. Nappe Flow

Nappe flow is described as flow free falling as a jet from a step, which then impinges on the next step. The flow directly after the nappe impingement is supercritical and, if the step is long enough, can lead to either a fully developed- or partially developed hydraulic jump (sub-regimes NA1 and NA2 respectively). Figure 2.9 illustrates the nappe flow sub-regimes NA1 and NA2. Nappe flow regimes NA 1 and NA 2 are discussed in more detail in Section 2.4.1.1. This is particularly true for small discharges or relatively flat spillways. However, for larger discharges, the nappe may hit the step, without the hydraulic jump even forming, and then fall onto the next step (sub-regime NA3). Sub-regime NA3 also occurs when the step is sloped downward in the direction of the flow and is discussed in more detail in Section 2.4.1.2.

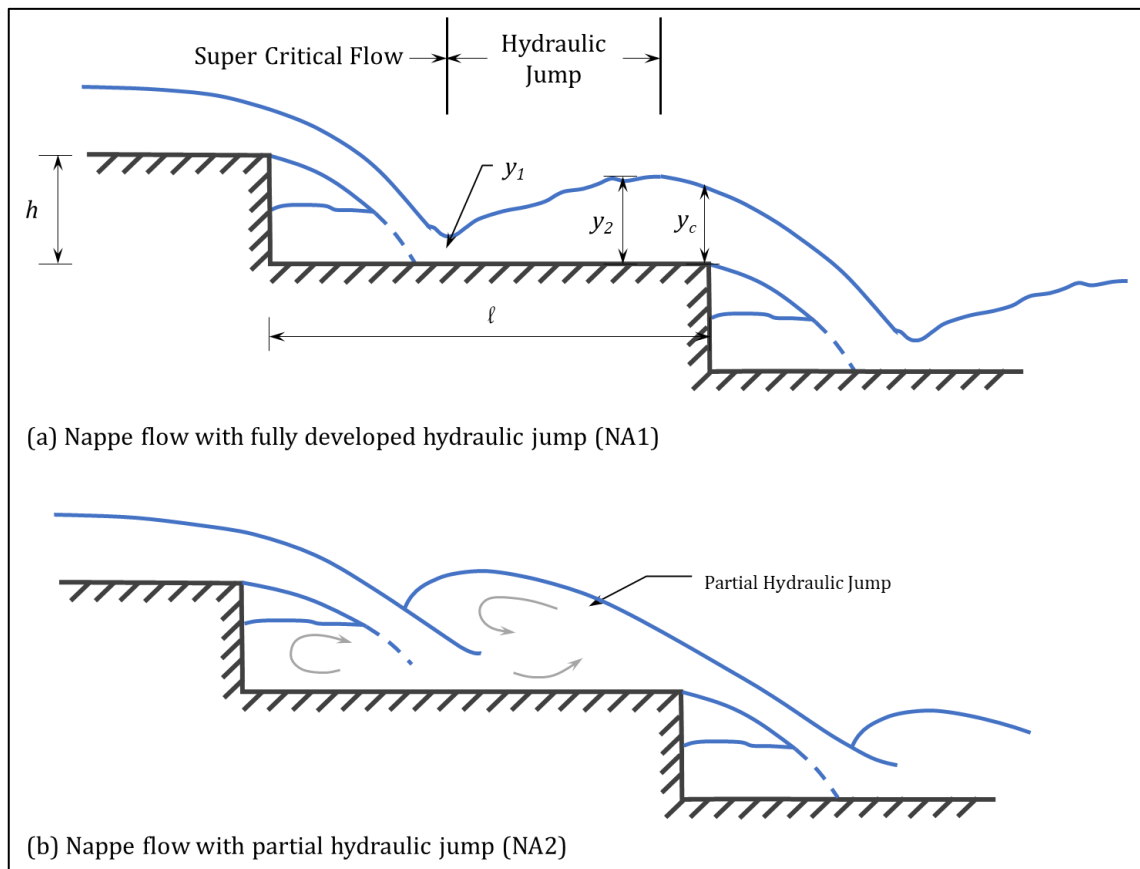


Figure 2.9: Nappe Flow with a Fully- and Partially Developed Hydraulic Jump

2.4.1.1. Nappe Flow with Hydraulic Jump (sub-regimes NA1 and NA2)

Nappe flow with hydraulic jump can be identified with the occurrence of critical flow conditions at each step edge. For horizontal steps, the flow may be analysed as a succession of drop structures with the flow conditions near the end of the step changing from subcritical to critical near the brink ($3 \times y_c$, where y_c is the critical depth) of the step (Chanson 2001:99). Figure 2.10 indicates the step height (h) and corresponding nappe geometry given the critical depth (y_c) before overflow.

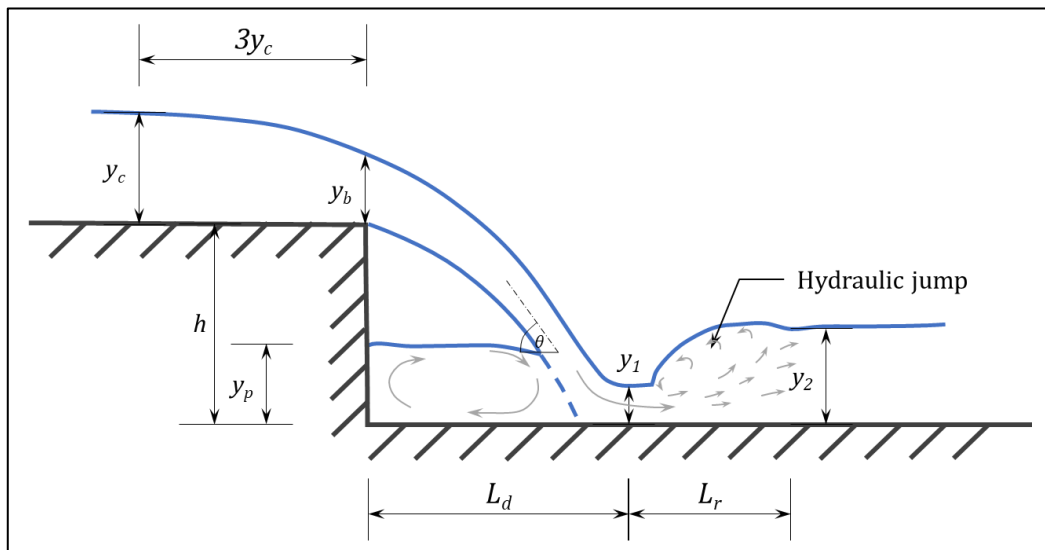


Figure 2.10: Nappe Geometry of Flow at a Drop Structure

Chanson (1994:71, 2001:100) proposed the following formulae to determine the nappe geometry for horizontal steps where the nappe is ventilated:

$$y_b = 0.715y_c \quad \text{Eq. 2.17}$$

$$y_1 = 0.54h \left(\frac{y_c}{h}\right)^{1.275} \quad \text{Eq. 2.18}$$

$$y_2 = 1.66h \left(\frac{y_c}{h}\right)^{0.81} \quad \text{Eq. 2.19}$$

$$y_p = h \left(\frac{y_c}{h}\right)^{0.66} \quad \text{Eq. 2.20}$$

$$L_d = 4.3h \left(\frac{y_c}{h}\right)^{0.81} \quad \text{Eq. 2.21}$$

where:

y_c is the critical flow depth (m);

y_1 is the flow depth at section 1 (m);

y_2 is the flow depth at section 2 (m);

y_p is the pool depth beneath the nappe (m);

y_b is the overflow depth at the brink of the step (m);

h is the step height (m); and

L_d is the horizontal length of the drop measured from the face of the drop (m).

Chanson (1994:71) recommended the use of Eq. 2.22, originally published by Hager *et al.* (1990), to determine the roller length of a fully developed hydraulic jump downstream of the nappe impact.

$$L_r = 8y_1(Fr_1 - 1.5) \quad \text{Eq. 2.22}$$

where:

L_r is the length of the hydraulic jump roller (m);

Fr_1 is the Froude number at section 1, defined as: $Fr_1 = \frac{q_w}{\sqrt{gy^3}}$ (dimensionless); and

y_1 is the flow depth at section 1 (m).

Peyras *et al.* (1991, 1992) indicated that equations Eq. 2.18 to Eq. 2.22 can be applied, with reasonable accuracy, to nappe flows with partially developed hydraulic jumps.

Chanson (1994: 72) asserted that, should the horizontal length of the drop (L_d) plus the length of the roller (L_r) be smaller than the length of the step (ℓ), a fully developed hydraulic jump may occur.

A comparison of the hydraulic jump length relationships from Eq. 2.13 to Eq. 2.15 and Figure 2.6 and Figure 2.7, and the relationship Chanson (1994) recommended be used, given a unit discharge of 1 m³/s/m, for Froude numbers ranging from 1.5 to 16 is illustrated in Figure 2.11.

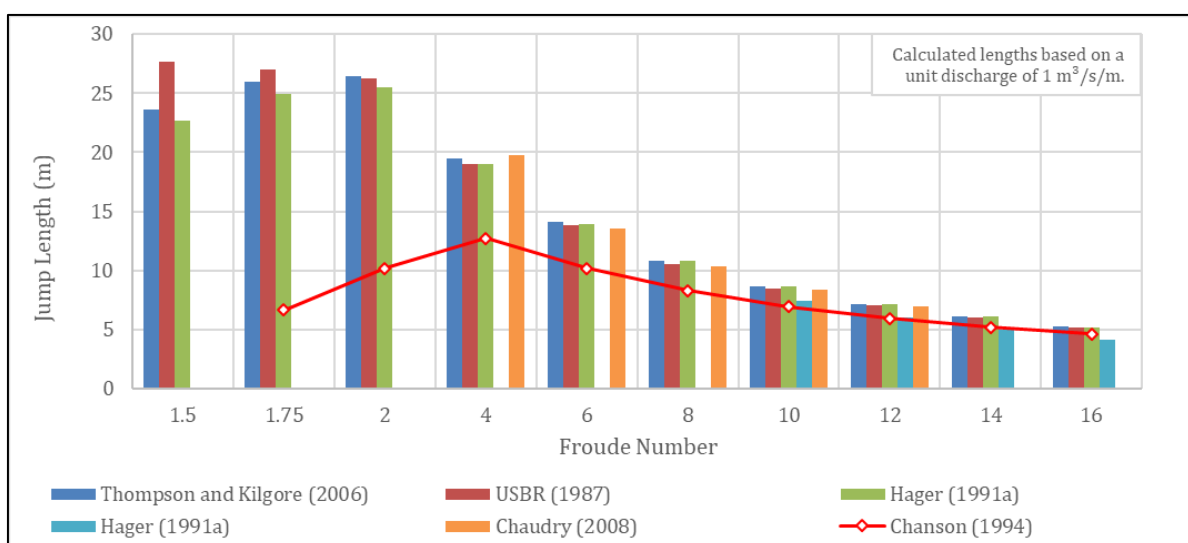


Figure 2.11: Comparison of Hydraulic Length Relationships

It is illustrated in Figure 2.12 that the relationship for a hydraulic jump length that Chanson (1994) recommended (red line) for stepped chute spillways correlates well with the relationships given in Eq. 2.13 to Eq. 2.15 and Figure 2.6 and Figure 2.7 for Froude numbers exceeding 4. The correlation also improved as the Froude number increased.

2.4.1.2. Nappe Flow without Hydraulic Jump (sub-regime NA3)

With nappe flow without hydraulic jump (sub-regime NA3), the flow is supercritical at any point and critical flow conditions are not observed at the step brink. According to Chanson (2001:104-105), the flow properties cannot be predicted analytically, and the best source of information would be from experimental investigations. Figure 2.12 illustrates the flow down a stepped chute without a hydraulic jump forming. The flow on the step at any point remains supercritical.

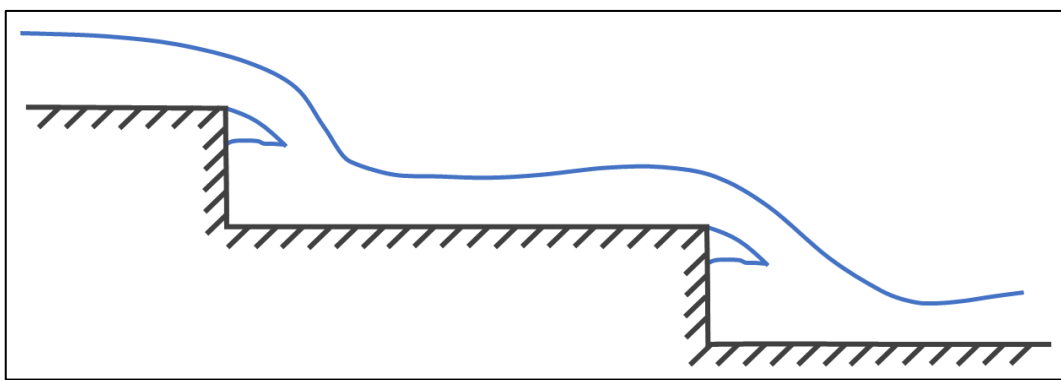


Figure 2.12: Nappe Flow with No Developed Hydraulic Jump (NA3) Down a Stepped Chute

2.4.1.3. Ventilation of the Nappe

Ventilation of uncontracted nappes may be required as the falling nappe draws air from the cavity between the nappe and the pool behind the nappe. Air is then transported downstream leading to sub-atmospheric pressure in the cavity behind the nappe (Chanson 2001). Chanson (2001) continued stating that thin nappes discharging from long free-flow spillways could be subject to nappe oscillations. Nappe oscillations are characterised by fluttering instabilities (also called "Kelvin-Helmholtz" instabilities). Air movement below the nappe could be strong enough to be heard for substantial distances. This poses little danger to a structure provided that the fluttering frequency of the water sheet does not match the natural frequency of the structure.

Chanson (2001) recommended using the following equation to determine the nappe aeration for Froude numbers between 3 to 10:

$$Q_{air} = 0.19 Q_w \left(\frac{h - y_p}{y_b} \right)^{0.95} \quad \text{Eq. 2.23}$$

where:

Q_{air} is the nappe aeration (m^3/s);

Q_w is the discharge of the nappe (m^3/s);

y_p is the pool depth beneath the nappe (m);

y_b is the overflow depth at the brink of the step (m); and

h is the step height (m).

Bos (1989) also formulated a relationship for the maximum air demand required for full aeration of a nappe:

$$Q_{air} = 0.1 \frac{Q_w}{\left(\frac{y_p}{y_{top}}\right)^{1.5}} \quad \text{Eq. 2.24}$$

where:

Q_{air} is the nappe aeration (m^3/s);

Q_w is the discharge of the nappe (m^3/s);

y_p is the pool depth beneath the nappe (m); and

y_{top} is the flow depth on the top step (m).

Eq. 2.24 had no limit on the approach flow Froude number.

2.4.2. Transition Flow

Chanson and Toombes (2004:52) demonstrated the existence of a transitory flow regime for intermediate flow rates between nappe and skimming flows. They found the transition regime flow to be chaotic with intense splashing and strong free-standing aeration. The distinctive succession of free-falling jets observed with nappe flow was not present, neither was the quasi-smooth free-surface appearance of skimming flows. Figure 2.13 illustrates transition flow on a stepped chute spillway.

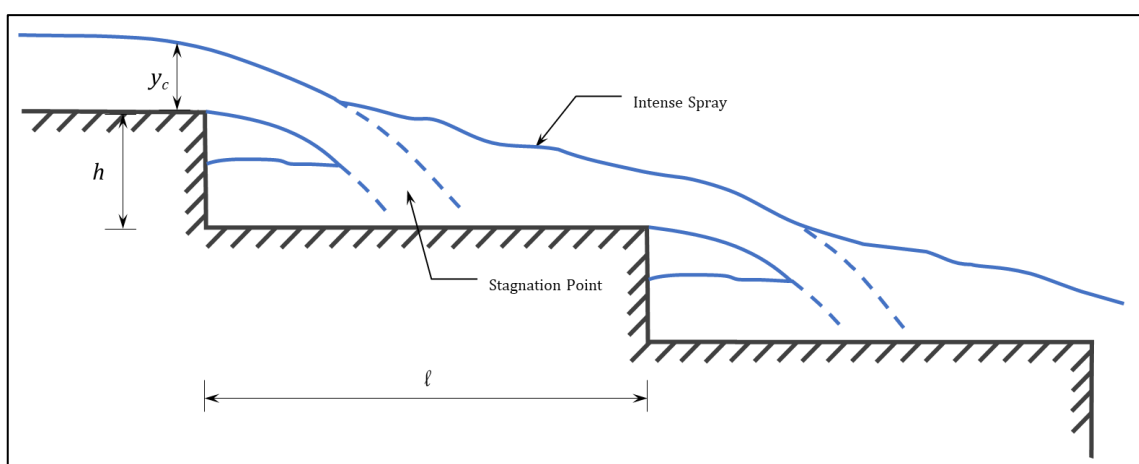


Figure 2.13: Transition Flow Down a Stepped Chute

Other researchers² who studied the boundaries of transition flow determined relationships demarcating the boundaries between the different flow regimes on stepped spillways. These boundaries are shown in Figure 2.14 and require two dimensionless inputs. The first input consists of the step height (h) divided by the step length (l). The second input is the critical flow depth (y_c) from the previous step divided by the step height (h). The zone where the intersect is found, indicates the expected flow regime.

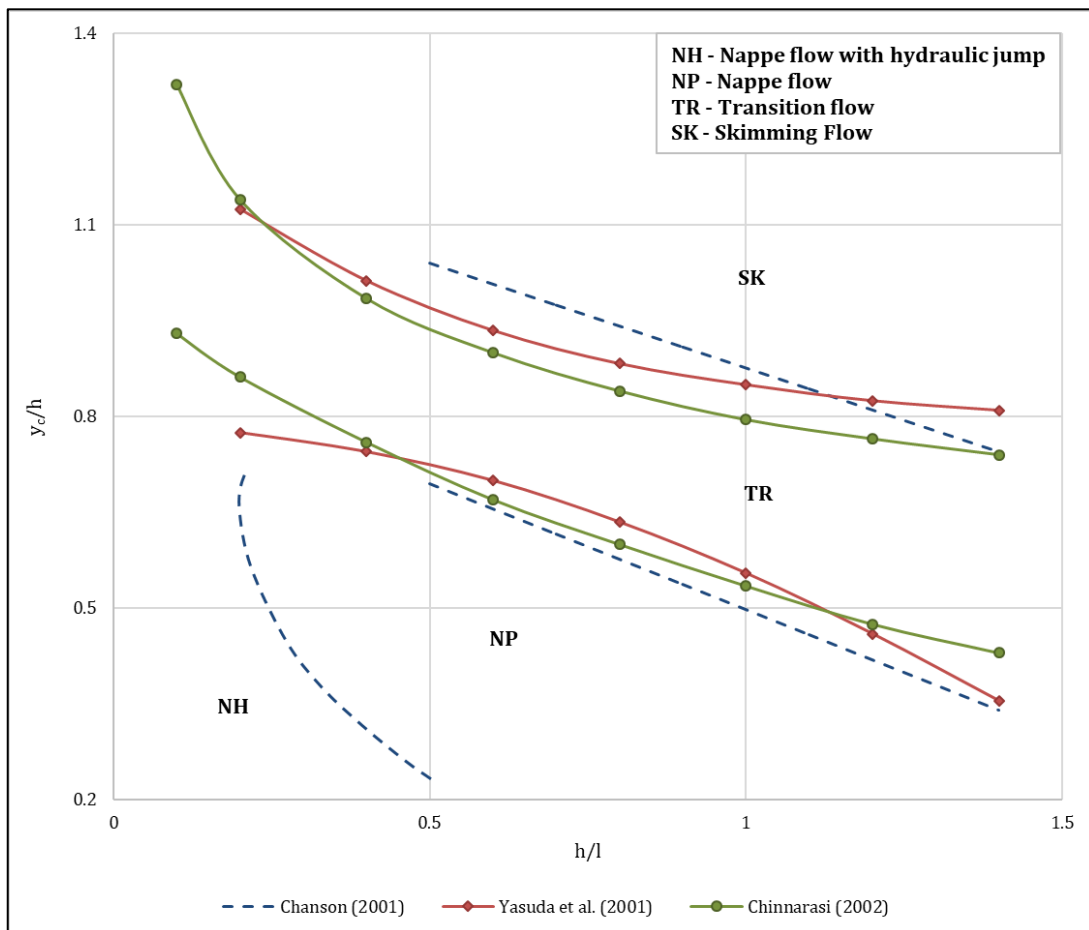


Figure 2.14: Flow Regimes on Stepped Spillways (adapted from Khatsuria:2005)

2.4.3. Skimming Flow

According to Khatsuria (2005), two distinct flow zones are present for skimming flow (illustrated in Figure 2.15), namely:

- an upper region over the external edges of the steps, forming a pseudo bottom; and
- a lower area, beneath the pseudo-bottom, formed by a triangular cell. Water remains caught, except water is exchanged with the upper flow due to turbulent flow conditions.

² Chanson (2001), Yasuda *et al.* (2001) & Chinnarasi (2002).

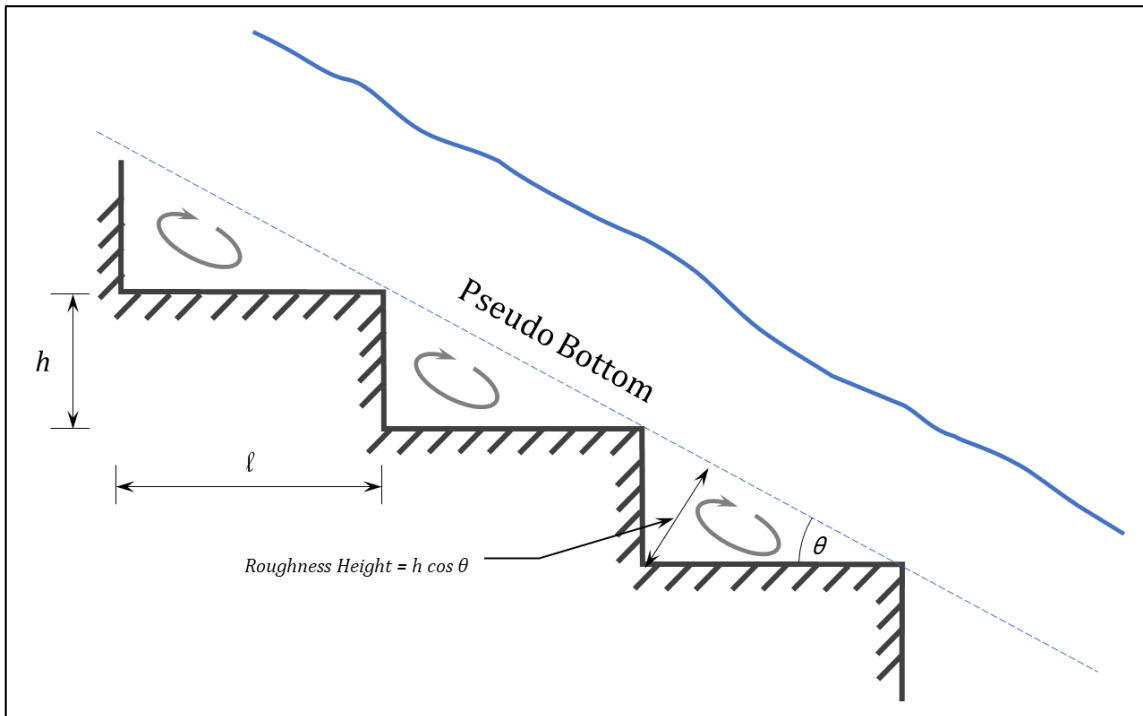


Figure 2.15: Skimming Flow with a Pseudo Bottom Down a Stepped Chute

Chanson (1994:219) found that for small discharges and flat slopes, the water flows as a succession of waterfalls (i.e. nappe flow regime) and that an increase of discharge and/or slope might induce the apparition of skimming flow regime. After reanalysing experimental data from previous researchers³, Chanson (1994:219) developed a relationship for determining the critical depth at which skimming flow would occur for step height to step length (h/ℓ) ratios ranging from 0.2 to 1.3:

$$y_{c,\text{onset}} = \left(1.057 - 0.465 \frac{h}{\ell} \right) h \quad \text{Eq. 2.25}$$

where:

$y_{c,\text{onset}}$ is the characteristic critical depth where skimming flow would occur (m);

ℓ is the step length (m); and

h is the step height (m).

2.4.3.1. Flow Regions in Skimming Flow

Stepped chutes with skimming flow conditions tend to have highly turbulent flow with free surface aeration conditions. Stepped chute spillways would normally have a boundary layer that starts at the crest of the ogee and grows progressively along the chute. The outer edge of

³ Essery and Horner (1978), Degoutte *et al.* (1992) & Beitz and Lawless (1992).

the boundary layer will eventually meet the free surface and initiate free surface aeration due to turbulence. The location at the start of air entrainment is also called the point of inception.

The layer downstream of the inception point contains an air-water mixture and extends far downstream until the flow becomes uniform. After flow has become uniform, air concentrations, flow depths and velocity distributions will remain constant along the chute. This region is known as the uniform equilibrium flow region. The flow regions on a skimming flow stepped chute are illustrated in Figure 2.16.

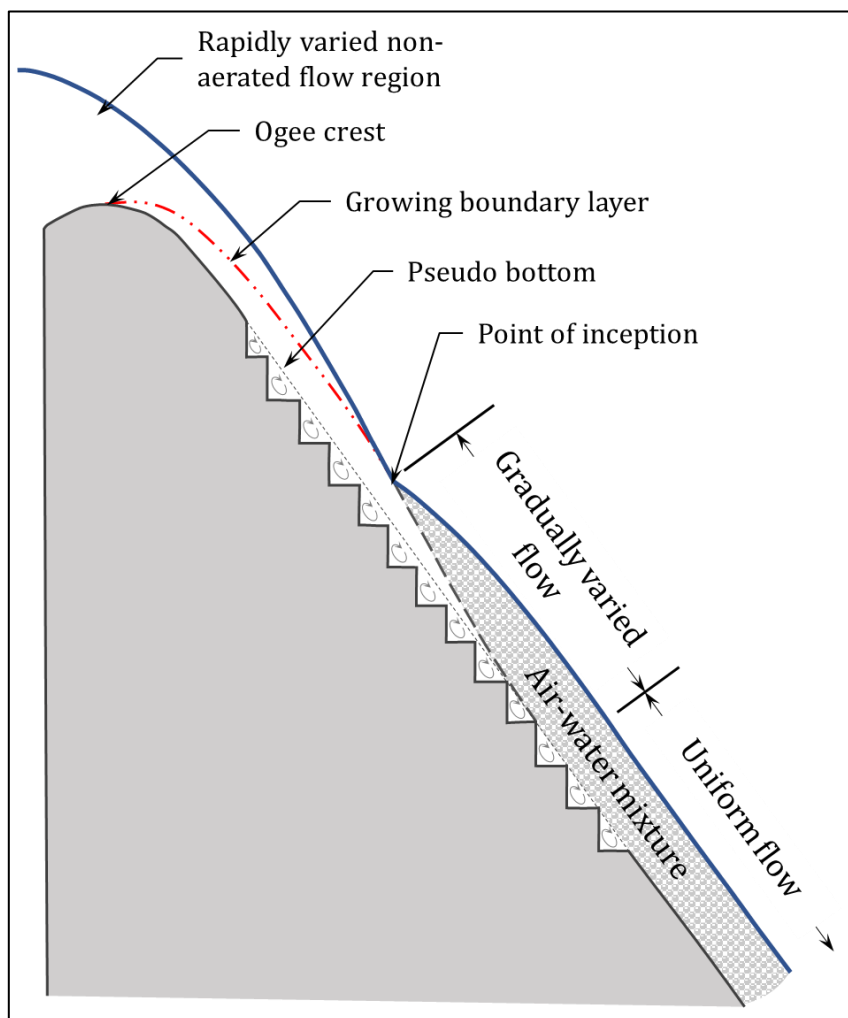


Figure 2.16: Flow Regions for Skimming Flow Stepped Chute Spillway

2.4.3.2. Air Entrainment

Air entrainment on stepped chute spillways may occur for both nappe and skimming flow regimes. The mechanism of occurrence, however, differs between nappe and skimming flow. Nappe flow air entrainment is caused by the turbulence at the impingement location whereas aeration for skimming flow starts when the boundary layer meets the free surface.

The process of aeration on stepped chutes closely resembles that of smooth, unstepped spillway chutes. The distance from the onset of the boundary layer to the inception point (onset of air entrainment) for stepped chute spillways is, however, shorter than that of smooth

spillway chutes due to the increase in surface roughness ($h \cos\theta$, as illustrated in Figure 2.15) caused by the steps.

The flow depth in the uniform flow region needs special consideration as the entrained air has a bulking effect on the flow volume. Boes and Minor (2002) proposed the relationship in Eq. 2.26 to be used for determining the uniform flow depth corresponding to a 90% air concentration:

$$y_{90,u} = 0.5h \left(\frac{q}{g \sin \theta_{chute} h^3} \right)^{0.1 \tan \theta + 0.5} \quad \text{Eq. 2.26}$$

where:

$y_{90,u}$ is the uniform flow depth corresponding to 90% air concentration (m);

h is the step height (m);

q is the unit discharge ($\text{m}^3/\text{s}/\text{m}$);

g is the gravitational acceleration constant taken as 9.81 m/s^2 ; and

θ_{chute} is the chute angle of inclination ($^\circ$).

Boes and Minor (2002) also provided Eq. 2.27 for the determination of the distance below the ogee crest level required for uniform flow to be reached:

$$H_{d,u} = 24y_c(\sin \theta)^{\frac{2}{3}} \quad \text{Eq. 2.27}$$

where:

$H_{d,u}$ is the vertical distance below the crest required for uniform flow to be reached (m); and

y_c is the critical flow depth (m).

Khatsuria (2005) recommended a safety factor of 1.2 to 1.5 be applied when determining the freeboard required for the training walls following the determination of the uniform flow depth ($y_{90,u}$).

2.4.3.3. Pressures Profiles on the Steps

In skimming flow, the triangular flow region below the pseudo-bottom, is highly turbulent. The pressure in this region is therefore expected to experience intense pressure fluctuations which could possibly lead to the inception of intermittent cavitation. As the region between the crest and the point of inception is not aerated, cavitation damage (if present) is most likely to occur in this region. Khatsuria (2005) believed that a velocity of 20 m/s (which could be attained with a unit discharge of $25 \text{ m}^3/\text{s}/\text{m}$) could cause cavitation in the region between the crest and

the inception point. The uniform flow region would be protected against cavitation as the air would have reached the bottom layer.

Sanchez *et al.* (2000) found that the upper half of the vertical face of the steps experienced negative pressures. The horizontal faces however, did not experience negative pressures.

2.4.4. Guidelines for the Design of Stepped Chute Spillways

Khatsuria (2005) recommended that transition flow regimes be avoided when designing stepped chute spillways. Avoiding flow conditions where y_c/h ratio is between approximately 0.8 and 1.2 should therefore be avoided when referring to Figure 2.14. Preventing transition flow regimes would, however, only be possible if outflow was controlled with spillway gates. Free, ungated spillway conditions would, however, cause flow to start as nappe flow for low discharges and would eventually pass through to the transition regime as the discharge increases, and ultimately reach skimming flow.

Khatsuria (2005) listed the following elements which need to be designed for a stepped chute spillway:

- the transition from the ogee crest to the stepped chute onset;
- determine the geometry of the steps, with particular attention being given to the step height;
- identifying the flow regime(s) applicable to the spillway;
- assessing the residual energy at the toe of the spillway;
- estimating the entrained air and concentration in proximity to the pseudo-bottom;
- determining the freeboard requirements for the training walls, taking into consideration the air concentration and uniform flow depth; and
- designing of the energy dissipation structure (stilling basin) at the toe of the spillway chute.

2.5. MODEL SCALING

Physical models are a viable option when it comes to solving complex hydraulic problems for which the characteristic of the physics and the boundaries of flow cannot be easily computed. A model can also be used to verify expected or numerically modelled prototype operation and performance. Whichever the case may be, hydraulic models should still behave accurately and sufficiently similar to that of the prototype (Bosman and Basson, 2012).

Chadwick *et al.* (2013:406) mentioned that scaled models are incapable of simultaneously replicating all the physical processes present in the prototype in correct proportions, which results in *scale effects*.

2.5.1. Hydraulic Similarity

2.5.1.1. Geometric Similarity

Geometric similarity refers to similarity of shape where the ratio of any two model dimensions remain the same as that of the same two dimensions for the prototype, provided that the model is undistorted. The relationship for geometric similarity is as expressed by Eq. 2.28 (Bosman and Basson, 2012):

$$\frac{(L_1)_{model}}{(L_2)_{model}} = \frac{(L_1)_{prototype}}{(L_2)_{prototype}} \quad \text{Eq. 2.28}$$

where:

$(L_n)_{model}$ is the linear dimension of the hydraulic model (m); and

$(L_n)_{prototype}$ is the linear dimension of the prototype (m).

2.5.1.2. Kinematic Similarity

Kinematic similarity refers to the motion of fluids which is obtained when equal ratios of velocities and accelerations remain the same at corresponding positions and time frames between the prototype and model. The relationship for kinematic similarity is as expressed by Eq. 2.29 (Bosman and Basson, 2012):

$$\frac{(v_1)_{model}}{(v_2)_{model}} = \frac{(v_1)_{prototype}}{(v_2)_{prototype}} \text{ and } \frac{(a_1)_{model}}{(a_2)_{model}} = \frac{(a_1)_{prototype}}{(a_2)_{prototype}} \quad \text{Eq. 2.29}$$

where:

$(v_n)_{model}$ is the velocity of fluid in the hydraulic model (m/s);

$(v_n)_{prototype}$ is the velocity of fluid in the prototype (m/s);

$(a_n)_{model}$ is the acceleration of fluid in the hydraulic model (m/s^2); and

$(a_n)_{prototype}$ is the acceleration of fluid in the prototype (m/s^2).

2.5.1.3. Dynamic Similarity

Dynamic similarity refers to the ratio of forces at the same relative positions between the model and the prototype and should act in the same direction. Eq. 2.30 expresses the relationship for dynamic similarity (Bosman and Basson, 2012):

$$\frac{(F_1)_{model}}{(F_2)_{model}} = \frac{(F_1)_{prototype}}{(F_2)_{prototype}} \quad \text{Eq. 2.30}$$

where:

$(F_n)_{model}$ is the force acting on the fluid in the model (kN); and

$(F_n)_{prototype}$ is the force acting on the fluid in the prototype (kN).

2.5.2. Laws of Hydraulic Similarity

Calitz (2016:45) emphasized that the main forces acting on a fluid in both the prototype and model and the associated hydraulic laws to determine the similarities between model and prototype are:

- Gravity: Froude's Law
- Fluid viscosity: Reynolds' Law
- Surface tension: Weber's Law
- Elasticity: Euler's Law

2.5.2.1. Froude's Law

In turbulent free surface flow, the main criteria for uniformity is that the Froude numbers of both the model and the prototype be the same as the gravity, while inertial forces are the dominant forces that influence the motion of the fluid. Although the effects of viscosity and surface tension are neglected, every effort should be made to minimise them by using large models and smooth boundaries. Dam spillways, weirs, open channels, harbours, water intake structures and energy dissipators are typical examples of hydraulic structures that adhere to Froude's law.

The effects of distorted friction in models are small in comparison to inertial effects with scale ratios of 1:30 to 1:60 and water surface profiles, pressure distributions and velocities closely resemble those of the prototype (USBR, 1948).

The Froude number is defined as follows (Bosman and Basson, 2012):

$$F_r = \frac{v}{\sqrt{gL}} \quad \text{Eq. 2.31}$$

where:

F_r is the Froude number (dimensionless);

v is the velocity (m/s);

g is the gravitational acceleration (taken as 9.81 m/s²); and

L is the characteristic linear dimension (m).

Assuming the scale factor (S) as a prototype linear dimension (L_p) divided by the same model linear dimension (L_m), the prototype fluid velocity can be determined from the model fluid velocity as follows (Bosman and Basson, 2012):

$$F_{rp} = F_{rm}$$

$$\frac{v_p}{\sqrt{gL_p}} = \frac{v_m}{\sqrt{gL_m}}$$

$$\frac{v_p}{L_p^{0.5}} = \frac{v_m}{L_m^{0.5}}$$

$$\frac{v_p}{v_m} = \frac{L_p^{0.5}}{L_m^{0.5}}$$

$$\frac{v_p}{v_m} = S^{0.5}$$

Eq. 2.32

2.5.2.2. Reynolds' Law

The dimensionless Reynolds number (Re) is defined as follows (Chadwick *et al.* 2004:70):

$$Re = \frac{vL}{\nu} \quad \text{Eq. 2.33}$$

where:

v is the fluid velocity (m/s);

L is the homologous section length (m); and

ν is the kinematic viscosity (taken as $1.13 \times 10^{-6} \text{ m}^2/\text{s}$).

The Reynolds law states that the corresponding velocities in the prototype and model must be related as per Eq. 2.34 below (Bosman and Basson, 2012):

$$\frac{v_p}{v_m} = \frac{v_p}{v_m} \frac{L_m}{L_p} = \frac{v_p}{v_m} \frac{1}{S} \quad \text{Eq. 2.34}$$

Viscous forces are generally a secondary influence on the fluid in the prototype due to the low viscosity of water but remains an important consideration due to their influence on boundary frictions and their role as the origin of turbulence in fluids (Bosman and Basson, 2012).

The Reynolds' law is applicable to steady flow through pressurised closed-conduits, or around deeply submerged bodies. The absence of a free surface also nullifies the effects of surface tension on a hydraulic model (USBR, 1948).

A model and prototype cannot be simultaneously satisfied by both Froude's and Reynolds' law. However, variations in the Reynolds number becomes less important should both the model and prototype have higher Reynolds numbers ($Re > 100 000$) (Bosman and Basson, 2012).

2.5.2.3. Weber's Law

Bosman and Basson (2012) state that Weber's law is of considerable importance when studying the influence of surface tension on fluids in models when very low weir heads, air entrainment, spray or splash is expected as the surface tension has a significant effect on the air-water boundary.

The Weber number can be calculated as follows (Chadwick *et al.*, 2004:89):

$$We = v \sqrt{\frac{\rho L}{\tau}} \quad \text{Eq. 2.35}$$

where:

v is the fluid velocity (m/s);

ρ is the fluid density (kg/m^3);

L is the homologous section length (m); and

τ is the surface tension of the fluid (N/m).

Weber's law states that the corresponding fluid velocities in the prototype and model can be related as per Eq. 2.36 below (Calitz, 2016:45):

$$\frac{v_p}{v_m} = \left(\frac{\tau_p \rho_m L_m}{\tau_m \rho_p L_p} \right)^{0.5} = \left(\frac{\tau_p \rho_m}{\tau_m \rho_p} \right)^{0.5} \frac{1}{S^{0.5}} \quad \text{Eq. 2.36}$$

Ensuring that the model is large enough, the effects of surface tension, and hence the need to comply with Weber's law, can be eliminated altogether (Bosman and Basson, 2012).

2.5.2.4. Euler's Law

Euler's equation describes the relationship between pressure (p) and velocity (v) (Bosman and Basson, 2012):

$$Eu = \frac{v}{v \sqrt{\frac{2\Delta p}{\rho}}} \quad \text{Eq. 2.37}$$

where:

v is the fluid velocity (m/s);

ρ is the fluid density (kg/litre); and

Δp is the fluid pressure drop (kN/m^2).

Euler's number is of particular significance when the inertial forces of the liquid are insignificant compared to the viscous forces (Calitz, 2016:47). Bosman and Basson (2012:12) noted that gravity and surface tension forces are absent from Euler's equation and that the applied pressure forces is therefore the controlling factor and consequently acts as an independent variable. Pressure force is, however, a dependant variable to most fluid phenomena as it is influential upon the motion of fluid.

Euler's law states that the corresponding fluid velocities in the prototype and model can be related as per Eq. 2.38 (Calitz, 2016:48):

$$\frac{v_p}{v_m} = \left(\frac{\Delta p_p \rho_m}{\Delta p_m \rho_p} \right)^{0.5} \quad \text{Eq. 2.38}$$

The scale factor (S), therefore, has no influence on the velocities as the pressure in the system is the only independent variable and the same fluid is used in both the model and prototype. This non-linear relationship is universally applicable when inertial forces are dominant, and gravity is insignificant (Calitz, 2016:48).

2.5.3. Summary of Hydraulic Model Scaling

In this model study, inertia and gravity were the dominant forces as free surface flow conditions were prevailed. No instances of pressurised flow in closed conduits were encountered. Froude's Law was, therefore, the selected criterion for the scaling of the hydraulic model. Bosman and Basson (2012:12) provided the relationships between model and prototype similarity (based of Froude's Law) in Table 2-1.

Table 2-1: Froude's Law Scale Ratios

Parameter	Unit (SI)	Model to Prototype Ratio
Distance	m	$L_m = \frac{L_p}{S}$
Area	m^2	$A_m = \frac{A_p}{S^2}$
Volume	m^3	$V_m = \frac{V_p}{S^3}$
Time	s	$t_m = \frac{t_p}{S^{1/2}}$
Velocity	m/s	$v_m = \frac{v_p}{S^{1/2}}$
Discharge	m^3/s	$Q_m = \frac{Q_p}{S^{5/2}}$
Unit Discharge	$\text{m}^3/\text{s/m}$	$q_m = \frac{q_p}{S^{3/2}}$

2.6. CONCLUSION OF LITERATURE REVIEW

The findings and conclusions from the literature review are summarised as follows:

- Low-level river crossings operate hydraulically similar to that of a culvert, with the exception of also allowing overtopping flow.
- Flow through culverts can be either upstream- or downstream controlled. The flow conditions downstream of the culvert (tailwater) normally dictates the operating condition.
- Erodible road embankments can be protected from road overtopping flow with the placement of a riprap layer/revetment on the downstream face of a road embankment.

- A steady hydraulic jump is an excellent method of dissipating excessive amounts of energy. The amount of energy lost from a hydraulic jump depends primarily on the height of the jump ($y_2 - y_1$) which is dictated by the sequent Froude number (Fr_1). Hydraulic jumps with sequent Froude numbers between 4.5 and 9.0 have the highest rates of energy dissipation.
- An increased interest in stepped chute spillways has been shown due to advances in roller compacted concrete dams. Stepped chute spillways have also been proven to have increased amounts of energy dissipation along the chute which lead to lower amounts of energy that need to be dissipated at the bottom, and hence reduced stilling basin sizes (Khatsuria 2005:95).
- Flow down stepped chutes can be classified as either nappe flow, transition flow or skimming flow.
- Nappe flow is characterised by the flow, free falling as a jet from a step, impinging on the next. The nappe impingement is followed with either a fully- or partially developed hydraulic jump, and in some cases, no jump at all.
- Uncontracted nappes tend to draw air from the cavity beneath the nappe and transport it downstream, leading to sub-atmospheric conditions in the cavity. Sub-atmospheric nappe cavities may cause nappe oscillations which do not pose an immediate danger unless the frequency thereof matches the natural frequency of the structure. Such cases may warrant the use of nappe ventilation installations.
- Transition flow on stepped chute is encountered as flow changes from the nappe flow regime to the skimming flow regime and is characterised by chaotic behaviour and intense splashing with strong free-standing aeration. Transition flow regimes should be avoided as far as possible by keeping the y_c/h ratio either below 0.8 or above 1.2.
- Skimming flow, normally associated with higher spillway discharges, is seen to have two distinctive flow zones. An upper region over the external edges of the steps forming a pseudo bottom and a lower area, beneath the pseudo-bottom, with an apparent triangular recirculating cell.
- For nappe flow, the regime can be maintained during the prototype design by keeping the y_c/h ratio below 0.8. Maintaining a high step height and increasing the overflow width (which in turn decreased the critical depth, y_c) will ensure nappe flow conditions.
- The Froude law was used to scale the hydraulic model from the prototype. The model would predominantly operate under free flow conditions, with gravitation and inertia being the main forces acting on the liquid.

CHAPTER 3: HYDRAULIC DESIGN OF THE PROTOTYPE AND MODEL

3.1. INTRODUCTION

A 1:15 scale hydraulic model of a low-level river crossing with a stepped chute was designed using symmetry and constructed in the Hydraulic Laboratory of Stellenbosch University.

The testing of the model consisted of four parts:

1. The model was tested with the culvert closed to eliminate the effects that the culvert outflow might have on the steps due to inundation - Figure 3.1 (a);
2. The culvert (one or more) was opened to observe the operation of the chute in combination with downstream normal flow conditions - Figure 3.1 (a);
3. A variation of the proposed model was tested by removing the chute wall and placing riprap directly downstream of the model, abutting to the chute steps. Again, the culvert was closed to achieve isolated flow on the chute only - Figure 3.1 (b);
4. Part three above was repeated with the culvert open (one or more) to observe operation of the chute and riprap in combination with downstream normal flow conditions - Figure 3.1 (b).

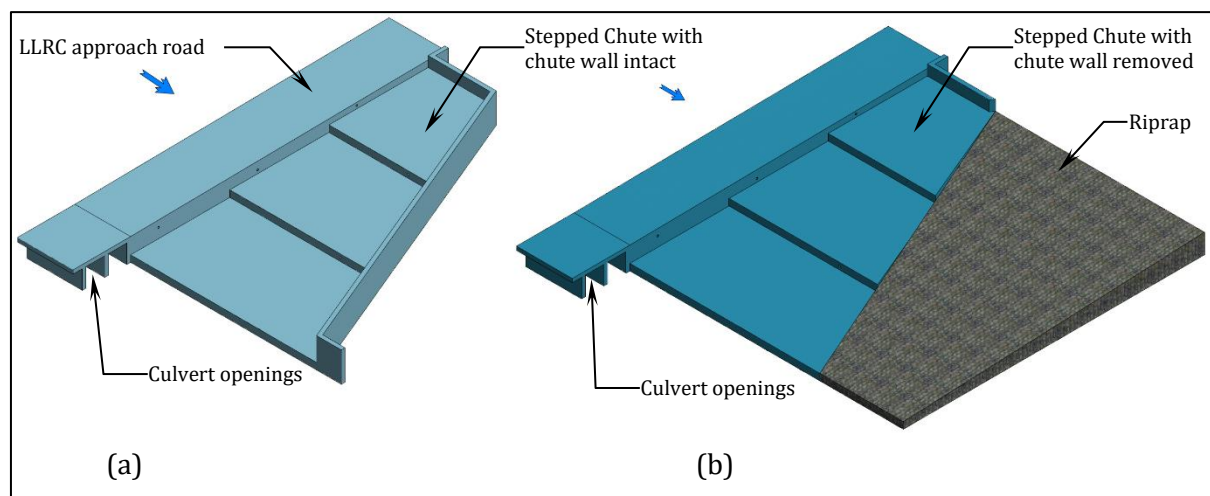


Figure 3.1: Model Setup Variations: (a) Model Setup 1: Chute Wall Intact; (b) Model Setup 2: Chute Wall Removed and Riprap Added

During all the tests, the pressures behind the nappes (from the road to the chute and from one chute step to another) were measured, flow profiles on the steps were recorded and attempts were made to record nappe ventilation inflows. This information was used to formulate recommendations on design guidelines and to identify areas for possible future research.

3.2. SCOPE OF THE HYDRAULIC MODEL TESTS

3.2.1. Model Scale

The model scale was selected based on widest available test channel at the Hydraulic Laboratory of the University of Stellenbosch. The 2 m wide test channel allowed for practically measurable flow depths and flow profile lengths, while reducing scale effects to as large an extent as possible.

The model scale was selected to be 1:15 with a prototype design flow of $23.5 \text{ m}^3/\text{s}$. The hydraulic model was bisected around the plane of symmetry (i.e. when looking from either downstream, upstream or in plan at the prototype, a vertical line drawn through the centre of the model would depict the plane of symmetry) to achieve as large as possible model which could fit into the 2 m wide test channel. This would minimise scale effects due to surface tension and viscosity, while maintaining hydraulic symmetry.

As concluded in Section 2.5.3, the model testing and operation was conducted in accordance with Froude's law of similitude. The ratio between inertial and gravitational forces as well as magnitude would be equal between the model and prototype, provided that geometric similarity was preserved, and flow was introduced into the model according to Froude's law (Calitz, 2016:52).

3.2.2. Laboratory Limitations

The design of the hydraulic model was governed by the widest available test channel (2 m wide test channel) at the Hydraulic Laboratory of the University of Stellenbosch. The design attempted to achieve the largest possible hydraulic model, which would improve the accuracy of flow depth and -profile measurements, and achieve the largest possible road overflow discharge, which would maximise the flow down the stepped chute.

3.2.3. Model Layout

The hydraulic model was built into the 2 m wide test channel at the Hydraulic Laboratory of the University of Stellenbosch. The longitudinal slope of the channel can be altered to suite the specific needs of a model. The longitudinal slope was set to 0% as the hydraulic model would act as a control, and upstream (subcritical flow) conditions would not have an effect on the model operation.

The channel was supplied with water (from a constant level stilling tank) via a DN100 steel pipe, as seen in Figure 3.2. A Flowmetrix Magflow DN100 electromagnetic flow meter was installed and used to measure flows exceeding 1.5 l/s (no flow was registered for flows smaller than 1.5 l/s). A DN100 gate valve (refer to Figure 3.3), placed approximately four diameters (400 mm) downstream of the flow meter, was used to control the flow rate to the model. A

DN100 flexible hose was connected to the end of the steel pipe and discharged into a V-notch weir channel placed inside the 2 m wide test channel.

The V-notch weir had an opening angle of 90° and was 200 mm deep. The V-notch weir was permanently fixed to the end of a rectangular steel channel that was 2 x 0.5 x 0.4 m (L x B x H) and had a maximum measuring capacity of 12 l/s. The V-notch weir was used to measure low flows (lower than 1.5 l/s), which the flow meter was unable to measure accurately. Water from the V-notch weir discharged directly into the 2 m wide test channel. A baffle wall was constructed inside the 2 m wide test channel, between the V-notch weir and the model to prevent severe wave action and to straighten the flow creating uniform flow.

Flows which exceeded the maximum capacity of the V-notch weir (i.e. H>200 mm), overtopped the rectangular steel channel but were still contained upstream of the 2 m wide test channel baffle wall. The model was placed 4 m (± 28 times the maximum flow depth of 140 mm) downstream of the baffle wall which enabled the flow to fully develop before reaching the model.

Two water level needles were used to measure the flow depth for the V-notch weir and the flow depth over the road deck section as this was one of the main design parameters of the prototype.

Figure 3.2 and Figure 3.3 illustrate the general model setup and layout.

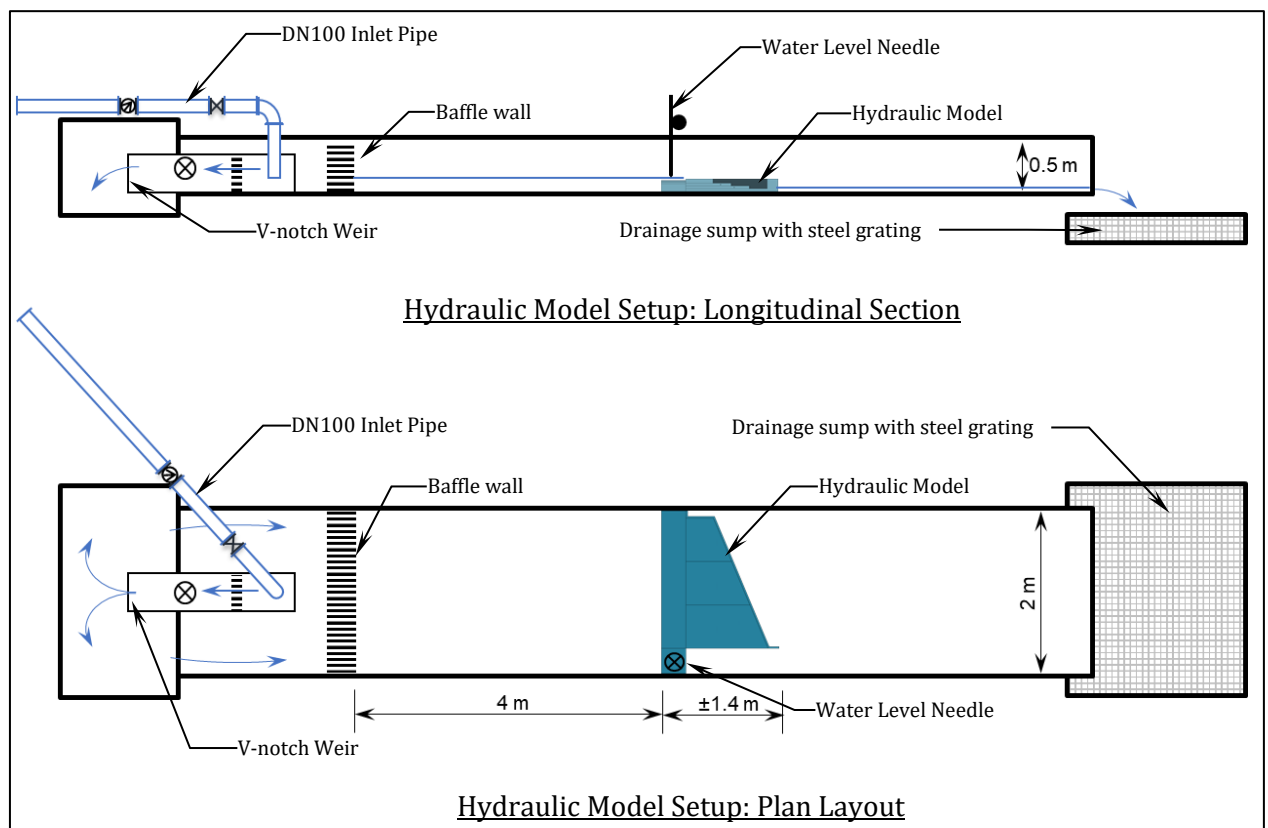


Figure 3.2: General Layout of Hydraulic Model Setup (Not to Scale)

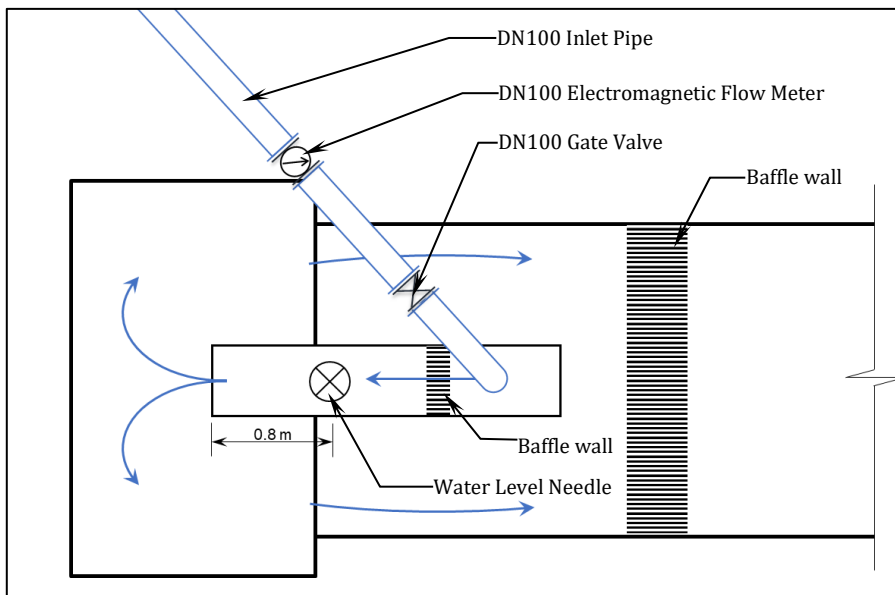


Figure 3.3: Enlargement of the V-notch Weir Layout (Not to Scale)

3.3. TEST CONDITIONS AND SCHEDULE

As mentioned at the beginning of this chapter, different model setup conditions were tested. Table 3-1 summarises the test conditions, with each operational permutation. APPENDIX D contains the complete testing schedule.

Table 3-1: Summarised Test Conditions

Test Number	Stepped Chute setup	One or more culverts open or closed	Nappe vents open or closed	Low level river crossing overflow depths (mm)
1.1.1	Stepped Chute with side wall	Closed	Closed	4, 8, 12, 16, 20
1.1.2		Closed	Open	4, 8, 12, 16, 20
1.1.3*		Closed	Closed	20
1.2.1		Open	Closed	4, 8, 12, 16, 20
1.2.2		Open	Open	4, 8, 12, 16, 20
1.2.3*		Open	Closed	20
2.1.1	Stepped Chute with side wall removed and riprap placed downstream of chute	Closed	Closed	4, 8, 12, 16, 20
2.1.2		Closed	Open	4, 8, 12, 16, 20
2.1.3*		Closed	Closed	20
2.2.1		Open	Closed	4, 8, 12, 16, 20
2.2.2		Open	Open	4, 8, 12, 16, 20
2.2.3*		Open	Closed	20

Note: Test Numbers denoted with a * refers to repeatability tests performed

Each test number listed in Table 3-1 consisted of five test runs (excluding the repeatability tests) where the prototype low level river crossing overflow depths were increased in 60 mm increments starting at a $y_{over road prototype} = 60$ mm and ending at $y_{over road prototype} = 300$ mm (where $y_{over road prototype}$ is the prototype overflow flow depth). In total, 44 test runs were performed. Repeatability tests were performed to verify that the hydraulic model state had not changed and that the results can be duplicated on demand. The repeatability of the tests is discussed in Section 4.3.5.

3.4. MODEL DESIGN

The main design aspects and considerations for the prototype and hydraulic model are discussed in this section. The complete design can, however, be found in APPENDIX B.

The hydraulic model consisted of a culvert structure that allowed for overflow, an approach road and the stepped chute. The hydraulic model with its main components is depicted in Figure 3.4.

The design recommendation and procedures followed for each of these components are summarised in Table 3-2 and are discussed in more detail in Section 3.4.2 to 3.4.3.

Table 3-2: Hydraulic Model Design Recommendations and Procedures

Model Component	Design Recommendations and/or Procedures
Low-level river crossing overflow	<ul style="list-style-type: none"> For 0% cross fall: assume critical flow over the river crossing For >0% cross fall in the downstream direction: use either Manning or Chezy's equation for open channel flow.
Approach road	Chapter 6, SANRAL's Drainage Manual, 6 th Ed.'s recommendations for low-level river crossing approach roads.
Culvert through low-level river crossing	Chapter 7, SANRAL's Drainage Manual, 6 th Ed.'s recommendations for inlet control.
Stepped Chute	Chanson's (1994) Hydraulics of nappe flow regime above stepped chutes and spillways.

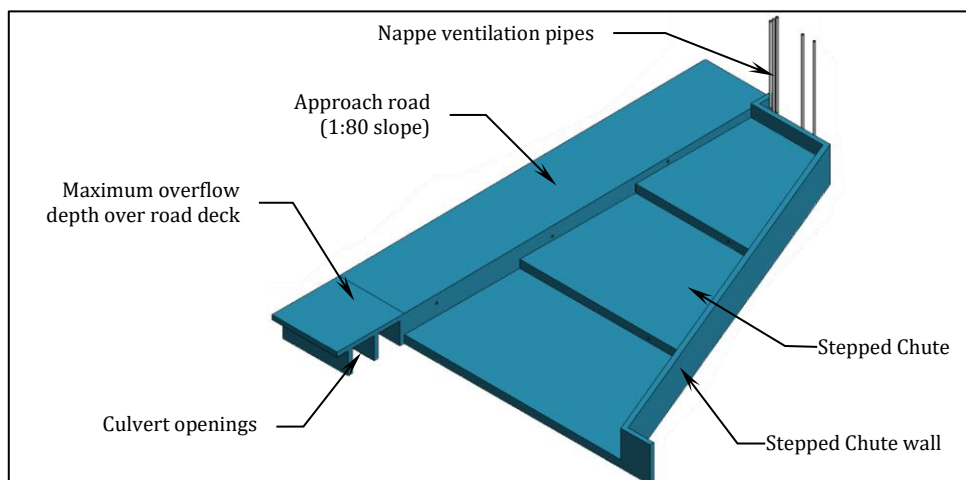


Figure 3.4: Isometric View of the Model with its Main Components Indicated

3.4.1. Determining of Design Flow

Multiple configurations were considered during initial prototype design stages where the slope of the approach to the main road deck was altered, as well as changes to the dimensions of the stepped chute were made. The maximum prototype design discharge, with 2.5 culvert openings and 300 mm overflow depth, was determined to be $23.5 \text{ m}^3/\text{s}$. The design discharge for the prototype consisted of $17 \text{ m}^3/\text{s}$ passing through the culvert and $6.5 \text{ m}^3/\text{s}$ overtopping the road.

3.4.2. Low-Level River Crossing

The design of the low-level river crossing consists of the flow through the culverts and the flow over the LLRC.

Figure 3.5 illustrates the vertically exaggerated downstream elevation, plan view and upstream elevation of the full-scale prototype (prototype prior to bisection). The design of flow over the LLRC and the flow through the culverts are discussed in Sections 3.4.2.1 to 3.4.2.3.

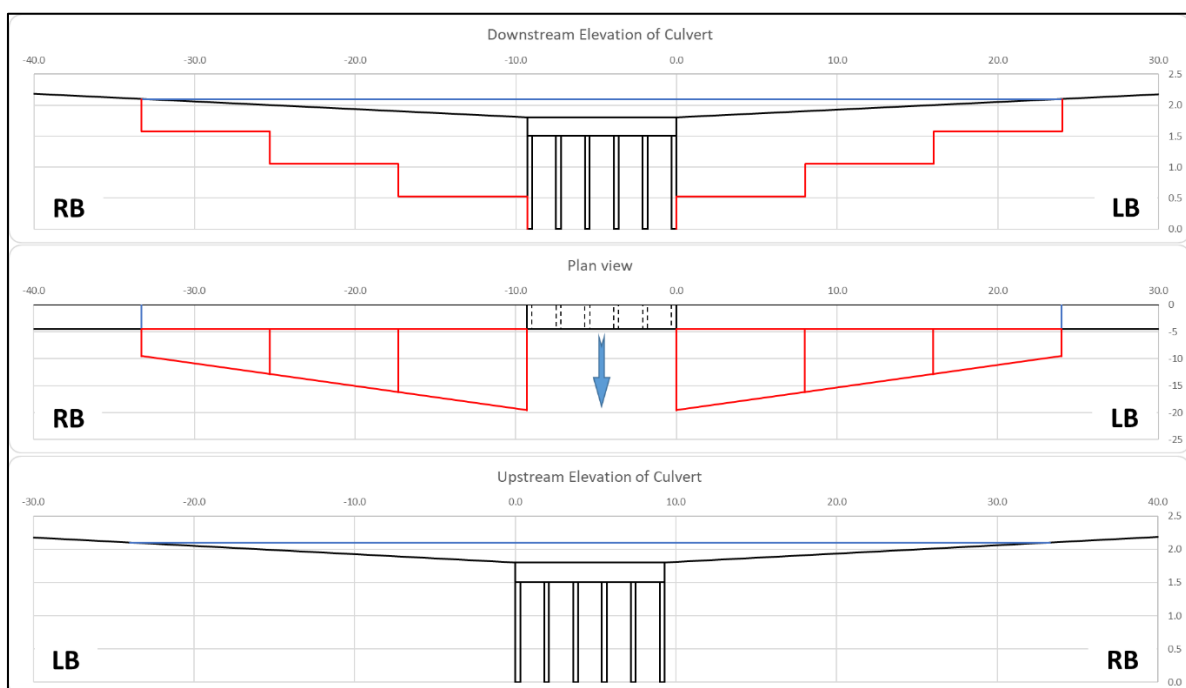


Figure 3.5: Full Prototype Elevations (Not to Scale)

3.4.2.1. Overflow Depth

Low level river crossings are typically designed to accommodate lower recurrence intervals (Pienaar & Kruger, 2013). The design flow would, therefore, be determined (by means of runoff calculations) for the appropriately selected return period. As mentioned in Section 2.2, low level river crossings are designed to allow for overtopping. This means that a portion of the design flow passes through the openings and the remaining flow flows over the low-level river crossing.

It is, however, sensible to consider a maximum overflow depth for a vehicle to still be able to safely cross (assuming the vehicle's under-body ground clearance is higher than the flow depth). The following maximum overflow depths are recommended for low level river crossings for the different flow regimes (Pienaar and Kruger, 2013):

- Supercritical flow: 100 mm; and
- Subcritical flow: 150 mm.

The design overflow depth would, however, be exceeded when the design flow of the low-level river crossing is exceeded (i.e. the selected recurrence interval is exceeded). Similarly, should the low-level river crossing have been designed for a 1:2 year return period, an increase in the design overflow depth for the stepped chute could also be considered as it is recommended that the approach road's slab be extended above the 1:5 to 1:10 year flood level (i.e. the deeper the design overflow depth, the further the stepped chute could be extended into the embankments) (Pienaar & Kruger, 2013). It was for these reasons that a prototype flow depth of 300 mm ($y_{over\ road\ model} = 20\ mm$) for which the stepped chute would be designed, was selected.

3.4.2.2. Approach Road

Pienaar and Kruger (2013) recommend using an approach road cross-fall of 2 to 3% in the direction of flow to prevent sedimentation on the road and a maximum gradient for the approach roads, in the direction of travel, as summarized in Table 3-3.

Table 3-3: Recommended Maximum Approach Road Gradients

Approach Road Construction	Desirable Maximum Grade (%)	Absolute Maximum Grade (%)
Paved Road	10	12
Unpaved Road	8	10

Pienaar and Kruger (2013) further recommend using a 4.0 m wide road width (measured from inside of guide blocks) for a single-lane crossing and a 7.5 m wide crossing for a two-lane crossing. Low level river crossings are typically provided for tertiary roads that normally have two lanes (one lane per direction). There may, however, be instances where a single lane could be considered such as significant cost savings on a long crossing or where the pedestrian and vehicular traffic volumes do not exceed 100 pedestrians per hour or 500 vehicles per day respectively.

The prototype approach road grade was set to 1.25%. This was selected to accommodate the width of the 2 m wide test channel as a flatter grade would have reduced the attainable overflow depth. The prototype approach road width was designed to be 4.5 m wide (typical

width for a single lane road with 0.25 m wide guide blocks on both sides⁴) with a level deck (i.e. 0% cross-fall). A level deck results in the road acting as a control, similar to that of a broad-crested weir (i.e. critical flow conditions over the low-level river crossing) and would simplify the measurement of the depth on the deck. The flow over the road can, therefore, be calculated by rearranging Eq. 2.11 and setting the Froude number equal to one ($F_r = 1$).

The discharge over the crossing, for the five different overflow depths, for both the prototype and model is summarised in Table 3-4.

Table 3-4: Flow Over the Crossing for the Different Overflow Test Depths

Prototype and Model Overflow Depths	Total Flow Over Prototype Crossing (m ³ /s)	Total Flow Over Model Crossing (l/s)
$y_{over road prototype} = 60 \text{ mm}$ $y_{over road model} = 4 \text{ mm}$	0.3	0.3
$y_{over road prototype} = 120 \text{ mm}$ $y_{over road model} = 8 \text{ mm}$	1.0	1.1
$y_{over road prototype} = 180 \text{ mm}$ $y_{over road model} = 12 \text{ mm}$	2.2	2.6
$y_{over road prototype} = 240 \text{ mm}$ $y_{over road model} = 16 \text{ mm}$	4.1	4.7
$y_{over road prototype} = 300 \text{ mm}$ $y_{over road model} = 20 \text{ mm}$	6.5	7.5

3.4.2.3. Culvert Openings

The prototype was designed to have five square culvert openings of 1.5 x 1.5 m. As mentioned in Section 3.2.1, the hydraulic model was bisected around the plane of symmetry. This resulted in two and a half (2.5) openings for the hydraulic model. This provided the option of blocking one or more of the openings which were used to control tailwater from the culvert during testing.

The discharge through a single and 2.5 culverts (under inlet control conditions using Eq. 2.2), for the five different overflow depths, for both the prototype and model is tabled in Table 3-5.

Table 3-5: Flow Through the Culvert for the Different Overflow Test Depths

Prototype and Model Overflow Depths (mm)	Discharge Through One Prototype Culvert $Q_{under prototype}$ (m ³ /s)	Total Flow Through Prototype Culverts (2.5 off) (m ³ /s)	Discharge Through One Model Culvert $Q_{under model}$ (l/s)	Total Flow Through Model Culverts (2.5 off) (l/s)
$y_{over road prototype} = 60 \text{ mm}$ $y_{over road model} = 4 \text{ mm}$	5.9	14.8	6.8	17.0
$y_{over road prototype} = 120 \text{ mm}$ $y_{over road model} = 8 \text{ mm}$	6.2	15.4	7.1	17.7
$y_{over road prototype} = 180 \text{ mm}$ $y_{over road model} = 12 \text{ mm}$	6.4	15.9	7.3	18.3

⁴ Guide blocks omitted from prototype design

Prototype and Model Overflow Depths (mm)	Discharge Through One Prototype Culvert $Q_{under\ prototype}\ (\text{m}^3/\text{s})$	Total Flow Through Prototype Culverts (2.5 off) (m}^3/s)	Discharge Through One Model Culvert $Q_{under\ model}\ (\text{l/s})$	Total Flow Through Model Culverts (2.5 off) (l/s)
$y_{over\ road\ prototype} = 240\ \text{mm}$ $y_{over\ road\ model} = 16\ \text{mm}$	6.6	16.5	7.6	18.9
$y_{over\ road\ prototype} = 300\ \text{mm}$ $y_{over\ road\ model} = 20\ \text{mm}$	6.8	17.0	7.8	19.5

Initial testing with 2.5 culverts caused complete inundation of the bottom step (step 1). It was therefore decided to execute model testing and data collection with one culvert open to prevent excessive inundation. This is discussed further in detail in Chapter 4.

3.4.3. Stepped Chute

Flow from the LLRC approach road to the stepped chute should form a nappe. After the nappe impingement on the step, flow is supercritical up to the point where a hydraulic jump should form on top of the step. The same effect is expected to take place from one step onto the next in the direction of the stepped chute.

Figure 3.6 indicates the elevation and plan view of the prototype stepped chute. The approach road maximum prototype overflow depth ($y_{over\ road} = 300\ \text{mm}$) and slope were used to determine the overflow width and consequently the step lengths in the direction of the chute.

The step height selection was the variable that ultimately determined the number of steps that would be required. Using three steps for the prototype was found to satisfy the design criteria for the stepped chute. Four chute steps were also considered but were found to have conjugate flow depths exceeding the step height. The design criteria for chute step height, width and lengths are discussed in Sections 3.4.3.1 and 3.4.3.2.

Nappe vents were also included to reduce sub-atmospheric pressures from developing that might collapse the nappe or cause nappe oscillations and also to study the differences in flow profiles between a vented and unvented nappe model. The nappe ventilation design is discussed in Section 3.4.3.3.

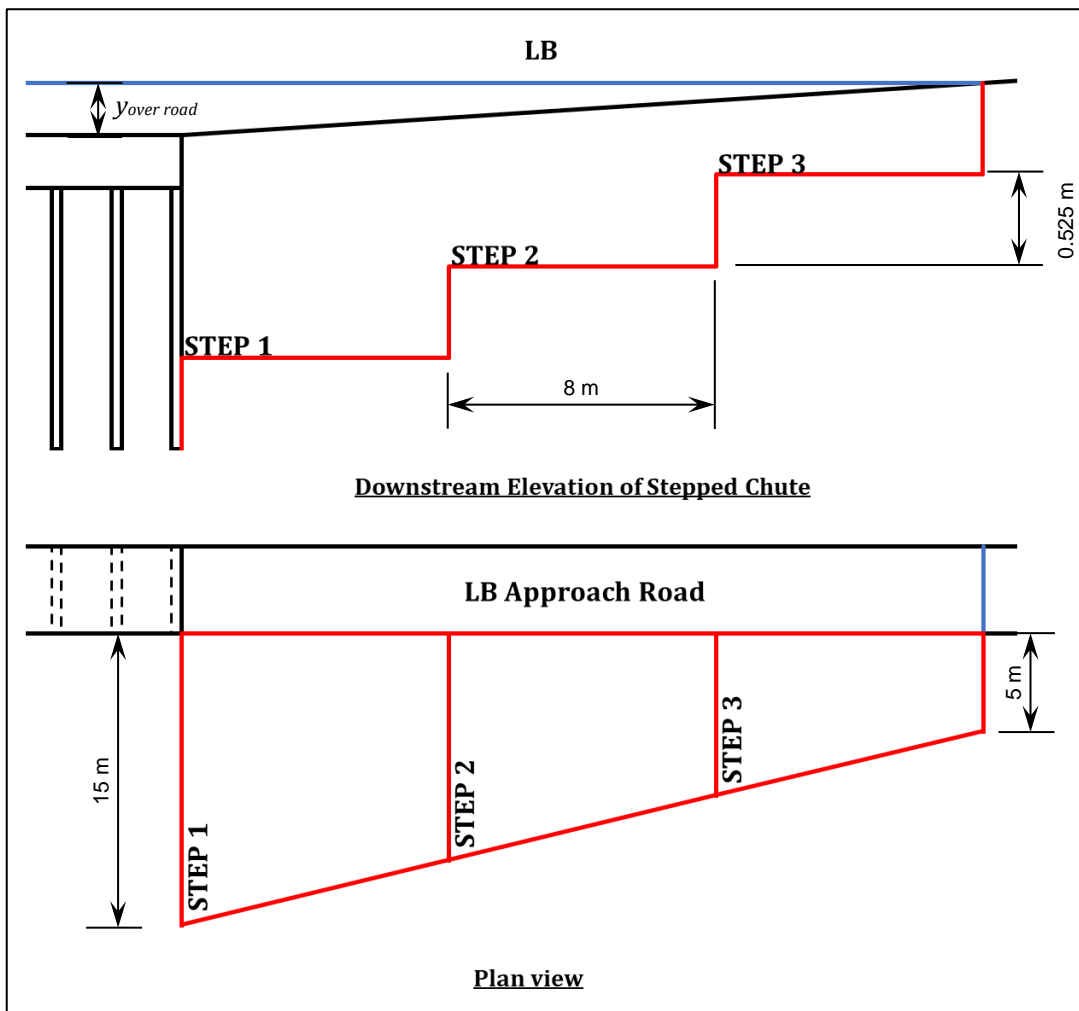


Figure 3.6: Prototype Step Chute Dimensions (Not to Scale)

3.4.3.1. Nappe Flow from the Approach Road onto the Stepped Chute

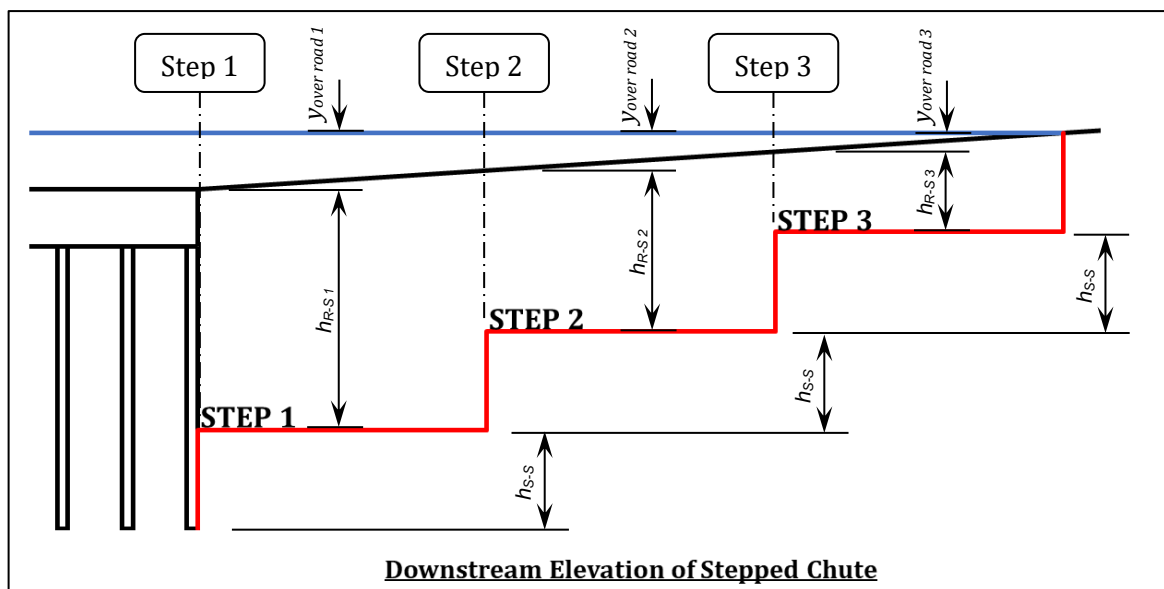
The cross-sectional flow area directly above each step was assumed to fall onto that particular step. For example, the triangular flow area above step 3 of 8 m width was assumed to impinge on step 3, the trapezoidal flow area above step 2 of 8 m width was assumed to impinge on step 2, etc. Although this approach simplifies the distribution of flow onto each step, it should be noted that effects of changing hydraulic radii of each flow area above each step could affect the flow distribution onto each step but was, however, not considered.

The total flow over the left bank approach road was distributed to each of the aforementioned flow areas according to the portion the flow area contributed to the total left bank approach road area. This principle was applied to the five different test overflow depths. The left bank approach road overflows impinging on each of the steps for a prototype overflow depth of 300 mm are tabulated in Table 3-6. The cumulative discharge is also listed as these values were used to determine the nappe geometries on each step in the direction of the chute. Refer to Appendix B for the flow impinging onto each step for all the overflow depths.

Table 3-6: Approach Road Overflows Impinging on Each Step

Prototype Flow Areas (m ²)	Prototype: Discharge onto Step Beneath Approach Road $Q_{Road-Step}$ (m ³ /s)	Prototype: Cumulative Discharge $Q_{Road-Step}$ (m ³ /s)	Model: Discharge onto Step Beneath Approach Road $Q_{Road-Step}$ (l/s)	Model: Cumulative Discharge $Q_{Road-Step}$ (l/s)
$A_{road-step 3} = 0.4 \text{ m}^2$	0.52	0.52	0.6	0.6
$A_{road-step 2} = 1.2 \text{ m}^2$	1.57	2.09	1.8	2.4
$A_{road-step 1} = 2.0 \text{ m}^2$	2.62	4.71	3.0	5.4

Following the determination of the flow impinging onto each step, the horizontal length of the nappe drops, and the length of the hydraulic jump rollers were determined for each step using Eq. 2.21 and Eq. 2.22. The input parameters to calculate the nappe drop length and hydraulic jump roller lengths included the critical depth on the approach road, the height of the step and the flow depth after the nappe impingement on the step. However, it can be seen from Figure 3.7 that the nappe fall height (h_{R-S}) differs over the nappe width. The nappe fall height (h_{R-S}) and overflow depth ($y_{over road}$) for each step was, therefore, taken at the point where the deepest flow depth (and flow concentration) would occur. For example, for flow impinging on step 2: if a line was projected upwards from the end of step 2, the step height would be taken as the difference in height between the approach road surface and the top of step 2. The same applies for the calculation of the flow depth after the nappe impingement for each step which is used to calculate the hydraulic jump roller length. Figure 3.8 illustrates the nappe and hydraulic jump geometry from the approach road to the steps.

**Figure 3.7: Positions for Overflow Depth ($y_{over road}$) and Nappe Fall Height (h_{R-S})**

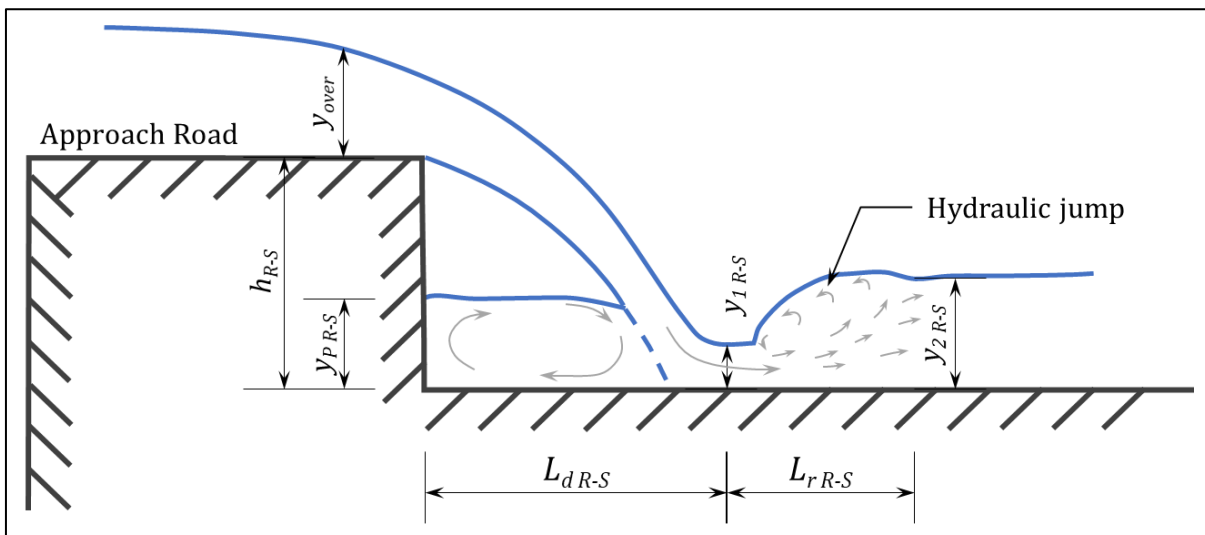


Figure 3.8: Nappe Geometry for Flow from the Approach Road

The calculated nappe drop length ($L_{d R-S}$) and hydraulic jump roller lengths ($L_{r R-S}$) due to flow from the approach road to each step, are summarised in Table 3-7.

Table 3-7: Nappe Drop-lengths and Hydraulic Jump Roller Lengths from Road to Steps

Prototype: Flow from Road to Steps (m^3/s)	Prototype: Nappe Drop Length ($L_{d R-S}$) (m)	Prototype: Hydraulic Jump Roller Length ($L_{r R-S}$) (m)	Prototype: Total Length ($L_{d R-S} + L_{r R-S}$) (m)	Model: Total Length ($L_{d R-S} + L_{r R-S}$) (mm)
$Q_{road-step\ 3} = 0.52$	0.57	0.44	1.01	67
$Q_{road-step\ 2} = 1.5$	1.13	0.99	2.12	141
$Q_{road-step\ 1} = 2.62$	1.70	1.23	2.93	195

3.4.3.2. Nappe Flow from One Chute Step to the Next

The flow down the stepped chute was accumulated from the top step (step 3) to the bottom step (step 1). For example, the flow over the edge of step 2 was equal to the flow from step 3 and the flow falling onto step 2 from the approach road. The cumulative discharges for the prototype and hydraulic model, as listed in Table 3-6, therefore represent the specific overflow from that particular step to the next step.

The same design procedure as used for Section 3.4.3.1 was used for the nappe drop length and hydraulic jump roller length determination. However, the step height (h_{S-S}) now remains constant and the overflow width is a function of the calculated lengths from Section 3.4.3.1. The effective flow area, as illustrated in Figure 3.9, down the chute, was assumed to exclude the nappe drop length and hydraulic jump length due to flow from the road onto the steps. The critical depth at the brink of each step was calculated and used to determine the nappe geometry with Eq. 2.18 to Eq. 2.21.

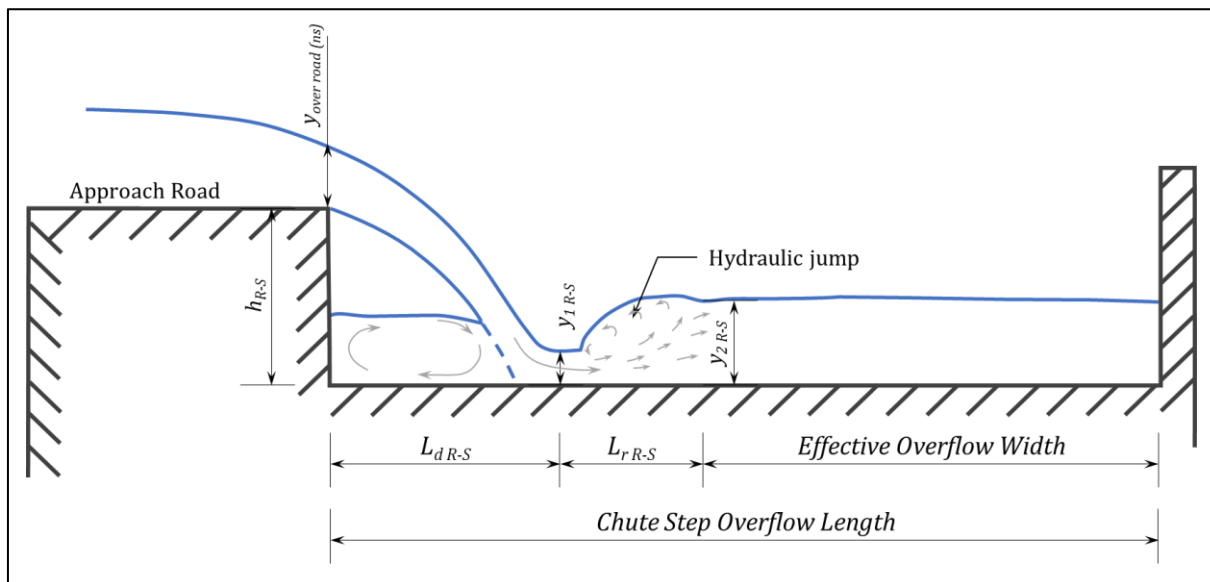


Figure 3.9: Cross-sectional View for Determining Stepped Chute Width

It is apparent then that the stepped chute dimensions are subject to an iterative selection process as the geometry of the nappe falling from the road overflow influences the nappe geometry from one step to the next. The final chute dimensions used for the prototype are indicated in Figure 3.6.

The resulting nappe drop length ($L_{d,S-S}$) and hydraulic jump roller lengths ($L_{r,S-S}$) due to flow from one step to the next are summarised in Table 3-8.

Table 3-8: Nappe Drop-lengths and Hydraulic Jump Roller Lengths from One Step to the Next

Prototype: Cumulative Flow from Step ($Q_{S-S}(ns)$) (m^3/s)	Prototype: Nappe Drop Length ($L_{d,S-S}$) (m)	Prototype: Hydraulic Jump Roller Length ($L_{r,S-S}$) (m)	Prototype: Total Length ($L_{d,S-S} + L_{r,S-S}$) (m)	Model: Total Length ($L_{d,S-S} + L_{r,S-S}$) (mm)
$Q_{step-step\ 3} = 0.523$	0.50	0.69	1.18	79
$Q_{step-step\ 2} = 2.092$	0.91	0.96	1.87	124
$Q_{step-step\ 1} = 4.708$	1.24	1.10	2.34	156

In summary, the following three conditions needed to be adhered to when selecting the appropriate chute dimensions:

- The *conjugate depth*, for a hydraulic jump formed in the direction of the chute (i.e. flow from one step to the next), on one step should not exceed the step height as this could lead to inundation of the previous step which would change the flow regime to either transition or skimming flow.
- As mentioned in Section 2.4.1.1, Chanson (1994: 72) asserted that, should the length of the drop (L_d) plus the length of the roller (L_r) be smaller than the length of the step (ℓ), a fully developed hydraulic jump may occur, leading to higher rates of energy

dissipation. Ensuring long enough step lengths for hydraulic jump formation is, therefore, advantageous to dissipate as much energy as possible.

- Maintain nappe flow conditions (refer to Figure 2.14 in Section 2.4.2).

3.4.3.3. Ventilation of the Nappe

A total of five nappe ventilation pipes were installed, three of which were provided for the nappe from the approach road to the stepped chute and one was installed for each nappe from step 2 and step 3 respectively.

As mentioned in Section 2.4.1.3, Chanson (2001) recommended using Eq. 2.23 to determine the nappe ventilation requirement on stepped chute spillways. The equation was, however, only valid for approach Froude numbers between 3 to 10, and the Froude numbers near the brink of each step was critical ($F_r = 1$) for both cases of flow from the approach road onto the step as well as flow from one step onto the next. Eq. 2.24 from Bos (1989) was, therefore, used as a first order estimation of the nappe air requirement for prototype design purposes as it had no limitation on the approach Froude number.

The input values used for the determination of the ventilation requirement of each vent are summarised in Table 3-9. The flow depth from the top step (y_{top}) was in this case the critical depth from the top step.

Table 3-9: Prototype Nappe Ventilation Requirement Variables

Model Component	Vent No.:	Q_w (m ³ /s)	y_p (m)	y_{top} (m)
Nappe Flow from Approach Road onto Step 1	V1	2.6	0.49	0.3
Nappe Flow from Approach Road onto Step 2	V2	1.6	0.33	0.2
Nappe Flow from Approach Road onto Step 3	V3	0.5	0.16	0.1
Nappe Flow from Step 3 onto Step 2	V4	0.5	0.15	0.08
Nappe Flow from Step 2 onto Step 1	V5	2.1	0.25	0.17

The maximum expected nappe air requirement for the prototype and model (based on a low-level river crossing prototype overflow depth of 300 mm) is listed in Table 3-10 .

Table 3-10: Nappe Ventilation Requirement

Vent No.:	Prototype: Nappe Ventilation ($Q_{air\ prototype}$) (m ³ /s)	Model: Nappe Ventilation ($Q_{air\ model}$) (l/s)
V1	0.125	0.144
V2	0.075	0.086
V3	0.025	0.029
V4	0.020	0.023
V5	0.118	0.135

The inside diameters of the prototype ventilation pipes were 150 mm (model inside diameter of 10 mm). The nappe ventilation size was determined using the maximum airflow requirement for flow from the approach road onto the steps ($Q_{air\ prototype - V1} = 0.125 \text{ m}^3/\text{s}$). The maximum airflow requirement for flow from the approach road onto the steps was used, as its nappe would be confined on both sides and ventilation of the nappe from the sides would not be possible. The nappes forming from one step onto the next were, however, not confined on both sides and ventilation of the nappe from one side of the nappe would, therefore, be possible. The use of a 150 mm prototype diameter for a maximum nappe aeration requirement of $0.125 \text{ m}^3/\text{s}$ (vent pipe V1 above step 1) would result in a prototype flow velocity of 7.1 m/s. The model equivalent airflow velocity would, therefore, be 1.8 m/s which is within the measuring capabilities of the anemometer as discussed in Section 3.6.5. The ventilation pipe installation for the hydraulic model is illustrated in Figure 3.10.

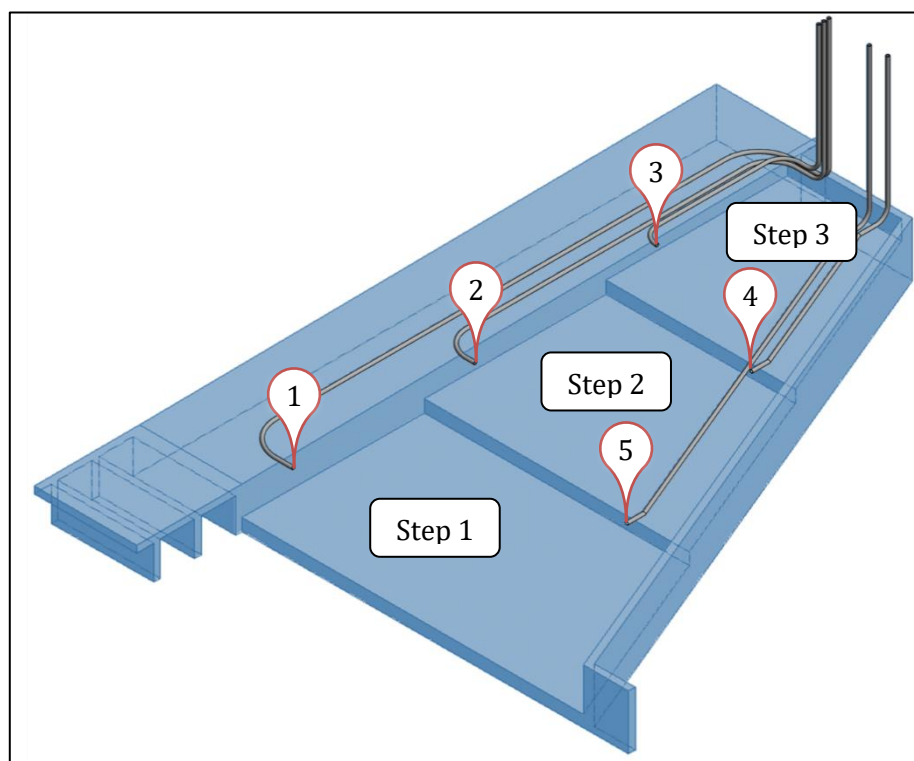


Figure 3.10: Illustration of ventilation pipe installation

3.4.4. Riprap Design

The design of the riprap size was determined using Eq. 2.8 with the following input parameters:

Table 3-11: Riprap Design Parameters

Parameter	Symbol	Prototype Values
Average flow velocity	v	1.3 m/s
Average flow depth	y_{avg}	0.15 m
Bank angle with the horizontal	θ	45 °
Riprap angle of repose	ϕ	42 °
Safety factor	S_F	2
Specific Gravity of riprap	S_S	2.5 kg/l
Dimensionless parameter	K_1	0.37
Coefficient for specific gravity and stability	C	2.48
Nominal 50% angular shaped stone size	D_{50}	0.37 m

The flow over the left bank approach road was used for the design of the prototype riprap as this was the flow that would directly interact with the riprap. The flow over the left bank had a maximum design flow depth of 0.3 m. However, as it had a triangular flow distribution over the left bank approach road, the average flow depth (y_{avg}) was taken as 0.15 m. The flow velocity over the left bank approach road was 1.3 m/s. The stability factor (S_F) was set to 2 as recommended by Jansen van Vuuren *et al.* (2013), for rapidly varied- and highly turbulent flow conditions, which would typically be found at the nappe impingement downstream of the low-level river crossing. The determined prototype D_{50} value of 0.37 m is equivalent to 24.7 mm for the hydraulic model. The grading of the riprap material is discussed further in Section 3.5.4.

3.5. MODEL CONSTRUCTION

The construction of the entire hydraulic model was undertaken by the hydraulic laboratory staff of the university. The final as-built drawings are contained in APPENDIX C. The particulars of the main model components are discussed in the following sub-sections.

3.5.1. Low-Level River Crossing

The low-level river crossing was constructed from 15 mm thick marine plywood with all joints sealed with silicone to waterproof it. The entire model was painted with a water-proof paint to prevent swelling and distortion during and after test runs as seen in Figure 3.11.



Figure 3.11: Upstream Elevation of the Left Bank Approach Road and River Crossing

The nappe ventilation pipes and the pressure sensors were housed in the cavity beneath the approach road of the hydraulic model as illustrated in Figure 3.12.



Figure 3.12: Installation of the Nappe Ventilation Pipes and Pressure Sensors

3.5.2. Stepped Chute

The stepped chute was also constructed from 15 mm marine plywood, sealed and painted in an analogous manner as that of the low-level river crossing. The stepped chute included the installation of a clear Perspex wall on the downstream end in order to observe the flow profile from the downstream end, as illustrated in Figure 3.13.



Figure 3.13: Installation of the Clear Perspex Chute Wall

3.5.3. Nappe Ventilation

As mentioned in Section 3.4.3.3, ventilation pipes were installed to aerate the nappes between the road and chute as well as the nappes flowing from step to step down the chute. The ventilation pipes were positioned as high as practically possible in an attempt to prevent submergence during operation. Figure 3.14 illustrates the installation of the ventilation pipe from the road deck to step 3 (in the background to the left) and the ventilation pipes on step 2 (in the background to the right) and step 3 (in the foreground).

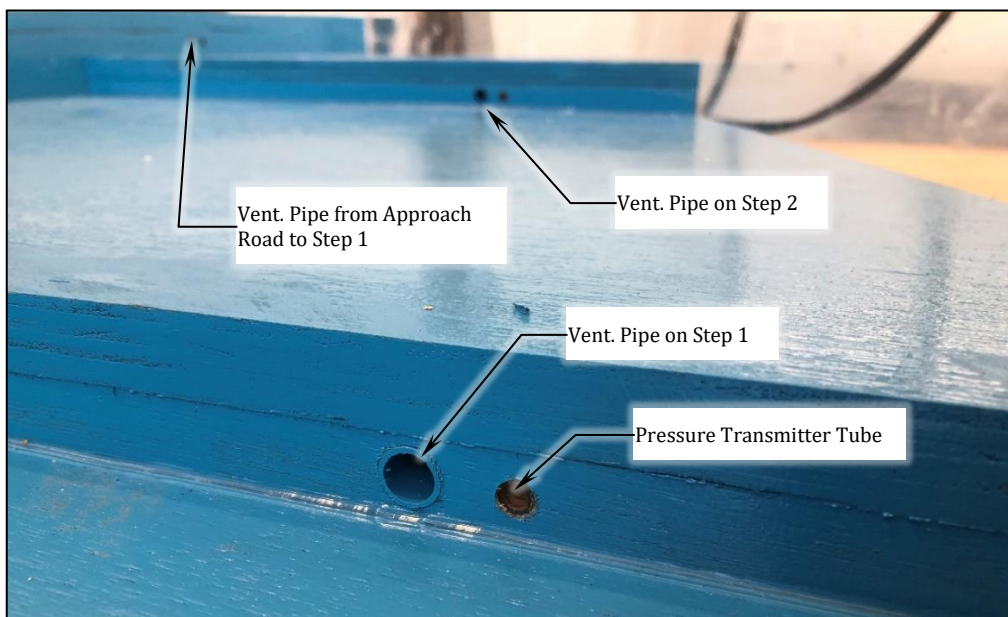


Figure 3.14: Installation of the Nappe Ventilation Pipes

3.5.4. Riprap

As mentioned in Section 3.4.4, the determined value of D_{50} was 24.7 mm for the hydraulic model. Using Figure 2.4 to determine the grading of the material would result in a grading requirement as tabled in Table 3-12:

Table 3-12: Hydraulic Model Riprap Grading Requirement

Sieve Size (mm)	Percentage Passing (%)
4.75	0
13.2	20
19.0	40
26.5	50
53.0	100

Obtaining material meeting this requirement was not practical and seeing that the minimum recommended riprap layer thickness should be at least equal to the D_{100} , the use of the single size of 53 mm (closest to a value of the hydraulic model $D_{100} = 49.4$ mm) was implemented.

Angular aggregates were sourced, and the fraction retained on the 53.0 mm sieve was placed downstream of the stepped chute after the chute wall was removed.

3.6. DATA COLLECTION

The methods and instruments used to measure and collect data from the hydraulic model are listed and described in this section.

3.6.1. Discharge

The flow for each test run was adjusted using the DN100 gate valve downstream of the flow meter. The flow meter reading was continuously monitored as the gate valve setting was adjusted to ensure that the correct flow rate was obtained prior to any testing and data recording taking place.

The second flow measurement device used for low flow conditions (flow smaller than 1.5 l/s) was the 90° V-notch weir. The water depth was determined for the required discharge. The gate valve was used to throttle the flow until the desired V-notch weir head was obtained prior to testing. The V-notch weir head was then verified after testing to ensure constant flow was maintained.

The testing conditions of the hydraulic model are listed in Section 3.3.

3.6.1.1. Instrumentation

A Flowmetrix Magflow DN100 electromagnetic flow meter, with a $\pm 0.5\%$ accuracy and reading repeatability of $\pm 0.1\%$, was used to measure flows exceeding 1.5 l/s (no flow was registered for flows smaller than 1.5 l/s). Figure 3.15 shows the flow gauge with zero flow.



Figure 3.15: Reading Gauge of Flowmetrix Magflow DN100 Flow Meter

The V-notch weir was used for low flow conditions. The V-notch weir did not have an automated gauge and required manual calculation of the discharge given the V-notch weir

dimensions. The BSI⁵ (1981) recommended the head-discharge relationship for the V-notch weir as per Eq. 3.1:

$$Q = \frac{8}{15} C_e \tan \frac{\theta}{2} \sqrt{2gh_e^{\frac{5}{2}}} \quad \text{Eq. 3.1}$$

where:

Q is the flow rate (m^3/s);

C_e is the coefficient of discharge (to be obtained from Figure 3.16) (dimensionless);

θ is the opening angle ($^\circ$);

g is the gravitational acceleration (taken as 9.81 m/s^2);

h_e is the effective head calculate as follows: $h_e = h + k_h$ (m);

h is the upstream head measured from the vertex of the V-notch (m);

k_h is an experimentally determined constant found to be 0.0085 for $\theta=90^\circ$ (m);

p is the height of the vertex of the notch with respect to the floor of the approach channel (m); and

B is the width of the approach channel (m).

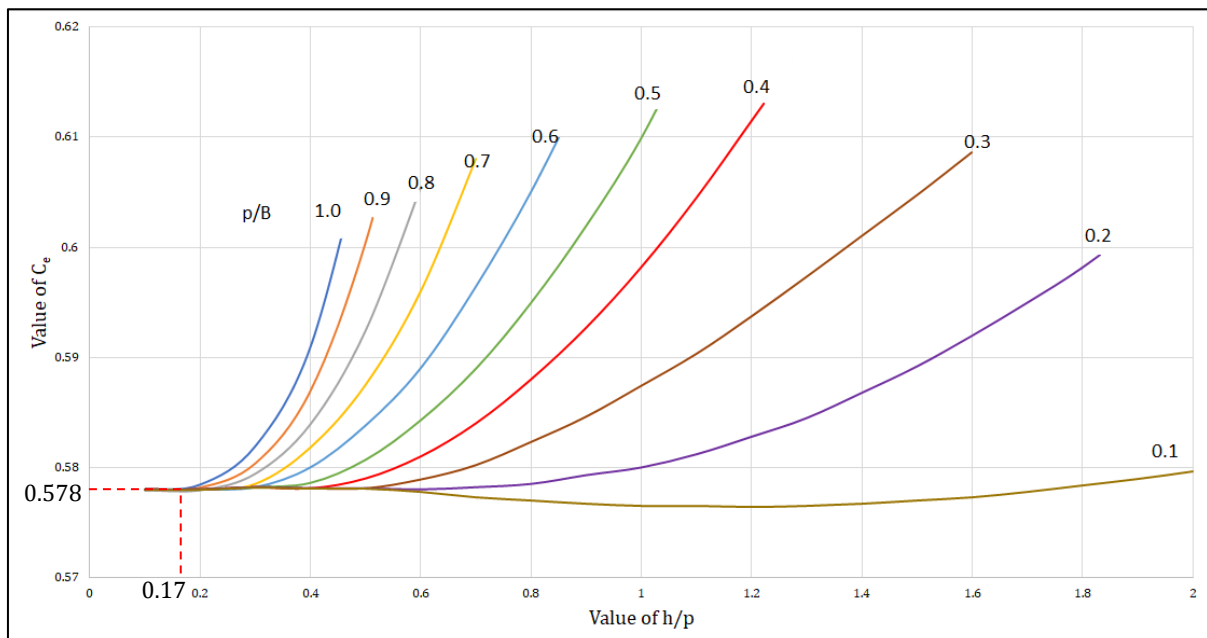


Figure 3.16: Coefficient of Discharge for $\theta=90^\circ$ V-Notch Weir

APPENDIX D contains the V-notch weir flow depths for the different flow rates used during testing of the hydraulic model.

⁵ British Standards Institution

3.6.1.2. Position

The flow meter was located on the DN100 steel pipe upstream of the V-notch weir channel. The recommended and actual laboratory setup up- and downstream straight lengths for the flow meter are tabulated in Table 3-13.

Table 3-13: Flowmetrix Magflow DN100: Recommended and Actual Minimum Up- and Downstream Straight Pipe Lengths⁶

Description	Upstream Length	Downstream Length
Recommended minimum lengths	300 mm (3 x DN)	200 mm (2 x DN)
Actual test setup lengths	1500 mm (15 x DN)	400 mm (4 x DN)



Figure 3.17: Flow Meter, Gate Valve and V-Notch Weir Setup

3.6.2. Water Level

The overflow depth on the low-level river crossing was measured for each test to verify the depths used during the design of the prototype. Instances where the V-notch weir was utilised also required the measurement of the weir flow depth to determine the corresponding discharge.

3.6.2.1. Instrumentation

The water level on the road at the culvert was measured, using a water level measurement needle mounted on a moving trolley, to verify the low-level river crossing overflow depth for each test.

A separate water level measuring needle was used to record the water depth upstream of the V-notch weir for low flow conditions. Testing of the model during low flow conditions where

⁶ Flow Metrix Beta Meter Electromagnetic Flow meter - User's Guide: Installation and Operation Instructions

the V-notch weir was used, only commenced after the correct flow depth and hence flow rate was obtained.

The accuracy of both measurement needles was 1 mm. Figure 3.18 shows the two water level measuring needles used for depth measurements.

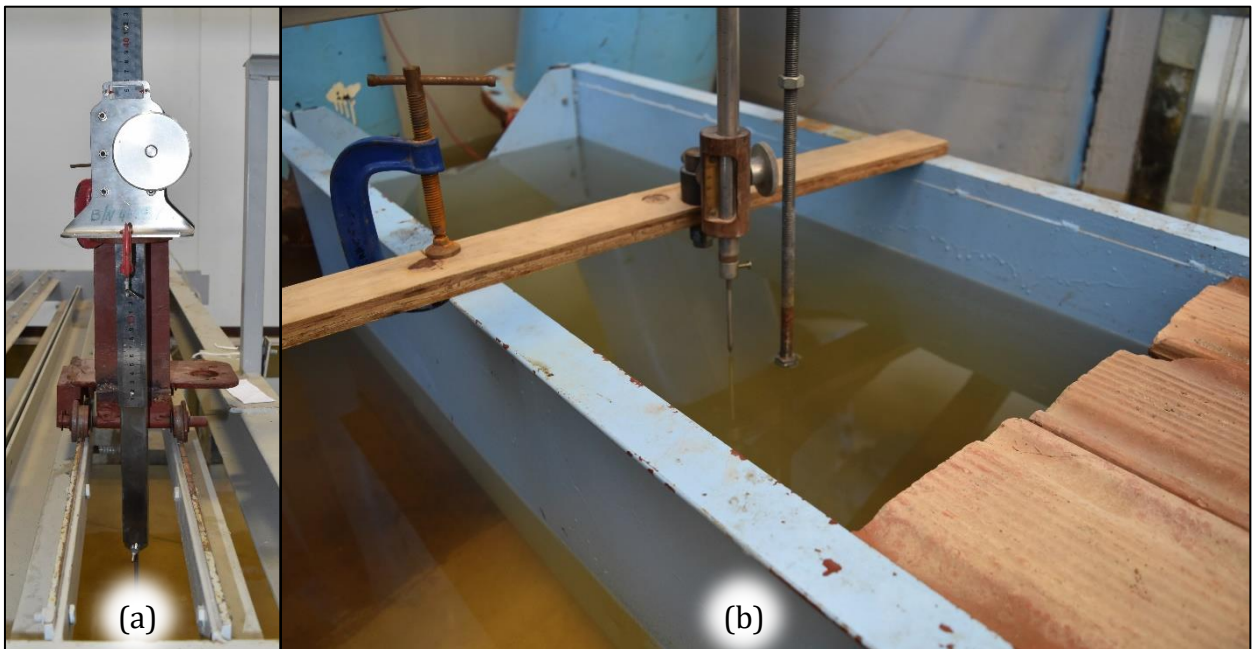


Figure 3.18: Flow Depth Water Measurement Needles: (a) LLRC Overflow Depth Measurements; (b) V-notch Weir Flow Depth Measurements

3.6.2.2. Position

The measurement position for the road overflow depth was on the centre line of the road (i.e. the middle of the road). The V-notch weir flow depth measurement was taken 800 mm upstream of the V-notch weir and could not be placed closer to the V-notch to provide access to the measurement needle. Backwater effect was negligible for the flows being measured.

3.6.3. Pressures Behind Nappes

The pressure behind the nappes was determined by measuring the dynamic flow pressures at certain position behind the nappe forming from the road and the nappes forming on the stepped chute.

3.6.3.1. Instrumentation

Five Wika S-10 high-quality pressure transmitters were used to measure the pressures behind the nappes. One end of each transmitter was connected to its specific location with a 3 mm outside diameter plastic tube while the other end of the plastic tube was located behind the stepped chute to allow for bleeding of the plastic tube prior to testing. Bleeding of the pressure sensor tubes was performed at the start of each test day.

The manufacturer of the transmitters listed the measuring range to be ± 100 mbar, a repeatability of $\pm 0.1\%$ and an accuracy of $\pm 0.2\%$. Figure 3.19 shows one of these pressure transmitters.



Figure 3.19: Wika S-10 High-Quality Pressure Transmitter

3.6.3.2. Position

The positioning of the pressure transmitters coincided with the placement of the nappe ventilation pipes as the objective of pressure measurements was to determine if sub-atmospheric conditions occurred behind the nappes.

Figure 3.10 and Figure 3.14 illustrate the positioning of the ventilation pipes and the installation of the pressure transmitter tubes relative to it.

3.6.3.3. Duration and Frequency

The pressure recording sampling interval and amount was set to 10 ms and 40 000 samples respectively. This translates to a frequency of 100 Hz and a length of 6 minutes and 40 seconds for each transmitter. Calitz (2016) showed that a 3-minute duration is adequate to obtain a statistically variable data set.

3.6.3.4. Data Conversion

The Wika S-10 pressure sensors do not provide a direct pressure reading output but rather an electrical signal (current output). The current output needs to be converted to a pressure head reading by using the manufacturer's transmitter range parameters as tabled in Table 3-14.

Table 3-14: Wika S-10 Pressure Transmitter Operating Ranges and Parameters

Transmitter Parameter	Symbol	Minimum Range	Maximum Range
Measurable pressure head of water (metres)	H	-1 m	1 m
Measurable pressure (atmospheric)	p	-100 mbar	100 mbar
Current output (ampere)	I	4 mA	20 mA
Resistance (Ohm)	R	120 Ω	

Each transmitter was connected to a data logging box that converted the electric signals from each transmitter, using Ohm's law, to a voltage over a 120Ω resistor.

The manufacturer recommends using Eq. 3.2 to convert either a voltage or ampere readings to pressure readings.

$$H_{measured} = (x - C_{min}) \frac{(H_{max} - H_{min})}{(C_{max} - C_{min})} \quad \text{Eq. 3.2}$$

where:

$H_{measured}$ is the pressure head for the corresponding measured signal (m);

H_{max} is the maximum pressure head of the transmitter (m);

H_{min} is the minimum pressure head of the transmitter (m);

C_{max} is the maximum voltage (V)/ampereage (A) of the transmitter;

C_{min} is the minimum voltage (V)/ampereage (A) of the transmitter; and

x is the measured voltage (V)/ampereage (A) signal from the transmitter.

The model transmitters were set up to measure voltage which results in Eq. 3.3.

$$H_{measured} = (x - V_{min}) \frac{(H_{max} - H_{min})}{(V_{max} - V_{min})} \quad \text{Eq. 3.3}$$

However, the minimum and maximum voltage limits of the pressure transmitters are unknown. Using Ohm's law ($V = I \cdot R$), Eq. 3.3 can be rewritten as follows:

$$H_{measured} = (x - V_{min}) \frac{(H_{max} - H_{min})}{R(I_{max} - I_{min})} \quad \text{Eq. 3.4}$$

The first set of brackets remains unchanged as the output signal is in volts; however, the base reference pressure is atmospheric pressure, resulting in $V_{min} = V_{atm}$. In the case where sub-atmospheric conditions exist, the value of x would be smaller than V_{atm} resulting in a negative measured head value which would then be recorded as the pressure head below atmospheric pressure.

Simplifying Eq. 3.4 results in the following relationship:

$$H_{measured} = (x - V_{atm}) \frac{(1 - (-1))}{120(0.02 - 0.004)} \quad \text{Eq. 3.5}$$

$$H_{measured} = (x - V_{atm}) \frac{25}{24}$$

A base measurement of atmospheric pressure was made for each transmitter in its final position to determine the corresponding voltage readings (V_{atm}) to be used in Eq. 3.5. The measured values are illustrated in Figure 3.20.

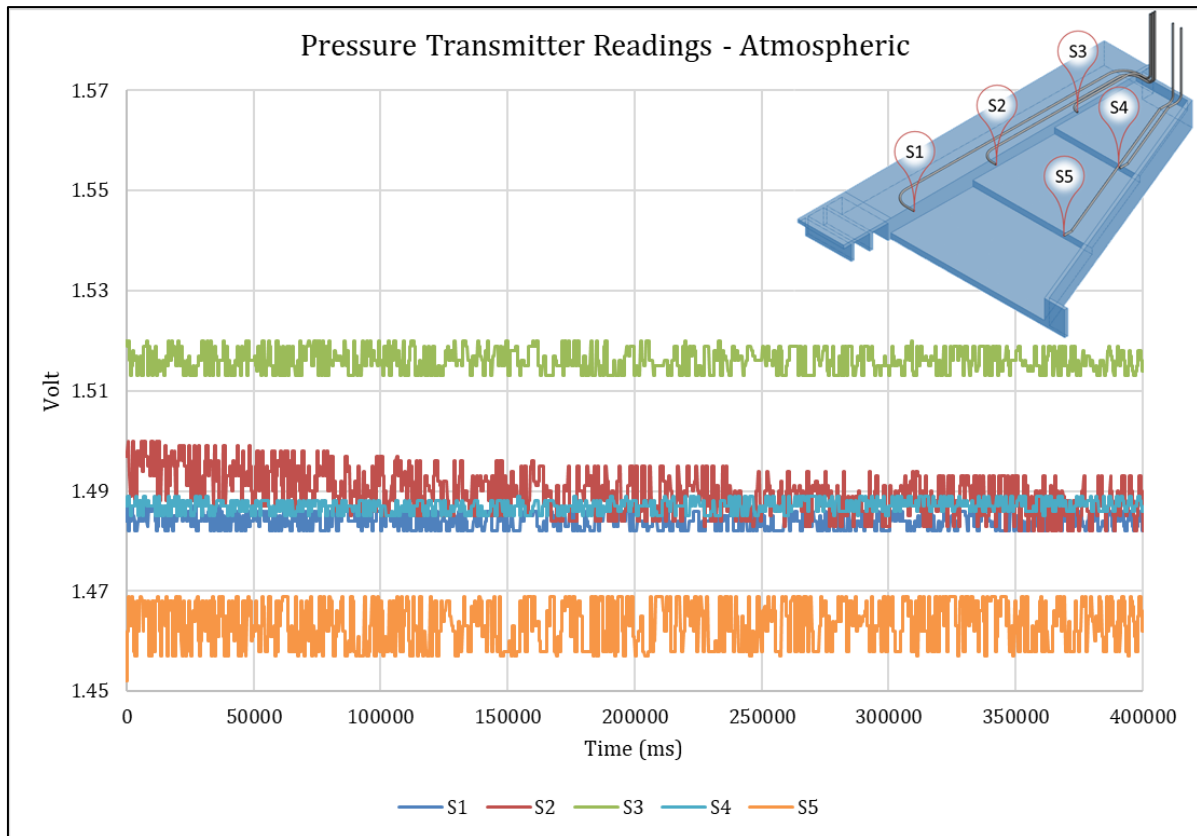


Figure 3.20: Pressure Transmitter Readings for Atmospheric Conditions

The transmitter readings had minor fluctuations, as seen in Figure 3.20 and reaffirmed by the low standard deviation values listed in Table 3-15. This prompted the use of the average values for each transmitter as the corresponding voltage for atmospheric conditions (V_{atm}). These values, together with their corresponding standard deviations, are tabulated in Table 3-15.

Table 3-15: Averaged Pressure Transmitter Readings and Standard Deviations for Atmospheric Conditions

Transmitter	Averaged Atmospheric Voltage (V_{atm})	Standard Deviation of Readings
S1	1.484	0.002
S2	1.490	0.004
S3	1.516	0.002
S4	1.487	0.001
S5	1.464	0.005

3.6.4. Flow Profiles on Chute Steps

The flow profiles on each step was determined by measuring the location of the hydraulic jumps relative to the model components.

3.6.4.1. Instrumentation

A Stanley 9 mm x 3 m PowerLock retractable tape rule, as illustrated in Figure 3.21, was used for measurement purposes. The tape rule was capable of measuring to an accuracy of 1 mm.

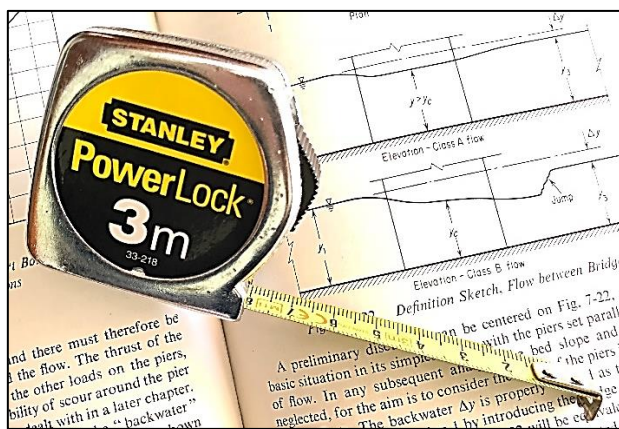


Figure 3.21: Stanley 9 mm x 3 m PowerLock Retractable Tape Rule

3.6.4.2. Position

The flow profiles were measured on all three steps using prominent model features as reference planes.

3.6.5. Nappe Ventilation

To determine the nappe ventilation requirement, an anemometer was used to measure the air flow velocities for each ventilation pipe.

3.6.5.1. Instrumentation

A Lutron hot-wire anemometer, as depicted in Figure 3.22, was used to measure airflow velocities. The anemometer functions with a combination of a hot-wire and a standard thermistor. The hot-wire is kept at a constant temperature via a regulating switch. The current drawn to maintain the constant temperature is directly proportional to the air velocity that extracts heat from the element due to the colder airflow.



Figure 3.22: Lutron Hot-Wire Anemometer

The anemometer was capable of measuring the temperature (in degrees Celsius and Fahrenheit) and five different velocity units at a sampling time of approximately 0.8 seconds. The measurement units with their respective operating ranges and display resolutions are tabulated in Table 3-16.

Table 3-16: Lutron Hot-Wire Anemometer Operating Parameters

Measurement Unit	Display Resolution	Accuracy	Range
°C	0.1	± 0.8 °C	0 – 50
°F	0.1	± 1.5 °F	32 - 122
m/s	0.1		0.2 - 20
km/h	0.1	± (5% + 1d) reading or	0.7 - 72
ft/min	1	± (5% + 1d) full scale <i>Dependant on which is larger</i>	40 - 3940
miles/h	0.1		0.5 – 44.7
knots	0.1		0.4 – 38.8

The anemometer did not have an automated logging functionality. Airflow velocities were, therefore, manually logged and recorded for each air ventilation pipe.

3.6.5.2. Position

As mentioned in Section 3.5.3, five nappe ventilation pipes were installed, three of which were to ventilate the nappe forming from the road onto the stepped chute. The remaining two ventilation pipes were installed to ventilate the nappe forming from step 3 to step 2 and from step 2 to step 1 respectively. The measurements with the anemometer probe were taken by resting the tip of the probe on top of the outlet of the vertical section of the ventilation pipes as indicated in Figure 3.23.

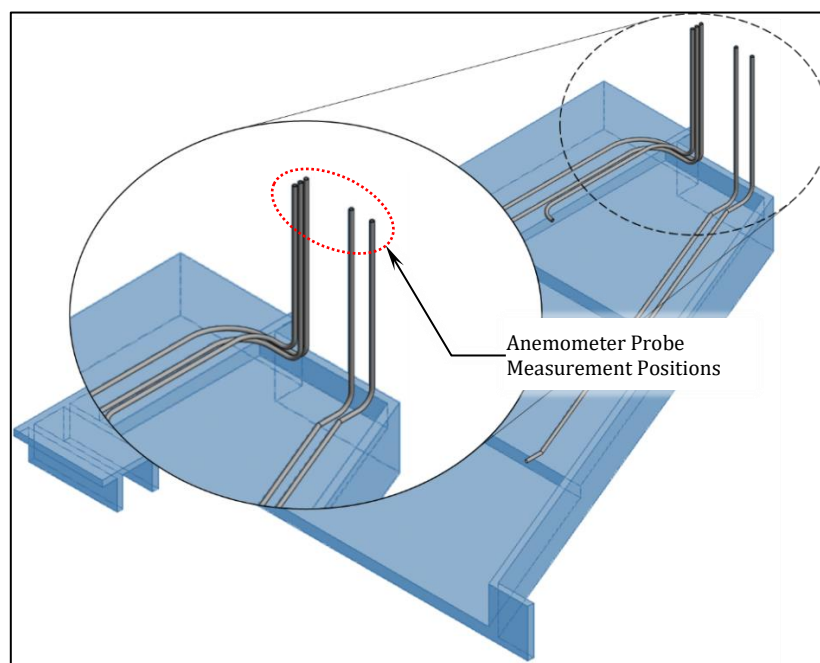


Figure 3.23: Airflow Measurement Positions

CHAPTER 4: TEST RESULTS

4.1. INTRODUCTION

This chapter contains the hydraulic model results and analyses, as well as a discussion on the performance of the model. The results are sorted according to the two different hydraulic model configurations (first model with chute wall intact and second model with the chute wall removed and riprap added). The results of the repeatability tests are also presented and discussed. The chapter is concluded with a discussion of the results and how the different model configurations compared with each other.

The model configurations with the corresponding test numbering convention used are summarised in Table 4-1.

Table 4-1: Test Number Convention

Model Configuration	Number of Culverts Open	Nappe Vents Open or Closed	Test Number	Model Low-level river crossing overflow depths (mm)				
				A	B	C	D	E
Stepped Chute with Chute Wall Intact	0	Closed	1.1.1	4	8	12	16	20
	0	Open	1.1.2	4	8	12	16	20
	0	Closed	1.1.3*	20				
	1	Closed	1.2.1	4	8	12	16	20
	1	Open	1.2.2	4	8	12	16	20
	1	Closed	1.2.3*	20				
Stepped Chute with side wall removed and riprap placed downstream of chute	0	Closed	2.1.1	4	8	12	16	20
	0	Open	2.1.2	4	8	12	16	20
	0	Closed	2.1.3*	20				
	1	Closed	2.2.1	4	8	12	16	20
	1	Open	2.2.2	4	8	12	16	20
	1	Closed	2.2.3*	20				

*Note: Test Numbers denoted with a * refers to repeatability tests performed*

The complete set of graphed pressure results, graphic illustrations of the model flow profiles and documented photographs are contained in APPENDICES E, F and G respectively.

4.2. RESULTS OF MODEL SETUP 1 (STEPPED CHUTE WITH WALL INTACT)

The results presented in this section are for the model with the stepped chute wall intact as illustrated in Figure 4.1.

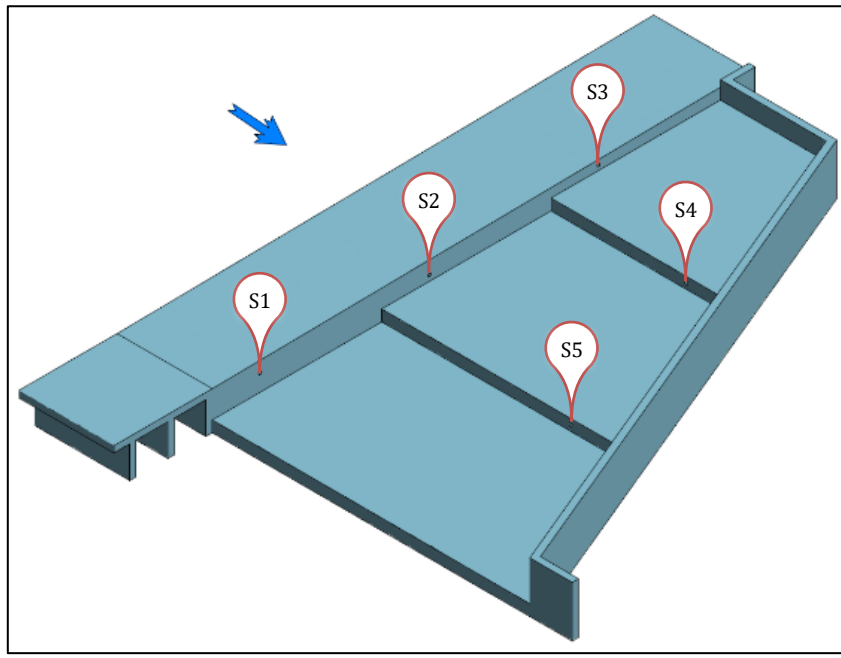


Figure 4.1: Hydraulic Model with Stepped Chute Wall Intact

4.2.1. Flow Profiles

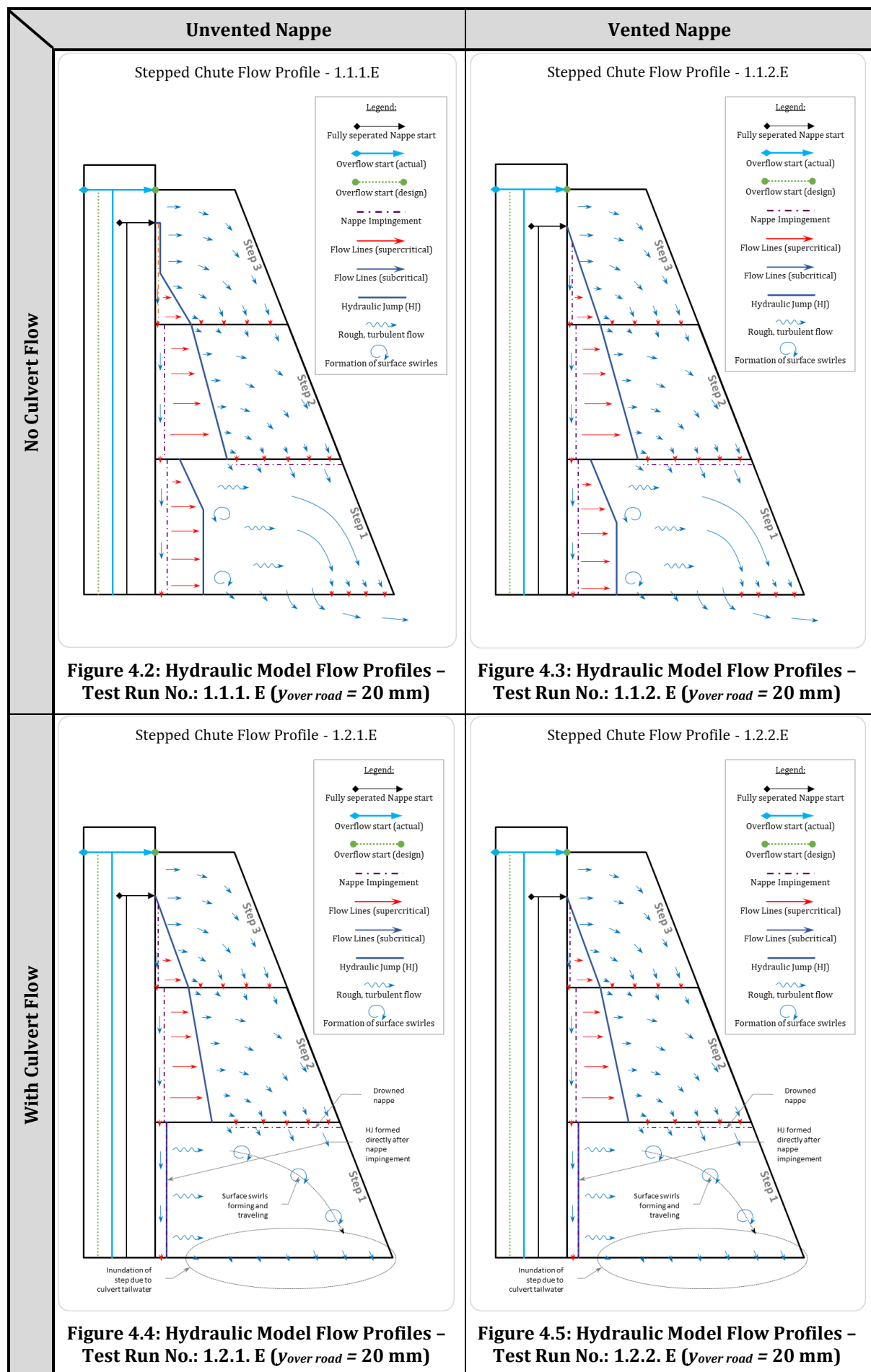
As mentioned in Section 3.6.4, the flow profiles on the stepped chute were recorded for each test run. The flow profiles with the maximum model overflow depth ($y_{over road} = 20 \text{ mm}$) for the unvented and vented model with no culvert flow and with culvert flow are illustrated in Figure 4.2 to Figure 4.5. The actual approach road overflow position, as well as the calculated design overflow position is also indicated for each test run.

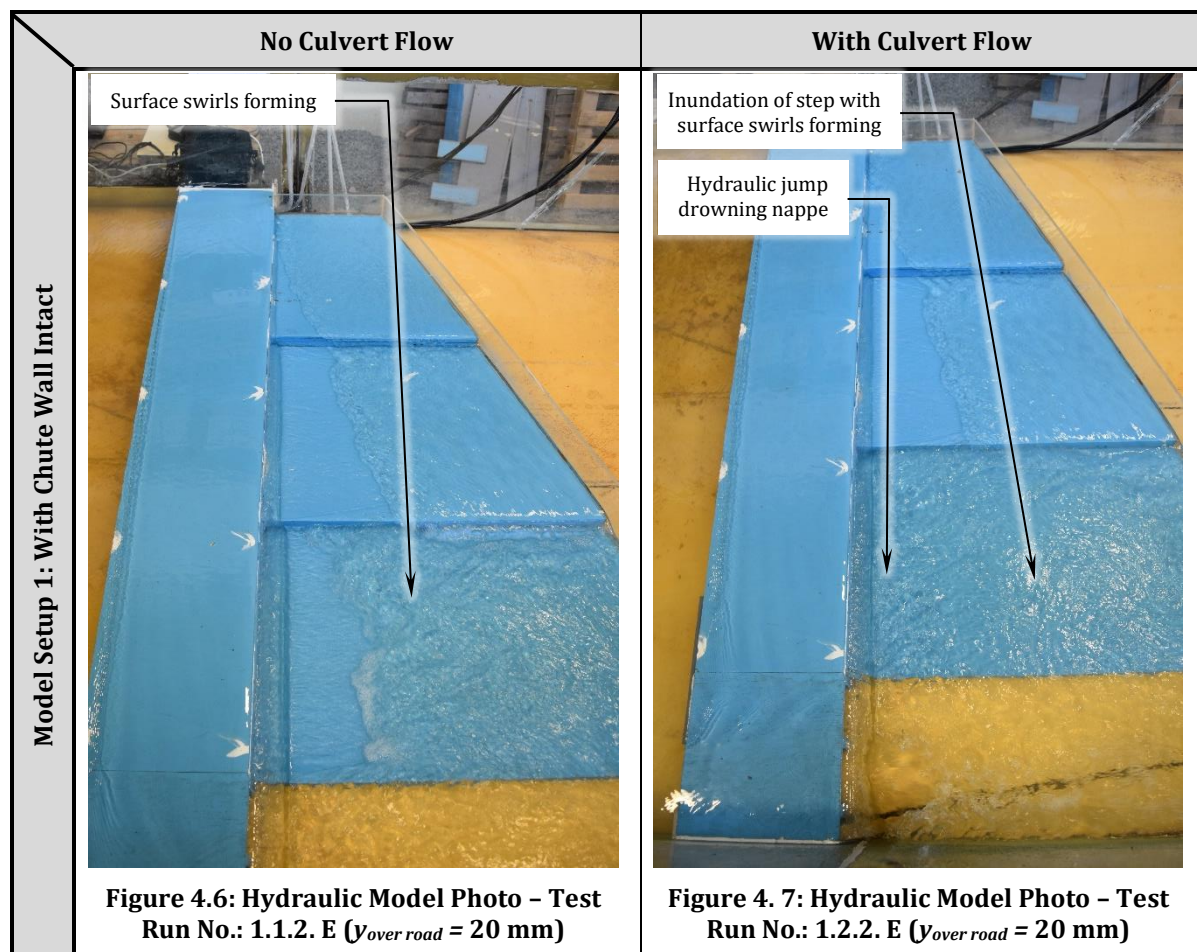
The flow profiles between the unvented and vented model seemed to correlate well in both instances with and without culvert flow. The first set of flow profiles without culvert flow (1.1.1.E and 1.1.2.E) mainly differed with the position of the hydraulic jump formation on step 3. The hydraulic jump positions on the remaining steps remained constant.

The second set of flow profiles with culvert flow, showed no apparent differences between the unvented (1.2.1.E) and vented (1.2.2.E) model. The effect of tailwater was, however, seen as step 1 was inundated, causing a partial hydraulic jump to form directly after nappe impingement on step 1. Surface swirls on step 1 could also be seen forming after the hydraulic jump and traveling towards the main channel.

Flow in the direction of the chute was also seen to form drowned nappes over the brink of step 3 and 2. Flow concentration from step 3 was, however, not enough to cause a separation between the step face and the nappe and therefore clung to the step face. A separated nappe was formed from step 2, but was drowned. The pool behind the nappe also submerged the ventilation pipe (V5) and the pressure sensor (S5).

Photographs of the model with and without culvert flow are illustrated in Figure 4.6 and Figure 4.7.





4.2.2. Pressure Behind the Nappe

The readings recorded for tests B to E (prototype overflow depths from 0.12 to 0.3 m) from transmitters S1 to S5 (as indicated in Figure 4.1) were converted to pressure heads, as discussed in Section 3.6.3.4. Test runs with the minimum prototype overflow depth of 0.06 m were not recorded as the nappe did not form from the approach road onto the steps. The calculated pressure heads were then scaled from model heads to equivalent prototype heads by multiplying the model head with the scale factor ($S = 15$). The equivalent prototype heads for prototype overflow depths from 0.12 to 0.3 m are listed in Table 4-2.

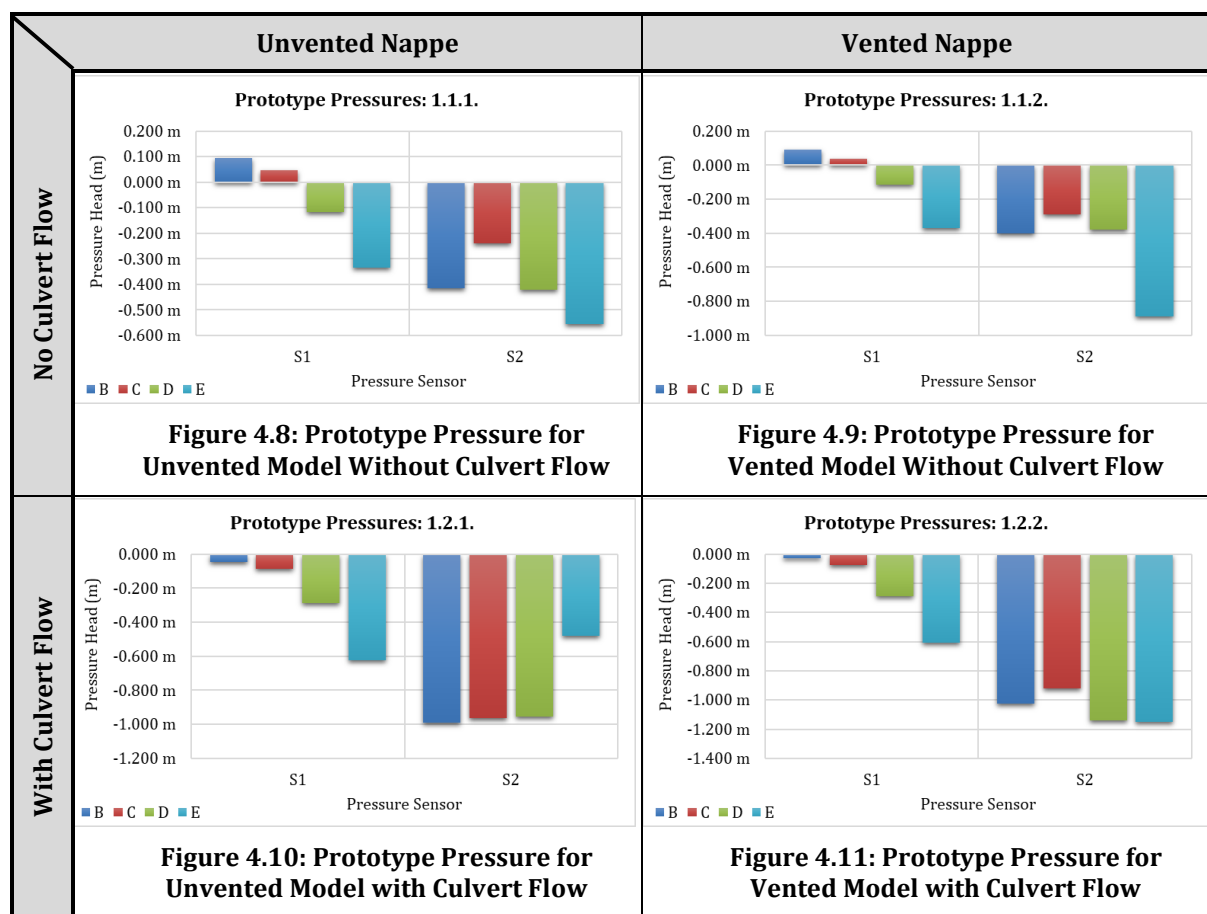
Table 4-2: Prototype Pressure heads for the Test Runs 1.1.1. to 1.2.2.

Transmitter	Test Run No.:	B ($y_{\text{over road}} = 0.12 \text{ m}$)	C ($y_{\text{over road}} = 0.18 \text{ m}$)	D ($y_{\text{over road}} = 0.24 \text{ m}$)	E ($y_{\text{over road}} = 0.3 \text{ m}$)
S1	1.1.1. (unvented) (no culvert)	0.094 m	0.046 m	-0.118 m	-0.335 m
S2		-0.414 m	-0.239 m	-0.422 m	-0.554 m
S3		0.040 m	0.028 m	0.104 m	0.194 m
S4		0.044 m	0.030 m	0.099 m	0.279 m
S5		0.037 m	0.092 m	0.298 m	0.311 m
S1	1.1.2. (vented)	0.093 m	0.036 m	-0.117 m	-0.370 m
S2		-0.403 m	-0.289 m	-0.379 m	-0.890 m

Transmitter	Test Run No.:	B ($y_{over road} = 0.12 \text{ m}$)	C ($y_{over road} = 0.18 \text{ m}$)	D ($y_{over road} = 0.24 \text{ m}$)	E ($y_{over road} = 0.3 \text{ m}$)
S3	(no culvert)	0.042 m	0.022 m	0.102 m	0.190 m
S4		0.048 m	0.032 m	0.098 m	0.300 m
S5		0.040 m	0.089 m	0.265 m	0.301 m
S1	1.2.1. (unvented) (with culvert)	-0.048 m	-0.087 m	-0.290 m	-0.622 m
S2		-0.989 m	-0.964 m	-0.954 m	-0.481 m
S3		0.029 m	0.034 m	0.099 m	0.180 m
S4		0.027 m	0.034 m	0.064 m	0.230 m
S5		0.038 m	0.079 m	0.265 m	0.499 m
S1	1.2.2. (vented) (with culvert)	-0.026 m	-0.077 m	-0.289 m	-0.608 m
S2		-1.024 m	-0.923 m	-1.138 m	-1.152 m
S3		0.014 m	0.008 m	0.100 m	0.207 m
S4		0.019 m	0.044 m	0.082 m	0.205 m
S5		0.036 m	0.080 m	0.296 m	0.522 m

As mentioned in Section 4.2.1 and illustrated in Figure 4.2 to Figure 4.5, a fully separated nappe formed only for flow from the approach road onto the chute steps and not from one step to another. The pressure sensors S4 and S5 were submerged and could therefore not measure negative pressures within the nappe cavity. The vent and pressure transmitter at position three (flow impinging from the approach road onto step 3) was also submerged during maximum flow conditions which meant that the S3 transmitter readings could not be used to measure negative pressures within the nappe cavity.

The pressure results for test cases B to E (model overflow depths 8 to 20 mm) are illustrated in Figure 4.8 to Figure 4.11. The pressure readings confirmed the presence of negative pressure behind a fully separated nappe. The S1 (lowest step, nappe impingement from approach road) transmitter was seen to have a gradual increase in negative pressure as the flow was increased for each test run, with the exception of no nappe formation for A and B (approach road model overflow depths of 4 and 8 mm respectively) which indicates pressures in proximity to atmospheric conditions. The increase in negative pressure is caused by the increase in discharge resulting in a higher rate of air removal from the nappe cavity.



The pressure readings from the S2 (flow impinging from approach road onto the middle step) transmitter, however, did not follow the same trend as the readings from transmitter S1. Seeing that the nappe forming from the road onto the stepped chute is a single barrel, as illustrated in Figure 4.12, measured pressures from transmitter S2 should closely resemble that of S1. This leads to the conclusion that transmitter S2 did not function as intended and was presumably faulty. The measured pressures of transmitter S2 could not be accepted as a true reflection of the nappe cavity pressures. Transmitter S1 was therefore used to describe the pressure behind the nappe from the approach road. The position of transmitter S1 also provided for data during lower road overflow depths due to its proximity to the culvert.



Figure 4.12: Downstream View of the Nappe Formation from the Approach Road onto the Stepped Chute

The prototype equivalent minimum, average and maximum pressure heads, from pressure sensor S1 (nappe cavity from approach road), for test runs 1.1.1. to 1.2.2. with prototype overflow depths of 0.12 to 0.3 m are graphically illustrated in Figure 4.13 to Figure 4.16.

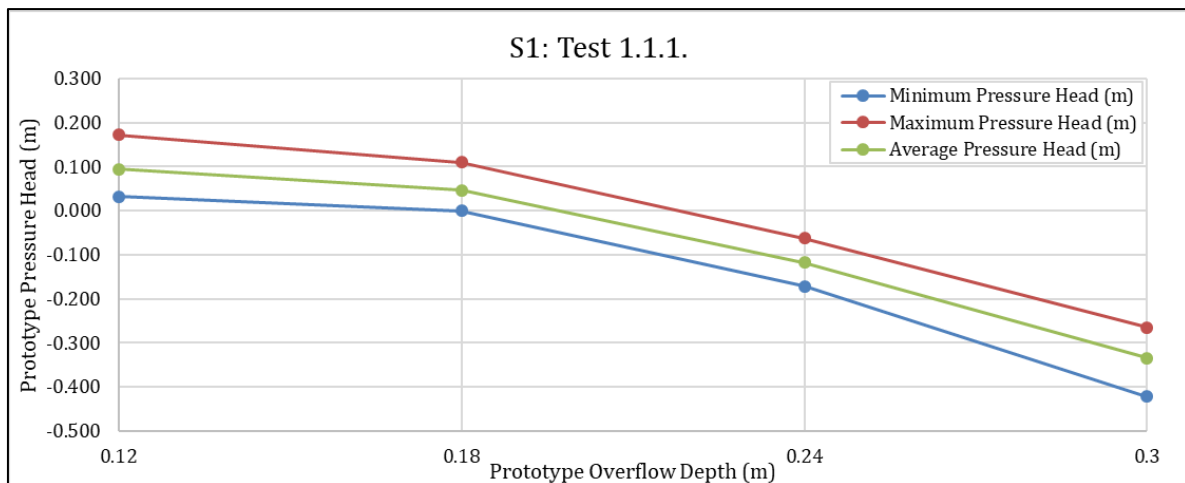


Figure 4.13: Summarised Prototype Nappe Cavity Pressures – Without Vents or Culvert Flow

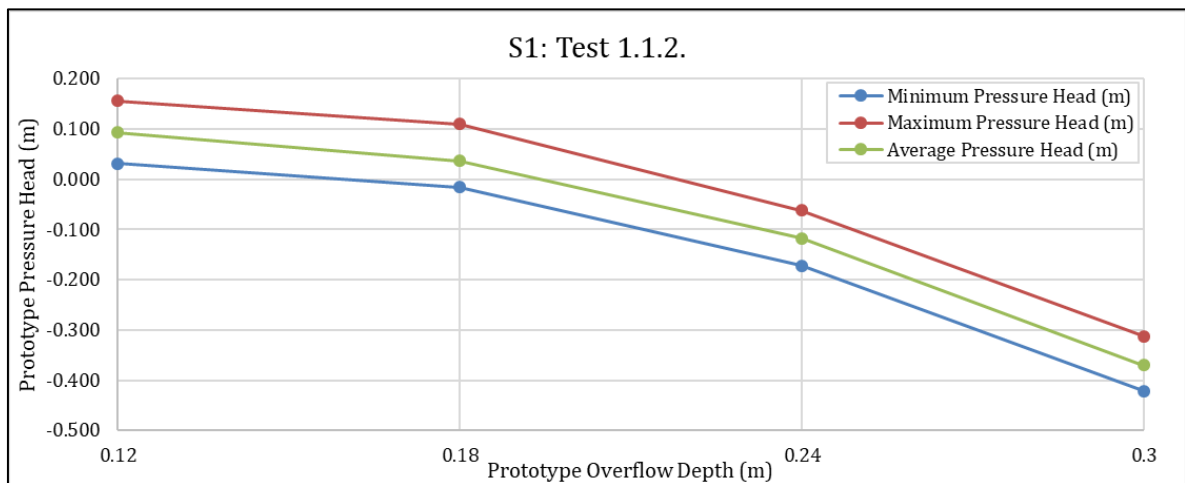


Figure 4.14: Summarised Prototype Nappe Cavity Pressures – With Vents, Without Culvert Flow

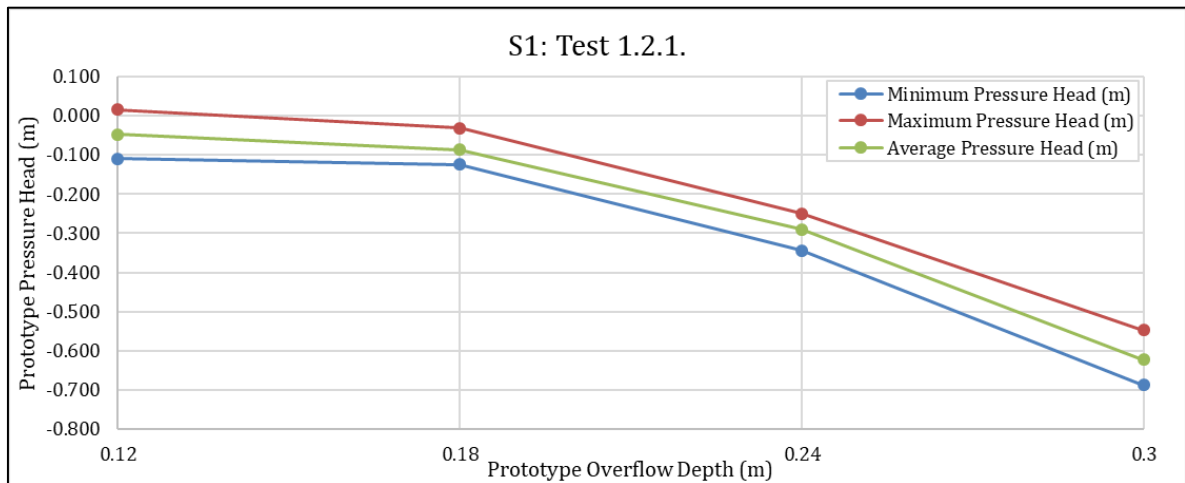


Figure 4.15: Summarised Prototype Nappe Cavity Pressures – Without Vents, With Culvert Flow

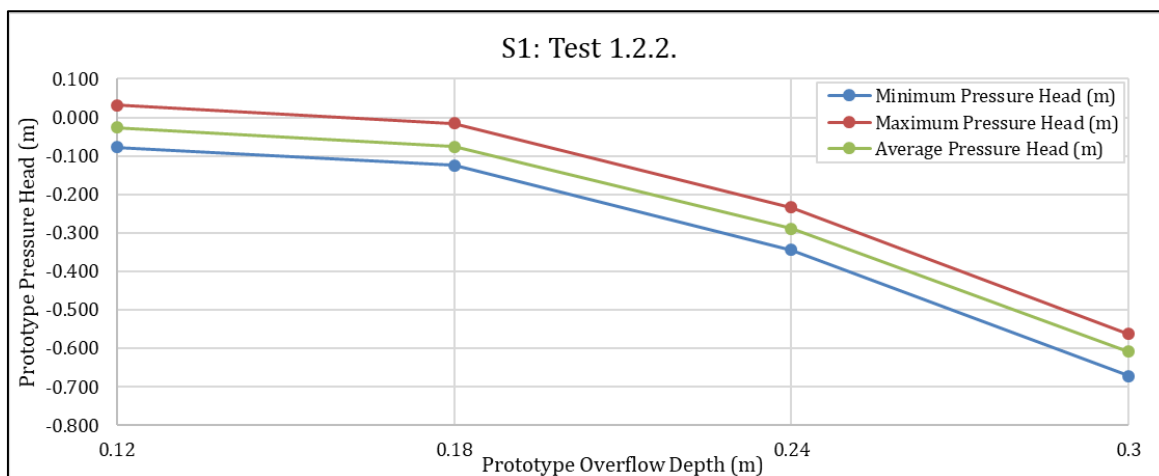


Figure 4.16: Summarised Prototype Nappe Cavity Pressures – With Vents and Culvert Flow

The unvented and vented model nappe pressures with- and without culvert flow are listed in Table 4-3.

Table 4-3: Model Setup 1 – Prototype Nappe Pressure Heads

Culvert Flow Conditions	Nappe Ventilation for Maximum Road Overflow Depth	
	Unvented Nappe	Vented Nappe
No Culvert Flow	-0.335 m	-0.370 m
With Culvert Flow	-0.622 m	-0.608 m

The pressure from the nappe forming directly after the approach road was of the same order of magnitude between the unvented and vented models. The average pressure behind the nappe for the tests without culvert flow (1.1.1.E and 1.1.2.E) was 0.35 m below atmosphere, and 0.62 m below atmosphere for tests with culvert flow (1.2.1.E and 1.2.2.E).

The significant difference in pressure was seen to be affected by the increase in tailwater levels between tests with culvert flow and without culvert flow. The reason the tailwater levels had such a pronounced impact on the nappe pressure is believed to be a function of the resulting nappe drop height. As the tests without culvert flow had a very low tailwater level, the nappe could more easily deform, thereby limiting the pressure drop. However, the tests with culvert flow, and therefore higher tailwater levels, had a shorter nappe drop height which could not deform as easily to accommodate the pressure drop as illustrated in Figure 4.17.

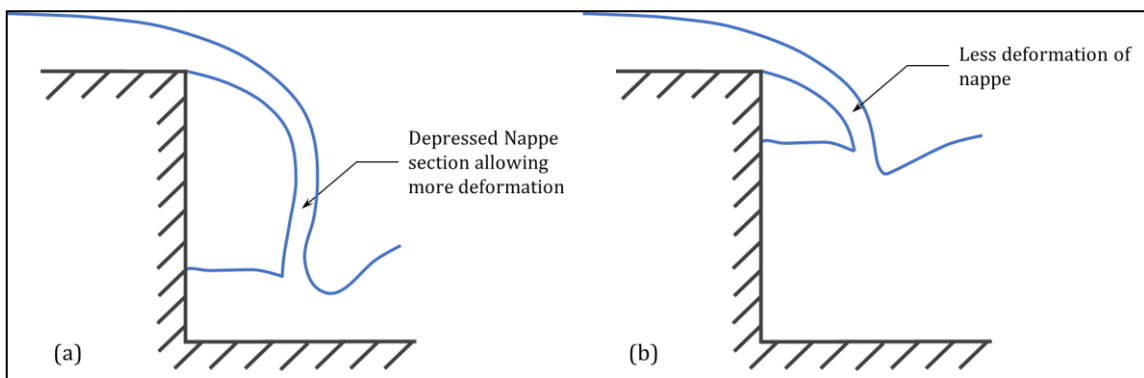


Figure 4.17: Nappe Deformation: (a) Low Tailwater Conditions; (b) High Tailwater Conditions

Chadwick *et al.* (2013) mentioned that the onset of cavitation is normally associated with the vapour pressure (~ 0.3 m sub-atmospheric at room temperature⁷) of a liquid, but due to dissolved gasses and small particles in suspension, cavitation damage may occur at higher pressures. They further advised that pressures not be allowed to fall below 3 m absolute (7 m below atmosphere). The maximum experienced sub-atmospheric pressure, recorded for pressure sensor S1, of 0.687 m (1.2.1.E - model without vents but with culvert flow) was within this margin and damage due to cavitation may therefore be disregarded.

Even though negative nappe cavity pressures were evident for tests without and with ventilation and for tests with and without culvert flow, no apparent changes in the flow profiles were noted. The positions where nappe hydraulic jumps formed, remained constant between unvented and vented states.

Complete collapse of the nappe from the approach road onto the steps was also not observed during tests. This leads to the conclusion that the addition of nappe ventilation did not influence the operation of the stepped chute and may be disregarded when designing the stepped chute.

4.2.3. Nappe Ventilation

As mentioned in Section 3.6.5, ventilation pipes were installed to ventilate the nappes. A Lutron hotwire anemometer was used to measure the airflow speed. The conduit inside diameter was known and could be used to determine the corresponding airflow.

Although the anemometer did not have the capability to indicate the direction of flow, it was safe to assume the direction would be towards the nappe and not from the nappe as explained in Section 2.4.1.

The air flow of each ventilation pipe was measured for the different overflow depths; however, a fully separated nappe only formed from the road to the stepped chute for test cases C to E

⁷ Calitz (2016)

(prototype overflow depths between 0.18 to 0.3 m) and no separated nappes formed on the chute steps.

The ventilation pipe V3 (top step, flow impinging from approach road) was submerged, due to a clinging nappe, for each test that had flow over vent V3 and therefore did not register any airflow. The airflow for ventilation pipes in the chute steps (vents V4 and V5) did not measure any flow as these ventilation pipes were submerged during test runs.

Given that the only separated nappe that formed was from the approach road onto the steps, the results for vents V1 and V2 (ventilation pipes for flow from the approach road onto step 1 and 2) were added to determine the total nappe airflow. The airflow was converted to equivalent prototype values as discussed in Section 2.5.3. The results of the combined airflow for V1 and V2 for test cases with nappe ventilation (1.1.2 and 1.2.2) are listed in Table 4-4 and can be seen in Figure 4.18.

Table 4-4: Prototype Nappe Ventilation Airflows

Test Run No. (Prototype overflow depth)	Total Prototype Airflow for Nappe from Approach Road to Stepped Chute (l/s)	
	1.1.2 (no culvert flow)	1.2.2 (with culvert flow)
C (0.18 m)	47.9	37.6
D (0.24 m)	102.7	61.6
E (0.3 m)	143.7	68.4

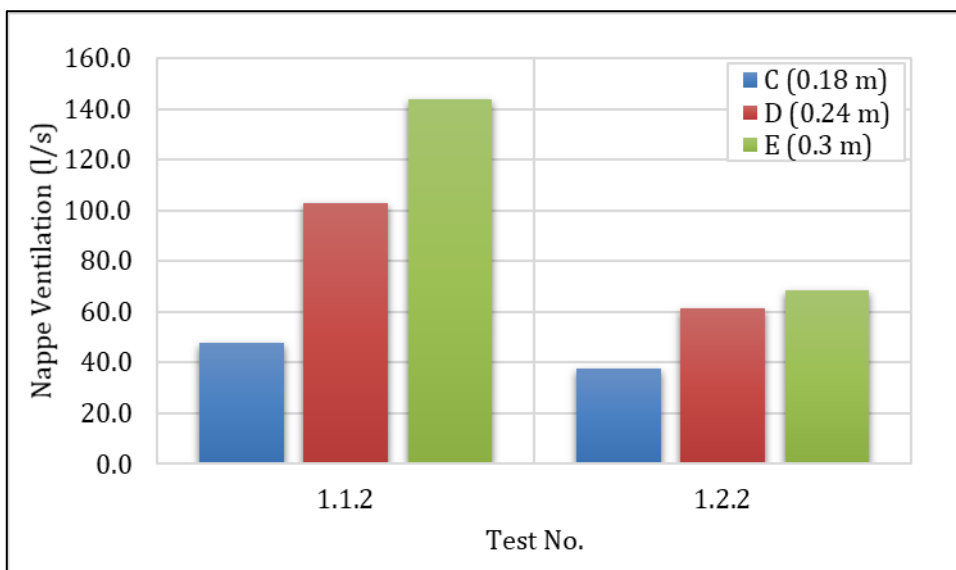


Figure 4.18: Total Prototype Nappe Ventilation Airflows – Model with Chute Wall

The nappe ventilation results for the first model setup (with the chute wall intact) indicated an increase in airflow as the approach road overflow depth, and corresponding discharge increased. This was caused by the pressure differential between atmospheric conditions and

the sub-atmospheric pressure within the nappe cavity. As the pressure differential increases (discussed in Section 4.2.2), so in turn does the rate of airflow. A decrease in the nappe ventilation was noted between tests without culvert flow and tests with culvert flow due to hydraulic ventilation of the nappe and is discussed in more detail in Section 4.5.3.

4.2.4. Brief Discussion of Stepped Chute with Wall Intact

The flow profiles on the stepped chute remained constant between unvented and vented test runs for both cases with and without culvert flow. The addition of culvert flow caused inundation of the bottom step and consequently causing a partial hydraulic jump to form immediately after the nappe. The inundation of the bottom step also caused highly turbulent flow conditions leading to surface swirls forming after the partial hydraulic jump and traveling to the main channel.

The pressures behind the nappe were found to be sub-atmospheric during tests where the nappe from the approach road to the steps were formed. The pressures remained within the same order of magnitude between tests with and without nappe ventilation (average prototype pressures of 0.35 m and 0.62 m below atmosphere for tests without culvert flow and tests with culvert flow respectively). An increase in sub-atmospheric pressure was, however, noted when culvert flow was added. The increase in sub-atmospheric pressure was believed to be due to increased tailwater levels reducing the ability of the nappe to deform with higher tailwater levels.

The nappe airflow was found to increase as the approach road discharge increased for both cases with and without culvert flow. A decrease in the nappe ventilation was noted as soon as the culvert flow was added due to the hydraulic transportation of air bubbles to the rear of the nappe as discussed in Section 4.5.3.

4.3. RESULTS OF MODEL SETUP 2 (STEPPED CHUTE WALL OMITTED, AND DOWNSTREAM RIPRAP ADDED)

The results presented in this section are for the model without the chute wall but with riprap downstream of the stepped chute as illustrated in Figure 4.19.

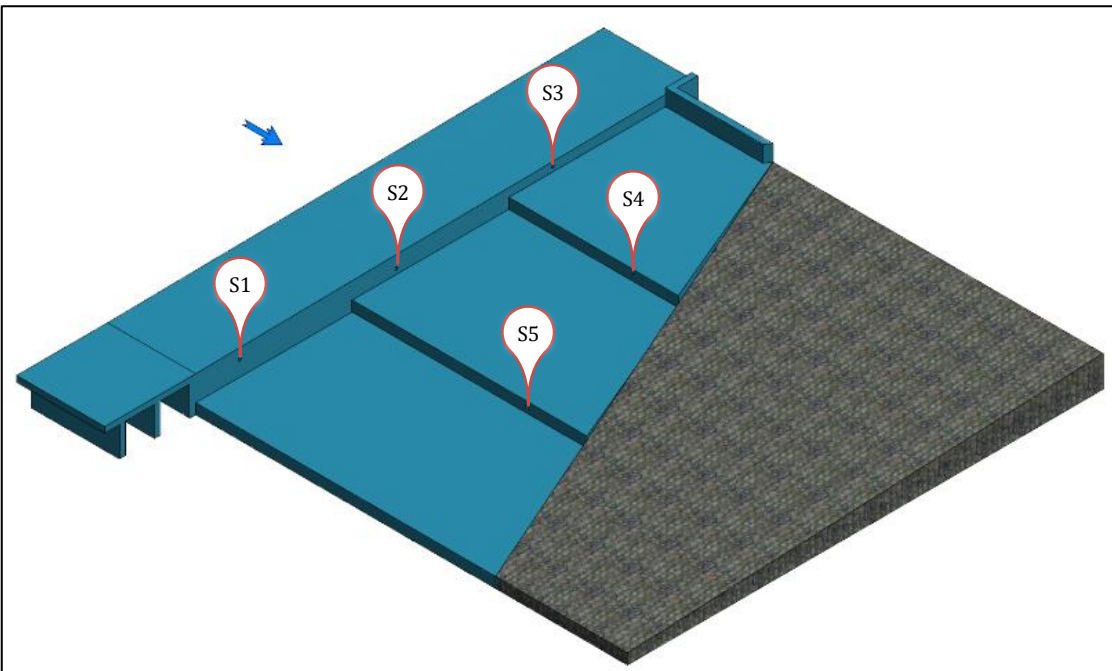


Figure 4.19: Hydraulic Model Without Stepped Chute Wall, and with Downstream Riprap Added

4.3.1. Flow Profiles

The flow profiles for the maximum model overflow depths ($y_{over road} = 20 \text{ mm}$) for the unvented and vented model with no culvert flow and with culvert flow are illustrated in Figure 4.20 to Figure 4.23. The actual overflow position as well as the calculated design overflow position is also indicated for each test run.

The flow profiles between the unvented and vented model compare well for both instances with and without culvert flow. The hydraulic jump positions on all three steps (steps 1 to 3) remained constant for the unvented and vented model during testing without culvert flow (2.1.1.E and 2.1.2.E). However, the effect of tailwater was evident as supercritical tailwater spilled onto step 1, joined the supercritical flow on step 1 and caused a standing wave.

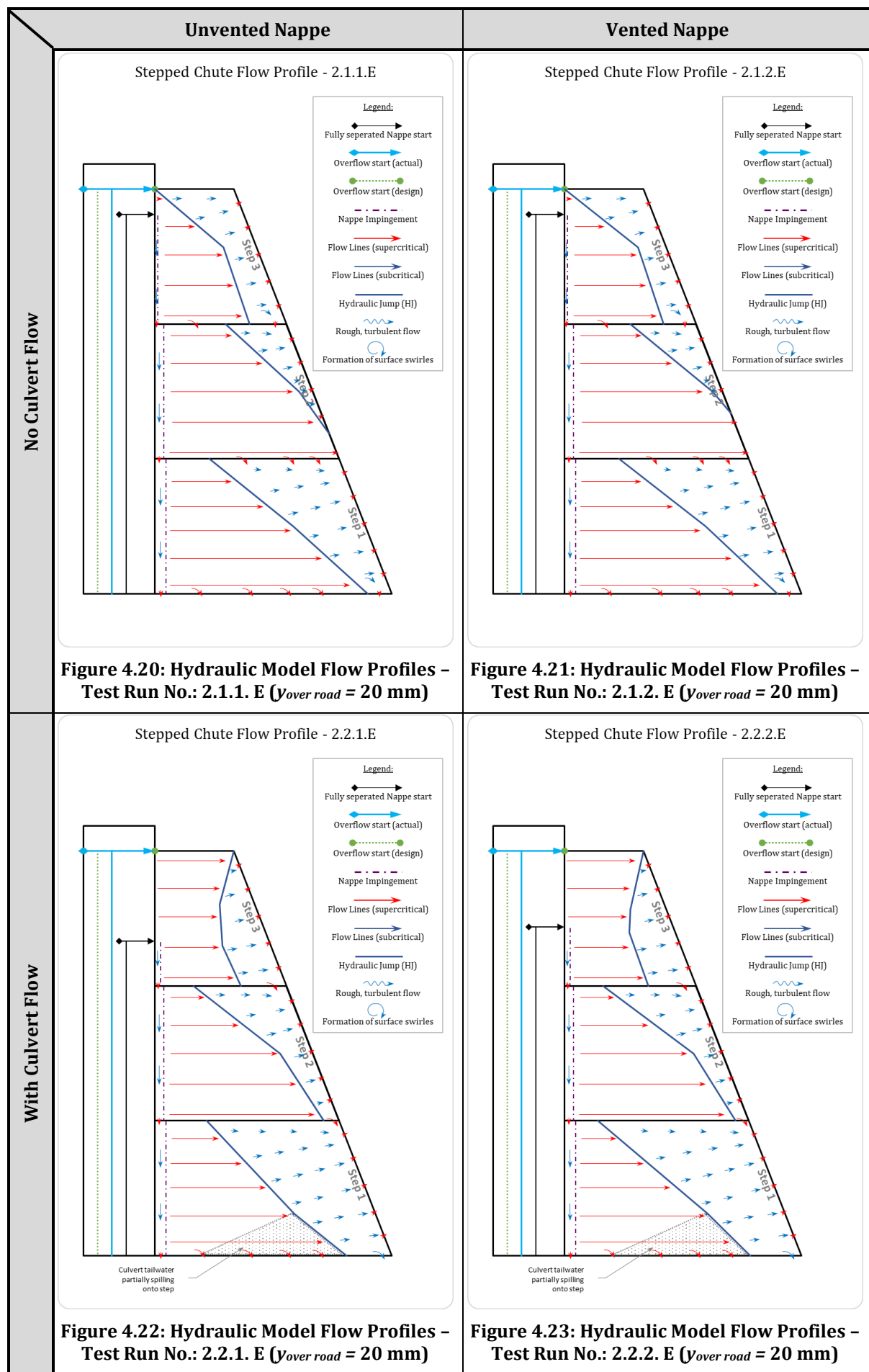
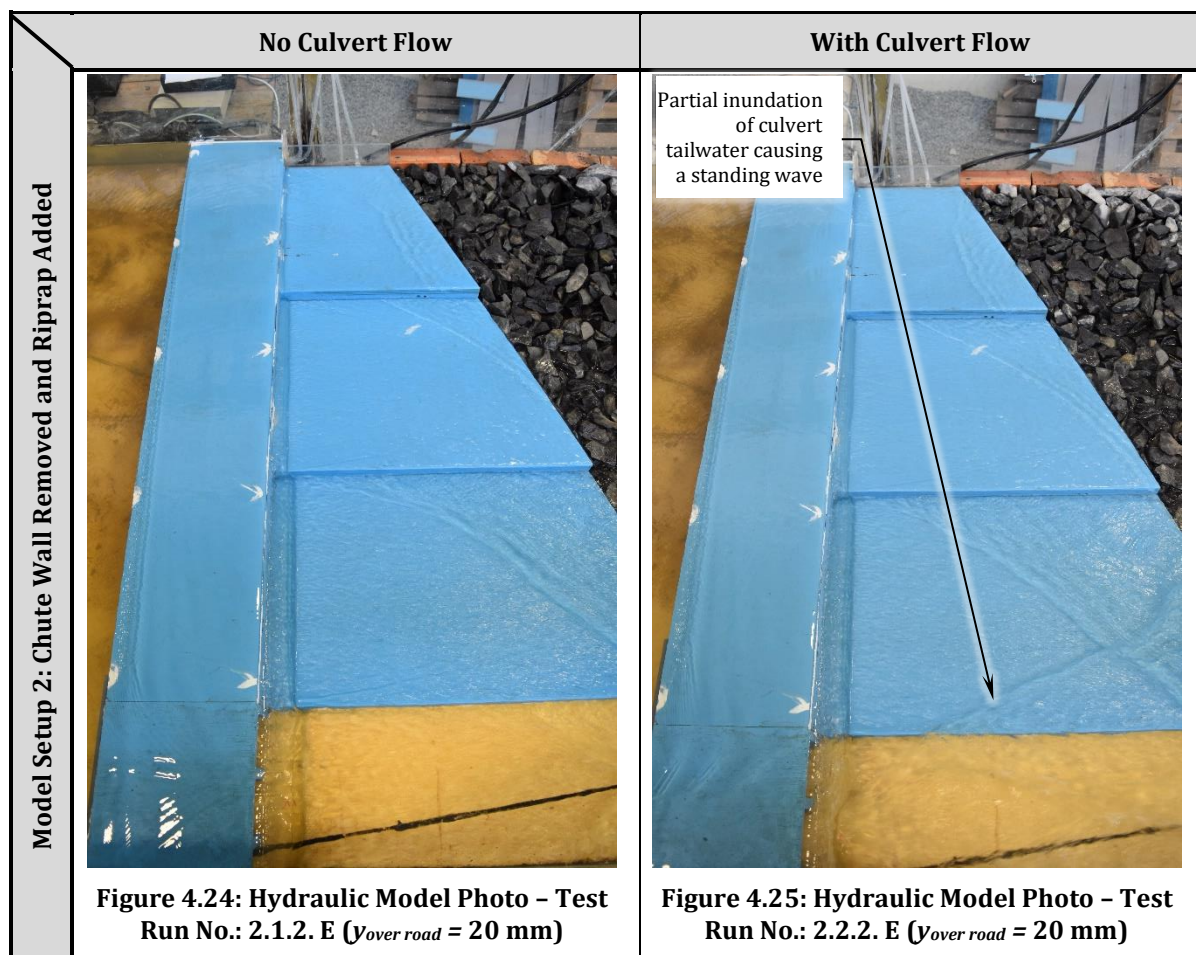


Figure 4.20 to Figure 4.23 illustrated that a nappe only formed from the approach road onto the steps for all instances with and without nappe ventilation and with and without culvert flow. No nappe formation was formed from one chute step onto the next. This was due to supercritical flow (that does not easily change direction), directly downstream of the nappe impingement from the approach road, that flowed for the majority of the step length until it formed a hydraulic jump. Little to no flow was seen to discharge from one chute step to the next and therefore not having any nappe formation from one chute step onto the next.

Photographs of the model with and without culvert flow is illustrated in Figure 4.24 and Figure 4.25.



The flow profiles from the first model configuration (chute with wall intact) was seen to have the hydraulic jump formed closely after nappe impingement whereas, for the second model configuration (chute wall omitted, and riprap added), the hydraulic jump moved further to the right as no accumulation of flow on the chute was encountered. The effect of culvert tailwater was present for the second model configuration but did not have the same level of inundation as for the first model configuration, again due to flow not being accumulated on the chute.

The hydraulic operation between the first and second model setup differed substantially, with the first model (with chute wall intact) accumulating the flow on the stepped chute and

channelling it to the main channel. The second model setup (with chute wall omitted) had weak hydraulic jump formation with instances of supercritical flow discharging from the chute steps onto the riprap.

4.3.2. Pressure Behind the Nappe

The readings recorded for tests B to E (prototype overflow depths from 0.12 to 0.3 m) from transmitters S1 to S5 (as indicated in Figure 4.19) were converted to prototype equivalent pressure heads, as discussed in Section 3.6.3.4 and are listed in Table 4-5. Test runs with the minimum prototype overflow depth of 0.06 m were not recorded as no nappe was formed from the approach road onto the steps.

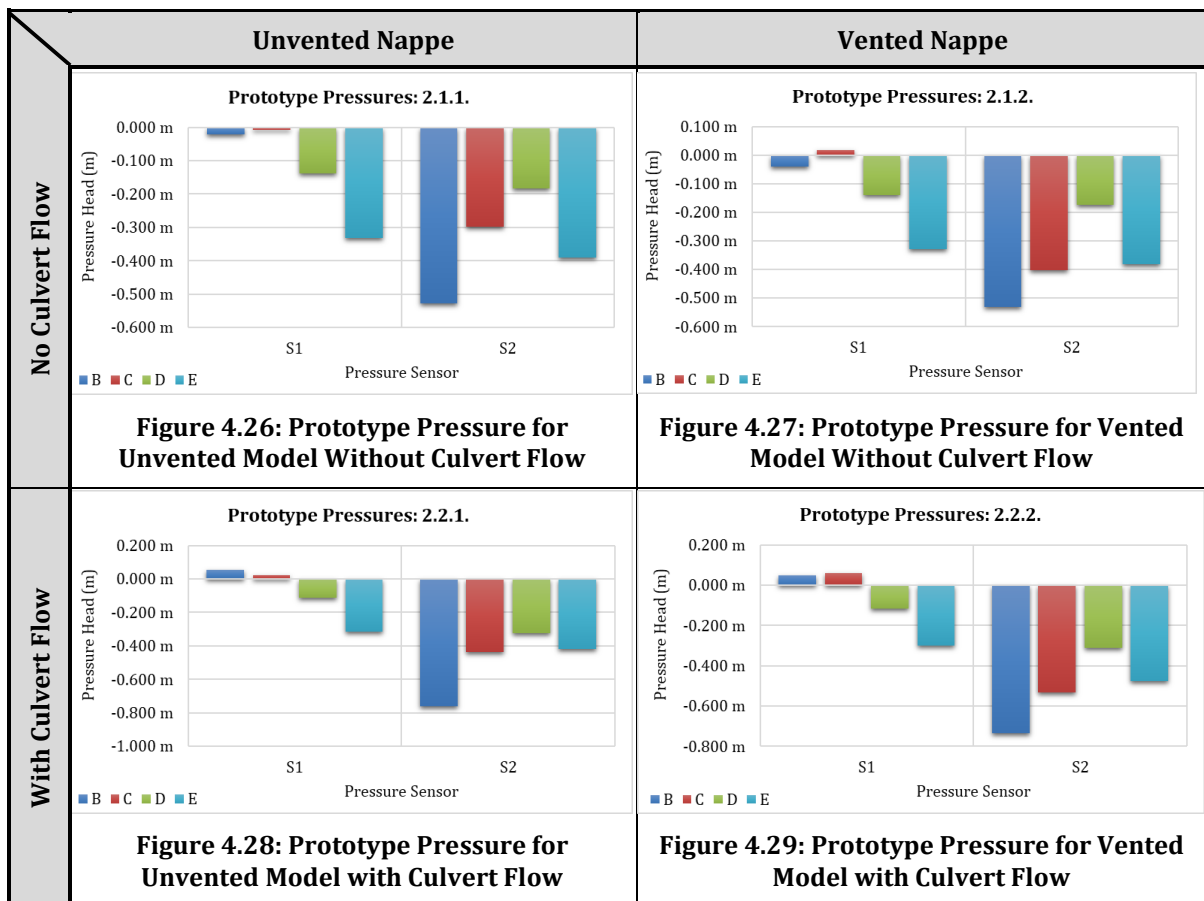
Table 4-5: Prototype Pressure heads for the Test Runs 2.1.1. and 2.2.2.

Transmitter	Test Run No.:	B ($y_{over road} = 0.12$ m)	C ($y_{over road} = 0.18$ m)	D ($y_{over road} = 0.24$ m)	E ($y_{over road} = 0.3$ m)
S1	2.1.1. (unvented) (no culvert)	-0.021 m	-0.008 m	-0.138 m	-0.332 m
S2		-0.528 m	-0.297 m	-0.183 m	-0.391 m
S3		0.038 m	0.014 m	0.104 m	0.199 m
S4		0.051 m	0.045 m	0.073 m	0.074 m
S5		0.028 m	0.058 m	0.093 m	0.115 m
S1	2.1.2. (vented) (no culvert)	-0.039 m	0.018 m	-0.139 m	-0.329 m
S2		-0.531 m	-0.403 m	-0.173 m	-0.381 m
S3		0.033 m	0.022 m	0.108 m	0.199 m
S4		0.044 m	0.051 m	0.065 m	0.075 m
S5		0.028 m	0.072 m	0.092 m	0.117 m
S1	2.2.1. (unvented) (with culvert)	0.052 m	0.022 m	-0.114 m	-0.315 m
S2		-0.763 m	-0.439 m	-0.324 m	-0.418 m
S3		0.035 m	0.034 m	0.103 m	0.203 m
S4		-0.221 m	-0.270 m	-0.011 m	-0.124 m
S5		0.031 m	0.044 m	0.099 m	0.102 m
S1	2.2.2. (vented) (with culvert)	0.048 m	0.059 m	-0.117 m	-0.299 m
S2		-0.734 m	-0.531 m	-0.311 m	-0.478 m
S3		0.032 m	0.023 m	0.099 m	0.205 m
S4		-0.212 m	-0.243 m	-0.028 m	-0.173 m
S5		0.030 m	0.064 m	0.098 m	0.114 m

It can be seen from Figure 4.20 to Figure 4.23 that a fully separated nappe only formed for flow from the approach road onto the chute steps and not from one step to another as discussed in Section 4.3.1. The vent and pressure transmitter at position three was also submerged due to a clinging nappe during maximum overflow conditions which meant that the S3 transmitter readings could not be used to measure negative pressures behind the nappe. As mentioned in

Section 4.3.1, very little flow discharged down the steps in the direction of the chute, resulting in no nappe formation between steps. Ventilation and pressure readings at positions four and five were therefore redundant.

The pressure results are illustrated in Figure 4.26 to Figure 4.29. The pressure readings again confirmed the presence of sub-atmospheric pressures behind a fully separated nappe. The S1 transmitter had a gradual increase in sub-atmospheric pressure as the flow was increased for each test run similar to what was observed for the first model setup discussed in Section 4.2.2.



The S2 pressure transmitter (flow impinging from approach road onto the middle step) did not follow the same trend as the readings from transmitter S1, similar to what was discussed in Section 4.2.2. Transmitter S1 was, therefore, used to describe the pressure behind the nappe from the approach road as pressure transmitter S2 was found to be faulty.

The prototype minimum, average and maximum pressure heads from pressure sensor S1 for test runs 2.1.1 to 2.2.2 with prototype overflow depths of 0.12 to 0.3 m are graphically illustrated in Figure 4.30 to Figure 4.33 .

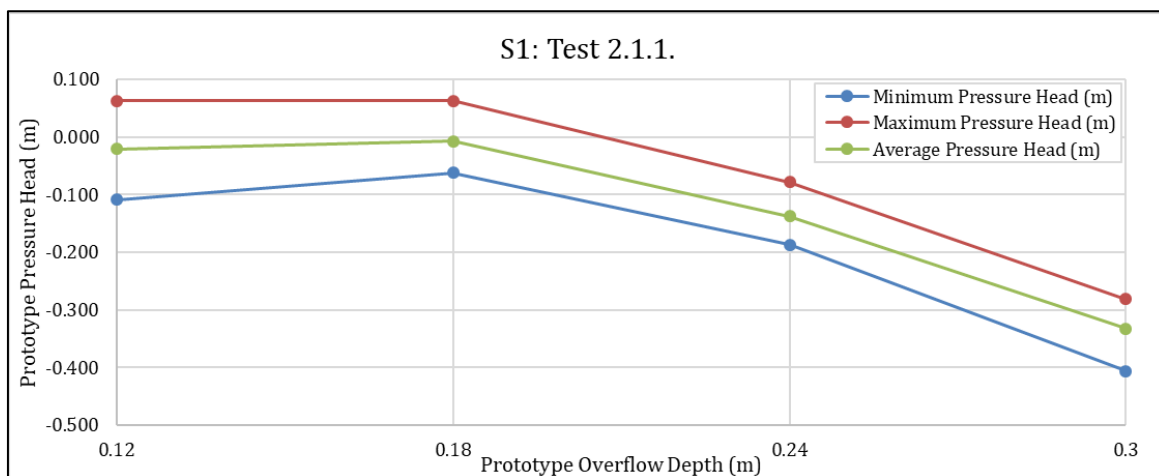


Figure 4.30: Summarised Prototype Nappe Cavity Pressures – Without Vents or Culvert Flow

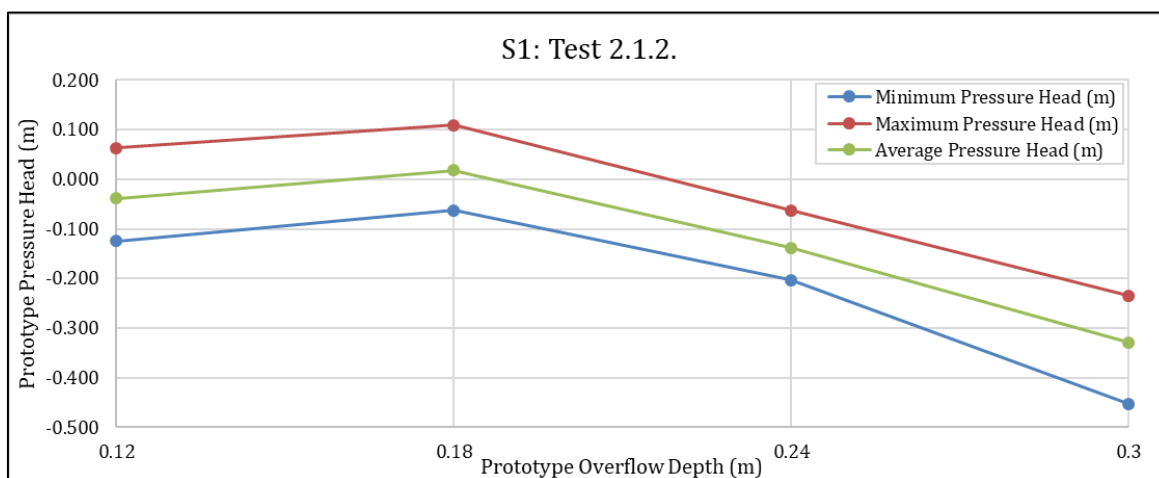


Figure 4.31: Summarised Prototype Nappe Cavity Pressures – With Vents, Without Culvert Flow

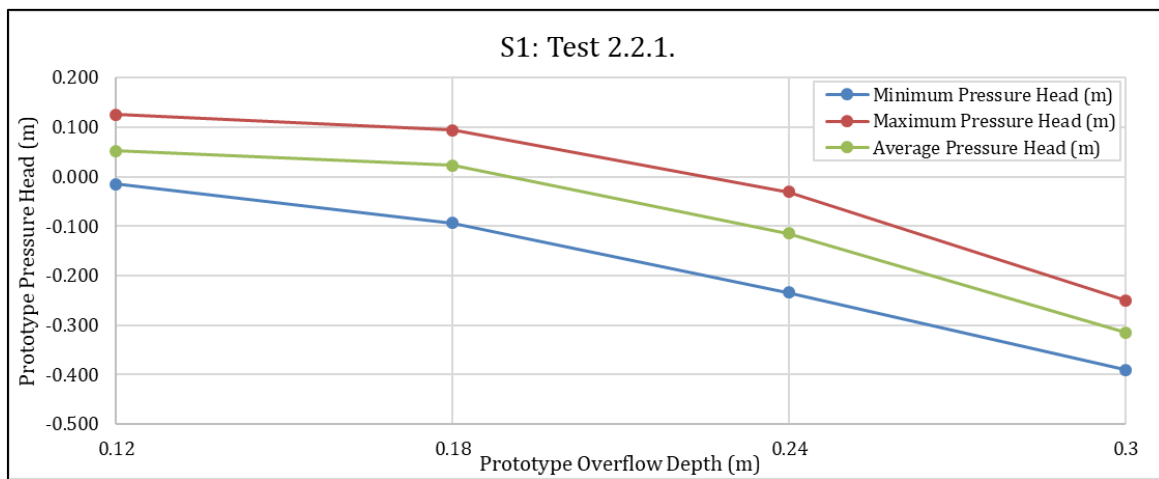


Figure 4.32: Summarised Prototype Nappe Cavity Pressures – Without Vents, With Culvert Flow

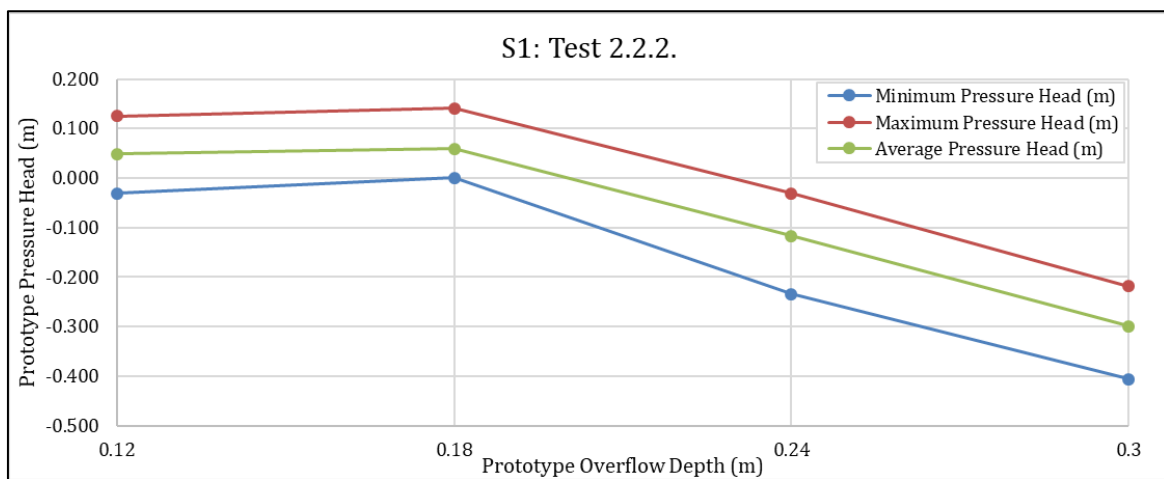


Figure 4.33: Summarised Prototype Nappe Cavity Pressures – With Vents and Culvert Flow

The unvented and vented model nappe pressures with- and without culvert flow are listed in Table 4-6.

Table 4-6: Model Setup 2 - Prototype Nappe Pressure Heads

Culvert Flow Conditions	Nappe Ventilation for Maximum Road Overflow Depth	
	Unvented Nappe	Vented Nappe
No Culvert Flow	-0.332 m	-0.329 m
With Culvert Flow	-0.315 m	-0.299 m

The pressure from the nappe forming directly after the approach road was of the same order of magnitude between the unvented and vented models for tests with and without culvert flow. The average pressure behind the nappe for the tests without culvert flow (2.1.1.E and 2.1.2.E) was 0.33 m below atmosphere and 0.31 m below atmosphere for tests with culvert flow (2.2.1.E and 2.2.2.E). Culvert tailwater therefore had no apparent effect on nappe cavity pressures as was the case with model setup 1 (chute wall intact). The tailwater did not reduce the nappe drop length, which allowed for nappe deformation, resulting in the same magnitude of nappe cavity pressures.

The maximum recorded sub-atmospheric pressure 0.453 m (2.1.2.E – with vents but without culvert flow) was well within the cavitation threshold, as discussed in Section 4.2.2, of 7 m below atmosphere, eliminating the possibility of cavitation damage.

4.3.3. Nappe Ventilation

The airflow was measured for each ventilation pipe but, similar to the discussion in Section 4.3.2 regarding the pressure readings, the nappe ventilation readings for vents V3 to V5 were redundant as each of these vents were either submerged or open to atmospheric conditions.

The results for vents V1 and V2 were again added to determine the total nappe airflow of the test cases with nappe ventilation (2.1.2 and 2.2.2). The nappe airflow results are listed in Table 4-7 and can be seen in Figure 4.34.

Table 4-7: Prototype Nappe Ventilation Airflows – Model without Chute Wall

Test Run No. (Prototype overflow depth)	Total Prototype Airflow for Nappe from Approach Road to Stepped Chute (l/s)	
	2.1.2 (no culvert flow)	2.2.2 (with culvert flow)
C (0.18 m)	61.6	34.2
D (0.24 m)	54.8	34.2
E (0.30 m)	109.5	61.6

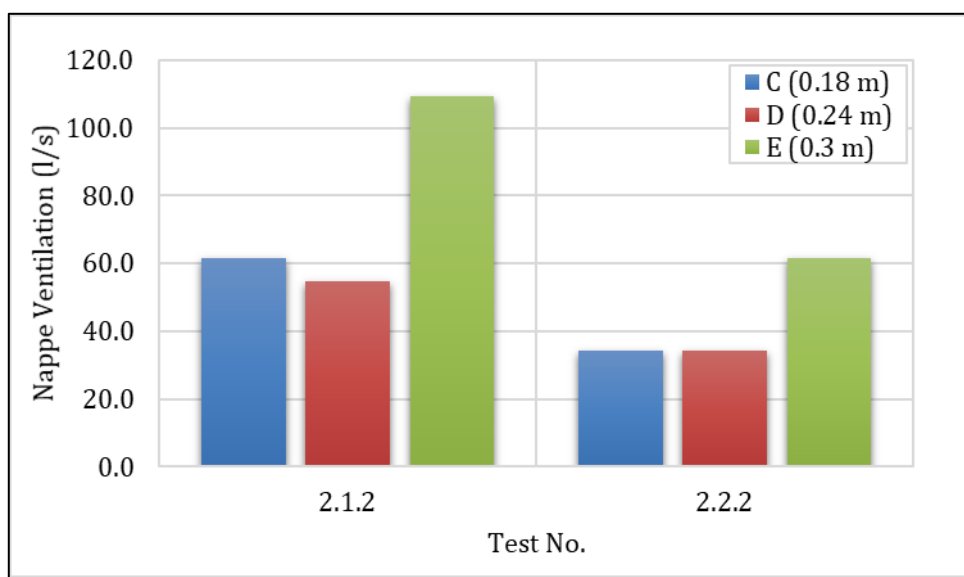


Figure 4.34: Prototype Nappe Ventilation Airflows – Model without Chute Wall

The nappe ventilation results for the second model setup (without the chute wall) indicated an increase in airflow as the approach road discharge increased with the exception of both C test cases (prototype approach road overflow depth of 0.24 m). The airflow was expected to follow the same trend as for the first model setup (stepped chute with wall intact), with an increase in airflow, and with an increase in overflow discharge.

The low quantity of airflow, and consequently low measured air velocities, were near the anemometer's minimum measurement limit of 0.2 m/s. The maximum measured air velocity for test cases with culvert flow was 0.5 m/s. An alternative method to measure the airflow with higher accuracy would possibly have verified the same trend as with the first model setup (stepped chute with sidewall intact).

4.3.4. Displacement of Riprap

None of the test runs where the chute wall was removed, and riprap was placed downstream of the stepped chute, had any indication of riprap displacement. Displacement of riprap only occurred during testing with all culverts open, causing an increased tailwater flow. This is discussed further in Section 4.5.5

4.3.5. Brief Discussion of Stepped Chute with Chute Wall Removed, and Downstream Riprap Added

The flow profiles remained constant between unvented and vented tests during cases with and without culvert flow. The effect of culvert tailwater was not as pronounced as for the first model setup (with chute wall intact). The test cases with culvert tailwater caused a small portion of supercritical culvert tailwater to spill onto the bottom step, joining the supercritical flow on the step and continuing to the hydraulic jump formation.

A decrease in nappe cavity pressures was noted as the approach road overflow discharge increased for test cases with and without nappe ventilation, as well as test cases with and without culvert flow. The average nappe pressure for the unvented and vented models, with and without culvert flow, was 0.319 m below atmosphere with little variation between the tests.

An increase in approach road overflow resulted in an increase in nappe airflow. A decrease in nappe airflow was also observed between tests without and with culvert flow. The addition of culvert flow resulted in the hydraulic transportation of air bubbles to the rear of the nappe, acting as an alternative source of air replenishment for the nappe cavity and is as discussed in Section 4.5.3.

Although changes in pressure and nappe airflow were evident for both model configurations (with and without chute sidewall), no apparent changes in the position of the hydraulic jump or flow conditions on the chute steps were noted between vented and unvented conditions.

No displacement of downstream riprap was noted indicating that smaller size riprap could be considered.

4.4. REPEATABILITY OF TESTS

As mentioned at the start of Chapter 3, the model testing consisted of four parts. The four parts comprised of two different model setups (chute with and without sidewall), each of which was tested with and without culvert flow. The four parts were tested with the ventilation pipes open and closed at five different flow depths. One test per part was repeated to verify that the data remained valid and no unforeseen changes to the hydraulic model, e.g. swelling and distortion of the marine ply, was experienced. Each repeatability test was undertaken with the maximum overflow depth (300 mm for the prototype) and the ventilation pipes closed. The

flow profiles on the stepped chute and the pressures behind the nappes were recorded and analysed.

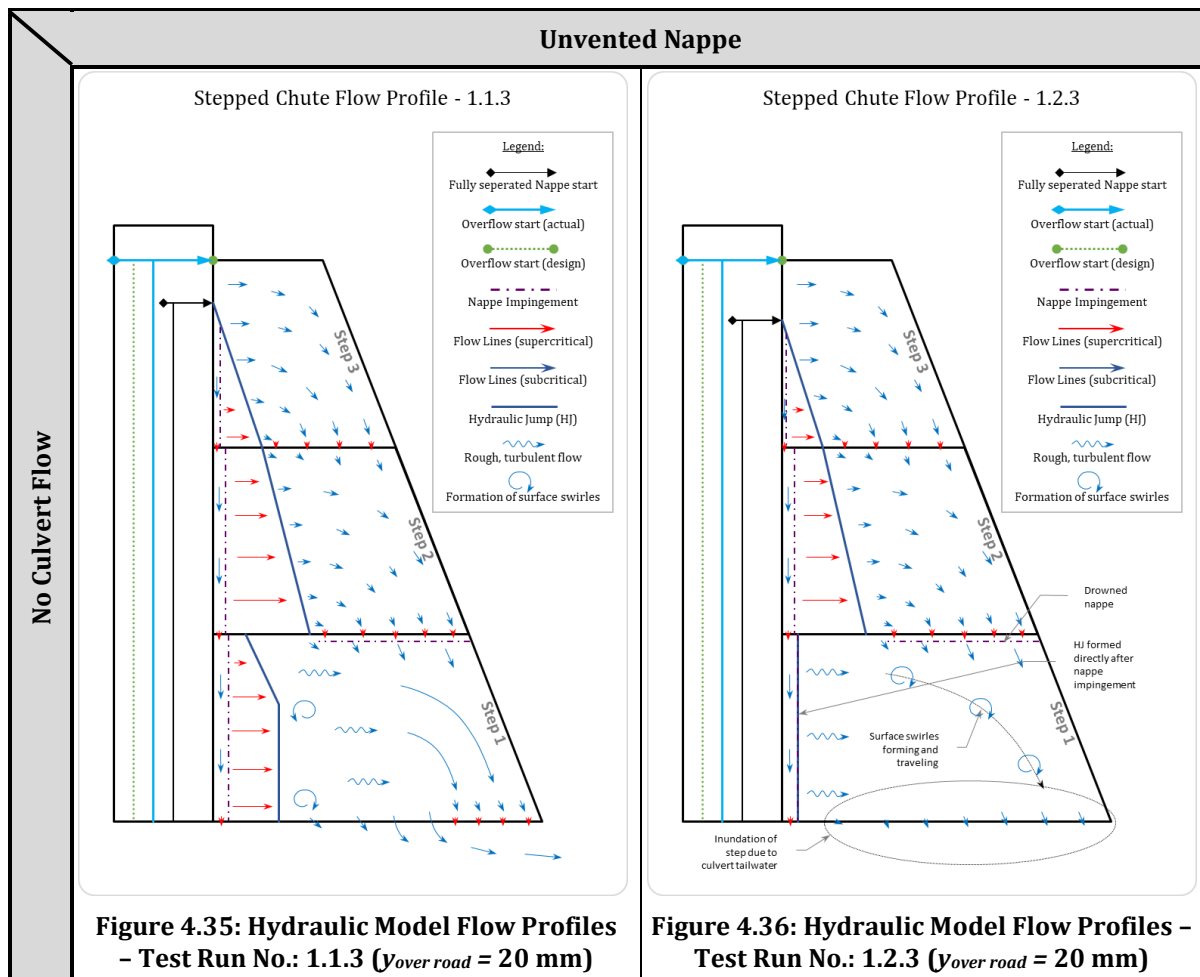
Table 4-8 lists the test runs and corresponding repeatability tests which were undertaken.

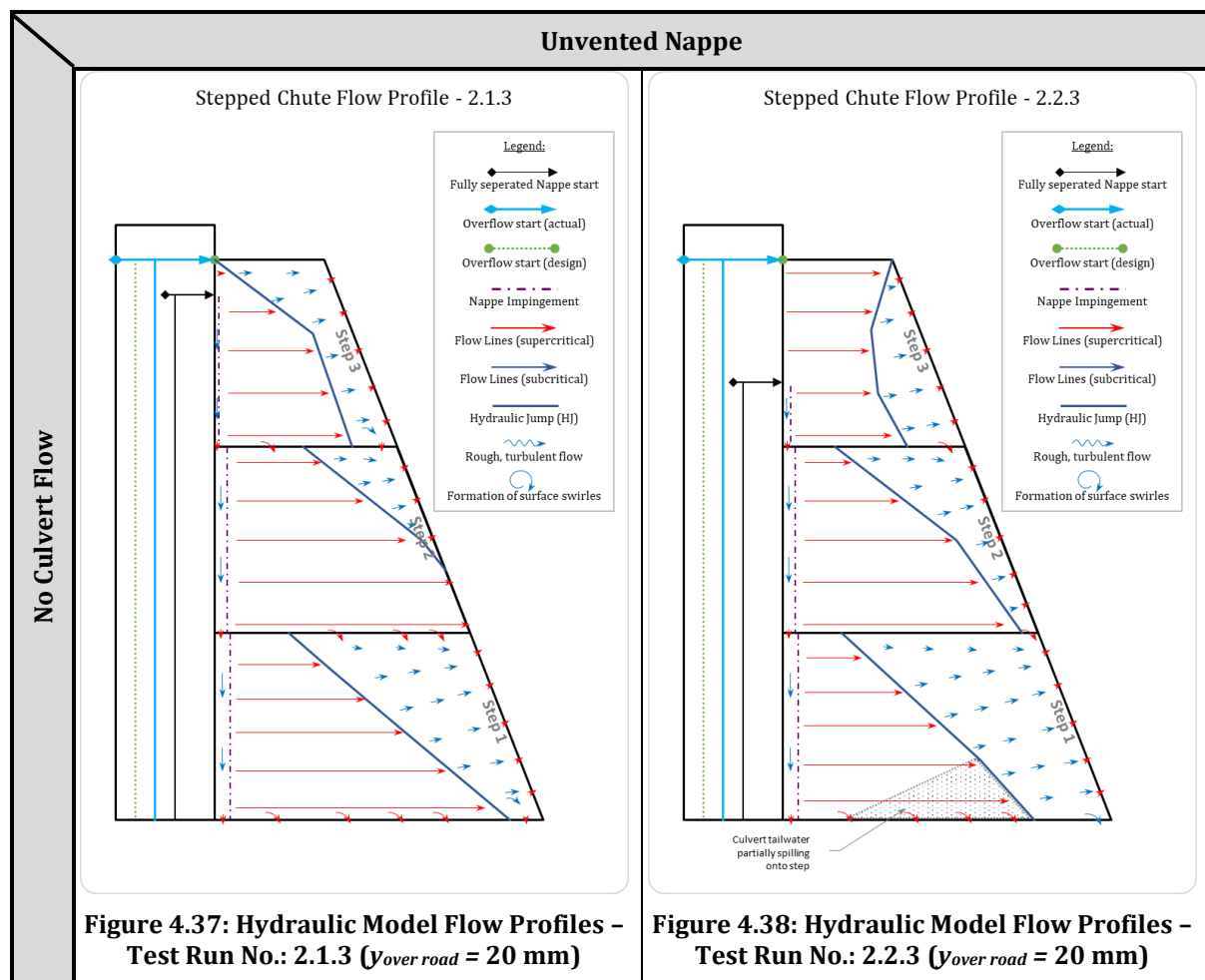
Table 4-8: Hydraulic Model Test Runs with Corresponding Repeatability Tests

Test Run	Repeatability Test	Test Conditions	Data Collected
1.1.1. E	1.1.3	<ul style="list-style-type: none"> • No nappe ventilation • No culvert flow 	<ul style="list-style-type: none"> • Flow profiles • Pressures behind the nappe
1.2.1. E	1.2.3		
2.1.1. E	2.1.3		
2.2.1. E	2.2.3		

4.4.1. Flow Profiles on Stepped Chute Steps

The flow profiles for the repeatability tests are illustrated in Figure 4.35 to Figure 4.38. The hydraulic jump positions are nearly identical between the normal tests and repeatability tests.





4.4.2. Pressure Behind the Nappe

The transmitter readings for both the normal tests and repeatability tests were converted to prototype equivalent pressures. The normal test run- (solid bars), and repeatability test (hatched bars) prototype pressure results are illustrated in Figure 4.39.

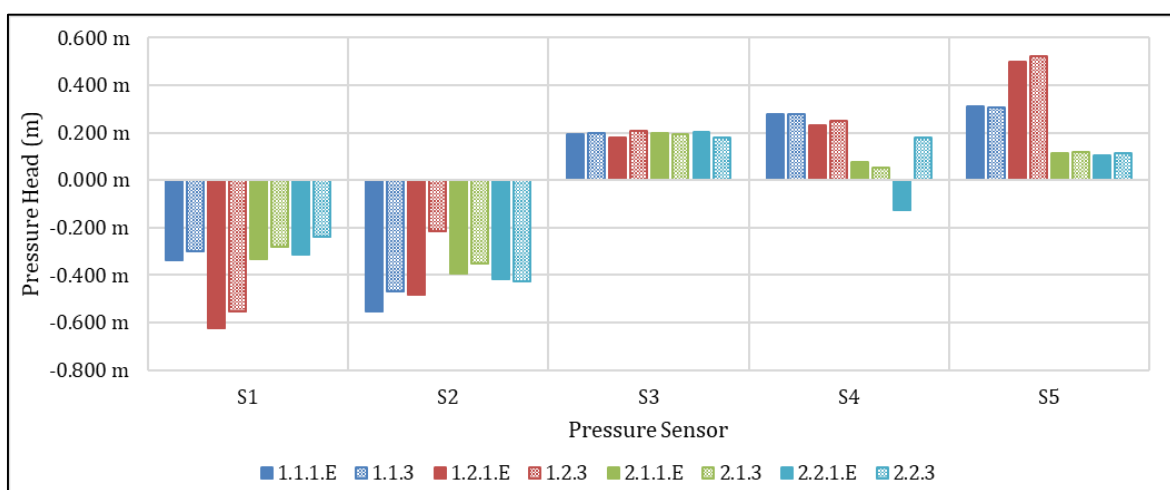


Figure 4.39: Prototype Pressure for Repeatability Tests

The percentage difference in pressures from the normal test and the repeatability test is summarised in Table 4-9.

Table 4-9: Prototype Pressure heads for Repeatability Tests

Transmitter	Test Run No.:			
	1.1.3	1.2.3	2.1.3	2.2.3
S1	-11%	-11%	-16%	-25%
S2	-16%	-55%	-10%	2%
S3	3%	16%	-2%	-11%
S4	-1%	9%	-32%	-245%
S5	-1%	5%	4%	14%

It is apparent from Figure 4.39 that there was a close correlation between the measured pressures for each normal test and the corresponding repeatability test, with the exception of pressure transmitter S4 which indicated a reading of 0.18 m for the repeatability test (2.2.3) and a -0.124 m reading for the normal test (2.2.1.E) (-245% difference) and for pressure transmitter S2 which indicated a reading of -0.217 m for the repeatability test (1.2.3) and -0.481 m for the normal test (1.2.1.E) (-55% difference). The reason for considerable differences in pressure for sensor S2 and S4 is believed to have been a loss of prime of the pressure transmitter tubes during setting and adjusting of the test flow rate.

4.5. ANALYSIS AND DISCUSSION

4.5.1. Comparison Between Vented and Unvented Hydraulic Models

A slight decrease in nappe pressure was experienced between tests without nappe ventilation and tests with nappe ventilation. A reduction in nappe airflow was also experienced between test runs without culvert flow and test runs with culvert flow.

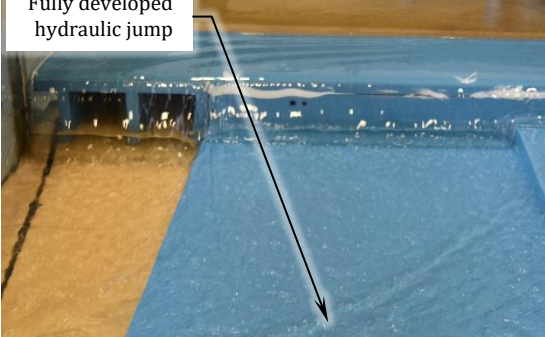
The nappe ventilation, from the approach road onto the steps, was considerably lower than the initial estimated prototype airflow of $0.225 \text{ m}^3/\text{s}$, determined in Section 3.4.3.3.

4.5.2. Comparison Between Two Different Hydraulic Models

The most notable difference between the two model configurations (with and without chute sidewall) was the flow profiles on each of the chute steps with the first model setup having shorter supercritical flow lengths before the hydraulic jump formed when compared to the second model setup.

For the first model setup (with the chute sidewall intact), the average pressure behind the nappe for the tests without culvert flow (1.1.1.E and 1.1.2.E) was 0.35 m below atmosphere and 0.62 m below atmosphere for tests with culvert flow (1.2.1.E and 1.2.2.E). For the second model setup (without the chute sidewall), the average pressure behind the nappe for the tests without culvert flow (2.1.1.E and 2.1.2.E) was 0.33 m below atmosphere and 0.31 m below atmosphere for tests with culvert flow (2.2.1.E and 2.2.2.E).

The differences in nappe pressures indicate that the first model setup was more sensitive to the addition of culvert flow whereas the second model setup was not. When viewing Figure 4.40 to Figure 4.43, it was apparent that test run 1.2.2.E ($y_{over road} = 20 \text{ mm}$) was the only test run where the partial hydraulic jump drowned the nappe impingement and drowned the culvert tailwater. Both model setups indicated a decrease in the nappe airflow between tests without culvert flow and tests with culvert flow.

	No Culvert Flow	With Culvert Flow
Model Setup 1: Chute Wall Intact	$H_{nappe} = -0.37 \text{ m}; Q_{air} = 143.7 \text{ l/s}$ 	$H_{nappe} = -0.61 \text{ m}; Q_{air} = 68.4 \text{ l/s}$ 
Model Setup 2: Chute Wall Removed	$H_{nappe} = -0.33 \text{ m}; Q_{air} = 109.5 \text{ l/s}$ 	$H_{nappe} = -0.299 \text{ m}; Q_{air} = 61.6 \text{ l/s}$ 

4.5.3. Notable Observations

4.5.3.1. Flow behind the nappe

During all the test runs where a fully separated nappe formed, it was noted that flow towards the main channel, behind the nappe, occurred and is illustrated in Figure 4.44. This resulted in a reduction in flow continuing to the hydraulic jump after nappe impingement.

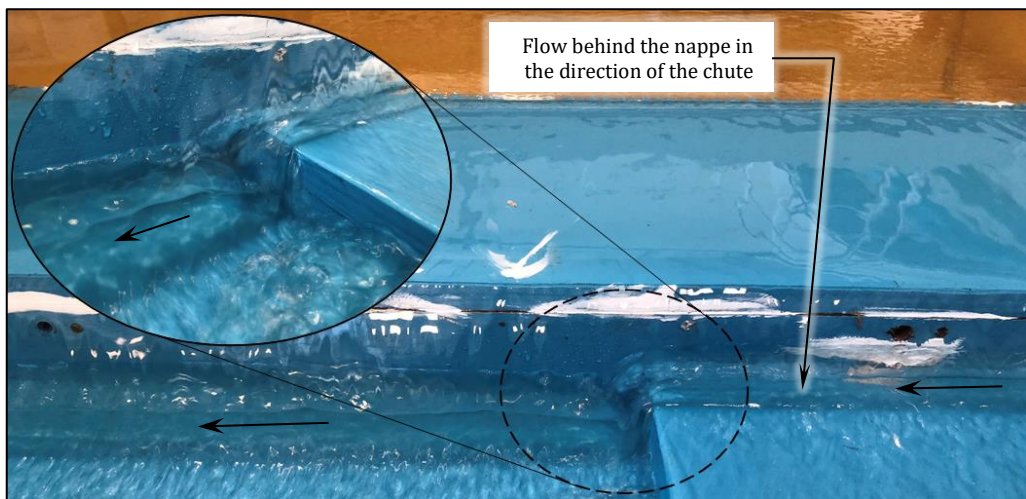


Figure 4.44: Flow Down the Chute Steps Behind the Nappe

4.5.3.2. Hydraulic ventilation of the nappe

It was observed, during tests that included culvert flow, that the nappe intersecting with the flow exiting the culvert, caused turbulence and lead to breakaway air bubbles which were transported along the intersection line to the rear of the nappe, thereby hydraulically ventilating the nappe. Although the quantity of air was not measured, it seemed to be an alternate source of nappe ventilation which would explain the reduction in nappe airflow requirement for tests with culvert flow compared to tests without culvert flow (for both model configurations – with chute wall intact and removed).

Figure 4.45 and Figure 4.46 illustrate the difference between the nappes downstream of the culvert. It can be seen from Figure 4.45 that no air bubble were formed downstream of the culvert whereas in Figure 4.46, the intersection line forms a string of air bubbles that is then transported in the directions indicated with the red arrows. Some of the air bubbles were transported to the rear of the nappe while others were merely transported further downstream.

No Culvert Flow	With Culvert Flow
	
Figure 4.45: Nappe Impingement without Culvert Flow ($y_{over road} = 20 \text{ mm}$)	Figure 4.46: Nappe Intersection with Culvert Outflow ($y_{over road} = 20 \text{ mm}$)

4.5.4. Discussion on the Hydraulic Model Performance with One Open Culvert

Model Setup 1: Model with Chute Wall Intact

The first model setup (with the chute wall intact) had short supercritical flow lengths before a hydraulic jump was formed. This length was influenced by the subcritical flow regions downstream of the hydraulic jumps. The flow on step 1 (bottom step) was also affected by culvert tailwater levels, causing the partial hydraulic jump to form directly downstream of the nappe impingement, rather than fully developed hydraulic jumps. The higher chute steps (step 2 and 3) were unhindered as they were not inundated.

Sub-atmospheric conditions were noted during testing but was still well within the cavitation threshold. The addition of nappe ventilation did not have any effect on the flow profiles and can therefore be disregarded during the design of a stepped chute in combination with a low-level river crossing.

The model performed well with the test runs excluding culvert flow. However, the addition of culvert flow and resulting tailwater conditions, for model setup 1 (with chute sidewall), indicated the importance of tailwater effects. Increased tailwater levels caused inundation of the bottom step. A partial hydraulic jump was, therefore, formed which drowned the nappe impingement on the bottom step. Measures to cater for high levels of tailwater that could be incorporated in the prototype design are briefly discussed in Section 4.5.5.

Model Setup 2: Model with Chute Wall Removed and Riprap Added

The second model setup (with the chute wall removed and riprap added) had longer supercritical flow lengths mainly due to the downstream water being quickly discharged after the hydraulic jump formation. There were also sections where the jump was not completely formed for the entire flow width. Flow was discharged under supercritical conditions from the stepped chute onto the riprap. This indicates the necessity of downstream riprap. The alternative could also be to increase the length of the chute steps in the direction of the main channel flow, but this would only resolve the problem for design flows and not flows exceeding design capacity. The observations from model setup indicated that the length and size of the riprap used in the prototype could, however, be further decreased and optimised.

The first model setup (with chute wall intact) was deemed to be the better option as the flow was contained on the chute, which caused stronger hydraulic jumps to be formed, leading to higher rates of energy dissipation. The flow was also channelled back to the main channel flow in a controlled manner, completely removing the necessity of adding riprap downstream of the chute.

4.5.5. Discussion on the Hydraulic Model Performance with All Culverts Open (2.5)

An additional separate test run was executed with all the culverts open (2.5 culverts) at a model flow rate of 27 l/s. This flow rate corresponded to a prototype flow rate that would still result in an overflow depth of 300 mm.

The operation of the model with all the culverts open was seen to cause excessive tailwater which completely inundated the bottom step (step 1) for both cases where the chute wall was intact and removed. A partial hydraulic jump formed directly after nappe impingement on step 1. This indicated that the prototype design should make provision for higher tailwater conditions by either:

- reducing the step heights in order for the bottom step to be higher, relative to the main channel floor;
- reducing the width of each step, which would offset the bottom step (step 1) from the closest culvert opening; or
- a combination of both, reducing the step height and length.

For instances where the chute wall was removed, and downstream riprap was added, the inception of riprap displacement at the toe of the riprap embankment was noted. This region is exposed to the high flow velocities from the main channel as well as the flow coming from step 1. The riprap thickness at this point comprised of a single layer of the riprap material ($D_{100} = 53$ mm), which was the minimum recommended thickness.



Figure 4.47: Downstream View of Step 1 with Culvert Tailwater and Riprap

In conclusion, the first model setup (with chute wall intact) was found to be the better performing configuration. Although sub-atmospheric nappe cavity pressures were present, they were still well within the cavitation threshold. No collapsing of the nappe was present either. The addition of nappe ventilation did not have any noticeable improvement on the model performance and can therefore be omitted.

CHAPTER 5: REGRESSION ANALYSIS

5.1. INTRODUCTION

This chapter contains the dimensional- and regression analyses using the hydraulic model test variables. The analyses were executed for the first model setup (with chute sidewall) as it was considered to be the better performing configuration. The chapter concludes with a set of equations which will enable the reader to determine the dimensions of a low-level river crossing stepped chute.

5.2. DIMENSIONAL ANALYSIS

Dimensional analysis involves the identification of relationships between different physical quantities. Physical quantities are identified by their base units of measure (dimensions) which include length (L), mass (M) and time (T) and can be either a single dimension, or a combination of dimensions (volume would for example be expressed as L^3 and flow rate as $\frac{L^3}{T}$). However, for any equation to be meaningful, the same dimensions need to be obtained on both the left and right sides. This is known as dimensional homogeneity.

5.2.1. LLRC Dimension of Interest

The dimensions to be determined for the LLRC stepped chute are listed as follows:

- Height of the steps (h_{S-S});
- Width of the steps (W_{Step}); and
- Length of the steps (L_{Step})

Figure 5.1 illustrates the known dimensions and physical quantities as well as the dimensions to be determined.

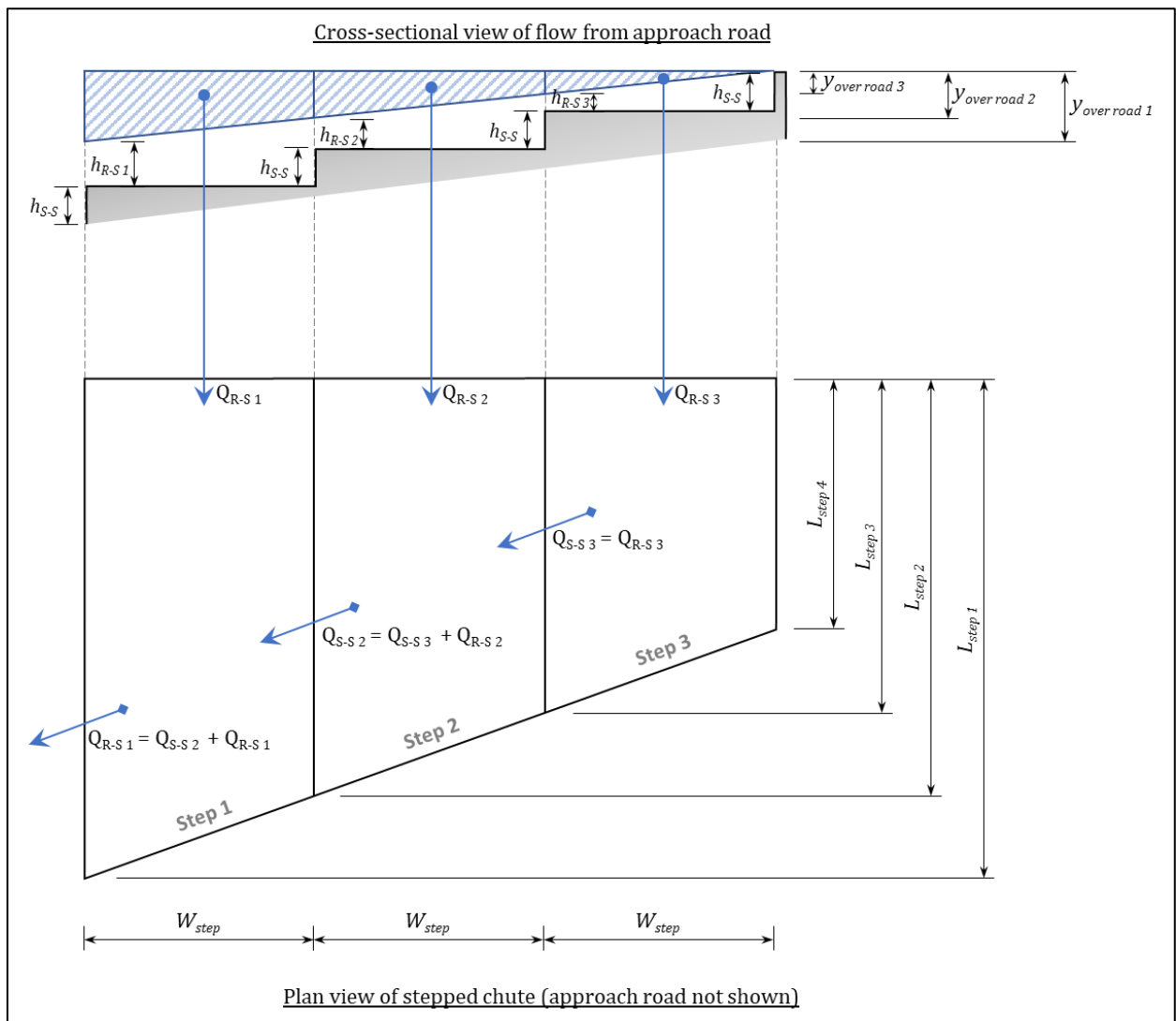


Figure 5.1: Definition sketch of physical quantities and dimensions (not to scale)

5.2.1.1. Height of the steps (h_{S-S})

As discussed in Section 3.4.3.2, the height of the steps (h_{S-S}) needs to be higher than the conjugate depth of the hydraulic jump formed due to flow from one chute step to the next. This is, however, a function of the effective flow area which in turn is a function of the step length (L_{step}). Seeing that the step length (L_{step}) is one of the stepped chute dimensions to be determined, it is apparent that an iterative calculation procedure will be necessary.

It is, therefore, advisable to start by choosing a number of steps. The height of the steps can then be calculated as follows:

$$h_{S-S} = \frac{h_{deck} + y_{over road}}{n_{steps} + 1} \quad \text{Eq. 5.1}$$

where:

h_{S-S} is the height of the chute steps (m);

h_{deck} is the height of the culvert measured from the culvert invert to the top of the deck (m);

$y_{over road}$ is the overflow depth on top of the culvert deck (m); and

n_{steps} is the number of steps (dimensionless).

5.2.1.2. Width of the steps (W_{Step})

The width of the steps (W_{Step}) is a function of the overflow depth, approach road slope and the number of steps and can be calculated as follows:

$$W_{step} = \frac{y_{over road}}{S_{approach} \times n_{steps}} \quad \text{Eq. 5.2}$$

where:

W_{Step} is the width of the chute steps (m);

$y_{over road}$ is the overflow depth on top of the culvert deck (m);

$S_{approach}$ is the approach road slope (m/m); and

n_{steps} is the number of steps (dimensionless).

5.2.1.3. Length of the steps (L_{Step})

The length of the steps (L_{step}) can be determined once the width of the steps (W_{Step}) is known, as the step width dictates the amount of flow to be discharged from the approach road onto each step. As discussed in Section 5.2.1.1, the length of each step influences the effective overflow width from one chute step to the next, which in turn affects the conjugate depth of the hydraulic jump formed after nappe impingement. The determination of the step lengths could, therefore, also be determined by means of iteration.

However, seeing that hydraulic model testing was performed and found to adhere to the requirement that the conjugate depth should not exceed the step height, the model testing variables could be used to perform a dimensional analysis. The results of the dimensional analysis are scalable and will therefore be usable for prototype design purposes.

5.2.1.4. Physical Quantities Affecting the Length of the Steps

The physical quantities that were found to affect the chute step lengths was the flow from the approach road onto each step (Q_{R-S}), the flow from one chute step onto the next (Q_{S-S}), the drop height from the approach road onto each step (h_{R-S}) and the depth of flow above each step ($y_{over road}$). Figure 5.1 indicates the exact positions of each dimension and quantity.

The dimensional equation for the step lengths can therefore be written as follows:

$$L_{step} = f(Q_{R-S}, Q_{S-S}, h_{R-S}, y_{over road}) \quad \text{Eq. 5.3}$$

In order to perform a regression analysis, using the physical quantities, a dimensionless equation was setup by dividing quantities with the same dimensions. Doing so reduces the terms to dimensionless values as the units are cancelled and retains dimensional homogeneity. The dimensionless equation for the step lengths is as follows:

$$\frac{L_{step}}{y_{over road}} = f\left(\frac{h_{R-S}}{y_{over road}}, \frac{Q_{S-S}}{Q_{R-S}}\right) \quad \text{Eq. 5.4}$$

Seeing that the flow onto each step (from both the previous step and the approach road) and the height of the drop from the approach road is known for each step, the data set could be divided for the parameters of each step. Eq. 5.4 was therefore altered to make provision for the parameters of individual steps.

$$\frac{L_{step(ns)}}{y_{over road(ns)}} = f\left(\frac{h_{R-S(ns)}}{y_{over road(ns)}}, \frac{Q_{S-S(ns+1)}}{Q_{R-S(ns)}}\right) \quad \text{Eq. 5.5}$$

where:

$L_{Step(ns)}$ is the length of chute step ns (m);

$y_{over road(ns)}$ is the overflow depth on top of the culvert deck above step ns (m);

$h_{R-S(ns)}$ is the height of the drop height from the approach road onto chute step ns (m);

$Q_{R-S(ns)}$ is the flow from the approach road onto chute step ns (m^3/s);

$Q_{S-S(ns+1)}$ is the flow from the previous chute step ($ns+1$) onto step ns (m^3/s); and

ns is the number of the chute step in question (dimensionless).

5.3. MULTI-LINEAR REGRESSION ANALYSIS

Eq. 5.4 in Section 5.2.1.4 showed that the ratio of the step length to the overflow depth (Q_o) is a function of two dimensionless independent variables (Q_1 and Q_2), written as follows:

$$Q_o = f(Q_1, Q_2) \quad \text{Eq. 5.6}$$

where:

$$Q_o = \frac{L_{step(ns)}}{y_{over road(ns)}}$$

$$Q_1 = \frac{h_{R-S(ns)}}{y_{over road(ns)}}$$

$$Q_2 = \frac{Q_{S-S(ns+1)}}{Q_{R-S(ns)}}$$

This presents a multidimensional relationship which can be solved using multi-linear regression. Three basic models of linear regression models were considered and are discussed in more detail in Section 5.3.1.

5.3.1. Regression Models

The three multi-linear regression models that were considered are listed with their respective notations.

Linear Regression Model:

$$Q_o = k + a \cdot Q_1 + b \cdot Q_2 \quad \text{Eq. 5.7}$$

Logarithmic Transformed Linear Regression Model:

$$\ln(Q_o) = \ln(k) + a \cdot \ln(Q_1) + b \cdot \ln(Q_2) \quad \text{Eq. 5.8}$$

Linear-Logarithmic Regression Model:

$$Q_o = \ln(k) + a \cdot \ln(Q_1) + b \cdot \ln(Q_2) \quad \text{Eq. 5.9}$$

The objective of regression is to obtain a relationship which will best describe the dependant variable from the independent variables. The coefficients a and b , from the regression model with the highest coefficient of determination (r^2) is the best representation of the variables.

5.3.2. Variables Dataset

The dataset of prototype equivalent dimensions and quantities used for the regression analysis is listed in Table 5-1. Test cases A and B (prototype approach road overflow depths of 60 and 120 mm) did not have overflow over at least one chute step and was therefore omitted. The variables for step 3 were also omitted as flow was only discharged onto the step during D test cases (prototype approach road overflow depth of 300 mm). Step 3 did not receive flow from another step as it was the last (highest) step in the chute. The C test cases (prototype approach road overflow depth of 180 mm) for chute step 2 was also omitted as no flow was discharged onto step 2 from step 3 ($Q_{S-S(3)} = 0 \text{ m}^3/\text{s}$).

Table 5-1: Data Set Used for Regression Analyses

Step ns:	Test No.:	$L_{Step\ (ns)}$ (m)	$y_{over\ road\ (ns)}$ (m)	$h_{R-S\ (ns)}$ (m)	$Q_{R-S\ (ns)}$ (m^3/s)*	$Q_{S-S\ (ns+1)}$ (m^3/s)*
Step 1	1.1.1.C	15	0.195	1.275	1.09	0.268
	1.1.1.D	15	0.255	1.275	1.803	0.93
	1.1.1.E	15	0.300	1.275	2.616	2.092
	1.1.2.C	15	0.195	1.275	1.09	0.268
	1.1.2.D	15	0.240	1.275	1.803	0.93
	1.1.2.E	15	0.300	1.275	2.616	2.092
	1.2.1.C	15	0.218	1.275	1.09	0.268
	1.2.1.D	15	0.255	1.275	1.803	0.93
	1.2.1.E	15	0.330	1.275	2.616	2.092
	1.2.2.C	15	0.203	1.275	1.09	0.268
	1.2.2.D	15	0.255	1.275	1.803	0.93
	1.2.2.E	15	0.323	1.275	2.616	2.092
Step 2	1.1.1.D	11.667	0.255	0.85	0.854	0.076
	1.1.1.E	11.667	0.300	0.85	1.569	0.523
	1.1.2.D	11.667	0.240	0.85	0.854	0.076
	1.1.2.E	11.667	0.300	0.85	1.569	0.523
	1.2.1.D	11.667	0.255	0.85	0.854	0.076
	1.2.1.E	11.667	0.330	0.85	1.569	0.523
	1.2.2.D	11.667	0.255	0.85	0.854	0.076
	1.2.2.E	11.667	0.323	0.85	1.569	0.523

*Note: the discharge from the approach road onto each step was not measured. The design values, as discussed in Section 3.4.3.1, were therefore used.

5.3.3. Results of Regression Analysis

The regression of the three regression models was performed using the *Microsoft Office 2016 Excel Analysis ToolPak* add-in. The *Regression Analysis* option was used which enables the user to select the list of dependant and independent variables and automatically performs the regression analysis. The output from the regression analysis includes the coefficients k, a and b as well as the regression statistics.

5.3.3.1. Linear Regression Model

The independent and dependant variable used for the linear regression model is listed in Table 5-2.

Table 5-2: Variables Used for Linear Regression Model

Q_0	Q_1	Q_2
76.92	6.54	0.25
58.82	5.00	0.52
50.00	4.25	0.80
76.92	6.54	0.25
62.50	5.31	0.52
50.00	4.25	0.80
68.97	5.86	0.25
58.82	5.00	0.52
45.45	3.86	0.80
74.07	6.30	0.25
58.82	5.00	0.52
46.51	3.95	0.80
45.75	3.33	0.09
38.89	2.83	0.33
48.61	3.54	0.09
38.89	2.83	0.33
45.75	3.33	0.09
35.35	2.58	0.33
45.75	3.33	0.09
36.18	2.64	0.33

The linear regression model statistics are listed in Table 5-3.

Table 5-3: Linear Regression Model Statistics

Regression Statistics	
Multiple r	0.999
r^2	0.999
Adjusted r^2	0.999
Observations	20

The coefficients k, a and b together with the final expression is listed in Table 5-4.

Table 5-4: Linear Regression Model Statistics

Regression Statistics	
k	12.774
a	10.05
b	-7.515
$\frac{L_{step(ns)}}{y_{over road(ns)}}$	$= 12.774 + 10.05 \cdot \frac{h_{R-S(ns)}}{y_{over road(ns)}} - 7.515 \cdot \frac{Q_{S-S(ns+1)}}{Q_{R-S(ns)}}$

The correlation between the actual independent variables and the predicted independent variable from the regression analysis can be seen in Figure 5.2.

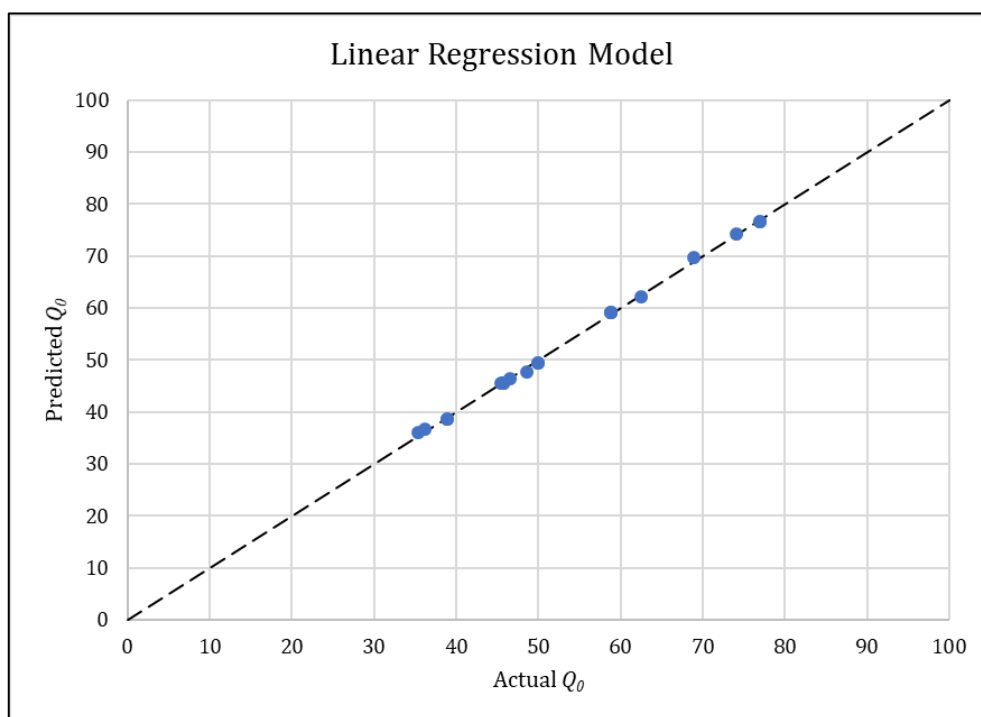


Figure 5.2: Linear Regression Model Predicted Q_0 vs. Actual Q_0

The coefficient of determination (r^2) was very high and approximated a value of one which indicated a good correlation between the actual and the regressed variables.

5.3.3.2. Logarithmic Transformed Linear Regression Model

The independent and dependant variables used for the logarithmic transformed linear regression model are listed in Table 5-5.

Table 5-5: Variables Used for Logarithmic Transformed Linear Regression Model

Q_0	Q_1	Q_2
4.343	1.878	-1.403
4.075	1.609	-0.662
3.912	1.447	-0.224
4.343	1.878	-1.403
4.135	1.670	-0.662
3.912	1.447	-0.224
4.234	1.769	-1.403
4.075	1.609	-0.662
3.817	1.352	-0.224
4.305	1.840	-1.403
4.075	1.609	-0.662
3.840	1.375	-0.224
3.823	1.204	-2.419
3.661	1.041	-1.099
3.884	1.265	-2.419
3.661	1.041	-1.099
3.823	1.204	-2.419
3.565	0.946	-1.099
3.823	1.204	-2.419
3.588	0.969	-1.099

The linear regression model statistics are listed in Table 5-6.

Table 5-6: Logarithmic Transformed Linear Regression Model Statistics

Regression Statistics	
Multiple r	0.998
r^2	0.997
Adjusted r^2	0.996
Observations	20

The coefficients k, a and b together with the final expression is listed in Table 5-7.

Table 5-7: Logarithmic Transformed Linear Regression Model Statistics

Regression Statistics	
k	2.735
a	0.810
b	-0.052
$\ln\left(\frac{L_{step(ns)}}{y_{over road(ns)}}\right) = 2.735 + 0.810 \cdot \ln\left(\frac{h_{R-S(ns)}}{y_{over road(ns)}}\right) - 0.052 \cdot \ln\left(\frac{Q_{S-S(ns+1)}}{Q_{R-S(ns)}}\right)$	

The correlation between the actual independent variables and the predicted independent variable from the regression analysis can be seen in Figure 5.3.

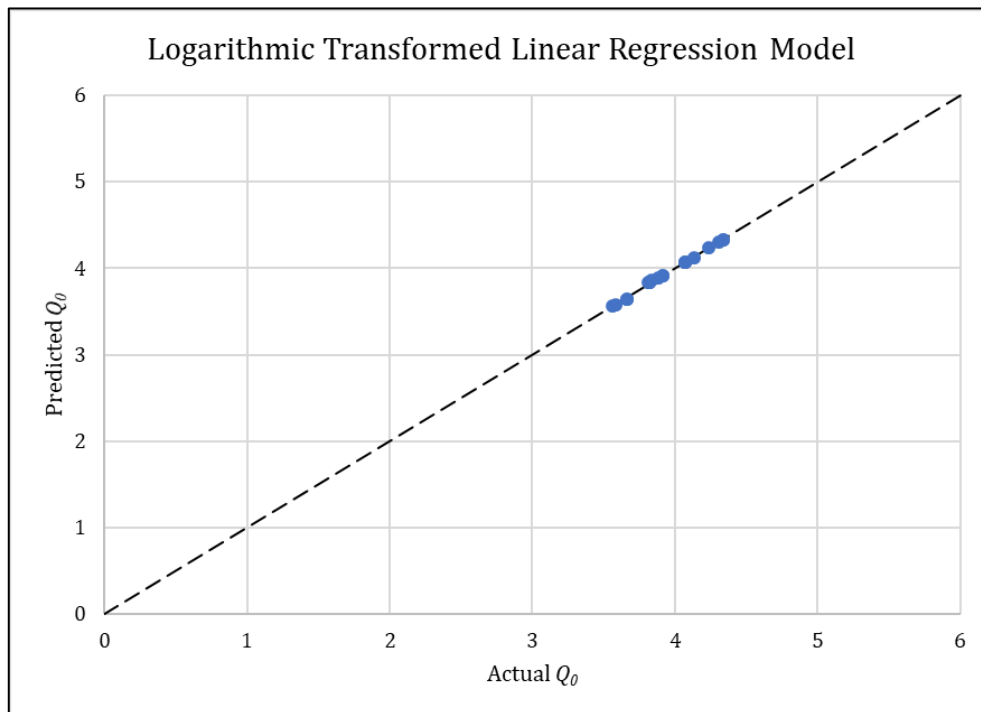


Figure 5.3: Logarithmic Transformed Linear Regression Model Predicted Q_0 vs. Actual Q_0

The coefficient of determination (r^2) was very high and approximated a value of one which indicated a good correlation between the actual and the regressed variables. The coefficient of determination was, however, slightly less than the linear regression model.

5.3.3.3. Linear-Logarithmic Regression Model

The independent and dependant variables used for the linear-logarithmic regression model are listed in Table 5-8.

Table 5-8: Variables Used for Linear-Logarithmic Regression Model

Q_0	Q_1	Q_2
76.923	1.878	-1.403
58.824	1.609	-0.662
50.000	1.447	-0.224
76.923	1.878	-1.403
62.500	1.670	-0.662
50.000	1.447	-0.224
68.966	1.769	-1.403
58.824	1.609	-0.662
45.455	1.352	-0.224
74.074	1.840	-1.403
58.824	1.609	-0.662
46.512	1.375	-0.224
45.752	1.204	-2.419
38.889	1.041	-1.099
48.611	1.265	-2.419
38.889	1.041	-1.099
45.752	1.204	-2.419
35.354	0.946	-1.099
45.752	1.204	-2.419
36.176	0.969	-1.099

The linear regression model statistics are listed in Table 5-9.

Table 5-9: Linear-Logarithmic Regression Model Statistics

Regression Statistics	
Multiple r	0.999
r^2	0.997
Adjusted r^2	0.941
Observations	20

The coefficients k, a and b together with the final expression are listed in Table 5-10.

Table 5-10: Linear-Logarithmic Regression Model Statistics

Regression Statistics	
k	0.000
a	36.410
b	-1.663
$\frac{L_{step(ns)}}{y_{over road(ns)}}$	$= 36.41 \cdot \ln\left(\frac{h_{R-S(ns)}}{y_{over road(ns)}}\right) - 1.663 \cdot \ln\left(\frac{Q_{S-S(ns+1)}}{Q_{R-S(ns)}}\right)$

The correlation between the actual independent variables and the predicted independent variable from the regression analysis can be seen in Figure 5.4.

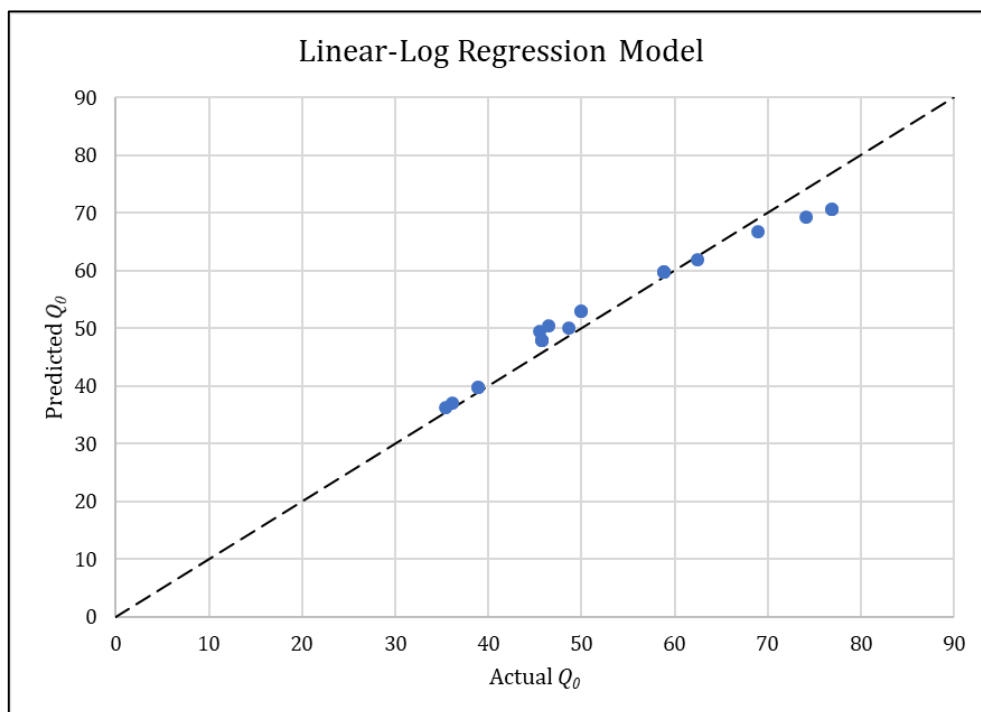


Figure 5.4: Linear-Logarithmic Regression Model Predicted Q_0 vs. Actual Q_0

The coefficient of determination (r^2) was very high and approximated a value of one which indicated a good correlation between the actual and the regressed variables. The coefficient of determination was slightly less than both the linear regression model and the logarithmic transformed linear regression model.

5.4. CONCLUSION OF REGRESSION ANALYSIS

All three regression models yielded good results as the coefficients of determination (r^2) of all three models approximated one which indicates good correlation between the regressed variables and the actual variables. The linear regression model, however, had the highest coefficient of determination. The explicit form of the equation to predict the length of a chute step, based on the linear regression model coefficients, can therefore be written as follows:

$$L_{step(ns)} = y_{over road(ns)} \cdot \left(12.774 + 10.05 \cdot \frac{h_{R-S(ns)}}{y_{over road(ns)}} - 7.515 \cdot \frac{Q_{S-S(ns+1)}}{Q_{R-S(ns)}} \right) \quad \text{Eq. 5.10}$$

The range of application based on the prototype experimental values are listed as follows:

- $h_{R-S} \leq 1.275 \text{ m}$
- $y_{over road} \leq 0.3 \text{ m}$
- LLRC deck crossfall = 0%

The fact that the discharge from the approach road onto each step could not be measured directly was a concern as these flows would have a direct impact on the regression analysis. No experimental data was obtained for a road crossfall exceeding 0% thereby limiting the application of Eq. 5.10. Future research with a road crossfall exceeding 0% should be considered and is discussed in Section 7.2.

After the chute step lengths had been determined, it would be advisable to confirm that the conjugate flow depths of the hydraulic jumps formed in the direction of the chute are still less than the step height ($h_{S,S}$), as discussed in Section 5.2.1.2. If this is not the case, the number of steps (n_{steps}) should be decreased to increase the step height.

APPENDIX B.4 contains an example calculation for the determination of the stepped chute length using Eq. 5.10.

CHAPTER 6: CONCLUSIONS

The use of stepped chute energy dissipation structures was recommended after ten low-level river crossings in the Skoenmakers River experienced excessive embankment erosion downstream of the approach roads. No formal design guidelines for the design of a stepped chute structure, used in combination with a low-level river crossing, were available.

A literature study was conducted to understand the anticipated hydraulic controls and features. The findings from the literature review, summarised in Section 6.1, were used to design a prototype low-level river crossing with a downstream stepped chute.

Following the design of the prototype model, a 1:15 scale hydraulic model was designed using Froude's law and constructed in the Hydraulic Laboratory of Stellenbosch University. The model would be used to verify initial hydraulic operations, identify unforeseen phenomena and to provide practical recommendations on the design and application of such a stepped chute.

The scaled model was tested with two configurations: the stepped chute added downstream of the low-level river crossing with the chute sidewall intact, and the same stepped chute with the chute wall removed and riprap added. The flow profiles, nappe cavity pressure and nappe airflow requirements were recorded and analysed.

6.1. FINDINGS FROM THE LITERATURE REVIEW

The following findings derived from the literature review provided acumens of what could be expected during the hydraulic model design and testing:

- The flow through low-level river crossings can be analysed as either inlet- or outlet controlled. Henderson (1966) reported that for $H/D > 1.2$, the water surface would come into contact with the culvert soffit at the entrance of a culvert, which would essentially act as a sluice gate. The flow through a sluice gate is normally computed using the orifice formula. The orifice formula has, however, been adapted to only take vertical contraction into account. The resulting formula is as per Eq. 2.2.
- Riprap is used to protect erodible river banks and road embankments from overtopping flow. The design of riprap is based on multiple factors such as channel velocity, flow depth and embankment slope, while also being mindful of the required dimensional properties and minimum layer thicknesses.
- Stepped chute spillways have enjoyed increased interest worldwide due to the technical advantages in the construction of roller compacted concrete dams and the immense energy dissipation along the chute which assists in reducing stilling basin sizes (Khatsuria 2005:95). The flow conditions down a stepped chute can either be

nappe flow, transition flow or skimming flow, depending on the step geometry and the discharge down the chute. Nappe flow conditions can either take place with, or without, a fully developed hydraulic jump.

- Uncontracted falling nappes may require ventilation to prevent clinging or collapse due to the transportation of air, from the cavity between the nappe and the pool behind the nappe, which leads to sub-atmospheric conditions behind the nappe.
- The scaling of the model study needed to adhere to Froude's Law as the dominant forces were identified as being inertial and gravitational forces.

6.2. FINDINGS FROM THE HYDRAULIC MODEL TESTS

A summary of the results obtained from the two different hydraulic model configurations and repeatability tests is as follows:

Model Setup 1 - Stepped chute with chute wall intact:

- The length of the hydraulic jump on each step could not be accurately predicted as the nappe flow from the approach road was not constant across the overflow width. The cumulative flow depths (conjugate depths) on the chute steps also affected the jump position.
- The pressure of the cavity behind the nappe for maximum road overflow conditions (based on the maximum overflow depth) was sub-atmospheric (with nappe cavity pressures ranging from -0.335 to -0.622 m) for tests with and without nappe ventilation as well as for tests with and without culvert flow. Although the pressures slightly differed for the two different culvert flow conditions, they were still within the same order of magnitude.
- The nappe airflow (nappe forming from the approach road) for tests with culvert flow was less than the nappe airflow for tests without culvert flow. The hydraulic transportation of air bubbles to the rear of the nappe was found to be an alternate source of air supply. The prototype nappe airflow for the maximum road overflow conditions was 143.7 l/s for no culvert flow and 68.4 l/s with culvert flow.
- Although differences were measured between nappe pressures and airflows, no major changes in the flow profiles between the different model permutations were noted.

Model Setup 2 - Stepped chute with chute wall omitted and riprap added:

- The length of the hydraulic jump on each step could not be accurately predicted as the nappe flow from the approach road was not constant across the overflow width.
- The pressure of the cavity behind the nappe for maximum road overflow conditions (based on the maximum overflow depth) was sub-atmospheric (with nappe cavity pressures ranging from -0.299 to -0.332 m) for tests with and without nappe

ventilation, as well as for tests with and without culvert flow. Although the pressure heads slightly differed, they were still within the same order of magnitude.

- A reduction in nappe airflow (nappe forming from the approach road) occurred between tests without culvert flow and tests with culvert flow. The prototype nappe airflow for the maximum road overflow conditions was 109.5 l/s for no culvert flow and 61.6 l/s with culvert flow.
- The addition of culvert flow did not have a significant effect on nappe pressures, but it did have a substantial effect on nappe airflow due to the hydraulic transportation of air bubbles to the rear of the nappe.
- The addition of riprap downstream of the chute indicated that the size could be reduced as no displacement of riprap was noted. It was only with increased culvert tailwater flow that the onset of riprap displacement was noted at the toe of the riprap layer.

Model Repeatability Tests:

The flow profile layouts and nappe pressures remained predominantly constant, which indicated that the hydraulic model remained intact and undistorted, and the results could be repeated on demand.

6.3. SUMMARY OF THE HYDRAULIC MODEL STUDY

The first hydraulic model (with chute wall intact) performed well, considering the initial design assumptions were based on empirical design formulae which were determined for one dimensional flow problems (flow in one direction), whereas the flow falling on the steps and flowing down the chute was a two-dimensional flow problem (disregarding vertical flow). Before opting for more computing-intensive and financially straining studies such as CFD (Computational Fluid Dynamic) modelling, which is capable of solving complex three-dimensional flow problems such as these, the attempt was made to use available literature to determine the anticipated hydraulic conditions while allowing for a certain degree of uncertainty. The use of the relationships provided by Chanson (1994) was a useful guide for the initial prototype sizing and design.

The performance of the second hydraulic model (with chute sidewall omitted) provided insightful results, especially when considering the pressures behind the nappe. The second model setup indicated that the nappe pressures remained roughly the same regardless of whether the nappe was ventilated or not, or for cases with- and without culvert flow. The nappe pressure results remained in the order of -0.3 to -0.33 m whereas the first model setup indicated a substantial increase in sub-atmospheric nappe conditions, in the order of -0.6 m, when culvert flow was added (test 1.2.1. E and 1.2.2. E). Although an increase in sub-

atmospheric nappe pressures was evident, the pressures were still well within the cavitation threshold (7 m below atmosphere). For this particular test case, the levels of tailwater which inundated the bottom chute step (step 1) were higher than the conjugate depth, thereby moving the hydraulic jump position up to the nappe from the approach road and nearly drowning it out.

The second model setup further indicated that the initial prototype riprap sizing ($D_{50}=0.37$ m) was overestimated for the flow coming from the stepped chute. The riprap function was only noticed when the onset of riprap displacement was noted with increased tailwater conditions where all the culverts (2.5 culverts) were open.

A decrease in airflow to the nappe was noted in both model setups between conditions of no culvert flow and conditions with culvert flow. The reduction in airflow requirement lead to the conclusion that another source of air supply should have been present and the nappe intersection with the flow exiting the culvert was seen to cause high turbulence and introduced air bubbles to the rear of the nappe.

The use of the first model setup (chute sidewall intact) was found to be the better option of the two model configurations. The hydraulic jump formation of flow from the approach road onto the chute steps was more pronounced leading to higher rates of energy dissipation. The flow falling onto each step was also contained on the stepped chute, accumulated in the direction of the chute and channelled down the chute in a controlled manner whereafter it rejoined the main channel flow. The nappe ventilation had no noticeable impact on nappe pressures or on the flow profiles when compared to cases without nappe ventilation. The addition of nappe ventilation was, therefore, deemed not to be needed as the pressures were not too negative. The regression analysis performed in Chapter 5 provided relationships which can be used to do the initial sizing of the stepped chute. Care should, however, be taken to ensure that the conjugate flow depths of hydraulic jumps formed in the direction of the stepped chute do not exceed the step height.

CHAPTER 7: RECOMMENDATIONS

The recommendations made from this hydraulic model study were categorised into two sections. The first section provided practical recommendations on the use of stepped chutes in combination with a low-level river crossing and the second section discussed areas of possible future research.

7.1. RECOMMENDATIONS ON THE USE OF A STEPPED CHUTE IN COMBINATION WITH A LLRC

The use of a stepped chute to protect downstream embankments of a low-level river crossing was proposed after ten LLRCs sustained substantial damage due to high levels of erosion. This model study provided insights into the design and application of a stepped chute with a LLRC and is listed as follows:

- Low-level river crossings should be designed for overtopping flow. The recommended overtopping flow depths (for annual floods and not extreme floods) for the different flow regimes are as follows (Pienaar and Kruger, 2013):
 - i. supercritical flow: 100 mm
 - ii. subcritical flow: 150 mm;
- The LLRC overflow may be selected to exceed the recommended values, even though access would become impossible, to protect the structure due to the downstream embankments eroding from higher flow depths (and flows);
- The desirable maximum slope for the approach road should be 10% and the crossing width should be 4 m for a single-lane crossing and 7.5 m for a two-lane crossing (Pienaar and Kruger, 2013);
- The transition flow regime should be avoided when designing stepped chutes. Stepped chutes should rather operate in the nappe flow regime. This will cause hydraulic jumps to form on the chute steps, thereby increasing energy dissipation;
- Provision of nappe ventilation pipes was found not to be necessary as the nappe cavity pressures (maximum sub-atmospheric pressure = 0.622 m) were well within cavitation threshold (7 m below atmosphere) and collapse of the nappe was not observed during testing. Hydraulic aeration of the nappe cavity was noted at the intersection between the nappe from the road deck and the flow exiting the culvert under inlet conditions.
- Three conditions need to be adhered to when determining appropriate stepped chute dimensions:
 - i. the conjugate depth, for the hydraulic jump formed from one chute step onto the next, should not exceed the step height as this would cause inundation of

- the top step and possibly change the flow regime to transition or skimming flow;
- ii. the length of the drop and the length of the roller combined (in the direction of the chute) should not exceed the length of the step. Ensuring a long enough step length would lead to a hydraulic jump formation and conversely higher rates of energy dissipation; and
- iii. maintain nappe flow conditions (refer to Figure 2.14 in Section 2.4.2).
- Particular attention needs to be given to tailwater conditions. If tailwater conditions are expected to exceed the bottom step height, one of the following mitigations could be applied:
 - i. reduce the top step heights and increase the bottom/last step height;
 - ii. reduce the width of the steps in order to create distance between the last step and the nearest culvert opening; or
 - iii. a combination of both.

7.2. FUTURE RESEARCH

Recommendations for possible future research on stepped chutes for LLRCs include the following:

- Investigate the effects of increased overflow rates, due to cross fall of the road, onto the stepped chute;
- Confirmation of the overall LLRC geometry should be done with a more detailed approach road flow distribution onto each of the chute steps as discussed in Section 3.4.3.1;
- Consider different chute setups with more, or less, steps, backward sloping steps or pooled stepped cascades to find the optimal stepped chute configuration;
- Develop a cost comparison/cost-benefit analysis of the LLRC vs. conventional erosion protection methods;
- Investigate the influence of the LLRC on downstream flow conditions;
- Investigate the effects of increased overflow depths on low-level river crossings, due to extreme floods (50 year or more recurrence intervals), and test whether a stepped chute could still be utilised for such instances;
- The three previously mentioned points would increase the data set to be used for regression and improve the relationship for determining the step lengths; and
- Hydraulic model testing of stepped chutes constructed out of gabions to determine if gabion mattress stepped chutes are a hydraulically feasible option. This could result in cost saving, versus having to construct a concrete stepped chute.

REFERENCES

1. BEITZ, E. & LAWLESS, M. 1992. *Hydraulic Model Study for Dam on GHFL 3791 Isaac River at Burton Gorge*. Water Resource Commission Report, Ref. No. REP/24.1, Sept., Brisbane, Australia.
2. BOES, R.M. & MINOR, H.E. 2002. *Hydraulic Design of Stepped Spillways for RCC Dams*. Intnl.Jnl of Hydropower and Dams – Issue 3. Pp. 87-91.
3. BOS, M.G. 1989. *Discharge Measurement Structures, 3rd ed.* The Netherlands. International Institute for Land Reclamation and Improvement.
4. BOSMAN, E. & BASSON, G.R. 2012. *Investigation of Unsteady Flow Conditions at Dam Bottom Outlet Works Due to Air Entrainment During Gate Closure: Physical Modelling* WRC Report TT528/12. Water Research Commission. Republic of South Africa.
5. BRAUNE, M. *The Rehabilitation of Skoenmakers River – Conducting Feasibility Studies for the Rehabilitation of Skoenmakers River – Feasibility Report*. Jul 2016. Vol. 1 of 2. BVi Consulting Engineers.
6. British Columbia. PUBLIC SAFETY SECTION. 2000. *Riprap Design and Construction Guide*. Province of British Columbia. Ministry of Environment, Lands and Parks.
7. BSI. 1981. *BS 3680: Methods of Measurement of Liquid Flow in Open Channels; PART 4A: Thin-plate weirs*. London: British Standards Institution.
8. CALITZ, G. 2016. *Aeration of Roberts Splitters Through an Internal Gallery of a Dam*. University of Stellenbosch. Stellenbosch.
9. CHADWICK, A., MORFETT, J. & BORTHWICK, M. 2004. *Hydraulics in Civil and Environmental Engineering*. 4th ed. Taylor and Francis Group. London.
10. CHADWICK, A., MORFETT, J. & BORTHWICK, M. 2013. *Hydraulics in Civil and Environmental Engineering*. 5th ed. Taylor and Francis Group. Boca Raton, Florida.
11. CHANSON, H. & TOOMBES, L. 2004. *Hydraulics of Stepped Chutes: The Transition Flow*. Jl of Hydraulic Research, International Association of Hydraulic Engineering and Research, Vol. 42, No. 1, pp. 43-54.
12. CHANSON, H. 1994. *Hydraulics of Nappe Flow Regime Above Stepped Chutes and Spillways*. Australian Civil Engineer Transactions, Vol. CE36, No.1, January, pp. 69-76.
13. CHANSON, H. 2001. Experimental Investigations of Air Entrainment in Transition and Skimming Flows Down a Stepped Chute. Research Report no CE 158; The University of Queensland, Australia. July.
14. CHANSON, H. 2001. *The Hydraulics of Stepped Chutes and Spillways*. The Netherlands: Balkema, Lisse.
15. CHANSON, H. 2001. *Transition Flow Regime on Stepped Spillways. The Facts*. 29th IAHR Congress, Beijing, China.

16. CHAUDHRY, M.H. 2008. *Open Channel Flow*. 2nd ed. Springer Science+Business Media. New York, New York.
17. CHINNARASRI, C. 2002. Assessing the Flow Resistance of Skimming Flow on the Step Faces of Stepped Spillways. *Dam Engineering*.
18. DEGOUTTE, G., PEYRAS, L. & ROYET, P. 1992. *Skimming Flow on Stepped Spillways – Discussion*. Jl of Hyd. Engrg., ASCE, Vol. 118, No. 1, pp. 111-114.
19. DEPARTMENT of WATER and SANITATION. 2018, *Fish-Sundays Transfer Scheme: Water Transfer Schemes in the Middle Orange* [Homepage of Department of Water and Sanitation], [Online]. Available: http://www.dwa.gov.za/orange/mid_orange/fish-sun.aspx [2018, 07 July].
20. ESSERY, I.T.S. & HORNER, M.W. 1978. *The Hydraulic Design of Stepped Spillways*. CIRIA Report No. 33, 2nd edition, London, UK.
21. HAGER, W.H. & BOES, R.M. 2000. *Backwater and Drawdown Curves in Stepped Spillway Flows*. Proc. Intl. Workshop on Hydr of Stepped Spillways. Swets & Zeitlinger, Rotterdam. Balkema Publishers.
22. HAGER, W.H., BREMEN, R. & N. KAWAGOSHI, N. 1990. *Classical Hydraulic Jump: Length of Roller*. Jl of Hyd. Res., IAHR, Vol. 28, No. 5. Pp. 591-608.
23. HENDERSON, F.M. 1966. *Open Channel Flow*. New York: Macmillan Publishing Co., Inc.
24. JANSEN VAN VUUREN, A.M., ROOSEBOOM, A. & KRUGER, E.J. 2013. *Chapter 8-Bridges and Major Culverts, Drainage Manual*, 6th ed. Pretoria. South African National Road Agency Soc Ltd.
25. JOHANNESSEN, B. 2008. *Building Rural Roads*. Bangkok: International Labour Organization (ILO).
26. KHATSURIA, R.M. 2005. *Hydraulics of Spillways and Energy Dissipators*. New York: Marcell Dekker.
27. PEYRAS, L., ROYET, P. & DEGOUTTE, G. 1991. *Ecoulement et Dissipation sur les Déversoirs en Gradins de Gabions. ('Flows and Dissipation of Energy on Gabion Weirs')*. Jl La Houille Blanche, No.1, pp. 37-47 (in French).
28. PEYRAS, L., ROYET, P. & DEGOUTTE, G. 1992. *Flow and Energy Dissipation over Stepped Gabion Weirs*. Jl of Hyd. Engrg. ASCE, Vol. 118, No.5, pp. 707-717.
29. PIENAAR, P.A. & KRUGER, E.J. 2013. *Chapter 6-Low-Level River Crossings, Drainage Manual*, 6th ed. Pretoria. South African National Road Agency Soc Ltd.
30. ROOSEBOOM, A. & VAN VUUREN, S.J. 2013. *Chapter 7-Lesser Culverts (and Stormwater Conduits), Drainage Manual*, 6th ed. Pretoria. South African National Road Agency Soc Ltd.
31. SANCHEZ, M., POMARES, J. & DOLZ, J. 2000. *Pressure Field in Skimming Flow Over Stepped Spillway*. *Hydraulics of Stepped Spillways*. Balkema Publishers. Netherlands.

32. South Africa. COMMITTEE OF STATE ROAD AUTHORITIES. 1994. *TRH 25: Guidelines for the Hydraulic Design and Maintenance of River Crossings – Vol. 3: Embankment and Protection*. Pretoria: Department of Transport.
33. THOMPSON, P.L. & KILGORE, R.T. 2006. *Hydraulic Design of Energy Dissipators for Culverts and Channels* – Hydraulic Engineering Circular No. 14, 3rd ed. Pub. No. FHWA-NHI-06-086; Federal Highway Administration, National Highway Institute, U.S. Department of Transportation. Arlington, Virginia. July.
34. UNIVERSITY of PRETORIA. 2004. *Physical Models* – SHC 320 Hydraulics. Class notes. Department of Civil & Biosystems Engineering. Pretoria.
35. USBR. 1987. *Design of Small Dams*. 3rd ed. United States Department of the Interior: Bureau of Reclamation.
36. USBR. RESEARCH AND GEOLOGY DIVISION. 1948. *Similitude in Hydraulic Models*. Hydraulic Laboratory Report No. Hyd -246. United States Department of the Interior: Bureau of Reclamation.
37. YASODA, Y. TAKAHASHI, M. & OHTSU, I. 2001. *Energy Dissipation of Skimming Flows on Stepped Channel Chutes*. 29th IAHR Congress, Beijing, China.

APPENDICES



APPENDIX A: PROTOTYPE DESIGN PROCEDURE

A.1. PROTOTYPE DESIGN PROCEDURE

The design procedure for the prototype stepped chute energy dissipation structure was a twofold process. The first was the design of the low-level river crossing which included the determination of the flow through the culverts and the flow over the crossing using the method described by Rooseboom and Van Vuuren (2013) and discussed in Section 2.2.1. The second process was the design of the stepped chute structure and determination of the required dimension of the chute steps using the literature from Chanson (1994 and 2001) as discussed in Section 2.4.1.

A.2. DESIGN STEPS OF THE PROTOTYPE LOW-LEVEL RIVER CROSSING

Step 1. Determine the dimensions and layout of the crossing and culvert(s) as listed in

Table A-1 and illustrated in Figure A.1.

Table A-1: Dimensions Used for Low-Level River Crossing Design

Symbol	Description	Dimension
$S_{approach}$	Approach road slope	m/m
R_w	Road width	m
R_{cf}	Road cross fall	%
h_{deck}	Deck height measure from the culvert invert to the deck top surface	m
d_{deck}	Deck depth measured from the culvert roof to the deck top surface	m
D	Culvert opening height measured from the culvert invert to the culvert roof	m
$W_{culvert}$	Culvert opening width measured from inside to inside	m
$n_{culverts}$	Number of culverts	dimensionless
$Sp_{culvert}$	Culvert spacing (c/c)	m
$y_{over road}$	Maximum road overflow depth	m

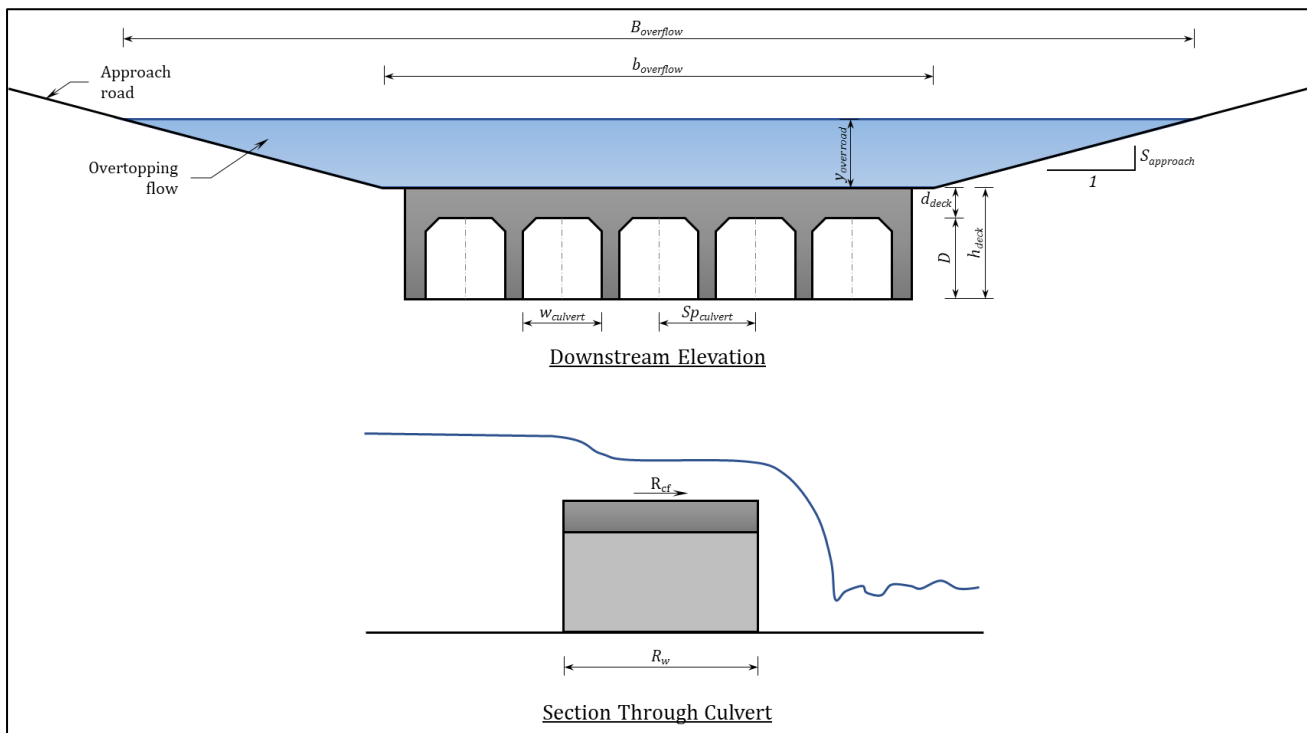


Figure A.1: Culvert Geometry (not to scale)

Step 2. Determine the flow over the road:

- For road cross fall = 0 %:

The LLRC deck will act as a control with critical flow conditions over the low-level river crossing ($Fr_{over} = 1$). The flow over the low-level river crossing can be calculated by rearranging Eq. 2.11 to the following form:

$$Q_{over} = \left(\frac{F_r^2 g A_{over}^3}{T_w} \right)^{\frac{1}{2}} \quad \text{Eq. A.1}$$

where:

Q_{over} is the flow rate over the LLRC (m^3/s);

F_r is the Froude number, equal to 1 for critical flow (dimensionless);

g is the gravitational acceleration constant taken as 9.81 m/s^2

T_w is the width of the top water surface (m); and

A_{over} is the cross-sectional area of flow over the LLRC (m^2).

- Road cross fall > 0 %:

The flow over the low-level river crossing can be calculated using either Manning's or Chezy's equation for channel flow.

$$\text{Manning: } Q_{over} = \frac{\frac{5}{2} A_{over}^{1/3} R_{cf}^{1/2}}{n P^3} \quad \text{Eq. A.2}$$

where:

Q_{over} is the flow rate over the LLRC (m^3/s);

R_{cf} is the road cross fall (m/m);

n is the Manning's n-value for flow over the LLRC ($\text{m}^{-1/3} \cdot \text{s}$);

P is the wetted perimeter of flow over the LLRC (m); and

A_{over} is the cross-sectional area of flow over the LLRC (m^2).

$$\text{Chezy: } Q_{over} = A_{over} \left(\frac{A_{over}}{P} \cdot R_{cf} \right)^{1/2} \cdot 18 \log \left(\frac{12 A_{over}}{P k_s} \right) \quad \text{Eq. A.3}$$

where:

Q_{over} is the flow rate over the LLRC (m^3/s);

R_{cf} is the road cross fall (m/m);

k_s is the absolute roughness for flow over the LLRC (m);

P is the wetted perimeter of flow over the LLRC (m); and

A_{over} is the cross-sectional area of flow over the LLRC (m^2).

It is advisable to calculate the Froude number to determine the flow regime over the LLRC and verify that the overflow depth recommendations are maintained:

- Supercritical flow ($Fr < 1$): 100 mm; and
- Subcritical flow ($Fr > 1$): 150 mm.

Step 3. Determine the flow through the culvert(s):

- For Inlet Control:

Use Eq. A.4 and Eq. A.5 as recommended by Rooseboom and Van Vuuren (2013):

For: $0 < H_1/D < 1.2$

$$Q_{under} = n_{culverts} \frac{2}{3} C_B w_{culvert} H_1 \sqrt{\frac{2}{3} g H_1} \quad \text{Eq. A.4}$$

For: $H_1/D > 1.2$

Eq. A.5



$$Q_{under} = n_{culverts} C_h w_{culvert} D \sqrt{2g(H_1 - C_h D)}$$

where:

Q_{under} is the discharge through all the culverts (m^3/s);

$n_{culverts}$ is the number of culverts of the same size (dimensionless);

C_b is the coefficient expressing the effect of width contraction in the flow (dimensionless). $C_b = 0.9$ for square inlets and $C_b = 1.0$ for rounded inlets where $r > 0.1B$;

r is the radius of the rounding at the inlet (m);

C_h is the coefficient of contraction in the vertical plane (dimensionless).

$C_h = 0.6$ for square inlets and $C_h = 0.8$ for rounded inlets;

$w_{culvert}$ is the width of the culvert opening (m);

D is the height of the culvert opening (m);

H_1 is the energy level upstream of the culvert (m); and

g is the gravitational acceleration constant taken as 9.81 m/s^2 .

The upstream energy level (H_1) is calculated as follows:

$$H_1 = h_{deck} + \frac{v_{over}^2}{2g}$$

$$H_1 = h_{deck} + \frac{Q_{over}^2}{A_{over}^2 2g} \quad \text{Eq. A.6}$$

where:

H_1 is the energy level upstream of the culvert (m);

h_{deck} is the height of the culvert deck (m);

Q_{over} is the flow rate over the LLRC (m^3/s);

A_{over} is the cross-sectional area of flow over the LLRC (m^2); and

g is the gravitational acceleration constant taken as 9.81 m/s^2 .

- For Outlet Control (effects of which were not considered for this model study), use Eq. 2.7 contained in Section 2.2.2.

A.3. STEPS FOR THE DESIGN OF THE PROTOTYPE STEPPED CHUTE

- Step 1.** Select an initial number of steps (n_{steps}), considering the height of the culvert deck (h_{deck}) and overflow depth ($y_{over road}$), and determine the step height ($h_{S-S(ns)}$) and step width (W_{step}). It is advisable to keep the number of steps to a minimum.
- Step 2.** Determine the flow from the approach road onto each step ($Q_{R-S(ns)}$) as detailed in Section 3.4.3.1.
- Step 3.** Determine the critical flow depth from the approach road onto the chute steps and the drop height ($h_{R-S(ns)}$) of each portion of flow onto each step as detailed in Section 3.4.3.1. Seeing as the prototype road cross fall was zero (level LLRC deck), critical flow conditions were encountered over the road and the critical depth was therefore equal to the overflow depth ($y_{over road(ns)}$).
- Step 4.** Determine the nappe geometry, listed in Table A-2 and illustrated in Figure A.2, from the approach road onto each step:

Table A-2: Nappe Geometry from Approach Road onto Chute Steps

Nappe Geometric component	Symbol	Equation	Unit
Flow depth after nappe impingement	$y_{1 R-S(ns)}$	$y_{1 R-S(ns)} = 0.54 h_{R-S(ns)} \left(\frac{y_{over road(ns)}}{h_{R-S(ns)}} \right)^{1.275}$	m
Nappe drop length	$L_{d R-S(ns)}$	$L_{d R-S(ns)} = 4.3 h_{R-S(ns)} \left(\frac{y_{over road(ns)}}{h_{R-S(ns)}} \right)^{0.81}$	m
Pool depth behind the nappe	$y_{p R-S(ns)}$	$y_{p R-S(ns)} = h_{R-S(ns)} \left(\frac{y_{over road(ns)}}{h_{R-S(ns)}} \right)^{0.66}$	m
Froude number of the flow after nappe impingement	$Fr_{1 R-S(ns)}$	$Fr_{1 R-S(ns)} = \left(\frac{Q_{R-S(ns)}^2 W_{step(ns)}}{g(w_{step(ns)} \times y_{1 R-S(ns)})^3} \right)^{\frac{1}{2}}$	-
Hydraulic jump roller length	$L_{r R-S(ns)}$	$L_{r R-S(ns)} = 8 y_{1 R-S(ns)} (Fr_{1 R-S(ns)} - 1.5)$	m

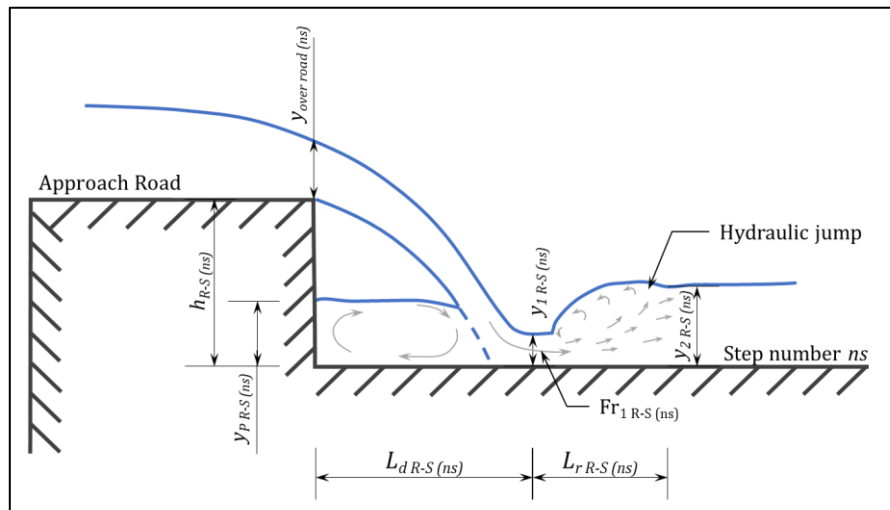


Figure A.2: Nappe Geometry from Approach Road onto Chute Steps

Step 5. Determine the nappe cavity ventilation requirement (Bos 1989):

$$Q_{air R-S(ns)} = 0.1 \frac{Q_{R-S(ns)}}{\left(\frac{y_{p R-S(ns)}}{y_{over road(ns)}}\right)^{1.5}} \quad \text{Eq. A.7}$$

where:

$Q_{air R-S(ns)}$ is the nappe aeration for flow onto step ns (m^3/s);

$Q_{R-S(ns)}$ is the nappe discharge onto step ns (m^3/s);

$y_{p R-S(ns)}$ is the pool depth beneath the nappe for step ns (m);

$y_{over road(ns)}$ is the flow depth on the top step (m); and

ns is the number of the chute step in question (dimensionless).

Step 6. Determine the accumulated flow over each step in the direction of the chute as discussed in Section 3.4.3.2 and illustrated in Figure A.3.

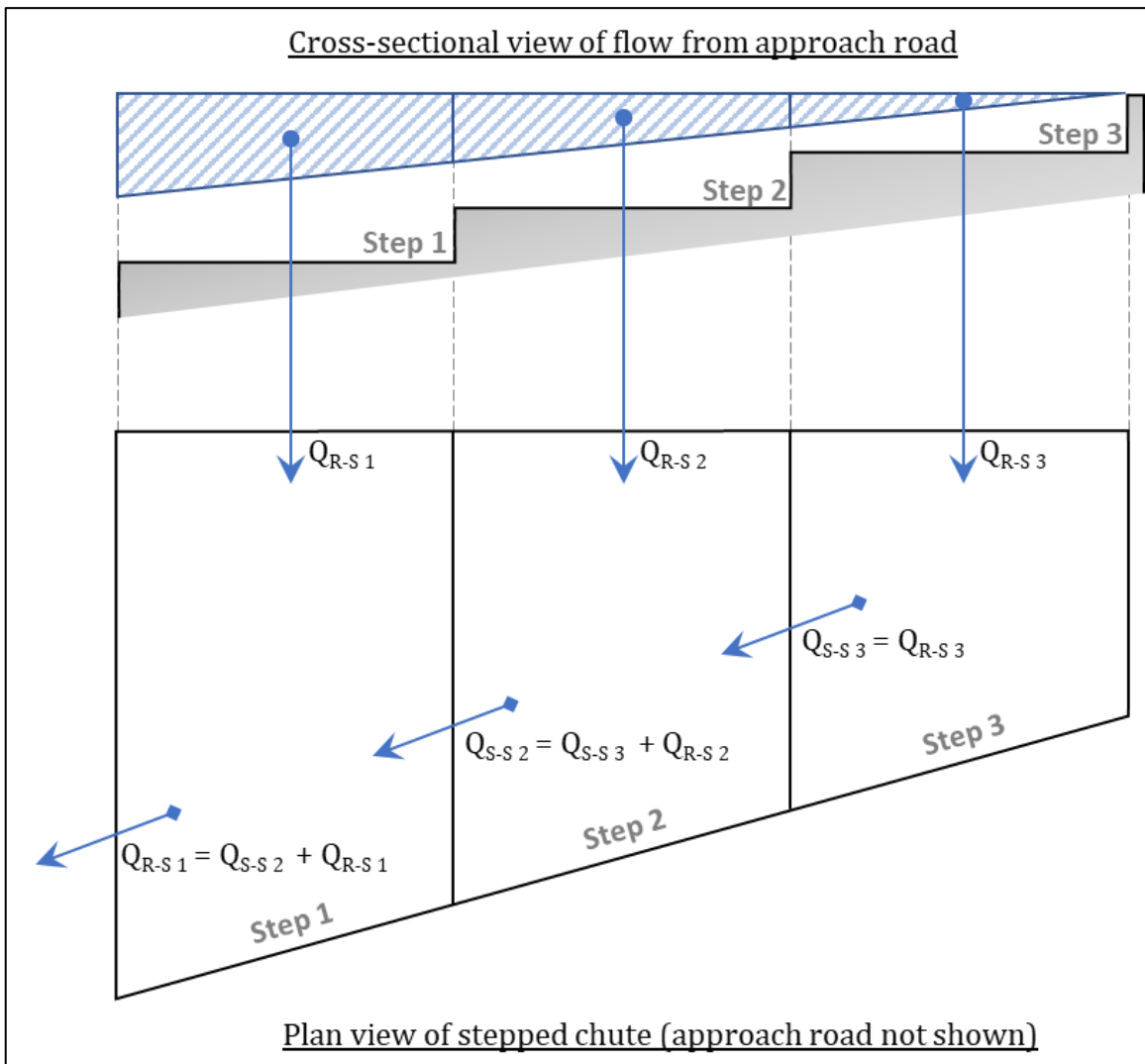


Figure A.3: Flow Accumulation Down the Stepped Chute

Step 7. Determine the effective overflow width ($W_{\text{effective } (ns)}$) at each step brink as discussed in Section 3.4.3.2 and illustrated in Figure A.4.

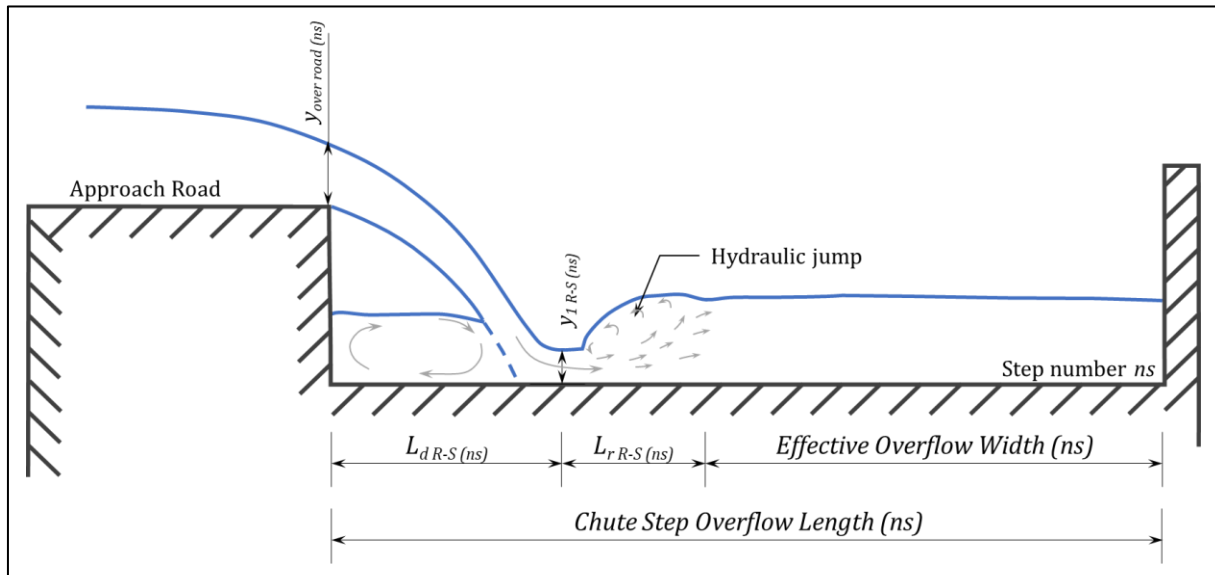


Figure A.4: Effective Chute Step Overflow Width

Step 8. Determine the nappe geometry from one chute step to the next in a similar manor as discussed in Step 4:

Table A-3: Nappe Geometry from One Chute Step onto the Next

Nappe Geometric component	Symbol	Equation	Unit
Critical depth at the brink of the step	$y_{c S-S (ns)}$	$y_{c S-S (ns)} = \left(\frac{Q_{S-S (ns)}^2}{g W_{\text{effective } (ns)}^2} \right)^{\frac{1}{3}}$	m
Flow depth after nappe impingement	$y_{1 S-S (ns)}$	$y_{1 S-S (ns)} = 0.54 h_{S-S (ns)} \left(\frac{y_{c S-S (ns)}}{h_{S-S (ns)}} \right)^{1.275}$	m
Conjugate flow depth	$y_{2 S-S (ns)}$	$y_{2 S-S (ns)} = 1.66 h_{S-S (ns)} \left(\frac{y_{c S-S (ns)}}{h_{S-S (ns)}} \right)^{0.81}$	m
Nappe drop length	$L_{d S-S (ns)}$	$L_{d S-S (ns)} = 4.3 h_{S-S (ns)} \left(\frac{y_{c S-S (ns)}}{h_{S-S (ns)}} \right)^{0.81}$	m
Pool depth behind the nappe	$y_{P S-S (ns)}$	$y_{P S-S (ns)} = h_{S-S (ns)} \left(\frac{y_{c S-S (ns)}}{h_{S-S (ns)}} \right)^{0.66}$	m
Froude number of the flow after nappe impingement	$Fr_{1 S-S (ns)}$	$Fr_{1 S-S (ns)} = \left(\frac{Q_{S-S (ns)}^2 W_{\text{effective } (ns)}}{g (W_{\text{effective } (ns)} \times y_{1 S-S (ns)})^3} \right)^{\frac{1}{2}}$	-
Hydraulic jump roller length	$L_{r S-S (ns)}$	$L_{r S-S (ns)} = 8 y_{1 S-S (ns)} (Fr_{1 S-S (ns)} - 1.5)$	m

Step 9. Ensure that the conjugate depths ($y_{2 S-S (ns)}$) determined in Step 8 do not exceed the step height ($h_{S-S (ns)}$) by either increasing the step length or decreasing the number of steps (resulting in increased step height).

Step 10. Determine the nappe cavity ventilation requirement (Bos 1989):

$$Q_{air\ S-S\ (ns)} = 0.1 \frac{Q_{S-S\ (ns)}}{\left(\frac{y_{p\ S-S\ (ns)}}{y_{c\ S-S\ (ns)}}\right)^{1.5}} \quad \text{Eq. A.8}$$

where:

$Q_{air\ S-S\ (ns)}$ is the nappe aeration for flow from step ns to the next (m^3/s);

$Q_{S-S\ (ns)}$ is the nappe discharge from step ns (m^3/s);

$y_{p\ S-S\ (ns)}$ is the pool depth beneath the nappe from step ns (m);

$y_{c\ S-S\ (ns)}$ is the critical flow depth on step ns (m); and

ns is the number of the chute step in question (dimensionless).

Step 11. Verify that the sum of the drop length and hydraulic jump roller length, for flow from one chute step to the next, is less than the step length (in the direction of the chute) ($L_{d\ S-S\ (ns)} + L_{r\ S-S\ (ns)} > W_{step}$).

Step 12. Ensure that nappe flow conditions are maintained by remaining in the NH and NP regions of Figure A.5.

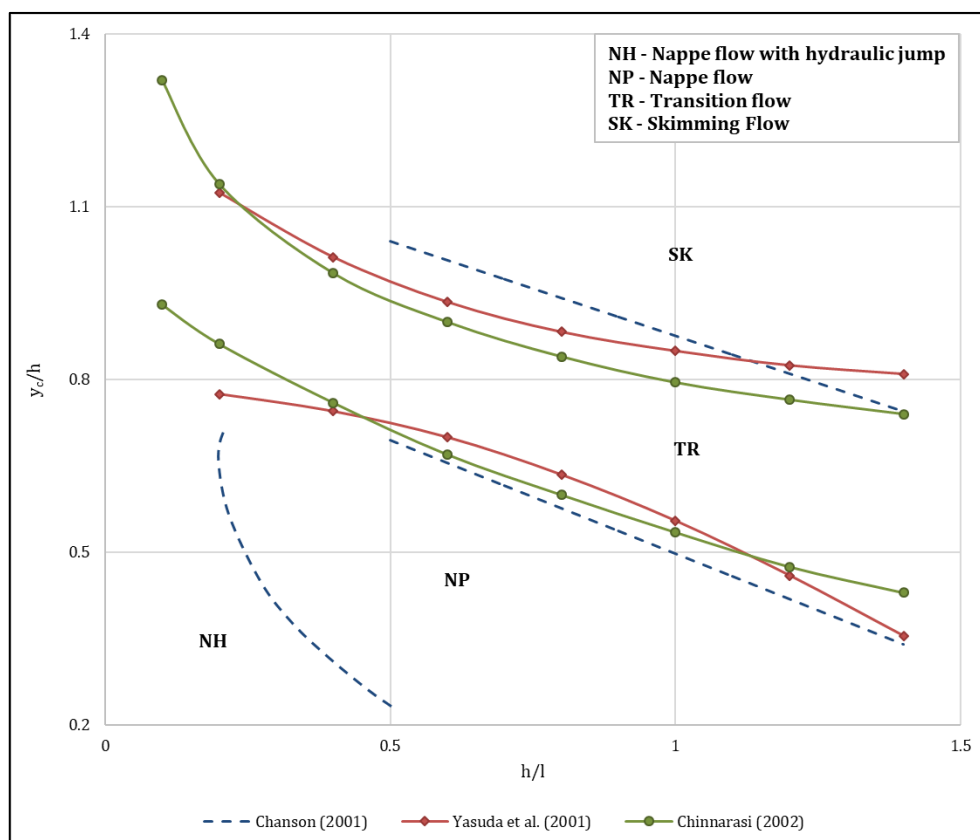


Figure A.5: Flow Regimes on Stepped Spillways (adapted from Khatsuria:2005)

Step 13. Review the chute dimensions and alter where necessary.



APPENDIX B: MODEL DESIGN

B.1. MODEL DESIGN

The detailed design calculations for the prototype and the scaled values for the model are contained in this appendix, as well as an example calculation of the stepped chute lengths using the relationship deduced in Chapter 5. The calculations for the model design were divided into two sections. The first section includes the design of the low-level river crossing and the second includes the design of the stepped chute. The design procedure followed for both the LLRC and the stepped chute is contained in APPENDIX A. The calculations were done using the prototype values and only the final calculated values were converted to the hydraulic model scaled values using the Froude law scale ratios listed in Table B-1. The model scale used was $S = 15$.

Table B-1: Froude's Law Scale Ratios

Parameter	Unit (SI)	Model to Prototype Ratio Relationship
Distance	m	$L_m = \frac{L_p}{S}$
Area	m^2	$A_m = \frac{A_p}{S^2}$
Volume	m^3	$V_m = \frac{V_p}{S^3}$
Time	s	$t_m = \frac{t_p}{S^{1/2}}$
Velocity	m/s	$v_m = \frac{v_p}{S^{1/2}}$
Discharge	m^3/s	$Q_m = \frac{Q_p}{S^{5/2}}$
Unit Discharge	$\text{m}^3/\text{s}/\text{m}$	$q_m = \frac{q_p}{S^{3/2}}$

B.2. DESIGN OF THE LOW-LEVEL RIVER CROSSING

Step 1. Dimensions of the LLRC:

Table B-2: Dimensions Used for Low-Level River Crossing

Parameter	Prototype Value	Model Value	Dimension
$S_{approach}$	0.0125	0.0125	m/m
R_w	4.500	0.300	m
R_{cf}	0 %	0 %	%
h_{deck}	1.800	0.120	m
d_{deck}	0.300	0.020	m
D	1.500	0.100	m
$w_{culvert}$	1.500	0.100	m
$n_{culverts}$	1 & 2.5	1 & 2.5	dimensionless
$S_{pculvert}$	1.800	0.120	m
$y_{over road}$	a. 0.060 b. 0.120 c. 0.180 d. 0.240 e. 0.300	a. 0.004 b. 0.008 c. 0.012 d. 0.016 e. 0.020	m

Step 2. Flow over the LLRC road:

$$Q_{over} = \left(\frac{F_r^2 g A_{over}^3}{B} \right)^{\frac{1}{2}} \quad \text{Eq. B.1}$$

Table B-3: Flow Over the Low-Level River Crossing

$y_{over road}$ (m)	F_{over} (dimensionless)	A_{over} (m^2)	B_{over} (m)	Q_{over} (Prototype) (m^3/s)	Q_{over} (Model) (l/s)
0.060	1	0.423	9.450	0.280	0.322
0.120	1	1.134	14.250	1.002	1.150
0.180	1	2.133	19.050	2.235	2.565
0.240	1	3.420	23.850	4.056	4.655
0.300	1	4.995	28.650	6.532	7.496

Step 3. Determine the flow through the culvert(s):

Inlet conditions were expected as no downstream controls, which would cause tailwater, was added. For Inlet Control use Eq. B.2 and Eq. B.3as recommended by Rooseboom and Van Vuuren (2013):

$$\text{For: } 0 < H_1/D < 1.2 \quad \text{Eq. B.2}$$

$$Q_{under} = n_{culverts} \frac{2}{3} C_B w_{culvert} H_1 \sqrt{\frac{2}{3} g H_1}$$

For: $H_1/D > 1.2$

Eq. B.3

$$Q_{under} = n_{culverts} C_h w_{culvert} D \sqrt{2g(H_1 - C_h D)}$$

H_1 is needs to be calculated for each overflow depth using Eq. B.4:

$$H_1 = h_{deck} + \frac{Q_{over}^2}{A_{over}^2 2g} \quad \text{Eq. B.4}$$

Table B-4: Upstream Energy Levels

$y_{over road}$ (m)	h_{deck} (m)	Q_{over} (m^3/s)	A_{over} (m^2)	H_1 (Prototype) (m)	H_1 (Model) (m)
0.060	1.8	0.280	0.423	1.882	0.125
0.120	1.8	1.002	1.134	1.960	0.131
0.180	1.8	2.235	2.133	2.036	0.136
0.240	1.8	4.056	3.420	2.112	0.141
0.300	1.8	6.532	4.995	2.187	0.146

Determine the upstream energy level (H_1) to culvert height (D) ratio:

Table B-5: H_1/D Ratios

$y_{over road}$ (m)	D (m)	H_1 (m)	H_1/D (dimensionless)
0.060	1.5	1.882	1.255
0.120	1.5	1.960	1.307
0.180	1.5	2.036	1.357
0.240	1.5	2.112	1.408
0.300	1.5	2.187	1.458

The minimum H_1/D ratio was 1.255. Eq. B.3 was therefore used to determine the flow through the culverts.

Table B-6: Culvert Flow Input Parameters

$y_{over\ road}$ (m)	D (m)	$w_{culvert}$ (m)	C_h (dimensionless)	H_1 (m)
0.060	1.5	1.5	0.6	1.882
0.120	1.5	1.5	0.6	1.960
0.180	1.5	1.5	0.6	2.036
0.240	1.5	1.5	0.6	2.112
0.300	1.5	1.5	0.6	2.187

Table B-7: Culvert Flow Results

$y_{over\ road}$ (m)	Q_{under} for 1 culvert (Prototype) (m^3/s)	Q_{under} for 1 culvert (Model) (l/s)	Q_{under} for 2.5 culverts (Prototype) (m^3/s)	Q_{under} for 2.5 culverts (Model) (l/s)
0.060	5.927	6.801	14.817	17.003
0.120	6.156	7.064	15.390	17.661
0.180	6.373	7.314	15.933	18.284
0.240	6.582	7.554	16.456	18.884
0.300	6.784	7.785	16.961	19.463

Table B-8: Total Prototype and Hydraulic Model Flows

$y_{over\ road}$ (m)	Q_{Total} for 1 culvert (Prototype) (m^3/s)	Q_{Total} for 1 culvert (Model) (l/s)	Q_{Total} for 2.5 culverts (Prototype) (m^3/s)	Q_{Total} for 2.5 culverts (Model) (l/s)
0.060	6.207	7.123	15.097	17.325
0.120	7.158	8.214	16.392	18.810
0.180	8.609	9.879	18.169	20.850
0.240	10.639	12.208	20.512	23.539
0.300	13.317	15.282	23.493	26.959

B.3. DESIGN OF THE STEPPED CHUTE

The stepped chute was designed for the maximum prototype overflow depth ($y_{over road}$) of 300 mm.

Step 1. Chute dimensions for 3 chute steps ($n_{steps}=3$):

Table B-9: Preliminary Prototype Chute Dimensions

n_{steps} (dimensionless)	h_{deck} (m)	$S_{approach}$ (m/m)	$y_{over road}$ (m)	h_{s-s} (Prototype) (m)	W_{Step} (Prototype) (m)
3	1.8	0.0125	0.3	0.525	8.000

Table B-10: Preliminary Hydraulic Model Chute Dimensions

h_{s-s} (Model) (m)	W_{Step} (Model) (m)
0.035	0.533

Step 2. Flow from the approach road:

Table B-11: Flow Distribution over the Left Bank ($y_{over road} = 60$ mm)

ns	$A_{over LB}$ (m ²)	$Q_{R-S(ns)}$ (Prototype) (m ³ /s)	$Q_{R-S(ns)}$ (Model) (l/s)
Step 1	0.144	0.095	0.110
Step 2	-	-	-
Step 3	-	-	-

Table B-12: Flow Distribution over the Left Bank ($y_{over road} = 120$ mm)

ns	$A_{over LB}$ (m ²)	$Q_{R-S(ns)}$ (Prototype) (m ³ /s)	$Q_{R-S(ns)}$ (Model) (l/s)
Step 1	0.560	0.495	0.568
Step 2	0.016	0.014	0.016
Step 3	-	-	-

Table B-13: Flow Distribution over the Left Bank ($y_{over road} = 180$ mm)

ns	$A_{over LB}$ (m ²)	$Q_{R-S(ns)}$ (Prototype) (m ³ /s)	$Q_{R-S(ns)}$ (Model) (l/s)
Step 1	1.040	1.090	1.251
Step 2	0.256	0.268	0.308
Step 3	-	-	-

Table B-14: Flow Distribution over the Left Bank ($y_{over road} = 240$ mm)

<i>ns</i>	$A_{over LB}$ (m ²)	$Q_{R-S(ns)}$ (Prototype) (m ³ /s)	$Q_{R-S(ns)}$ (Model) (l/s)
Step 1	1.520	1.803	2.069
Step 2	0.720	0.854	0.980
Step 3	0.064	0.076	0.087

Table B-15: Flow Distribution over the Left Bank ($y_{over road} = 300$ mm)

<i>ns</i>	$A_{over LB}$ (m ²)	$Q_{R-S(ns)}$ (Prototype) (m ³ /s)	$Q_{R-S(ns)}$ (Model) (l/s)
Step 1	2	2.616	3.002
Step 2	1.2	1.569	1.801
Step 3	0.4	0.523	0.600

Step 3. The cross fall of the deck was 0 %. Critical flow conditions were therefore assumed and the flow over the deck ($y_{over road}$) was therefore equal to the critical flow depth.

Table B-16: Drop Height from Approach Road onto Each Step

<i>ns</i>	$h_{R-S(ns)}$ (Prototype) (m)	$h_{R-S(ns)}$ (Model) (m)
Step 1	1.275	0.085
Step 2	0.850	0.057
Step 3	0.425	0.028

Step 4. Nappe geometry (approach road onto the stepped chute):

Table B-17: Nappe Geometry from Approach Road onto Each Chute Step ($y_{over road} = 300$ mm)

Nappe Component	Step 1		Step 2		Step 3	
	Prototype (m)	Model (m)	Prototype (m)	Model (m)	Prototype (m)	Model (m)
$y_{1 R-S(ns)}$	0.109	0.007	0.073	0.005	0.036	0.002
$L_{d R-S(ns)}$	1.698	0.113	1.132	0.075	0.566	0.038
$y_{P R-S(ns)}$	0.491	0.033	0.327	0.022	0.164	0.011
$F r_{1 R-S(ns)}$	2.908	2.908	3.205	3.205	3.022	3.022
$L_{r R-S(ns)}$	1.226	0.082	0.990	0.066	0.442	0.029

Step 5. Nappe cavity ventilation requirement (approach road onto the stepped chute):

Table B-18: Nappe Cavity Ventilation Requirement from Approach Road onto Each Chute Step
 $(y_{over\ road} = 300\ mm)$

Nappe Component	Step 1		Step 2		Step 3	
	Prototype (m ³ /s)	Model (l/s)	Prototype (m ³ /s)	Model (l/s)	Prototype (m ³ /s)	Model (l/s)
$Q_{air\ R-S\ (ns)}$	0.125	0.144	0.075	0.086	0.025	0.029

Step 6. Flow accumulation down the stepped chute:

Table B-19: Flow Accumulation Down the Chute ($y_{over\ road} = 300\ mm$)

<i>ns</i>	$Q_{R-S\ (ns)}$ (Prototype) (m ³ /s)	$Q_{S-S\ (ns)}$ (Prototype) (m ³ /s)	$Q_{S-S\ (ns)}$ (Model) (l/s)
Step 3	0.523	0.523	0.600
Step 2	1.569	2.092	2.401
Step 1	2.616	4.708	5.403

Step 7. Effective overflow width:

Table B-20: Flow Accumulation Down the Chute ($y_{over\ road} = 300\ mm$)

<i>ns</i>	$L_{Step\ (ns)}$ (Prototype) (m)	$W_{effective(ns)}$ (Prototype) (m)	$W_{effective(ns)}$ (Model) (m)
Step 3	8.333	7.326	0.488
Step 2	11.667	9.545	0.636
Step 1	15.000	12.076	0.805

The step lengths were selected to ensure that the conjugate depths ($y_{2\ S-S\ (ns)}$) calculated in step 8 do not exceed the step height ($h_{S-S\ (ns)}$).

Step 8. Nappe geometry (step to step):

Table B-21: Nappe Geometry from One Chute Step onto the Next ($y_{over\ road} = 300\ mm$)

Nappe component	From Step 3 onto Step 2		From Step 2 onto Step 1	
	Prototype (m)	Model (m)	Prototype (m)	Model (m)
$y_{c\ S-S\ (ns)}$	0.080	0.005	0.170	0.011
$y_{1\ S-S\ (ns)}$	0.026	0.002	0.067	0.004
$y_{2\ S-S\ (ns)}$	0.191	0.013	0.349	0.023
$L_{d\ S-S\ (ns)}$	0.494	0.033	0.905	0.060
$y_{P\ S-S\ (ns)}$	0.152	0.010	0.249	0.017
$Fr_{1\ S-S\ (ns)}$	4.804	4.804	3.284	3.284
$L_{r\ S-S\ (ns)}$	0.685	0.046	0.960	0.064

Step 9. The maximum conjugate depth ($y_{2S-S(2)}$) of 0.349 m was less than the step height ($h_{S-S(2)}$) of 0.525 m.

Step 10. Nappe cavity ventilation requirement (step to step):

Table B-22: Nappe Cavity Ventilation Requirement from One Chute Step onto the Next
($y_{over road} = 300 \text{ mm}$)

Nappe Component	From Step 3 onto Step 2		From Step 2 onto Step 1	
	Prototype (m^3/s)	Model (l/s)	Prototype (m^3/s)	Model (l/s)
$Q_{air S-S(ns)}$	0.020	0.023	0.118	0.135

Step 11. Verify that the step length exceeds the nappe drop length and hydraulic jump length:

Table B-23: Comparison of Drop Length ($L_{dS-S(ns)}$) Plus Hj Roller Length ($L_{rS-S(ns)}$) with Step Length in Direction of Flow ($y_{over road} = 300 \text{ mm}$)

Nappe Component	From Step 3 onto Step 2		From Step 2 onto Step 1	
	Prototype (m)	Model (m)	Prototype (m)	Model (m)
$L_{dS-S(ns)} + L_{rS-S(ns)}$	1.179	0.079	1.865	0.124

The calculated drop length ($L_{dS-S(ns)}$) plus the hydraulic jump roller length ($L_{rS-S(ns)}$) for both step 3 and step 2 were shorter than the step length in the direction of the chute (W_{step}) of 8 m.

Step 12. Ensure nappe flow conditions:

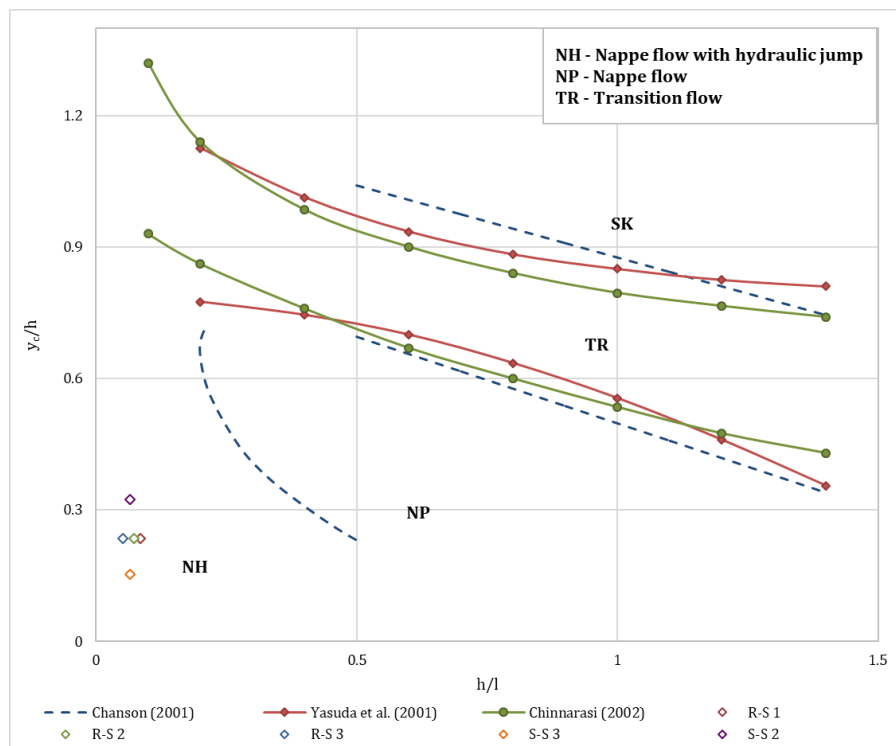


Figure B.1: Flow Regimes on Stepped Chute (adapted from Khatsuria:2005)

B.4. APPLICATION OF THE REGRESSION ANALYSIS EQUATION FOR THE STEPPED CHUTE LENGTH

An example calculation of the stepped chute dimensions (including the use of the regression analysis equation for the stepped chute lengths) is illustrated below.

The following information was derived following the design of a LLRC:

Table B-24: Dimensions Determined for a Low-Level River Crossing

Parameter	Value	Dimension
$S_{approach}$	0.010	m/m
R_w	4.500	m
R_{cf}	0 %	%
h_{deck}	0.900	m
d_{deck}	0.150	m
D	0.750	m
$w_{culvert}$	1.500	m
$n_{culverts}$	5	dimensionless
$s_{culvert}$	1.800	m
$y_{over road}$	0.150	m

Flow over the LLRC road:

$$Q_{over} = \left(\frac{F_r^2 g A_{over}^3}{B} \right)^{\frac{1}{2}} \quad \text{Eq. B.5}$$

Table B-25: Flow Over the Low-Level River Crossing

$y_{over road}$ (m)	Fr_{over} (dimensionless)	A_{over} (m^2)	B_{over} (m)	Q_{over} (m^3/s)
0.150	1	3.645	39.300	3.480

Following the determination of the flow over the LLRC, the design of the stepped chute is detailed below:

The number of steps was selected to be equal to three ($n_{steps} = 3$) with the resulting step height and width (using Eq. B.6 and Eq. B.7) as per Table B-26:

$$h_{s-s} = \frac{h_{deck} + y_{over road}}{n_{steps} + 1} \quad \text{Eq. B.6}$$

$$W_{step} = \frac{y_{over road}}{S_{approach} \times n_{steps}} \quad \text{Eq. B.7}$$

Table B-26: Preliminary Chute Dimensions

n_{steps} (dimensionless)	h_{deck} (m)	$S_{approach}$ (m/m)	$y_{over road}$ (m)	h_{s-s} (m)	W_{Step} (m)
3	0.9	0.010	0.150	0.263	5.000

The flow from the approach road onto each step, as well as the flow accumulation down the chute is listed in Table B-27 (with step 1 referring to the bottom step):

Table B-27: Flow distribution over Both the Left and Right Bank ($y_{over road} = 150$ mm)

ns	$A_{over LB}$ (m ²)	$Q_{R-S(ns)}$ (m ³ /s)	$Q_{S-S(ns)}$ (m ³ /s)
Step 1	0.63	0.596	1.073
Step 2	0.38	0.358	0.477
Step 3	0.13	0.119	0.119

The flow depth above each step and the drop height from the approach road onto each step was calculated and is listed in Table B-28:

Table B-28: Drop Height from Approach Road onto Each Step

ns	$y_{over road(ns)}$ (m)	$h_{R-S(ns)}$ (m)
Step 1	0.150	0.638
Step 2	0.100	0.425
Step 3	0.050	0.213

The chute lengths were calculated using Eq. B.8 and is listed in Table B-29:

$$L_{step(ns)} = y_{over road(ns)} \cdot \left(12.774 + 10.05 \cdot \frac{h_{R-S(ns)}}{y_{over road(ns)}} - 7.515 \cdot \frac{Q_{S-S(ns+1)}}{Q_{R-S(ns)}} \right) \quad \text{Eq. B.8}$$

Table B-29: Calculated Chute Step Lengths

ns	$L_{step(ns)}$ (m)
Step 1	7.421
Step 2	5.298
Step 3	2.774

The calculated chute lengths were adjusted to more practical lengths and are listed in Table B-30:

Table B-30: Altered Chute Step Lengths

<i>ns</i>	<i>L_{step (ns)}</i> (m)
Step 1	7.500
Step 2	5.333
Step 3	3.167

The nappe geometry from the approach road onto each step as well as the nappe geometry from one chute step to the next is as listed in Table B-31 and Table B-32 :

Table B-31: Nappe Geometry from Approach Road onto Each Chute Step ($y_{over road} = 150$ mm)

Nappe Component	Step 1 (m)	Step 2 (m)	Step 3 (m)
$y_{1 R-S (ns)}$	0.054	0.036	0.018
$L_{d R-S (ns)}$	0.849	0.566	0.283
$y_{P R-S (ns)}$	0.245	0.164	0.082
$F_{r 1 R-S (ns)}$	2.999	3.306	3.117
$L_{r R-S (ns)}$	0.653	0.524	0.235

Table B-32: Nappe Geometry from One Chute Step onto the Next ($y_{over road} = 150$ mm)

Nappe component	From Step 3 onto Step 2	From Step 2 onto Step 1
$y_{c S-S (ns)}$	0.059 m	0.109 m
$y_{1 S-S (ns)}$	0.021 m	0.046 m
$y_{2 S-S (ns)}$	0.130 m	0.214 m
$L_{d S-S (ns)}$	0.337 m	0.553 m
$y_{P S-S (ns)}$	0.098 m	0.147 m
$F_{r 1 S-S (ns)}$	3.899	2.883
$L_{r S-S (ns)}$	0.407 m	0.510 m

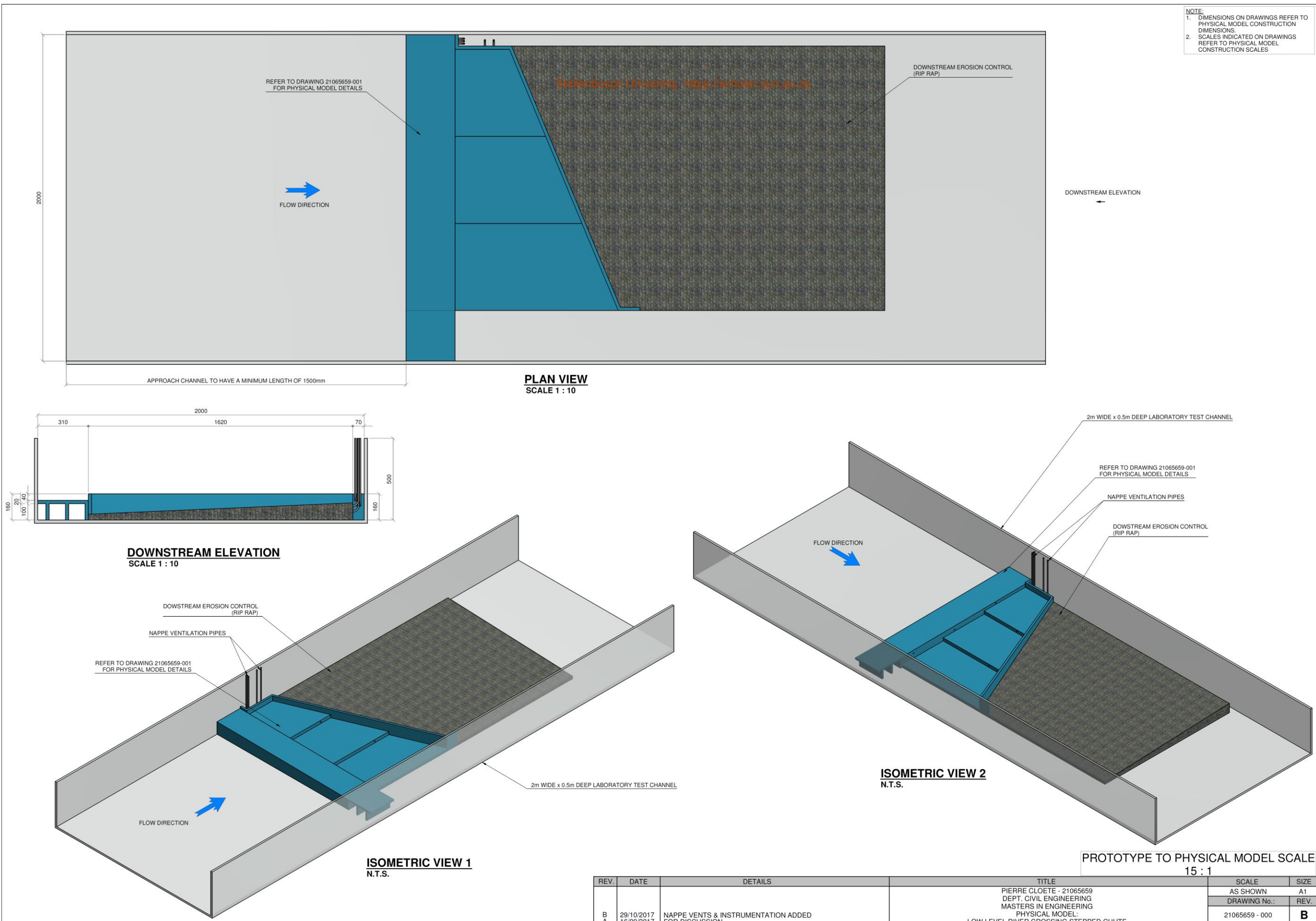
The maximum conjugate depth ($y_{2 S-S (2)}$) of 0.214 m was less than the step height ($h_{S-S (2)}$) of 0.263 m.

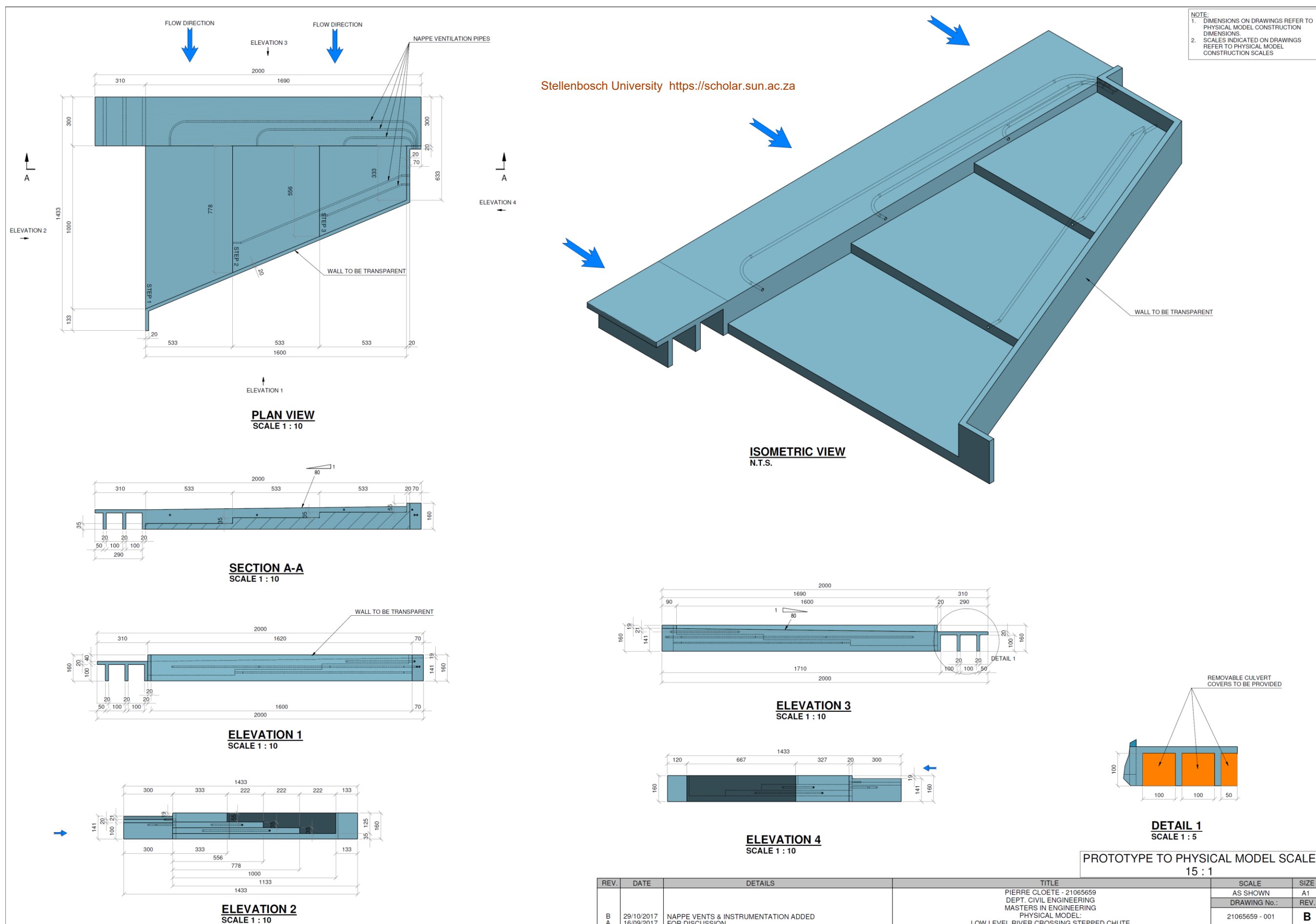
The step length, in the direction of the stepped chute, ($W_{Step} = 5$ m) also exceeded the sum of the corresponding step nappe drop lengths and hydraulic jump lengths, as listed in Table B-33, indicating ample distance for a hydraulic jump to form on the step:

Table B-33: Comparison of Drop Length ($L_{dS-S(ns)}$) Plus Hj Roller Length ($L_{rS-S(ns)}$) with Step Length in Direction of Flow ($y_{over road} = 150$ mm)

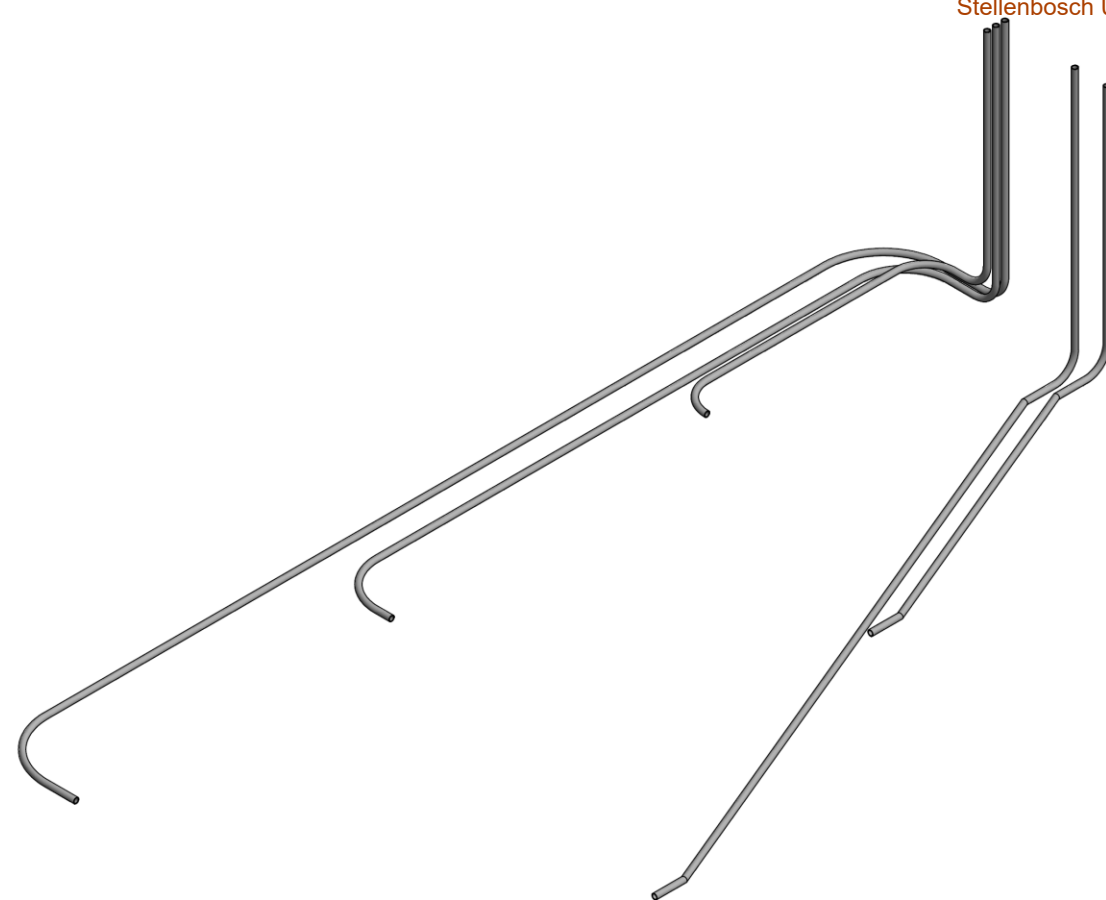
Nappe Component	From Step 3 onto Step 2	From Step 2 onto Step 1
$L_{dS-S(ns)} + L_{rS-S(ns)}$	0.744 m	1.063 m

APPENDIX C: DESIGN DRAWINGS OF THE MODEL

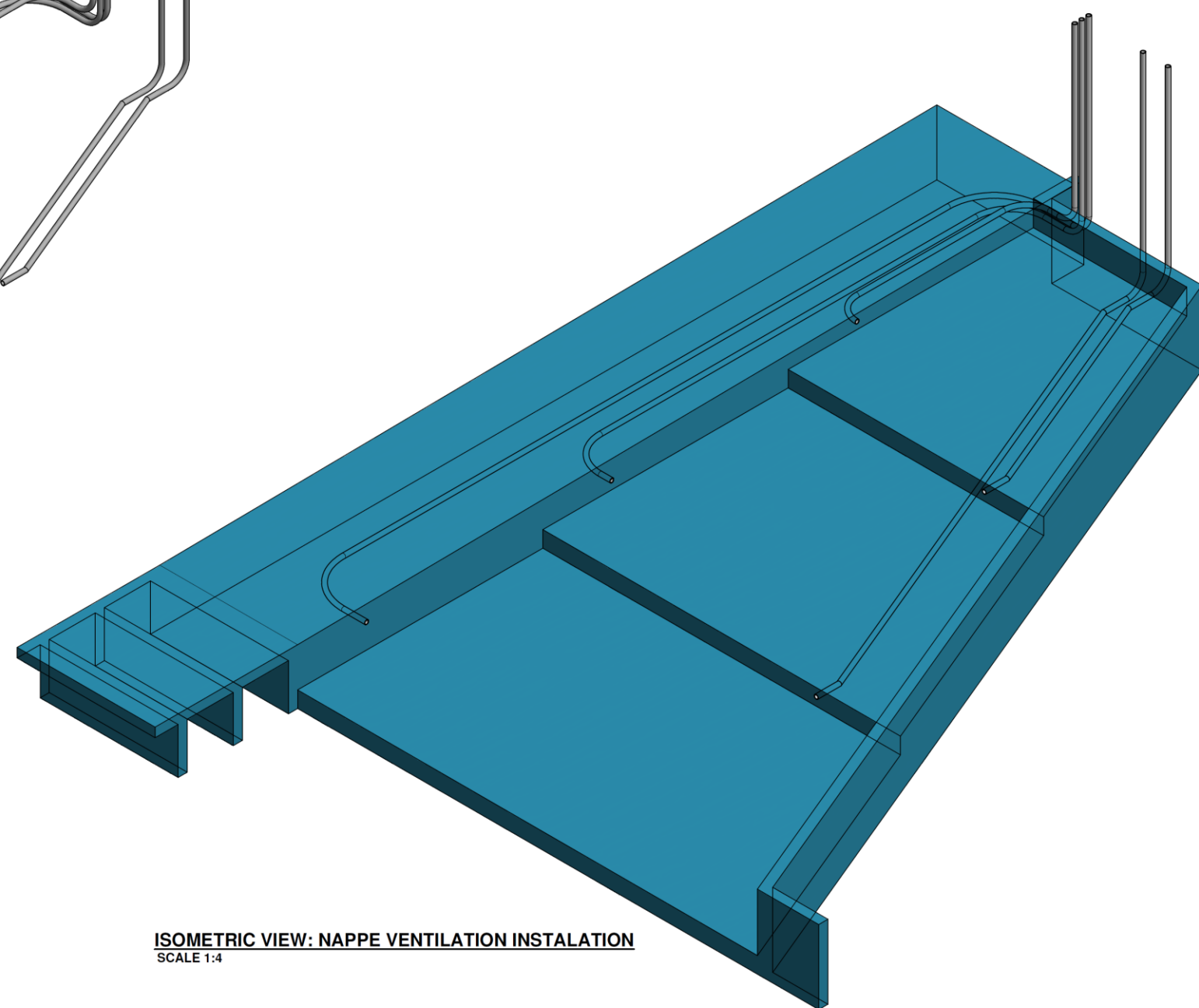




NOTE:
 1. DIMENSIONS ON DRAWINGS REFER TO PHYSICAL MODEL CONSTRUCTION DIMENSIONS.
 2. SCALES INDICATED ON DRAWINGS REFER TO PHYSICAL MODEL CONSTRUCTION SCALES

Stellenbosch University <https://scholar.sun.ac.za>

ISOMETRIC VIEW: NAPPE VENTILATION
SCALE 1:4



ISOMETRIC VIEW: NAPPE VENTILATION INSTALATION
SCALE 1:4

PROTOTYPE TO PHYSICAL MODEL SCALE
15 : 1

REV.	DATE	DETAILS	TITLE	SCALE	SIZE
A	29/10/2017	FOR DISCUSSION	PIERRE CLOETE - 21065659 DEPT. CIVIL ENGINEERING MASTERS IN ENGINEERING PHYSICAL MODEL: LOW LEVEL RIVER CROSSING STEPPED CHUTE	AS SHOWN DRAWING No.: 21065659 - 001	A1 REV. A

APPENDIX D: COMPLETE TESTING SCHEDULE

Table D-1: Test Run Details

No.:	Test Run:	Flow (l/s)	V-notch head (mm)	Apparatus required			
				Flow depth measurement needle with overhead trolley	V-Notch weir	Wika S-10 Pressure sensors	Lutron Hotwire Anemometer
1.1.1	Culverts blocked - Vents blocked - No rip rap						
	a. LLRC overflow depth = 4 mm	0.32	34	X	X	X	
	b. LLRC overflow depth = 8 mm	1.15	58	X	X	X	
	c. LLRC overflow depth = 12 mm	2.57	80	X	X	X	
	d. LLRC overflow depth = 16 mm	4.65	102	X	X	X	
	e. LLRC overflow depth = 20 mm	7.50	124	X	X	X	
1.1.2	Culverts blocked - Vents open - No rip rap						
	a. LLRC overflow depth = 4 mm	0.32	34	X	X	X	X
	b. LLRC overflow depth = 8 mm	1.15	58	X	X	X	X
	c. LLRC overflow depth = 12 mm	2.57	80	X	X	X	X
	d. LLRC overflow depth = 16 mm	4.65	102	X	X	X	X
	e. LLRC overflow depth = 20 mm	7.50	124	X	X	X	X
1.1.3	Repeat test 1.1.1.e - Run with maximum flow depth over LLRC						
	LLRC overflow depth = 20 mm	7.50	124	X	X	X	
1.2.1	Culverts open - Vents blocked - No rip rap						
	a. LLRC overflow depth = 4 mm	7.12	121	X	X	X	
	b. LLRC overflow depth = 8 mm	8.21	128	X	X	X	
	c. LLRC overflow depth = 12 mm	9.88	138	X	X	X	
	d. LLRC overflow depth = 16 mm	12.21	151	X	X	X	
	e. LLRC overflow depth = 20 mm	15.28	165	X	X	X	
1.2.2	Culverts open - Vents open - No rip rap						
	a. LLRC overflow depth = 4 mm	7.12	121	X	X	X	X
	b. LLRC overflow depth = 8 mm	8.21	128	X	X	X	X
	c. LLRC overflow depth = 12 mm	9.88	138	X	X	X	X
	d. LLRC overflow depth = 16 mm	12.21	151	X	X	X	X
	e. LLRC overflow depth = 20 mm	15.28	165	X	X	X	X
1.2.3	Repeat test 1.2.1.e - Run with maximum flow depth over LLRC						
	LLRC overflow depth = 20 mm	15.28	165	X	X	X	

Table D-2: Test Run Details (cont.)

No.:	Test Run:	Flow (l/s)	V-notch head (mm)	Apparatus required			
				Flow depth measurement needle with overhead trolley	V-Notch weir	Wika S-10 Pressure sensors	Lutron Hotwire Anemometer
2.1.1	Culverts blocked - Vents blocked - Chute wall removed with rip rap						
	a. LLRC overflow depth = 4 mm	0.32	34	X	X	X	
	b. LLRC overflow depth = 8 mm	1.15	58	X	X	X	
	c. LLRC overflow depth = 12 mm	2.57	80	X	X	X	
	d. LLRC overflow depth = 16 mm	4.65	102	X	X	X	
	e. LLRC overflow depth = 20 mm	7.50	124	X	X	X	
2.1.2	Culverts blocked - Vents open - Chute wall removed with rip rap						
	a. LLRC overflow depth = 4 mm	0.32	34	X	X	X	X
	b. LLRC overflow depth = 8 mm	1.15	58	X	X	X	X
	c. LLRC overflow depth = 12 mm	2.57	80	X	X	X	X
	d. LLRC overflow depth = 16 mm	4.65	102	X	X	X	X
	e. LLRC overflow depth = 20 mm	7.50	124	X	X	X	X
2.1.3	Repeat test 2.1.1.e - Run with maximum flow depth over LLRC						
	LLRC overflow depth = 20 mm	7.50	124	X	X	X	
2.2.1	Culverts open - Vents blocked - Chute wall removed with rip rap						
	a. LLRC overflow depth = 4 mm	7.12	121	X	X	X	
	b. LLRC overflow depth = 8 mm	8.21	128	X	X	X	
	c. LLRC overflow depth = 12 mm	9.88	138	X	X	X	
	d. LLRC overflow depth = 16 mm	12.21	151	X	X	X	
	e. LLRC overflow depth = 20 mm	15.28	165	X	X	X	
2.2.2	Culverts open - Vents open - Chute wall removed with rip rap						
	a. LLRC overflow depth = 4 mm	7.12	121	X	X	X	X
	b. LLRC overflow depth = 8 mm	8.21	128	X	X	X	X
	c. LLRC overflow depth = 12 mm	9.88	138	X	X	X	X
	d. LLRC overflow depth = 16 mm	12.21	151	X	X	X	X
	e. LLRC overflow depth = 20 mm	15.28	165	X	X	X	X
2.2.3	Repeat test 2.2.1.e - Run with maximum flow depth over LLRC						
	LLRC overflow depth = 20 mm	15.28	165	X	X	X	

APPENDIX E: PRESSURE DATA

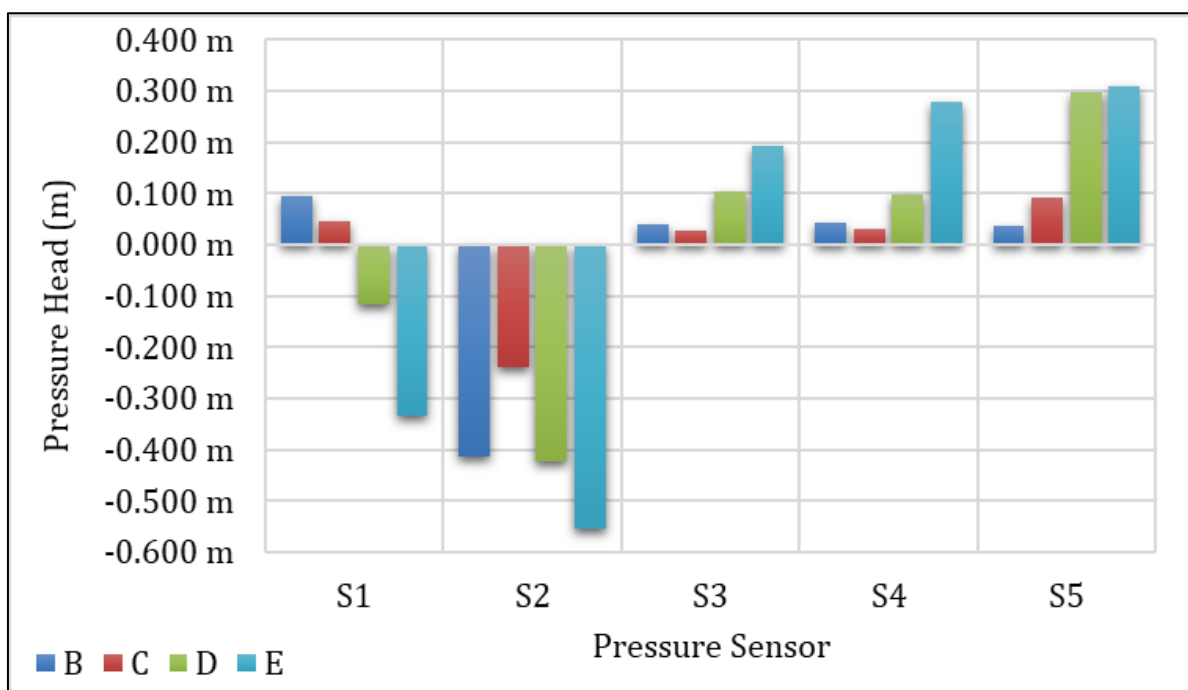


Figure E.1: Prototype Pressures – Test Run No.: 1.1.1.

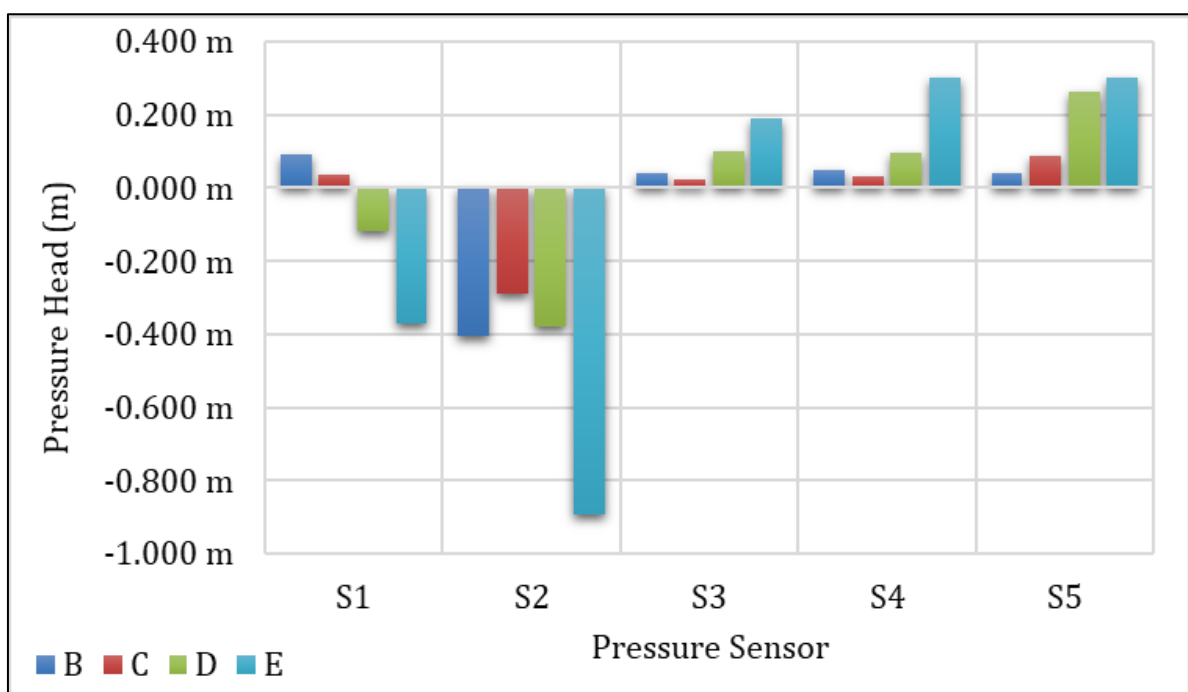


Figure E.2: Prototype Pressures – Test Run No.: 1.1.2.

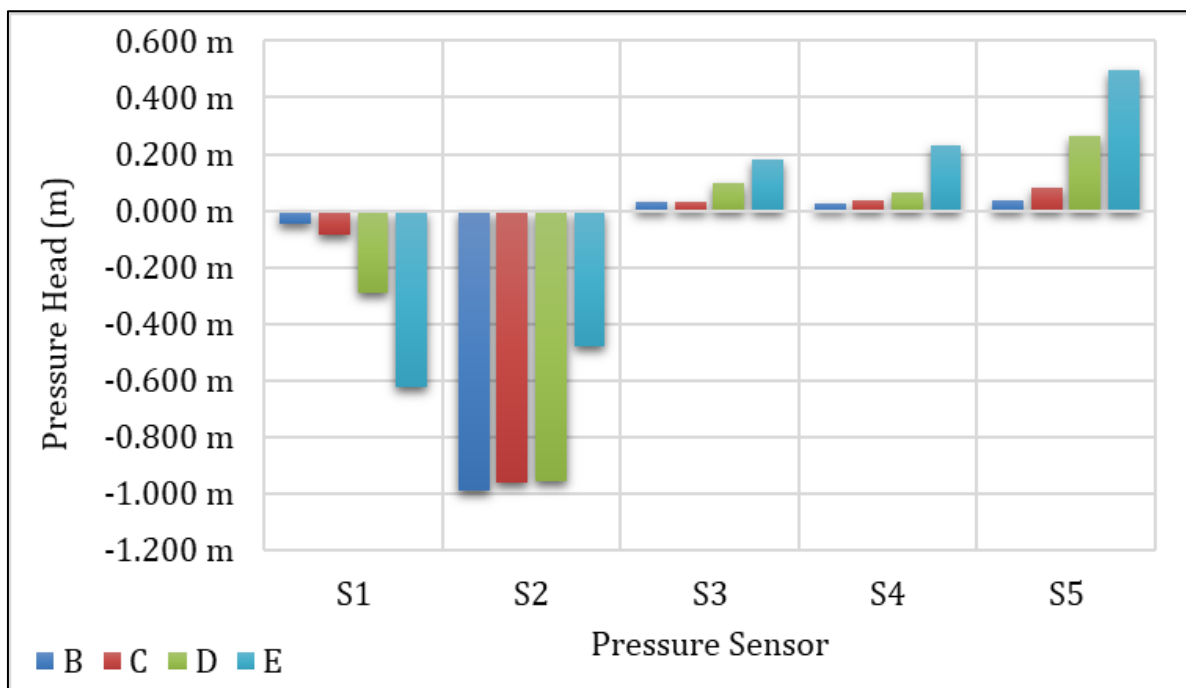


Figure E.3: Prototype Pressures – Test Run No.: 1.2.1.

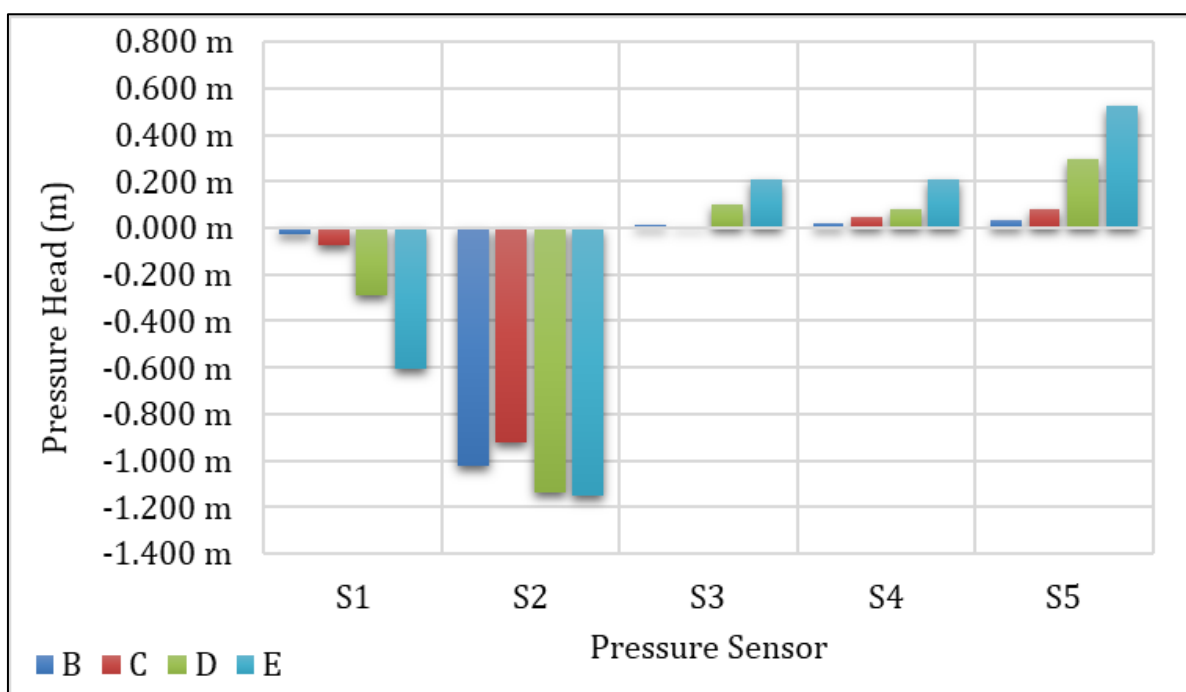


Figure E.4: Prototype Pressures – Test Run No.: 1.2.2.

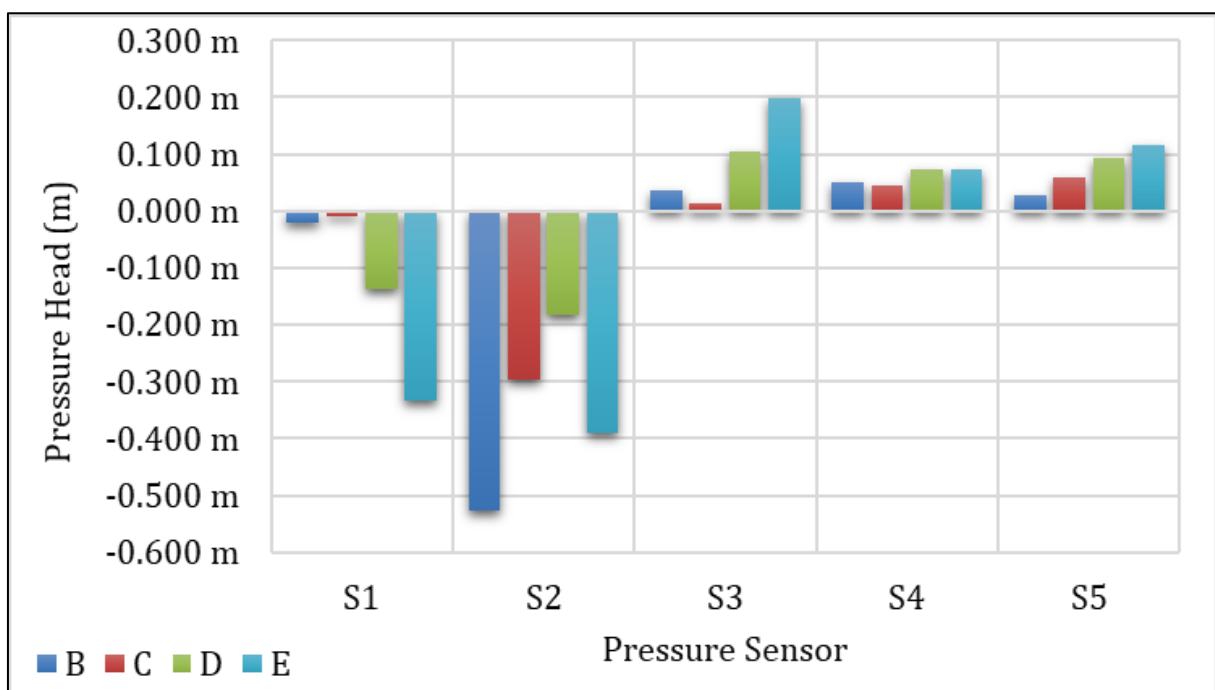


Figure E.5: Prototype Pressures – Test Run No.: 2.1.1.

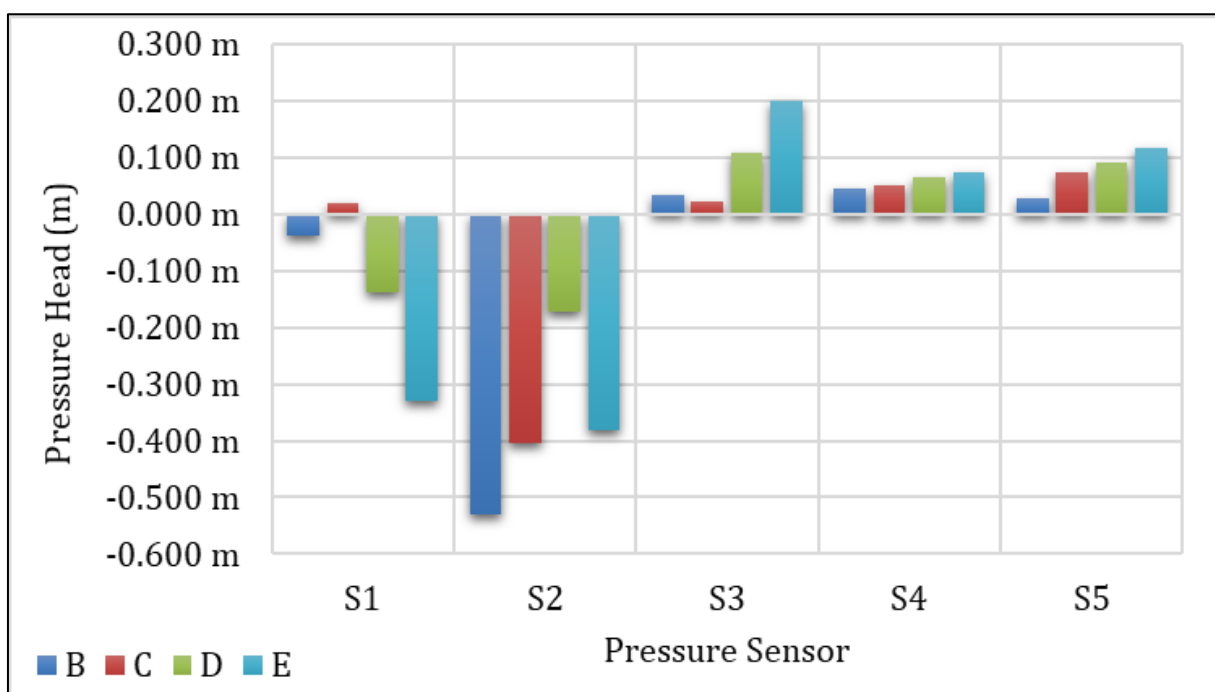


Figure E.6: Prototype Pressures – Test Run No.: 2.1.2.

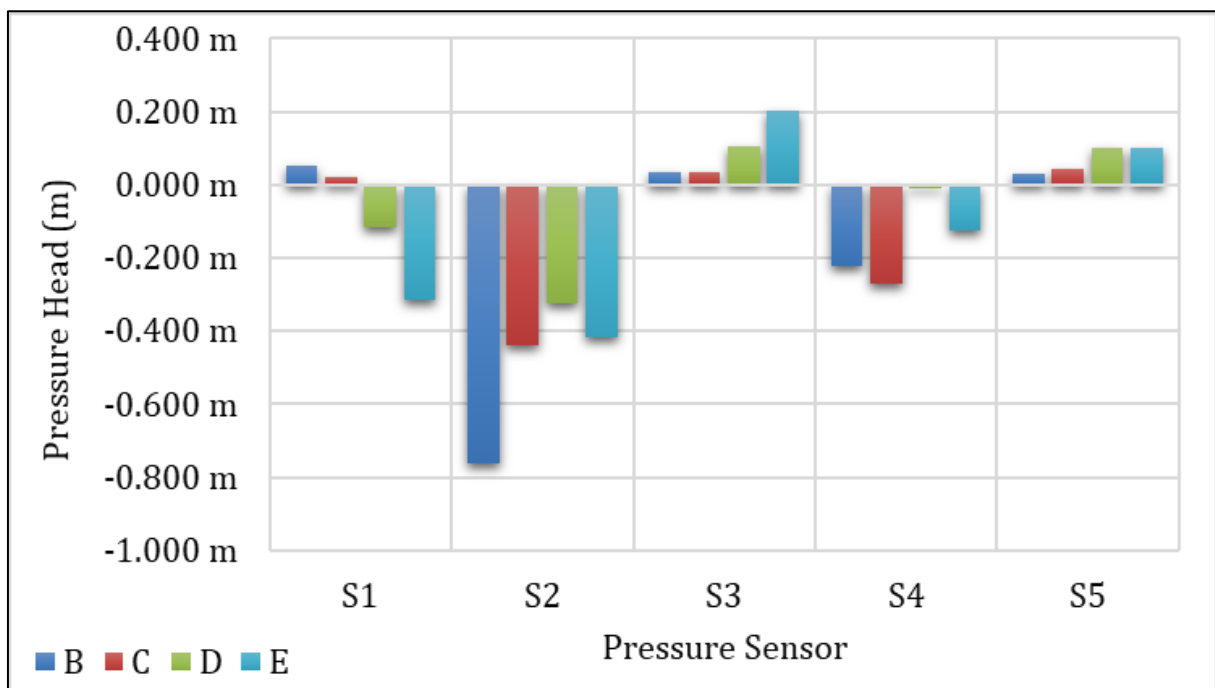


Figure E.7: Hydraulic Model Pressures – Test Run No.: 2.2.1.

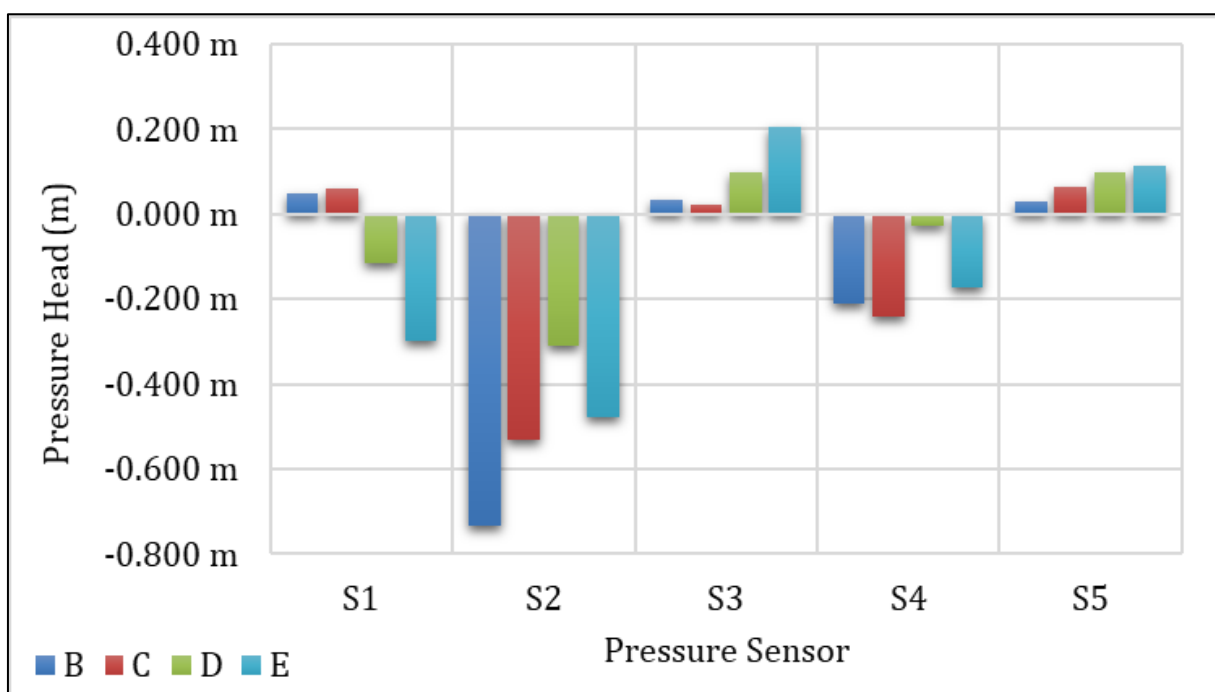


Figure E.8: Hydraulic Model Pressures – Test Run No.: 2.2.2.

APPENDIX F: FLOW PROFILES

Stepped Chute Flow Profile - 1.1.1.A

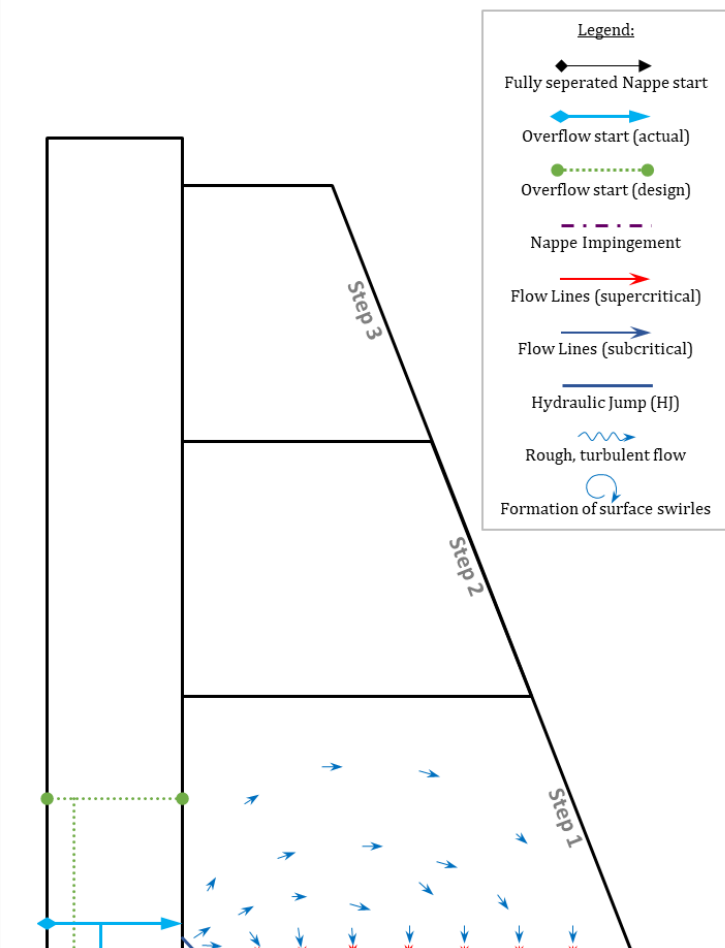


Figure F.1: Hydraulic Model Flow Profiles – Test Run No.: 1.1.1.A

Stepped Chute Flow Profile - 1.1.1.B

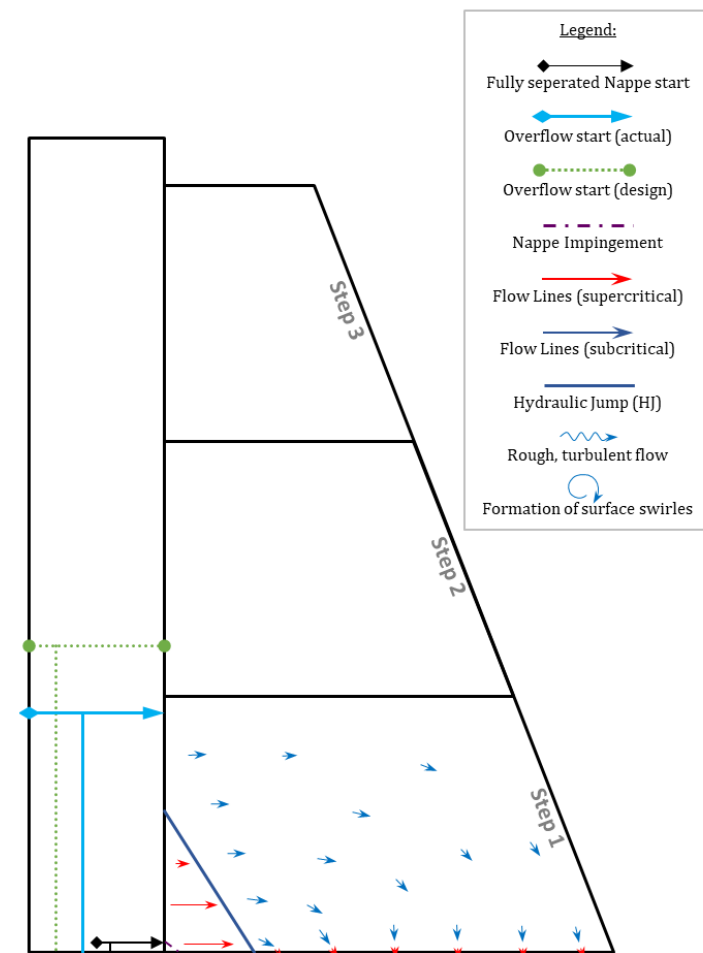


Figure F.2: Hydraulic Model Flow Profiles – Test Run No.: 1.1.1.B

Stepped Chute Flow Profile - 1.1.1.C

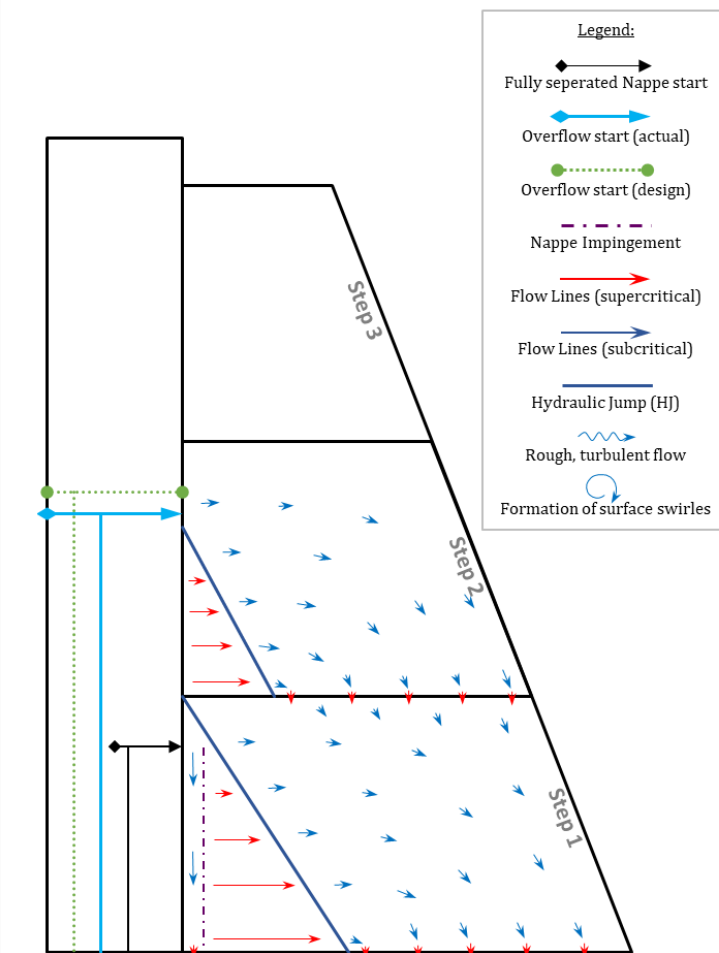


Figure F.3: Hydraulic Model Flow Profiles – Test Run No.: 1.1.1.C

Stepped Chute Flow Profile - 1.1.1.D

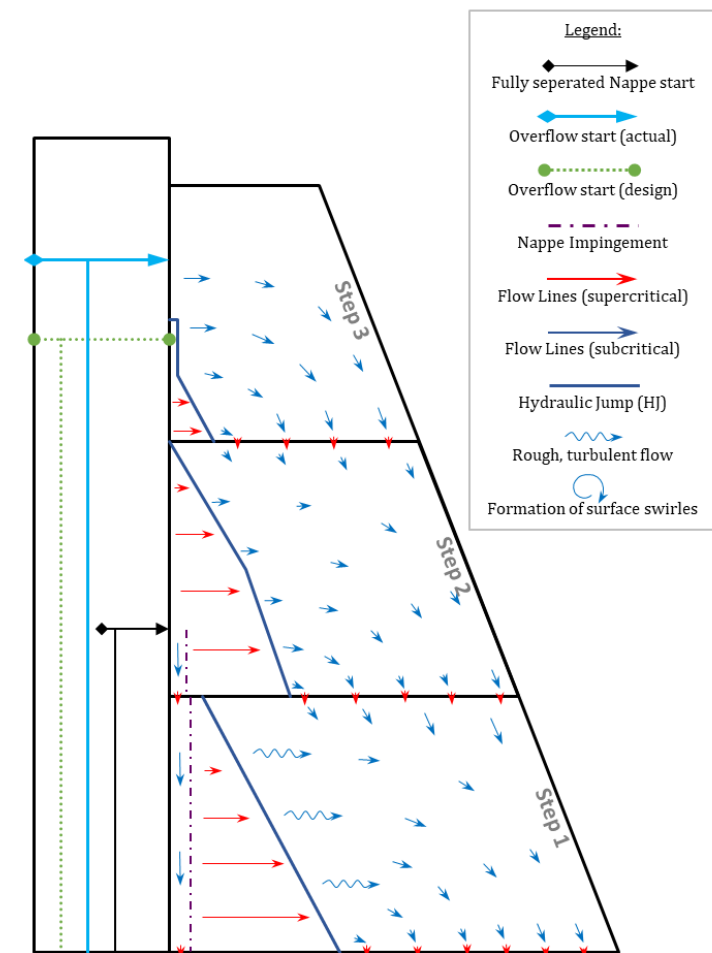
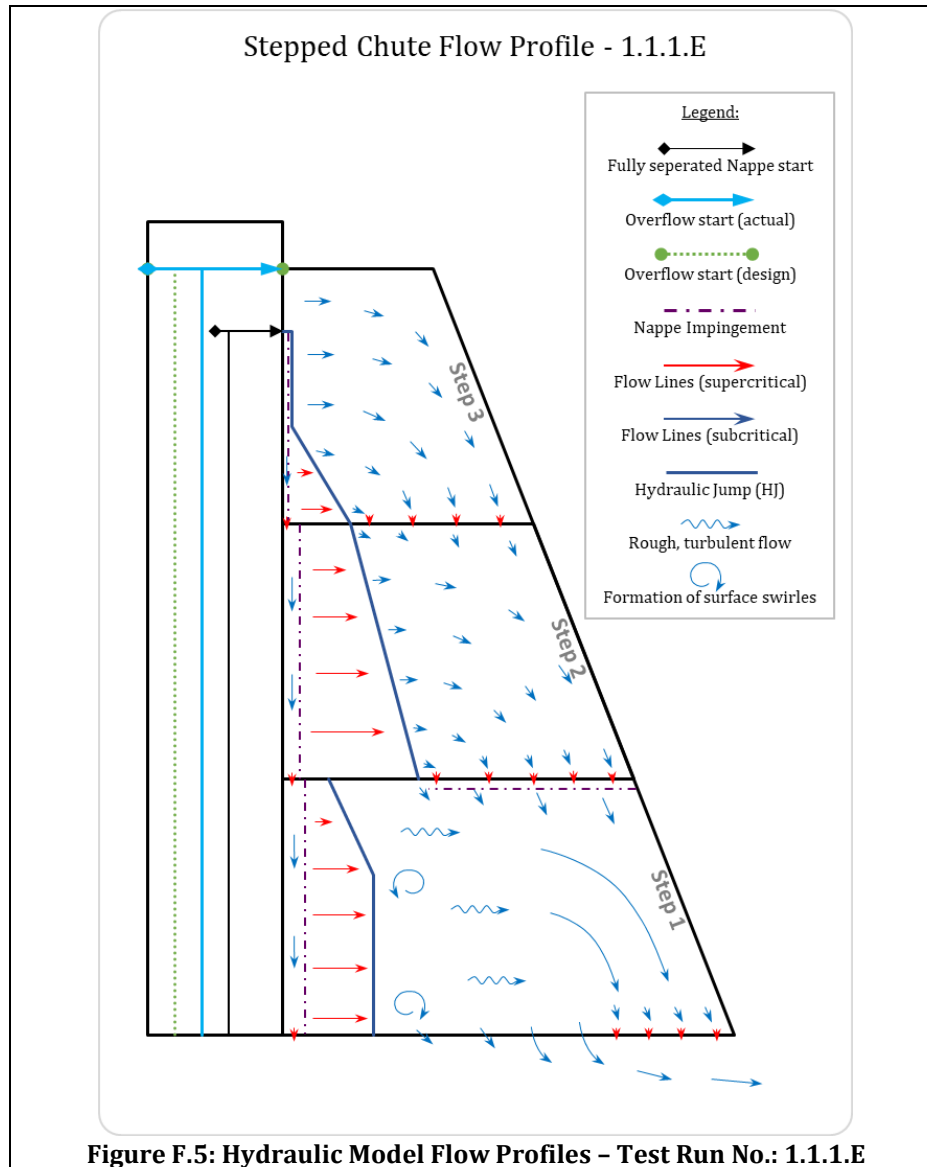


Figure F.4: Hydraulic Model Flow Profiles – Test Run No.: 1.1.1.D



Stepped Chute Flow Profile - 1.1.2.A

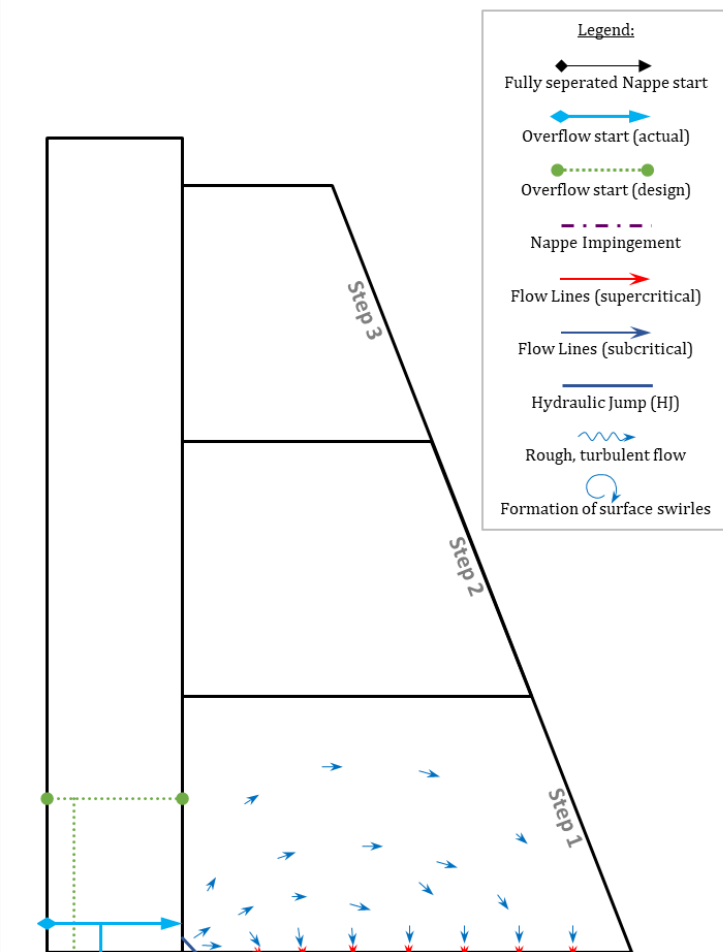


Figure F.6: Hydraulic Model Flow Profiles – Test Run No.: 1.1.2.A

Stepped Chute Flow Profile - 1.1.2.B

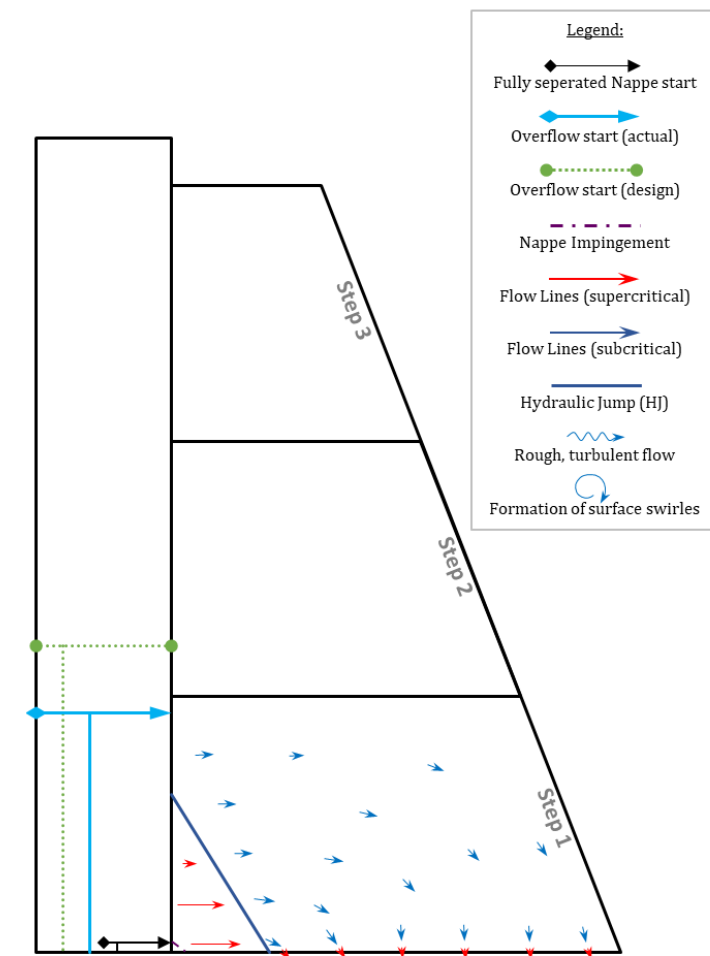


Figure F.7: Hydraulic Model Flow Profiles – Test Run No.: 1.1.2.B

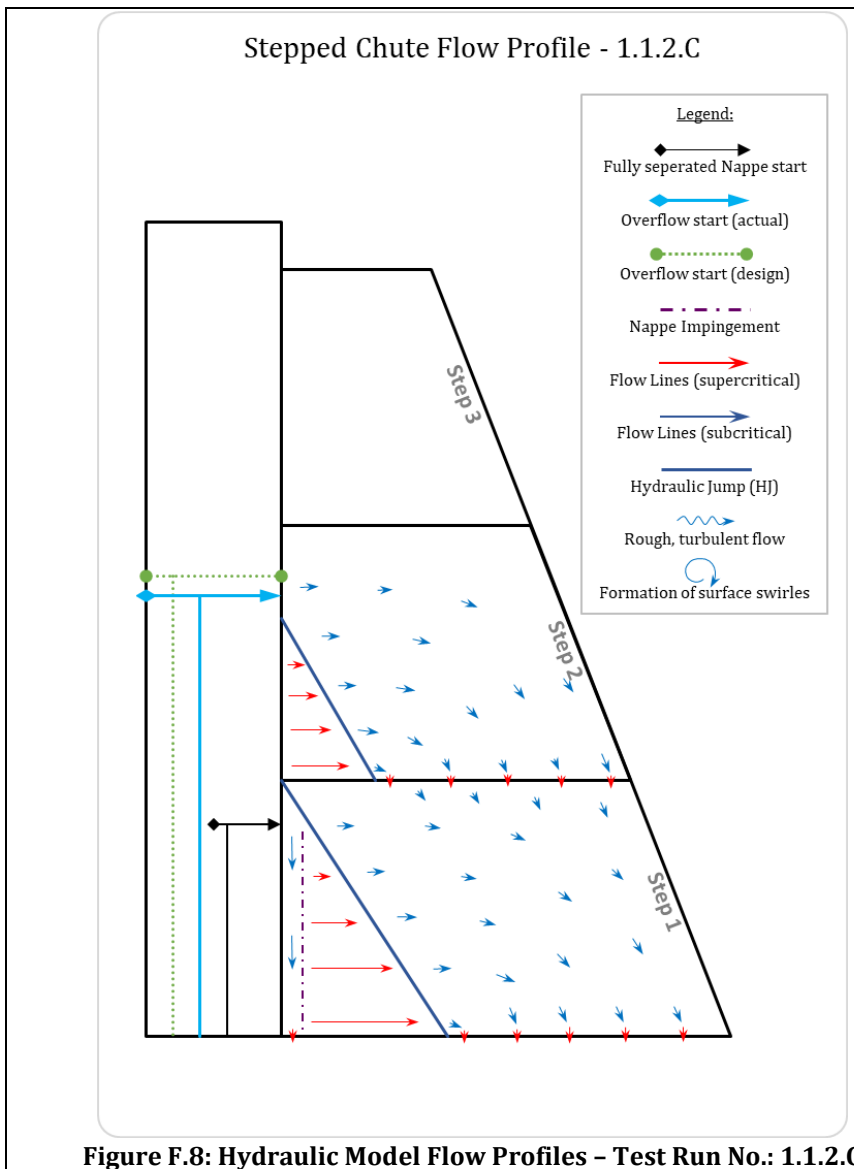


Figure F.8: Hydraulic Model Flow Profiles – Test Run No.: 1.1.2.C

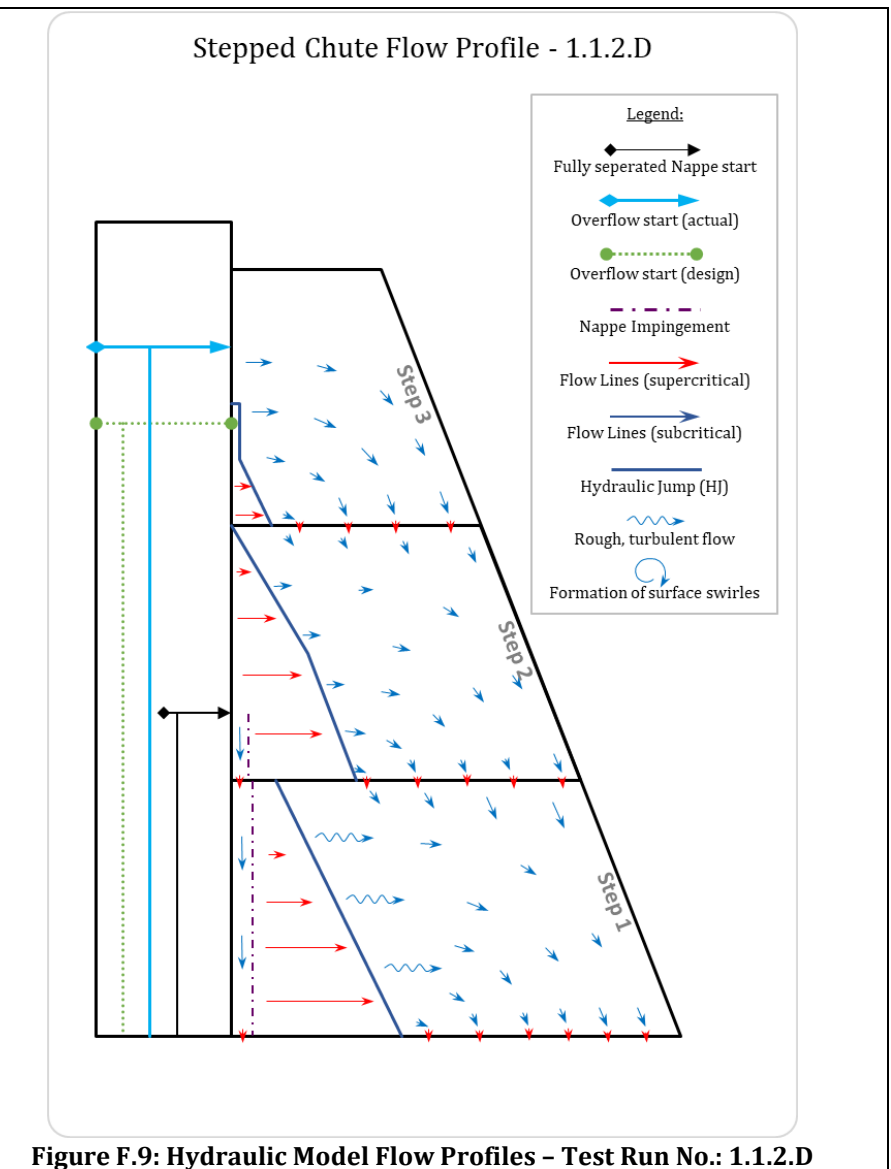
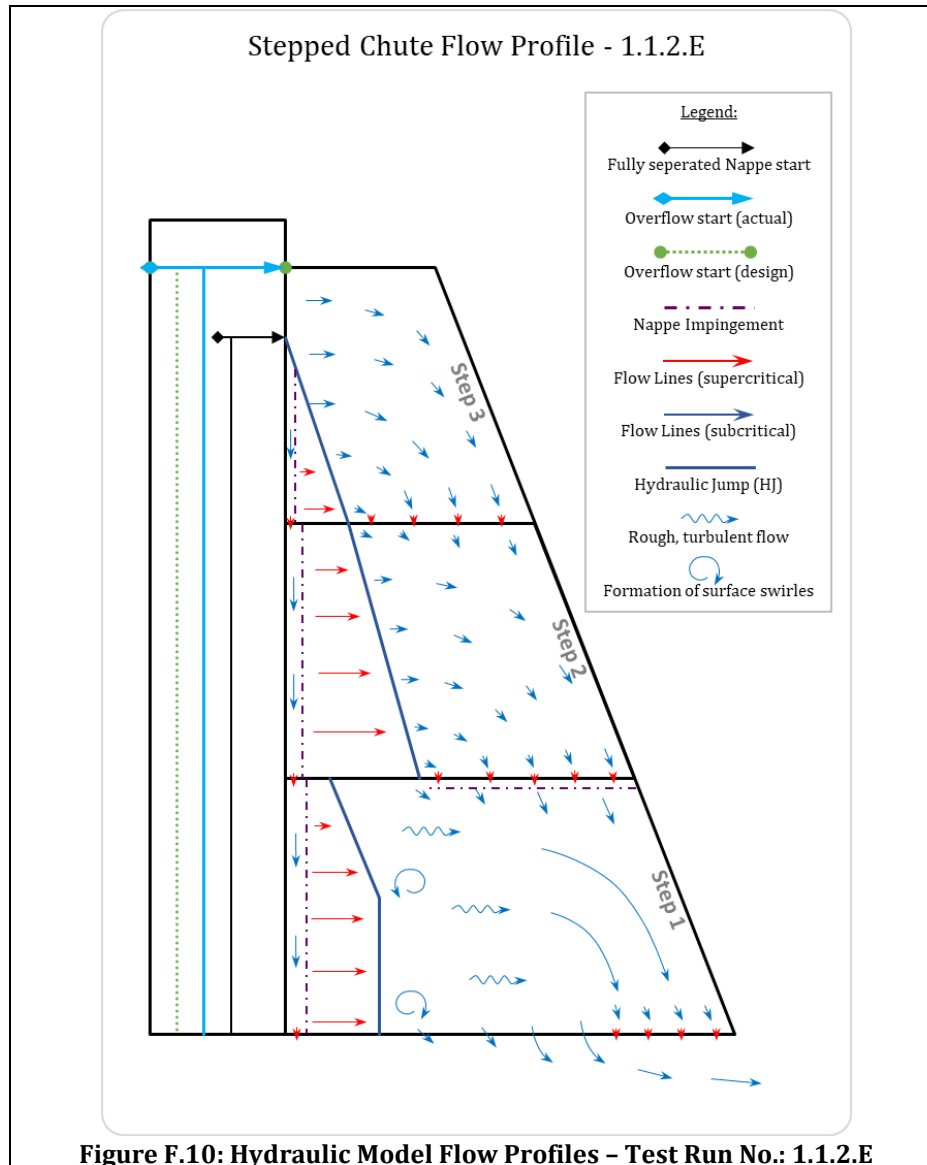
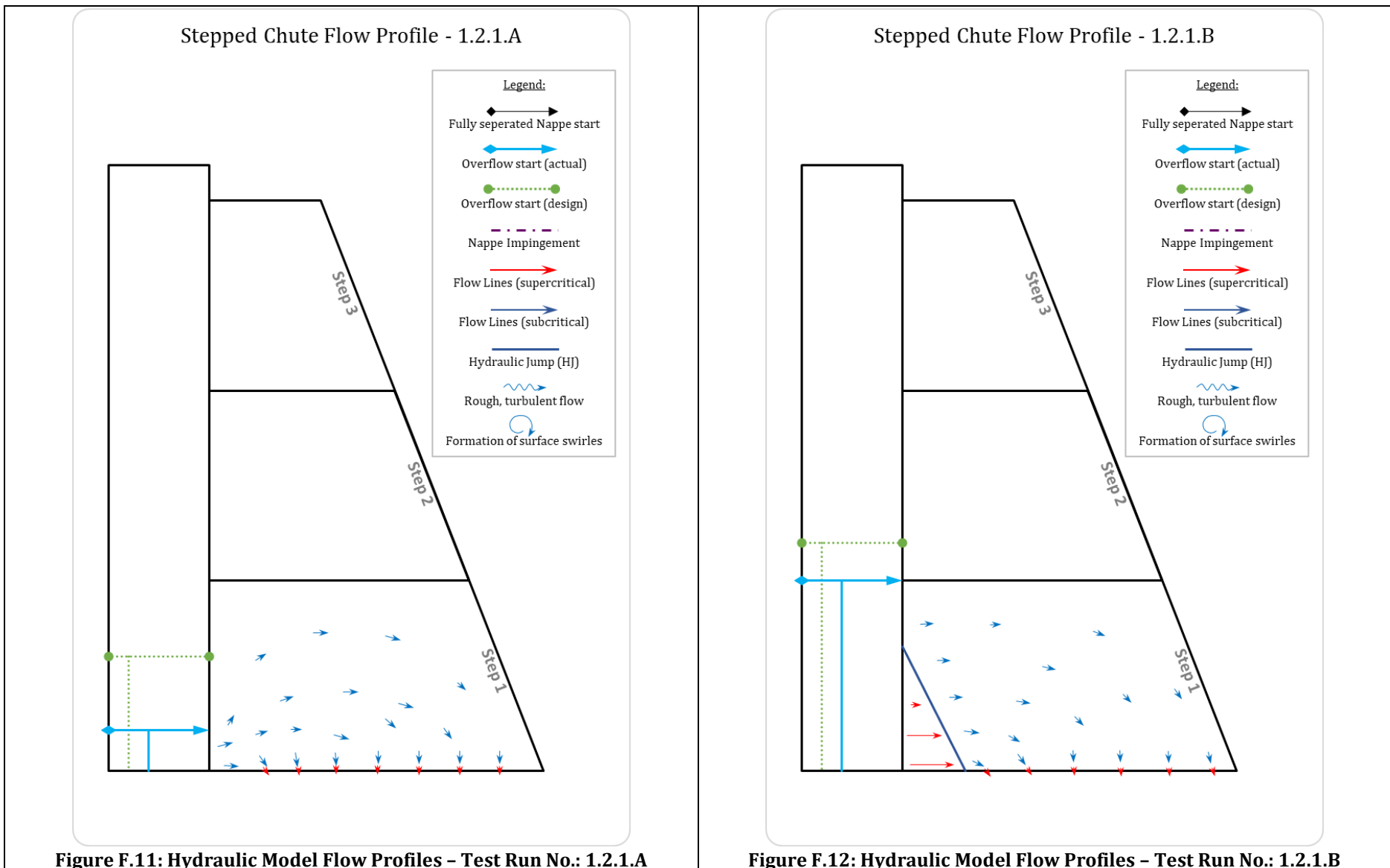


Figure F.9: Hydraulic Model Flow Profiles – Test Run No.: 1.1.2.D





Stepped Chute Flow Profile - 1.2.1.C

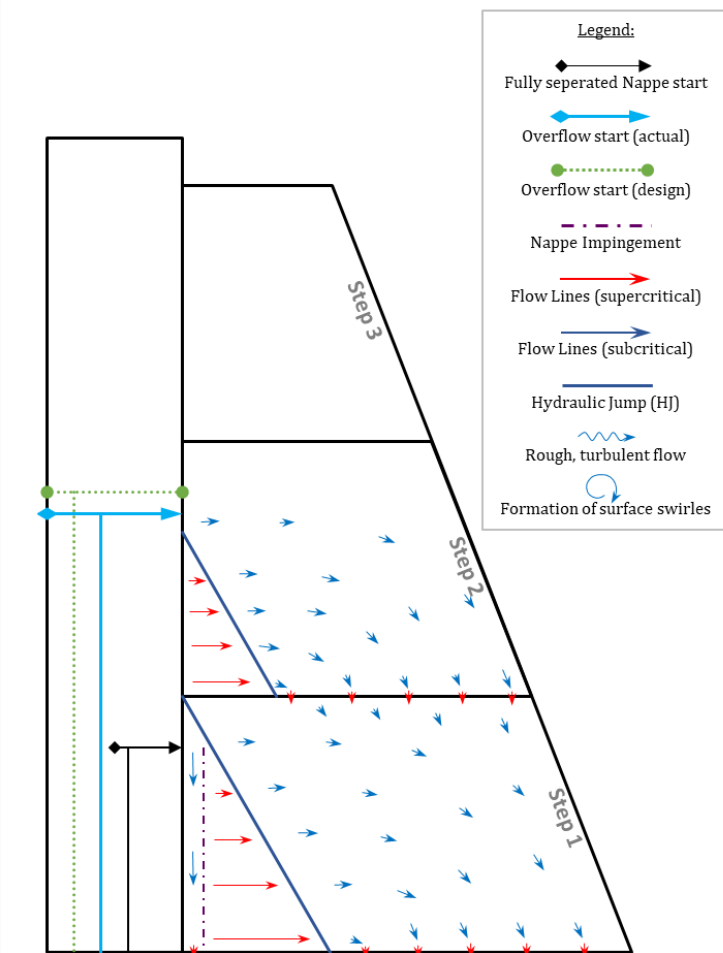


Figure F.13: Hydraulic Model Flow Profiles - Test Run No.: 1.2.1.C

Stepped Chute Flow Profile - 1.2.1.D

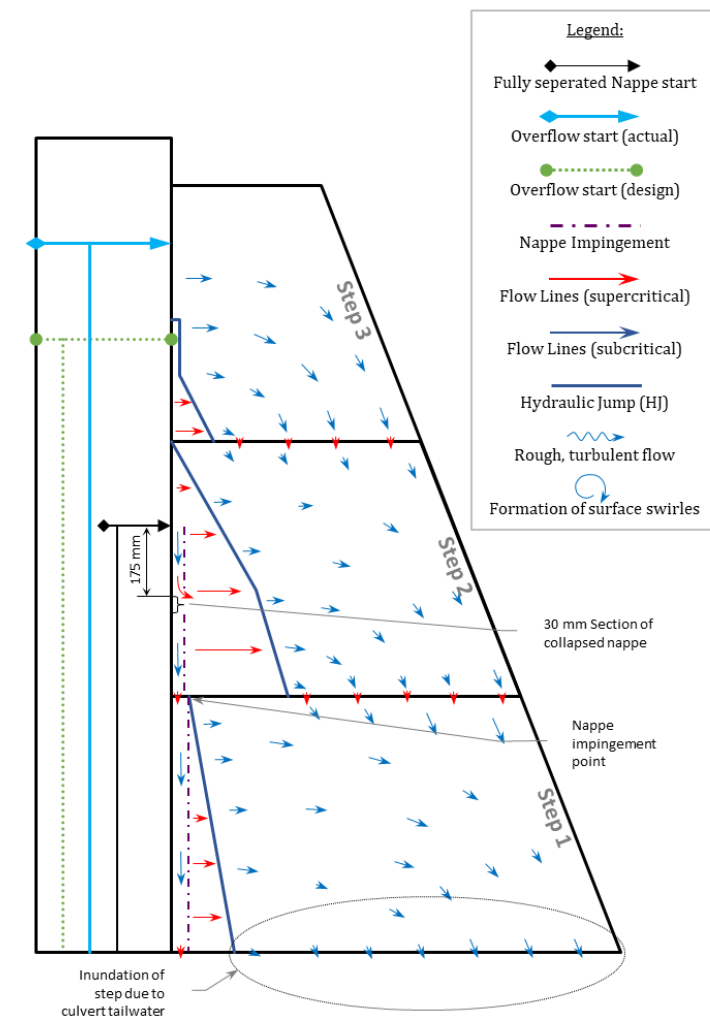
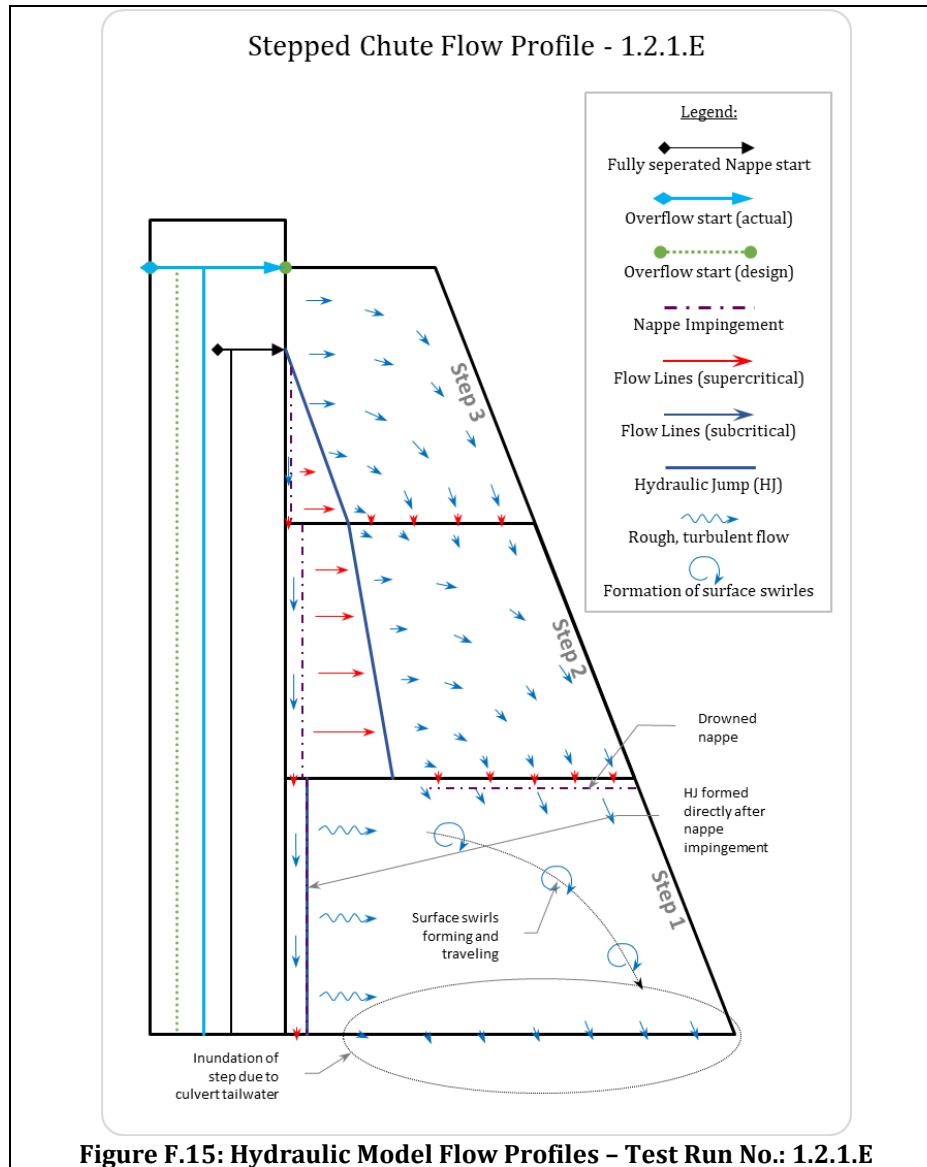
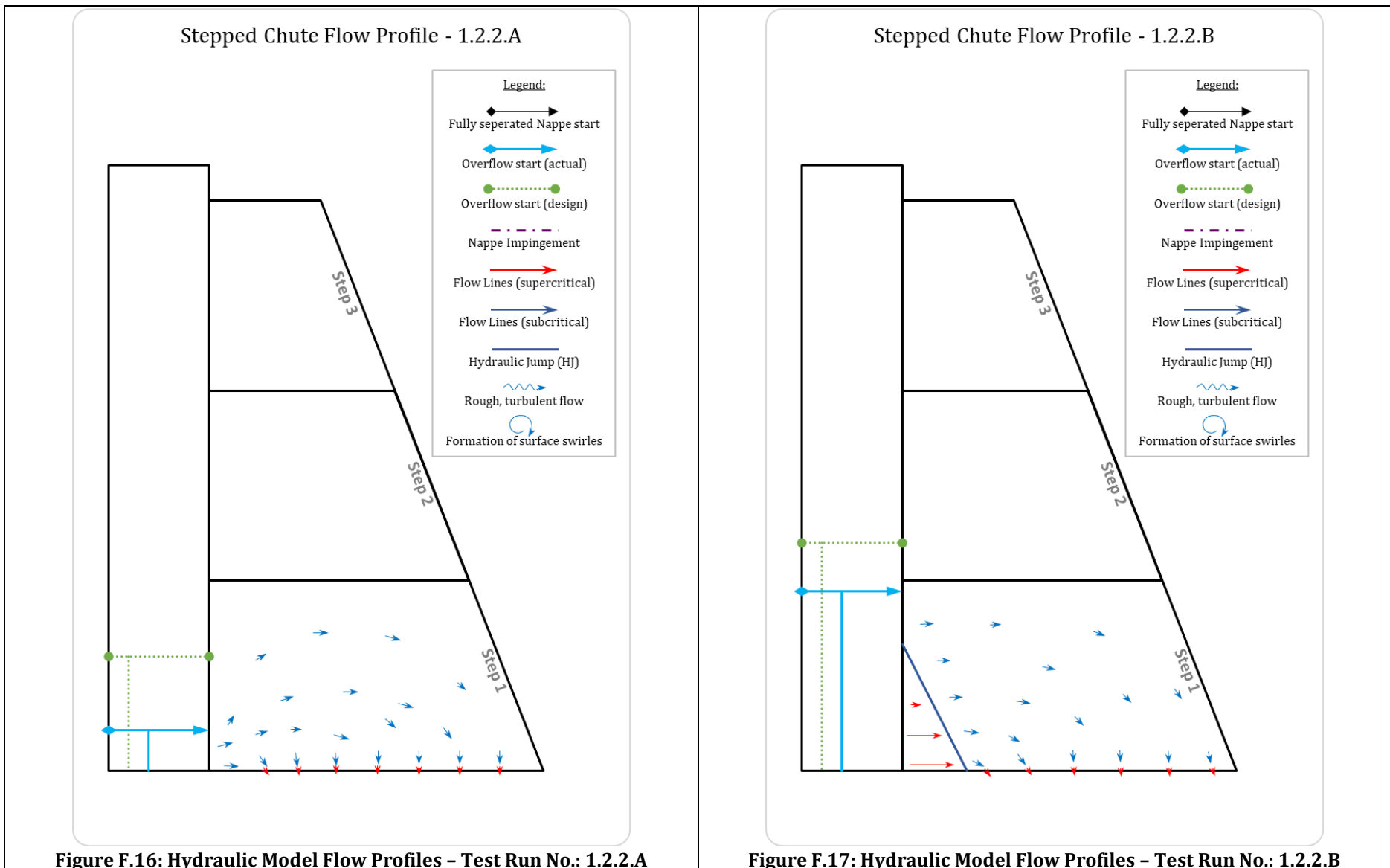


Figure F.14: Hydraulic Model Flow Profiles - Test Run No.: 1.2.1.D





Stepped Chute Flow Profile - 1.2.2.C

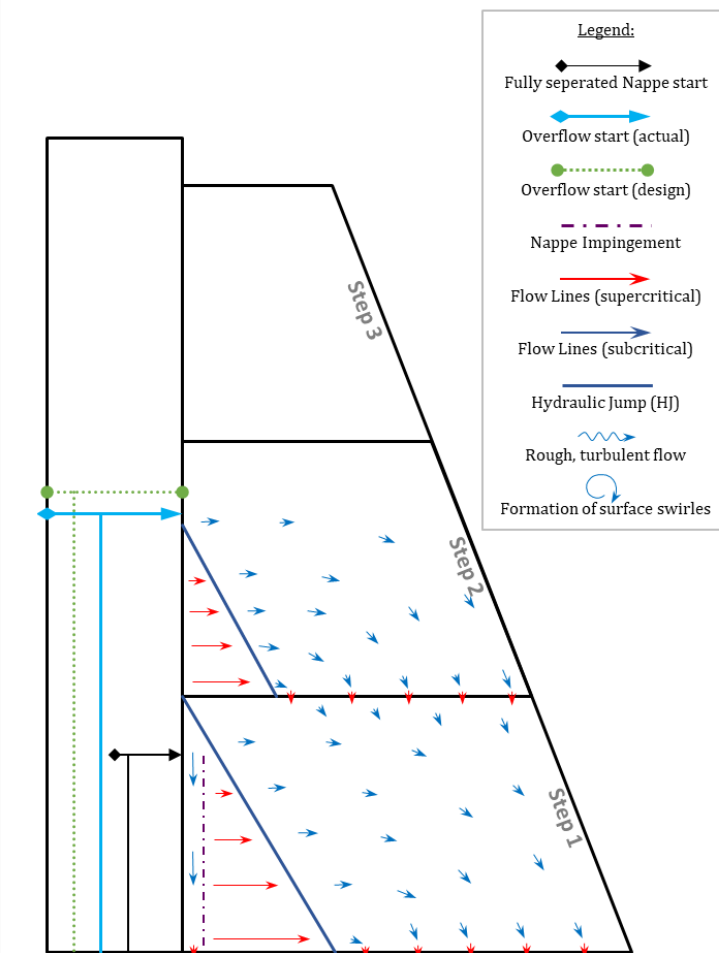


Figure F.18: Hydraulic Model Flow Profiles - Test Run No.: 1.2.2.C

Stepped Chute Flow Profile - 1.2.2.D

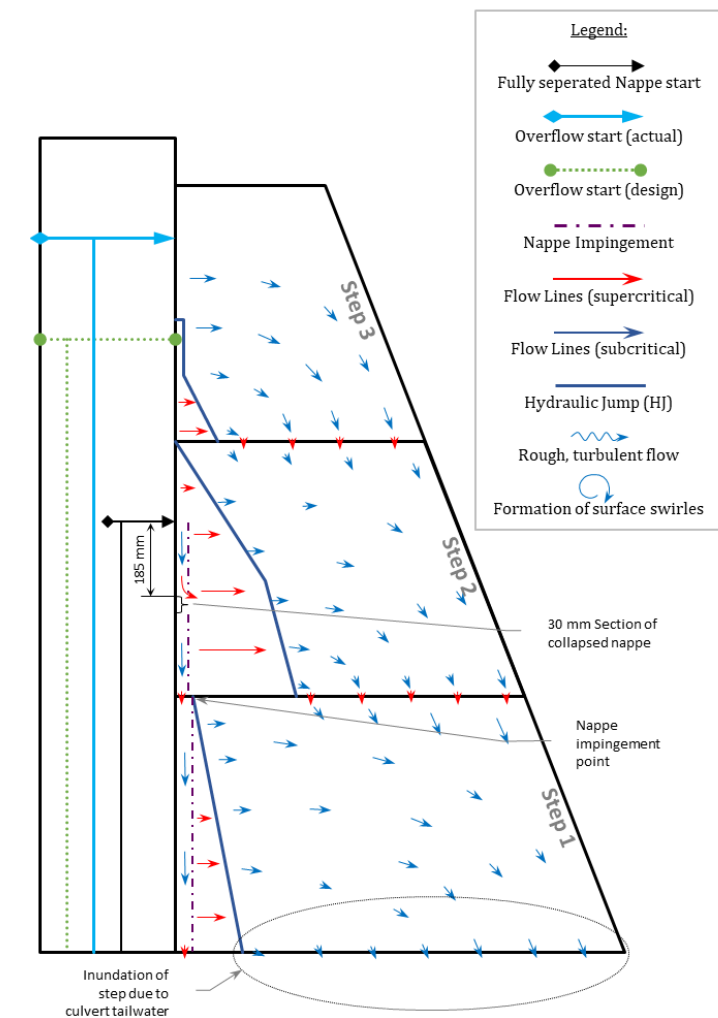
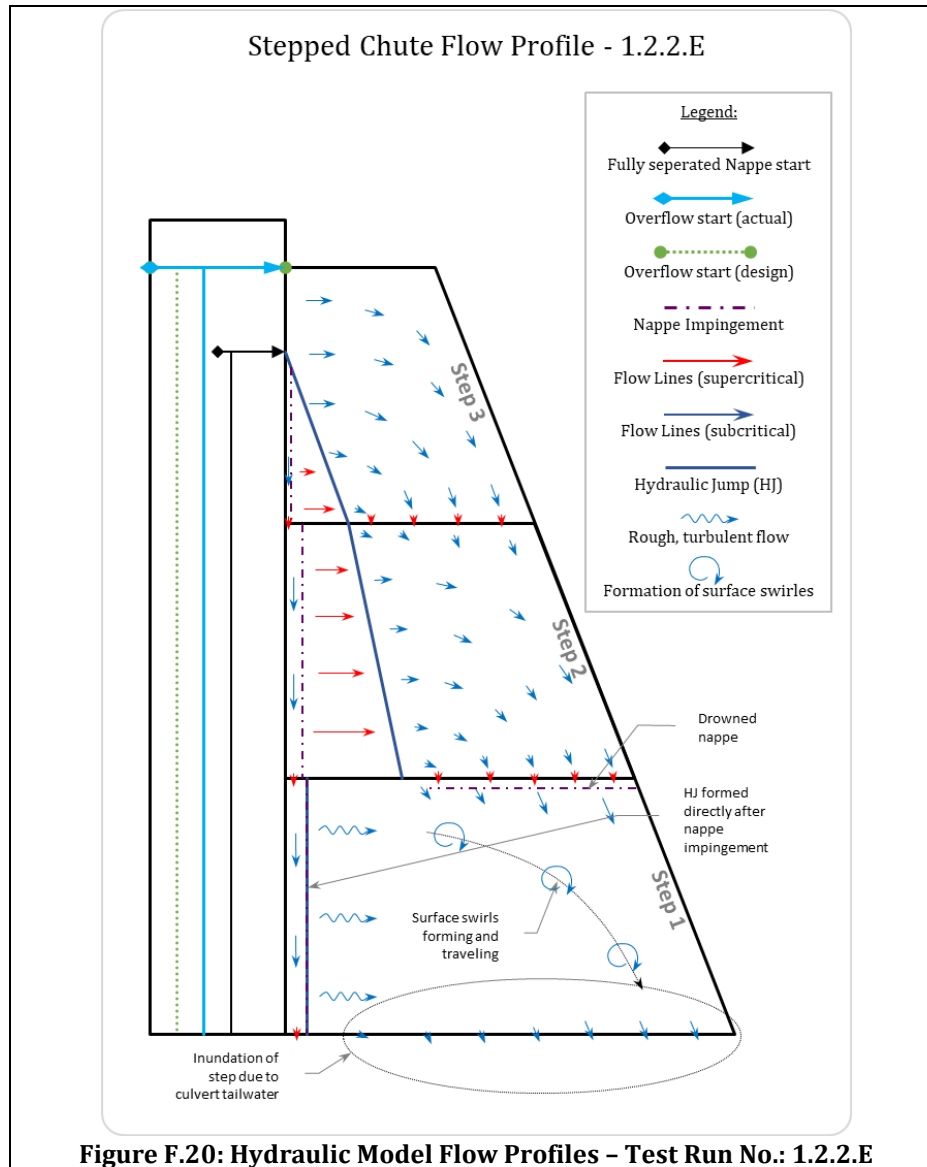
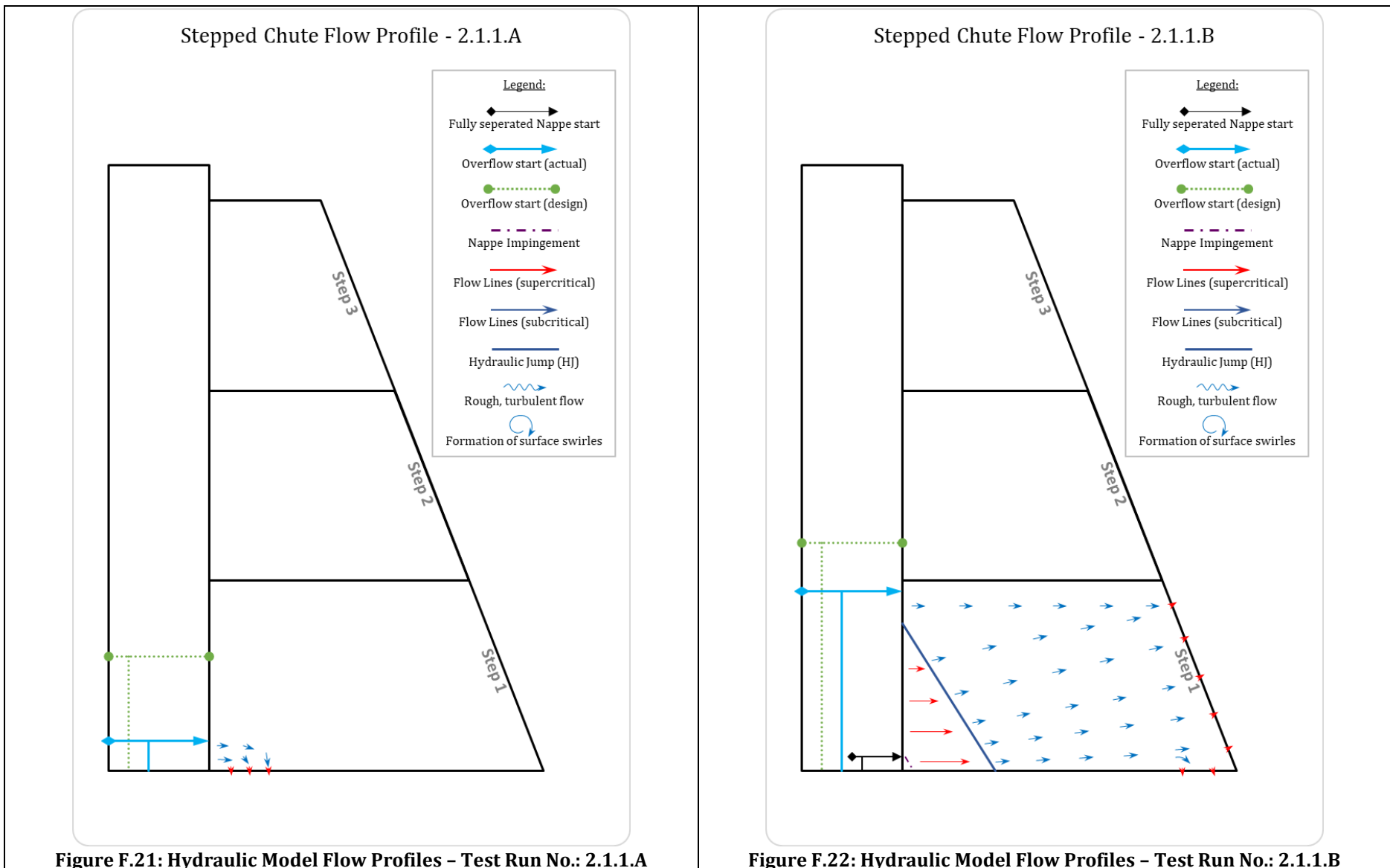


Figure F.19: Hydraulic Model Flow Profiles - Test Run No.: 1.2.2.D





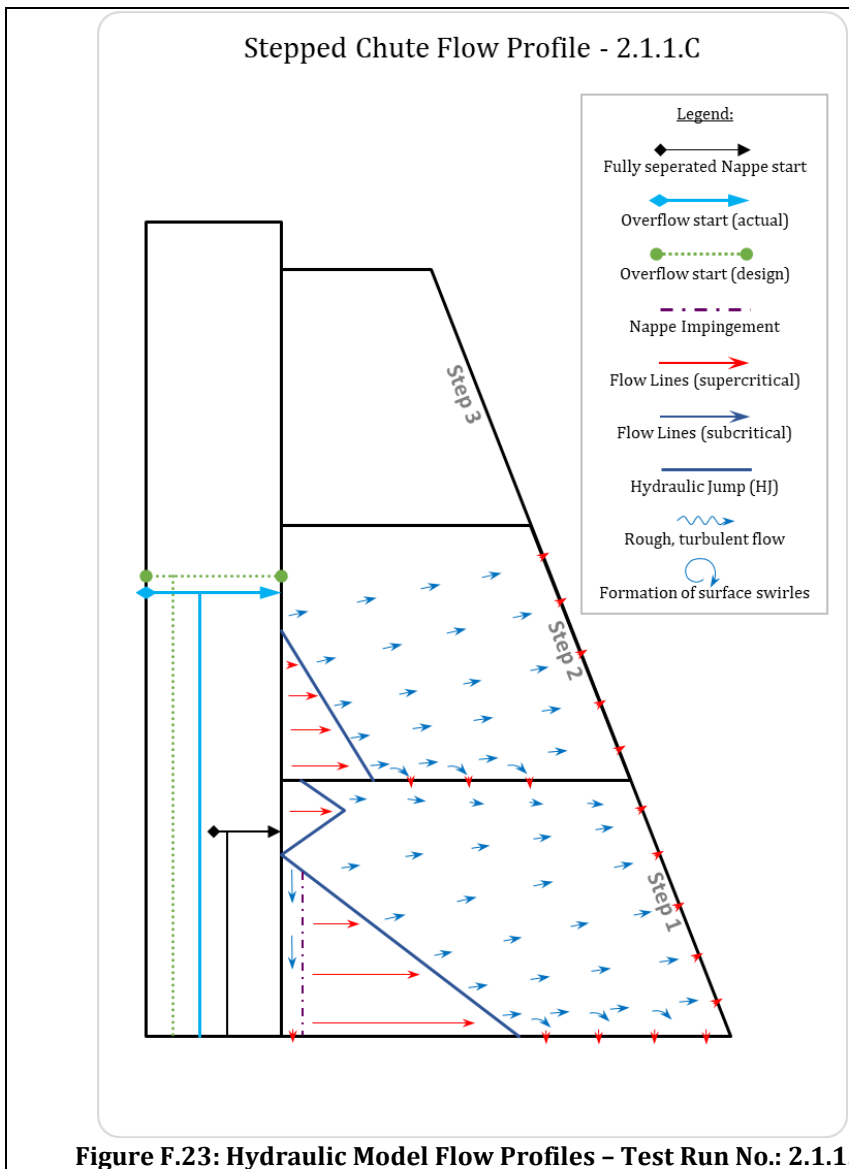


Figure F.23: Hydraulic Model Flow Profiles - Test Run No.: 2.1.1.C

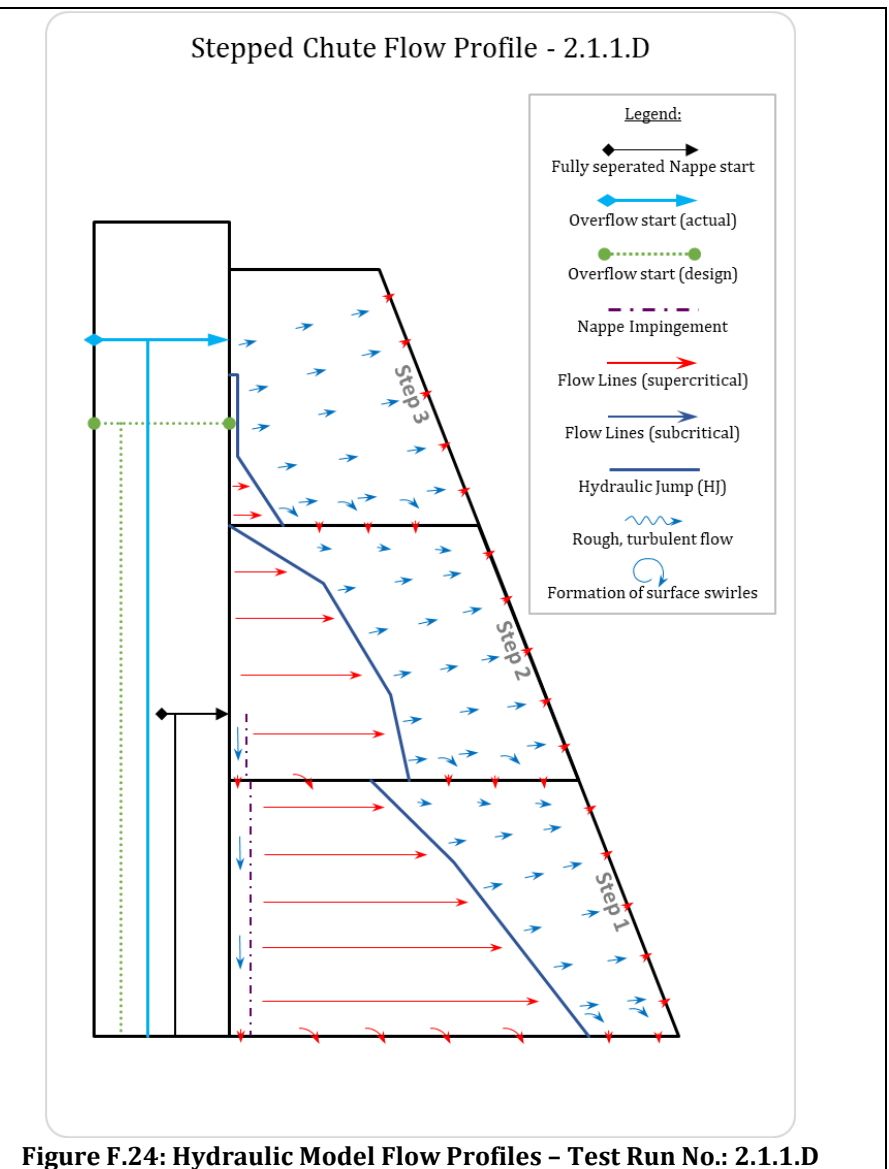
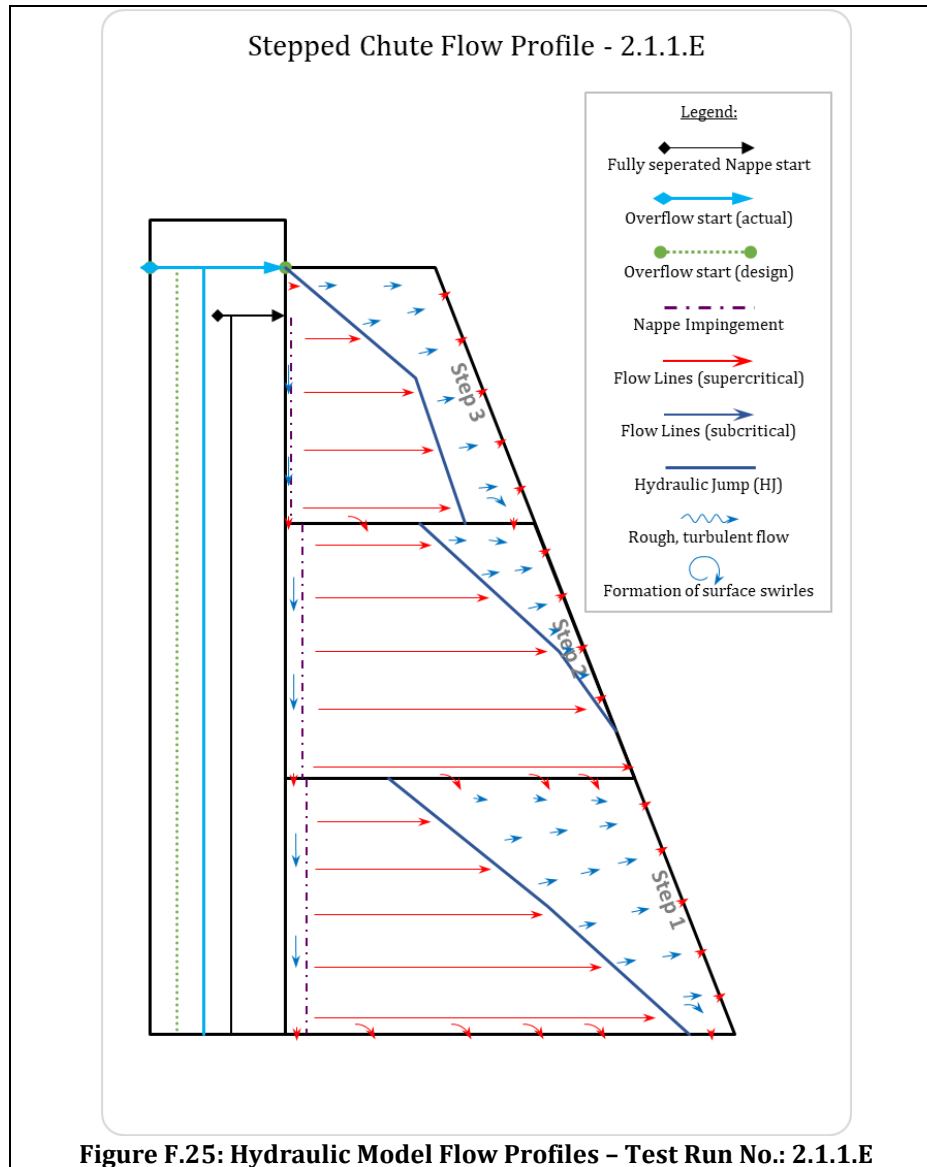
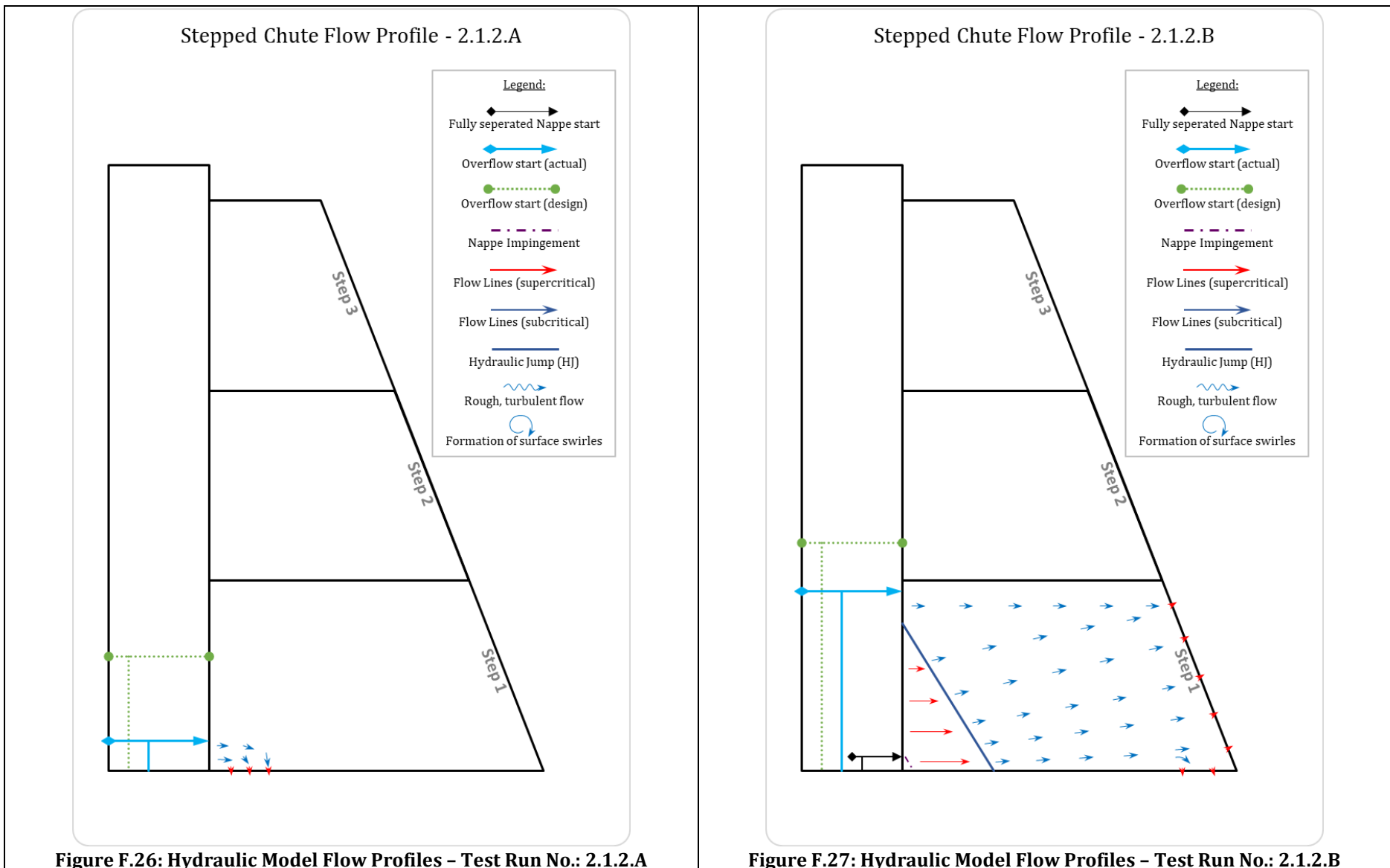


Figure F.24: Hydraulic Model Flow Profiles - Test Run No.: 2.1.1.D





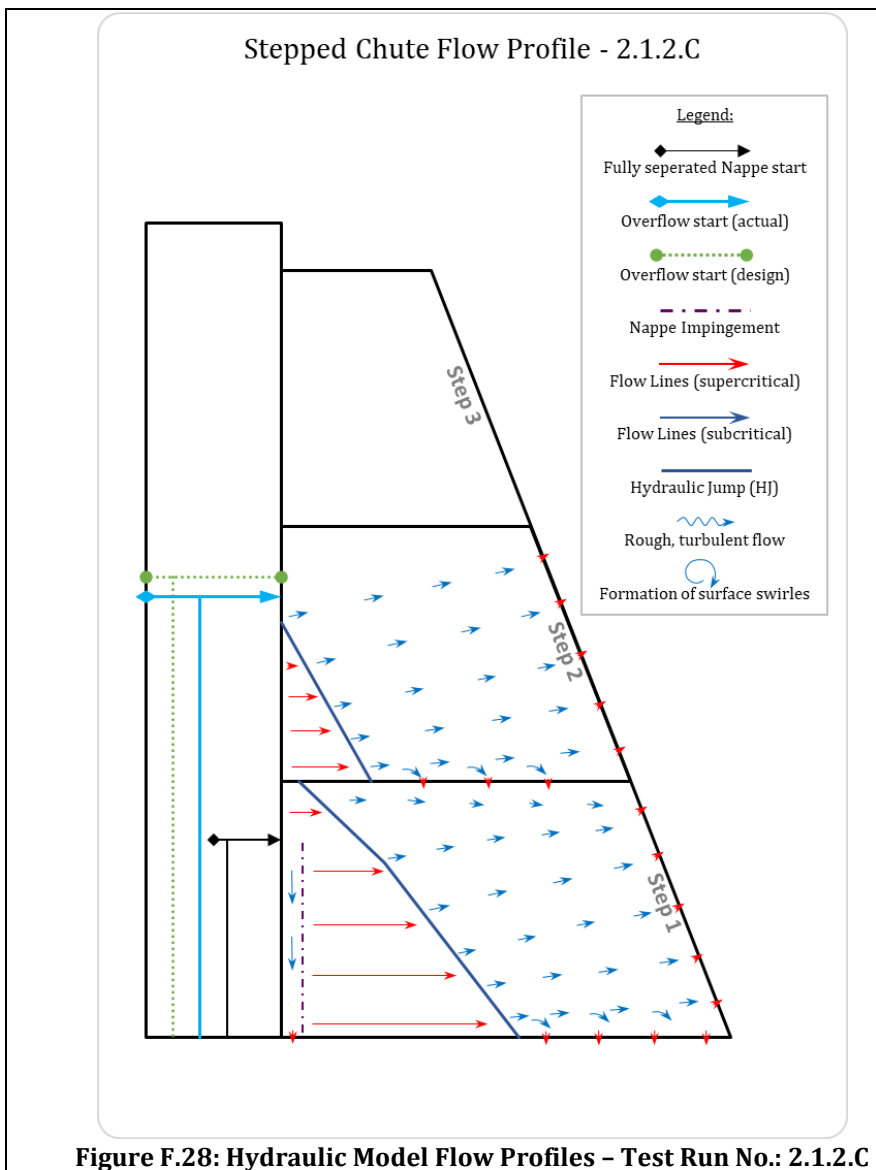


Figure F.28: Hydraulic Model Flow Profiles – Test Run No.: 2.1.2.C

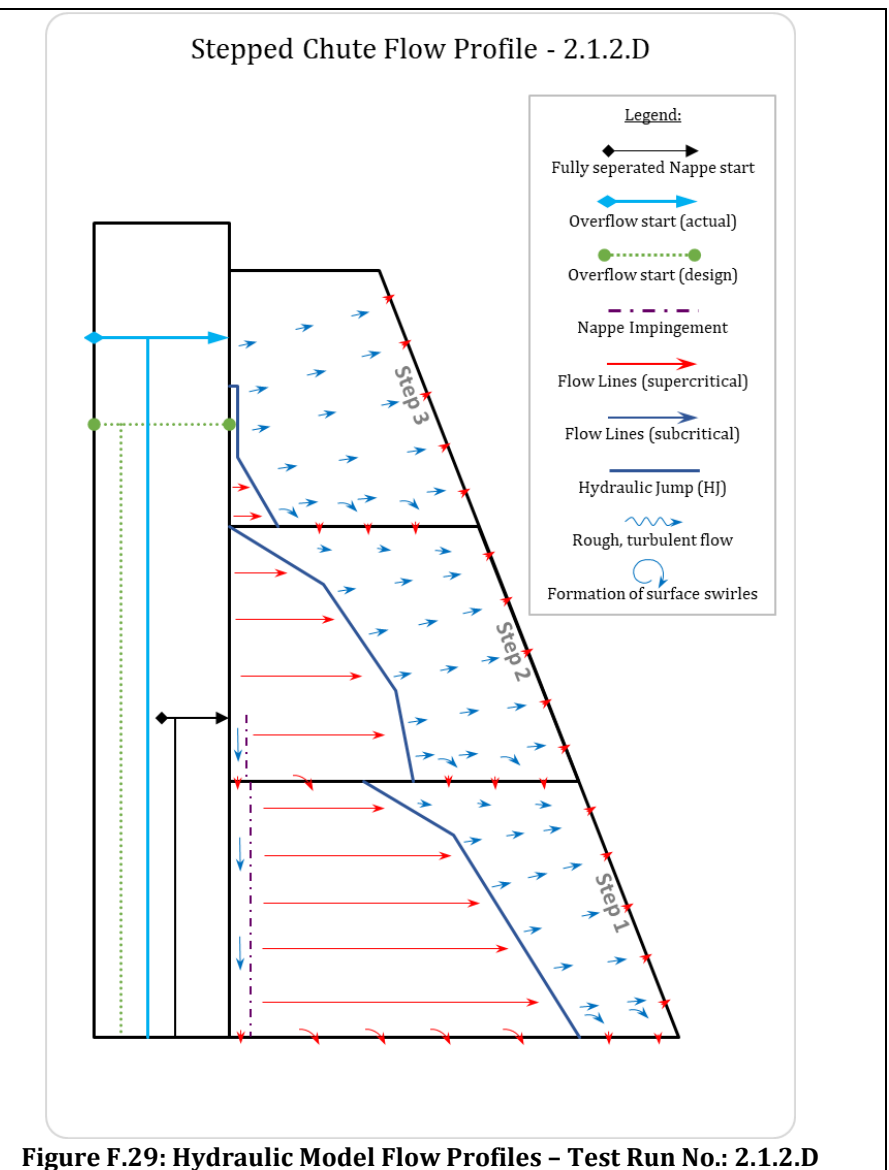
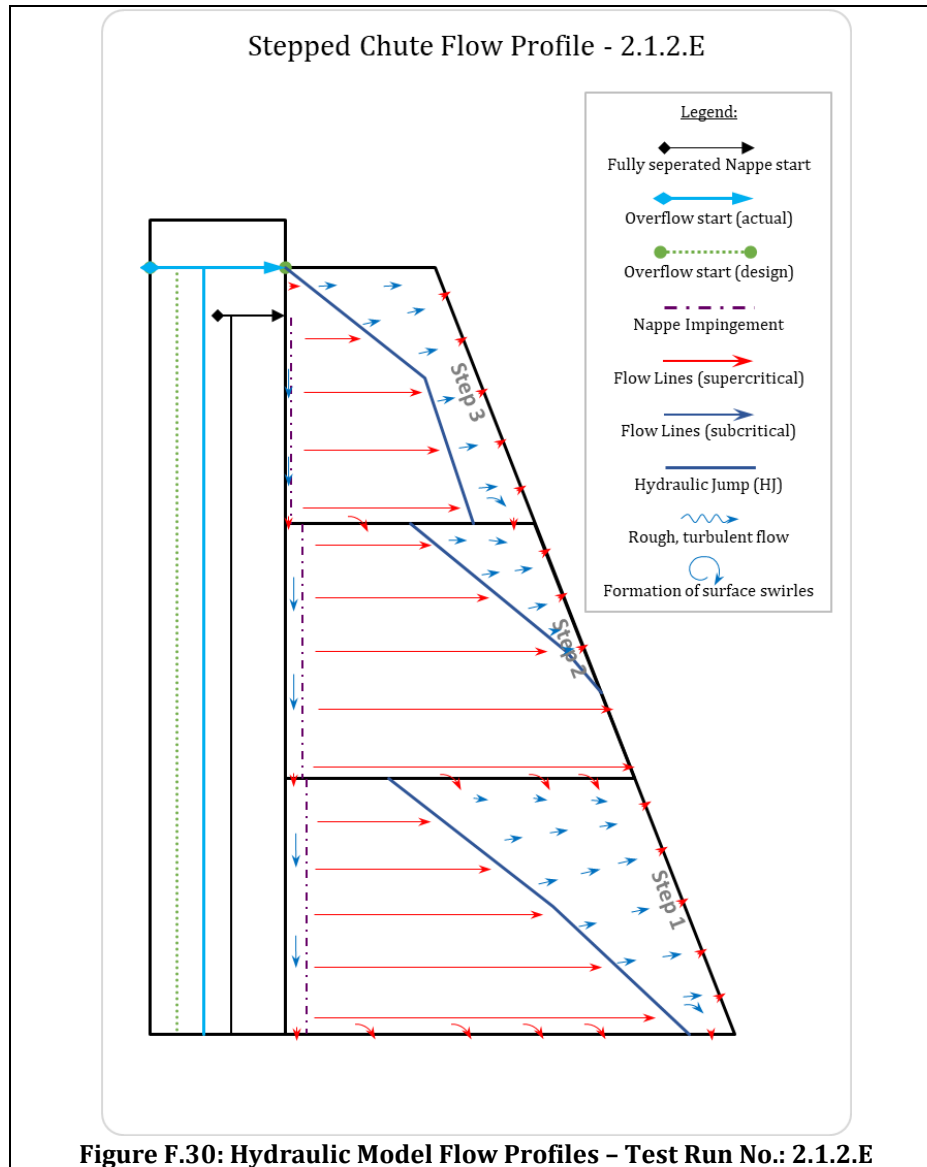
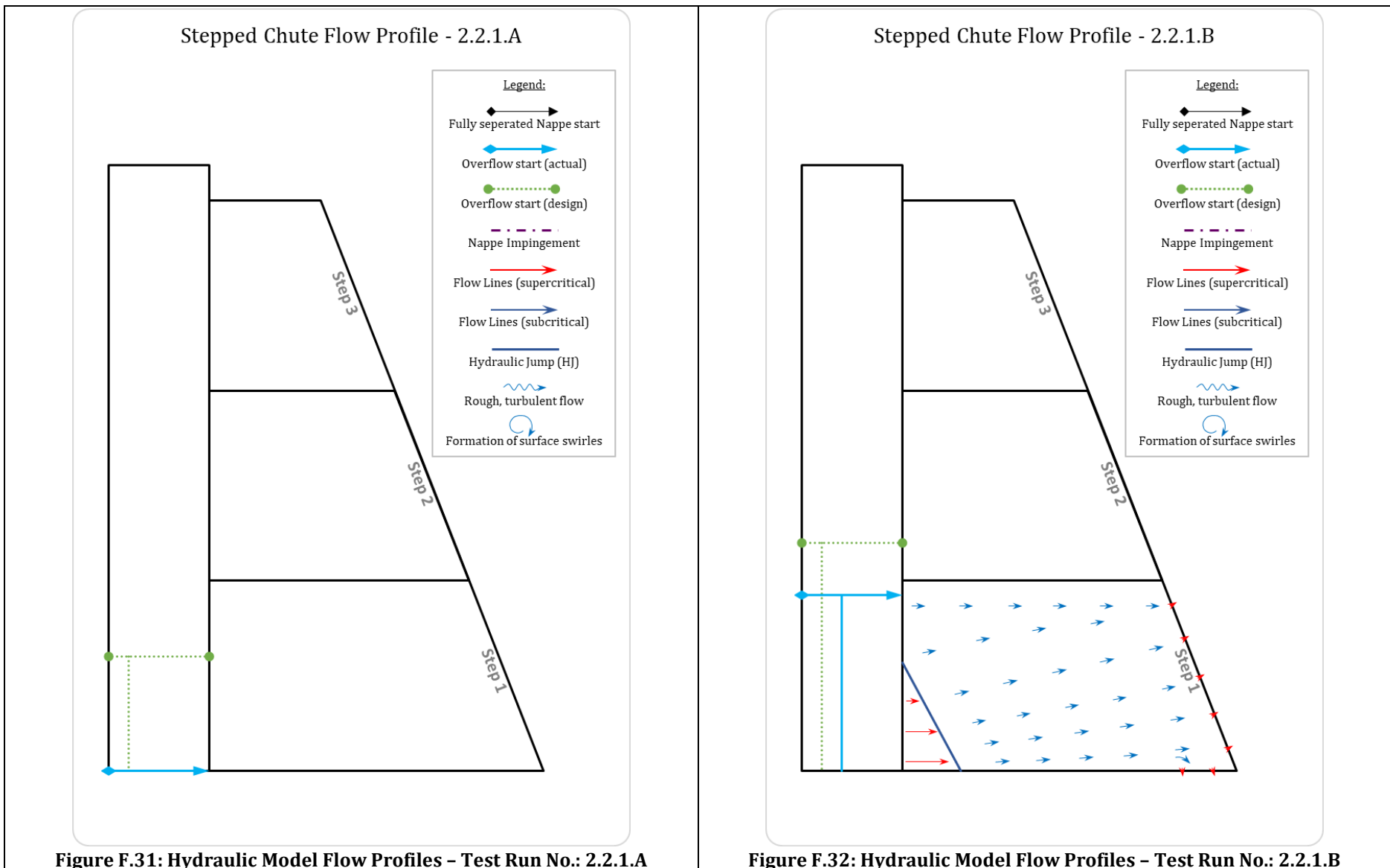


Figure F.29: Hydraulic Model Flow Profiles – Test Run No.: 2.1.2.D





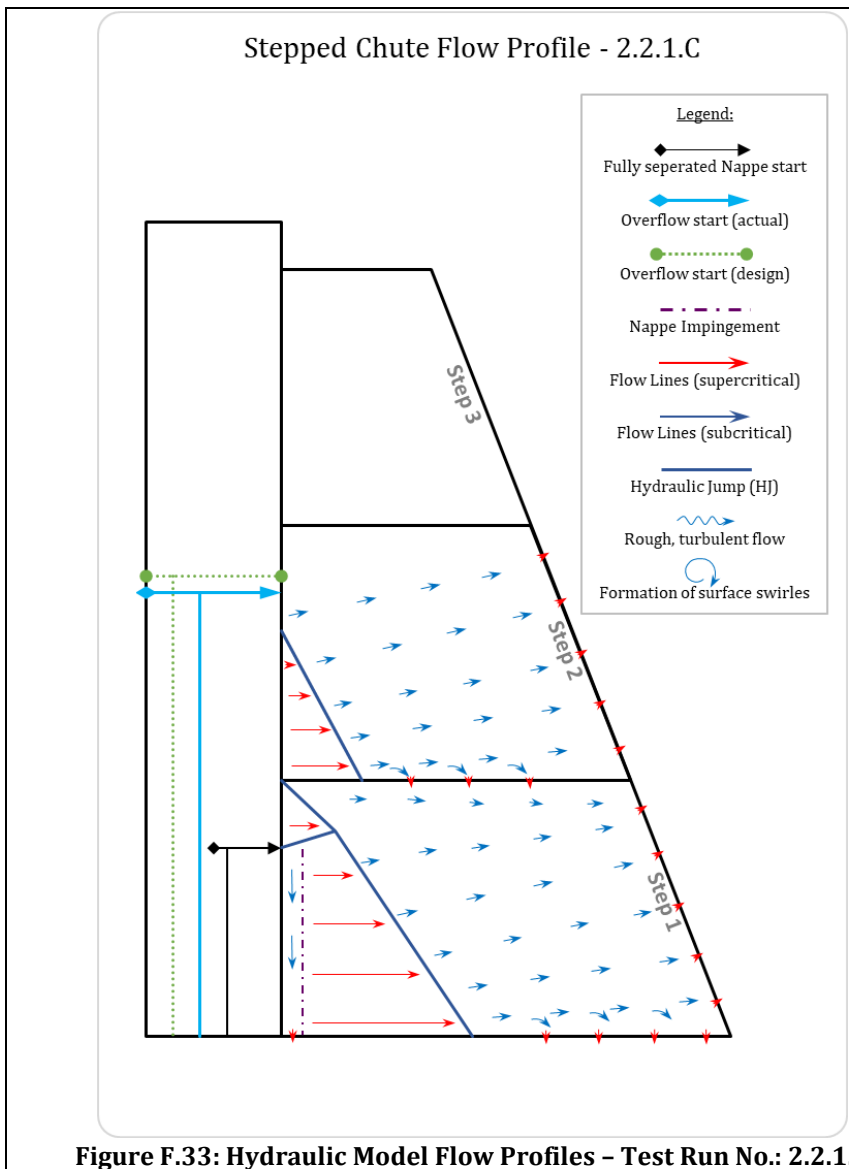


Figure F.33: Hydraulic Model Flow Profiles - Test Run No.: 2.2.1.C

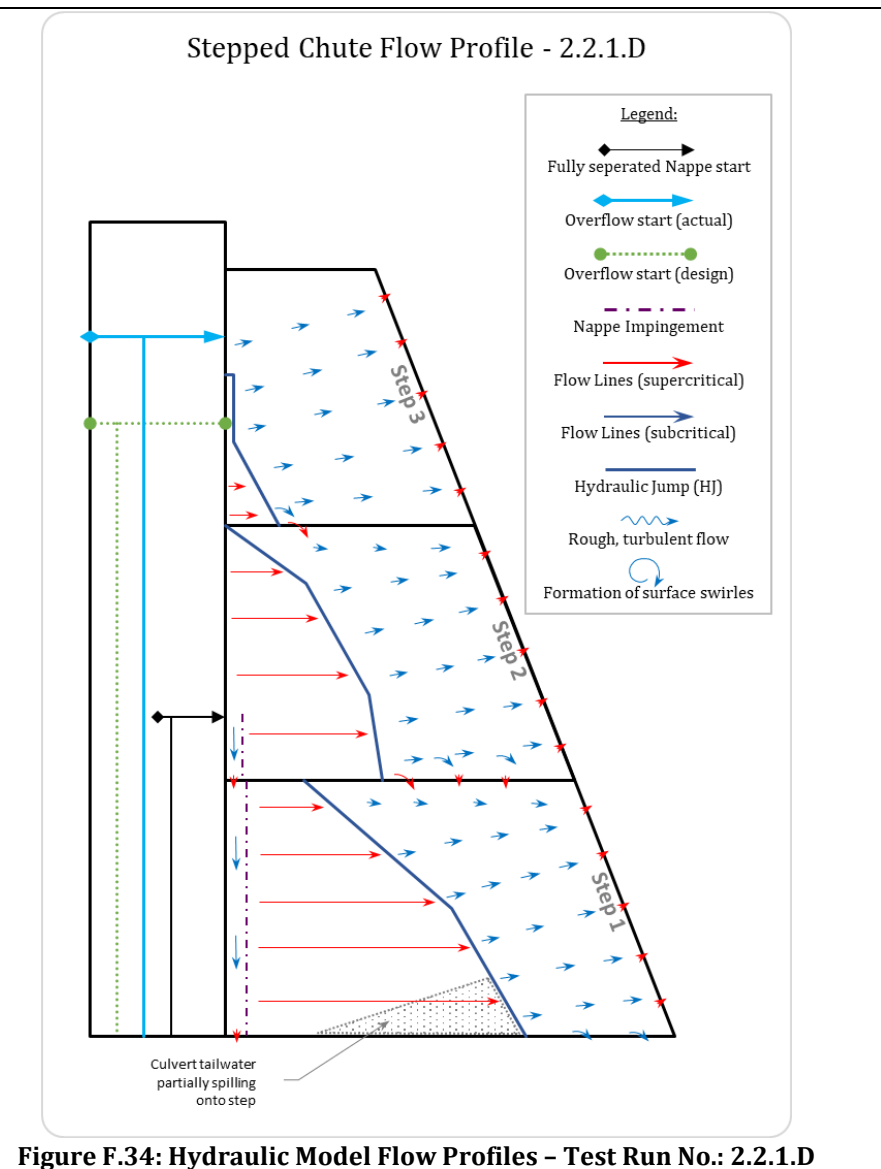
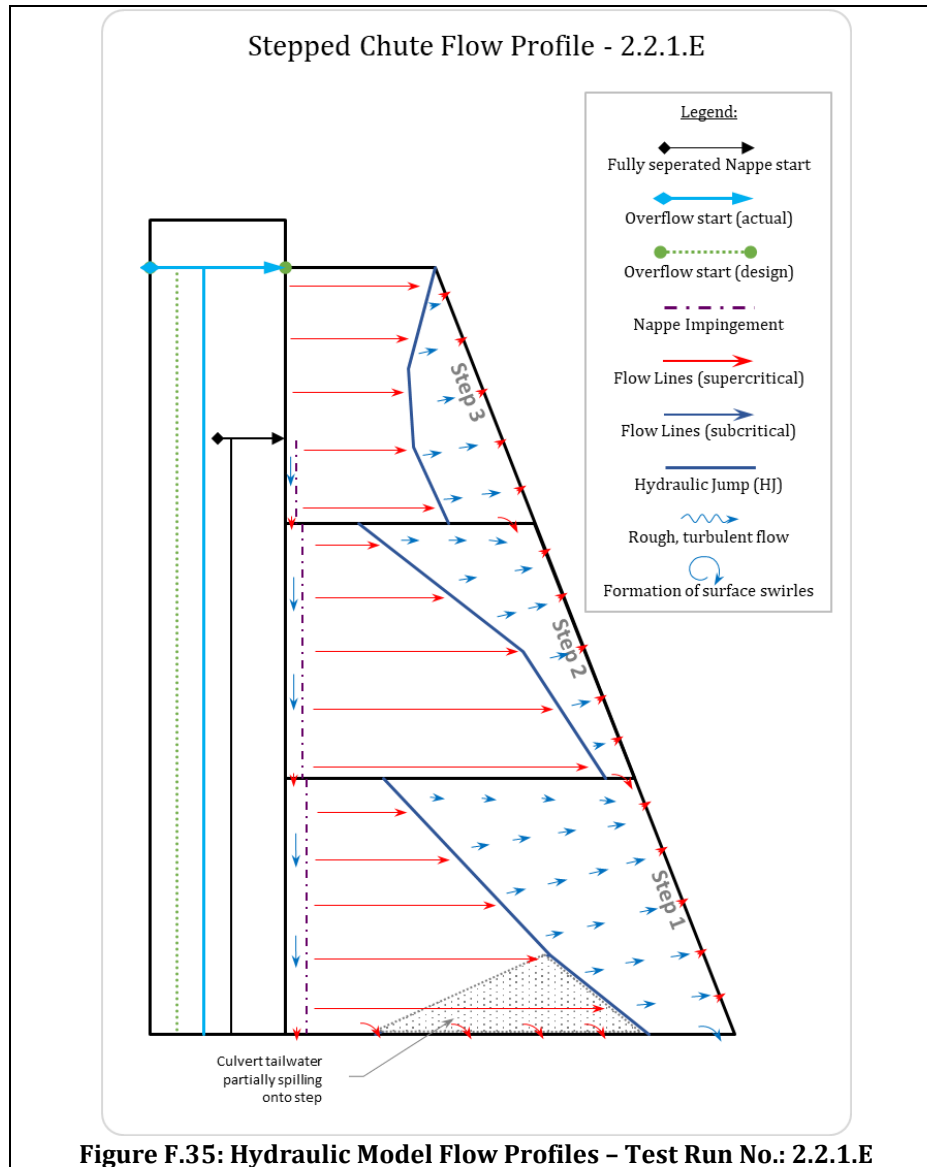
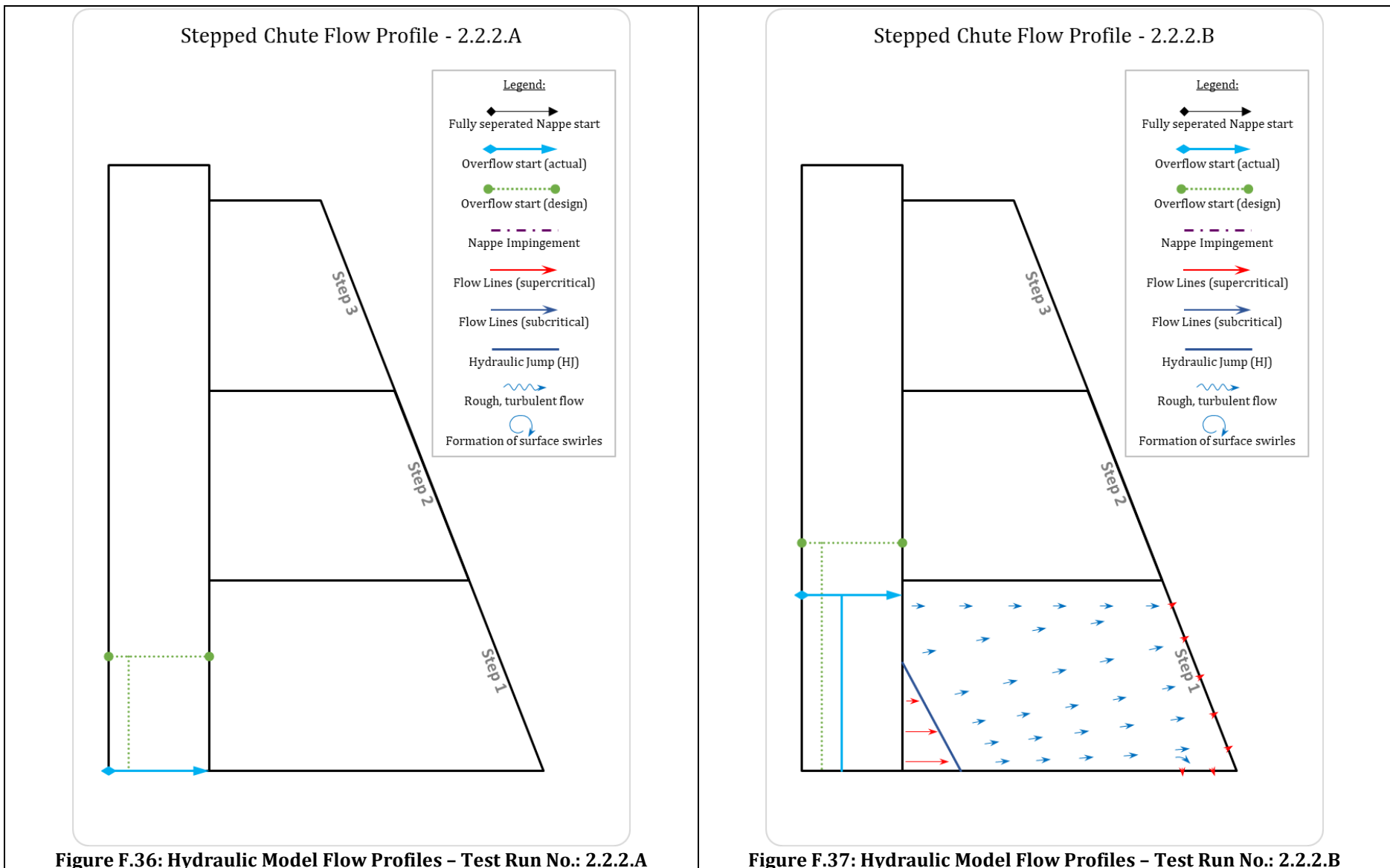


Figure F.34: Hydraulic Model Flow Profiles - Test Run No.: 2.2.1.D





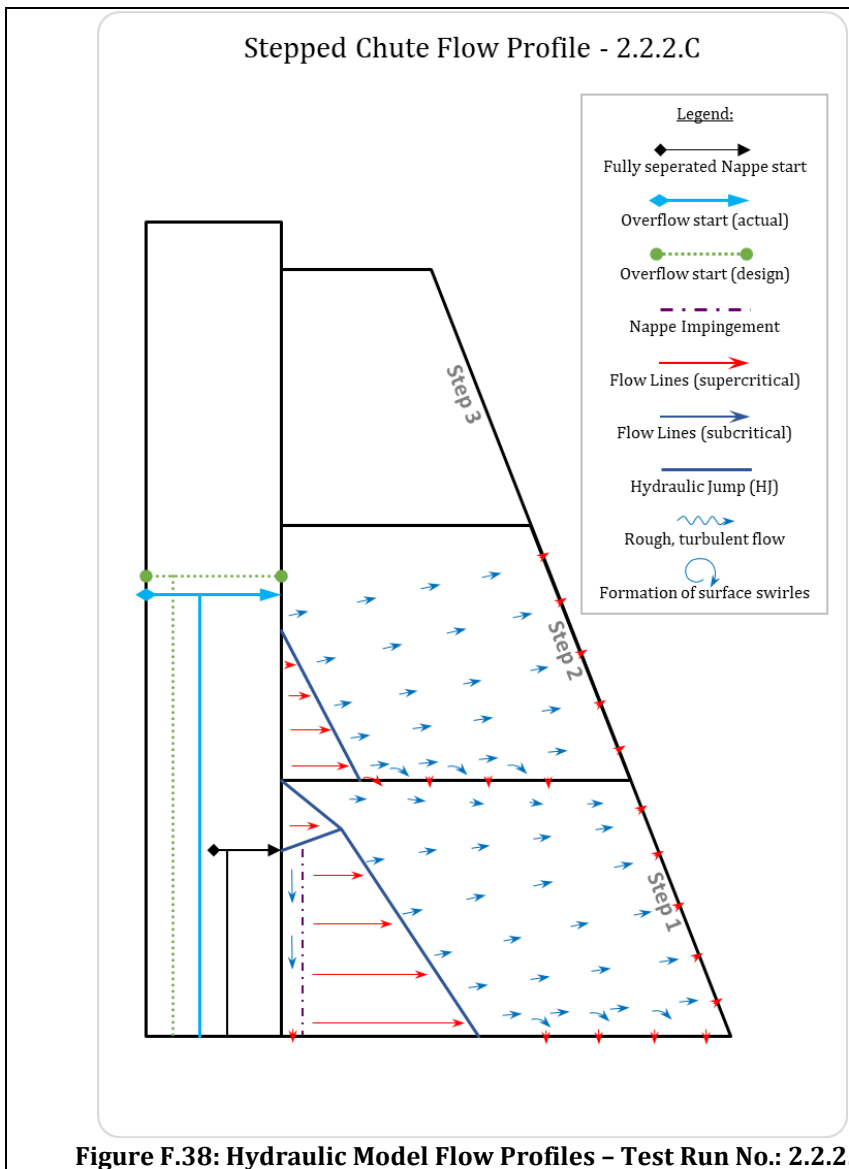


Figure F.38: Hydraulic Model Flow Profiles - Test Run No.: 2.2.2.C

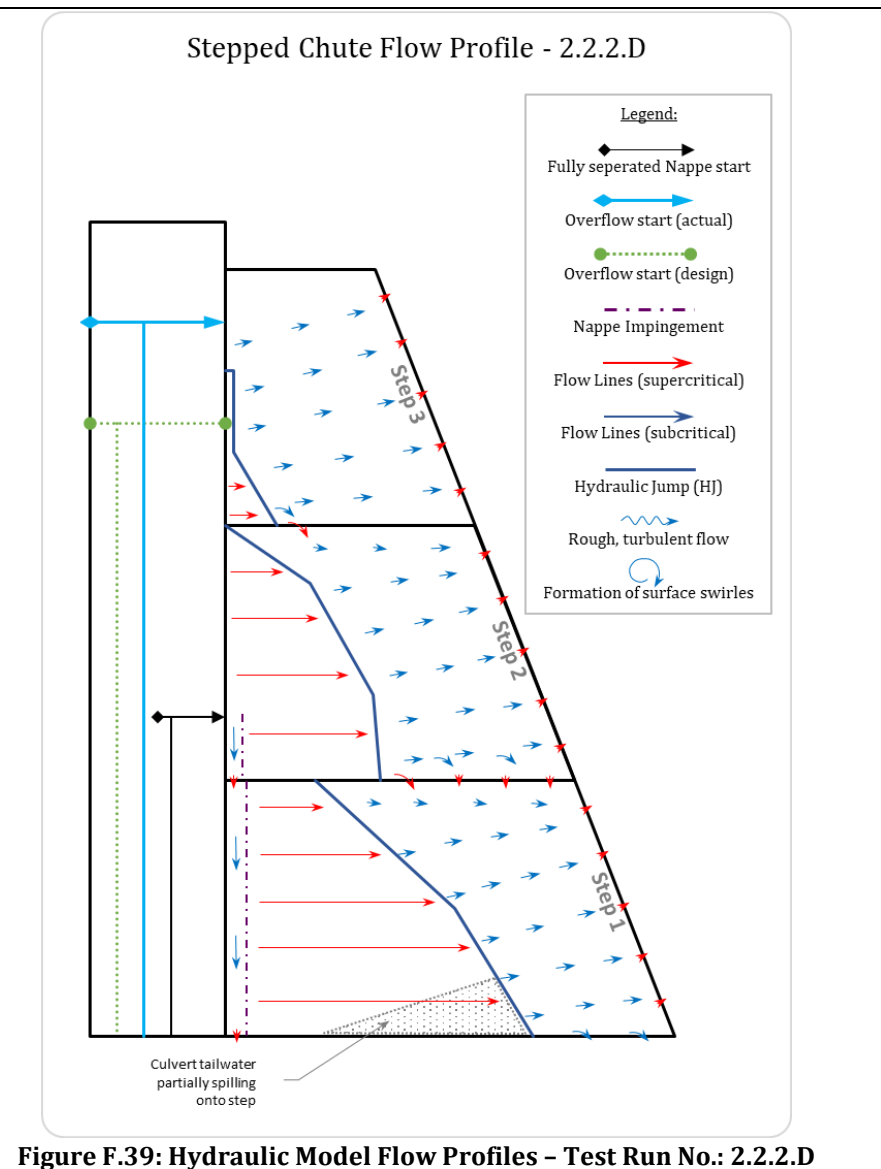
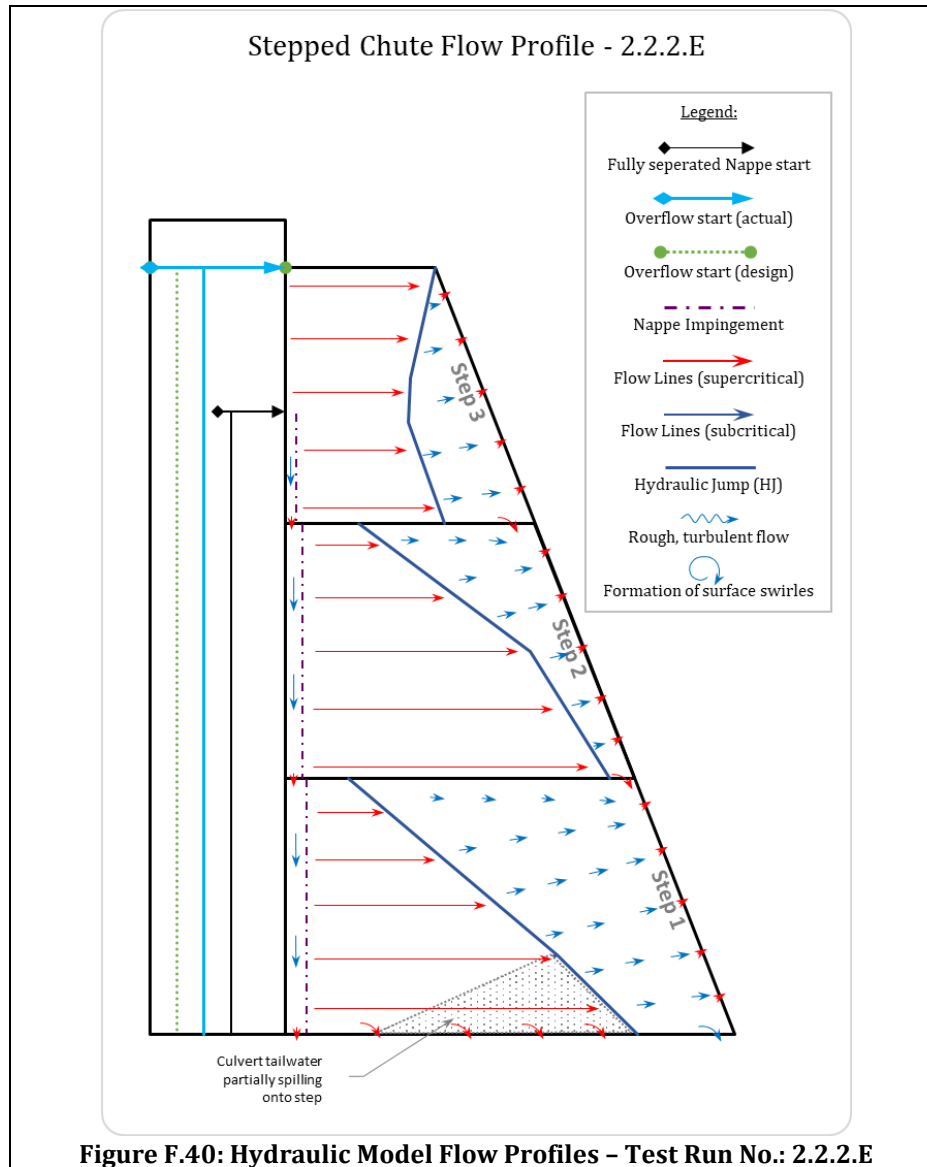
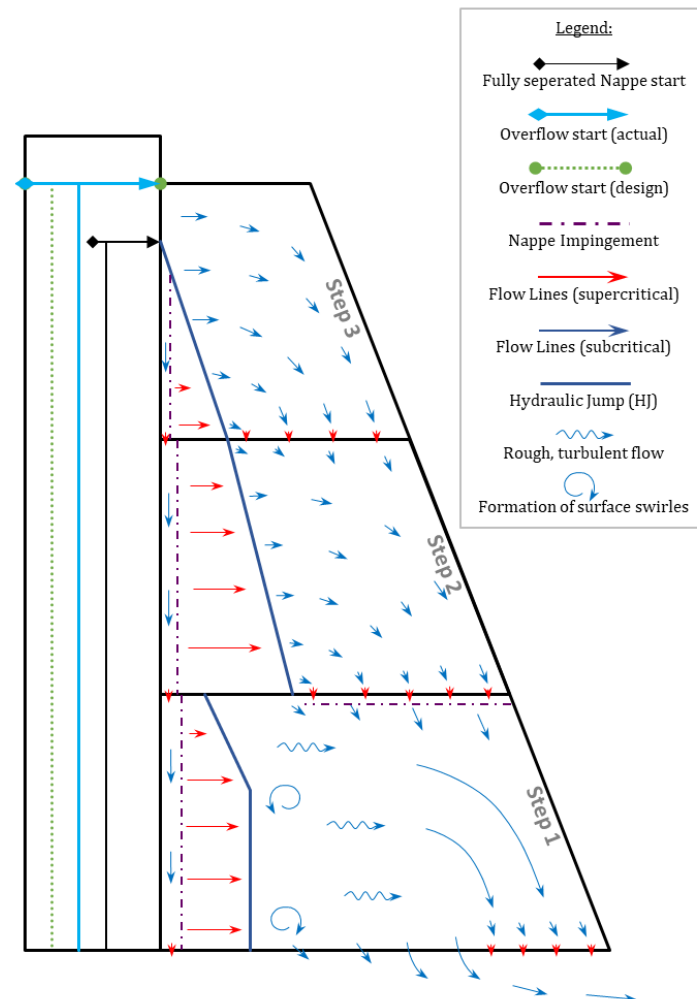


Figure F.39: Hydraulic Model Flow Profiles - Test Run No.: 2.2.2.D



Stepped Chute Flow Profile - 1.1.3



Stepped Chute Flow Profile - 1.2.3

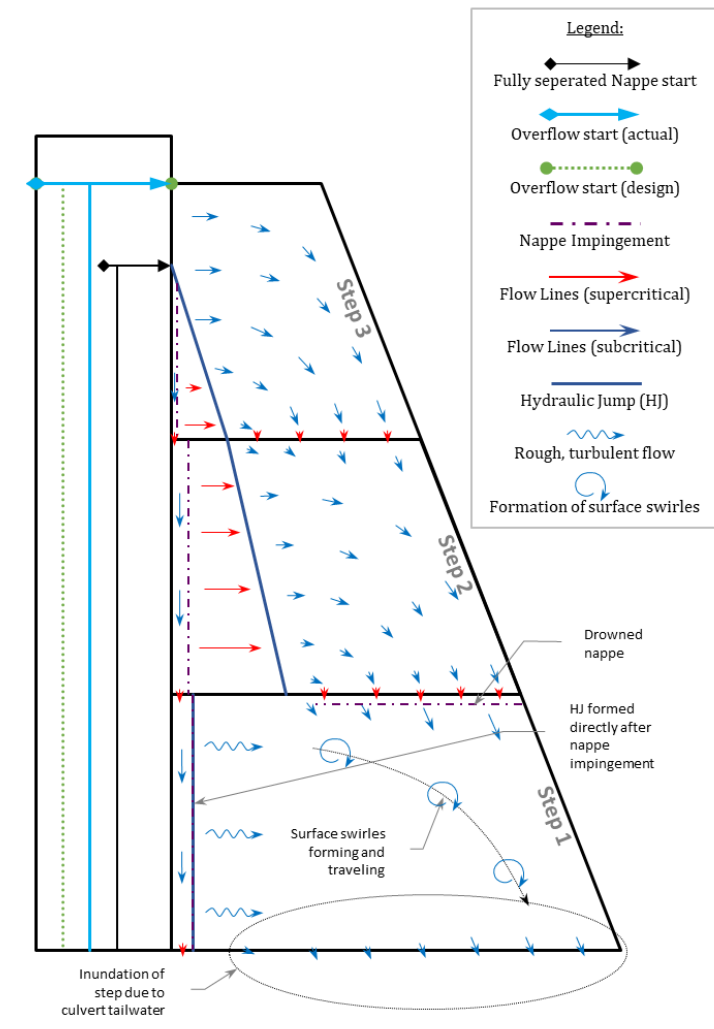


Figure F.41: Hydraulic Model Flow Profiles – Test Run No.: 1.1.3.

Figure F.42: Hydraulic Model Flow Profiles – Test Run No.: 1.2.3.

Stepped Chute Flow Profile - 2.1.3

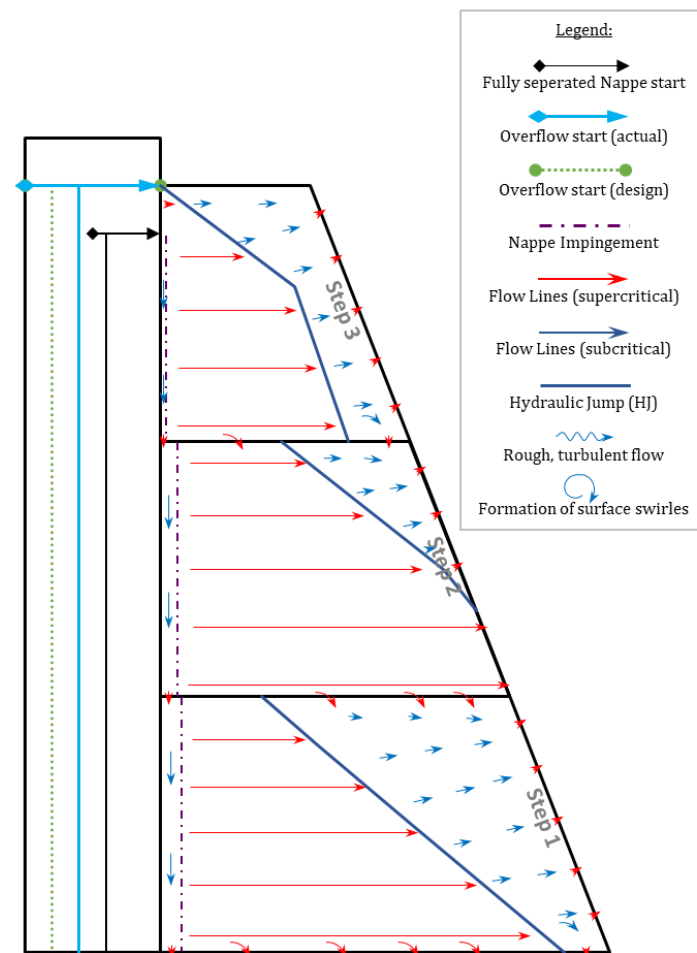


Figure F.43: Hydraulic Model Flow Profiles – Test Run No.: 2.1.3.

Stepped Chute Flow Profile - 2.2.3

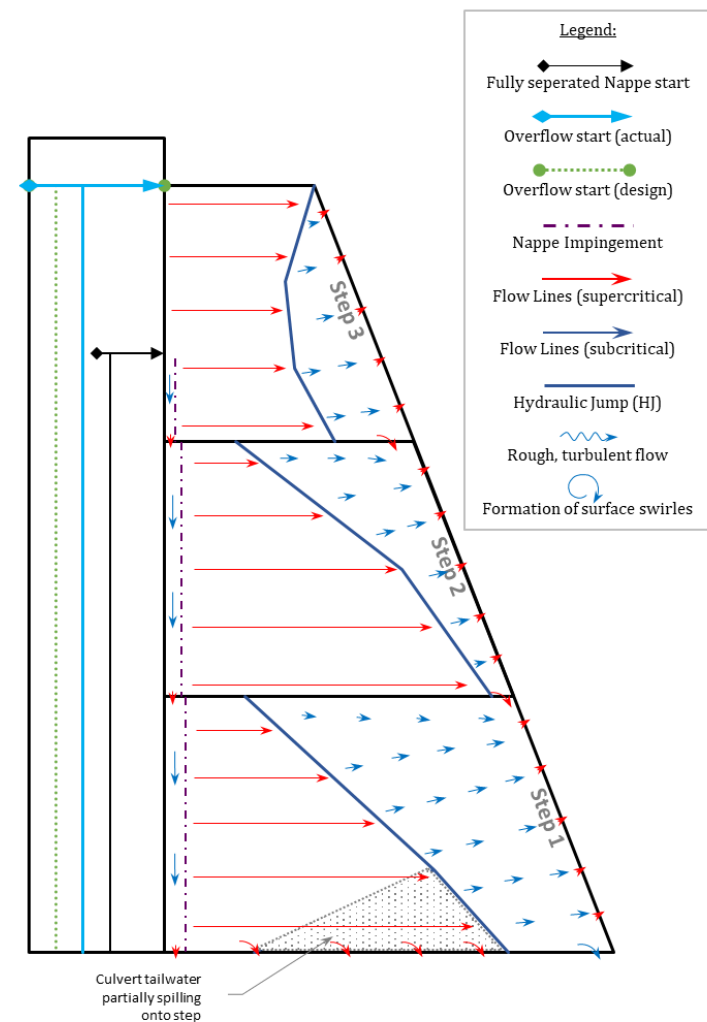
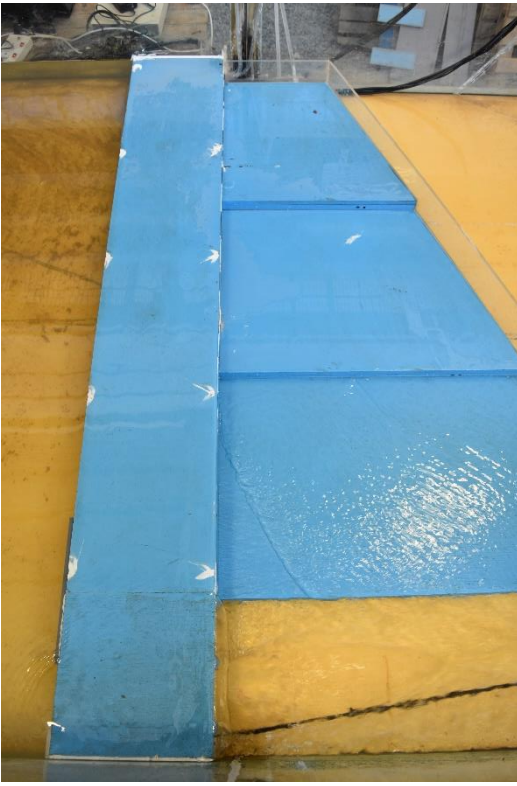
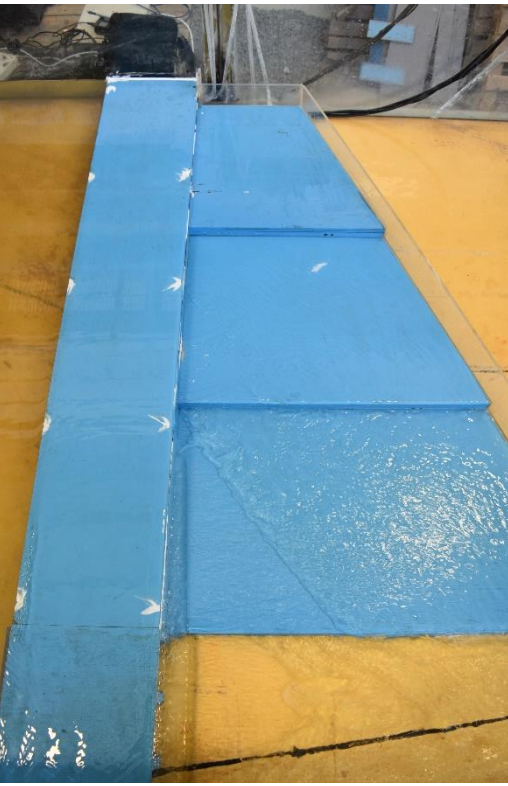


Figure F.44: Hydraulic Model Flow Profiles – Test Run No.: 2.2.3.

APPENDIX G: PHOTOGRAHPS OF MODEL TESTS

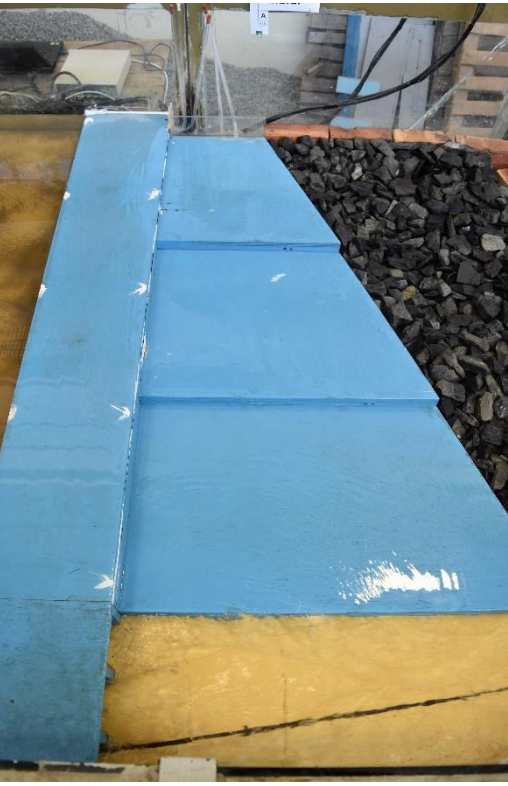
	Unvented Nappe	Vented Nappe
No Culvert Flow		
With Culvert Flow		
Figure G.1: Hydraulic Model Photograph – Test Run No.: 1.1.1. A ($y_{over road} = 4 \text{ mm}$)	Figure G.2: Hydraulic Model Photograph – Test Run No.: 1.1.2. A ($y_{over road} = 4 \text{ mm}$)	Figure G.3: Hydraulic Model Photograph – Test Run No.: 1.2.1. A ($y_{over road} = 4 \text{ mm}$)
Figure G.4: Hydraulic Model Photograph – Test Run No.: 1.2.2. A ($y_{over road} = 4 \text{ mm}$)		

	Unvented Nappe	Vented Nappe
No Culvert Flow		
With Culvert Flow		
Figure G.5: Hydraulic Model Photograph – Test Run No.: 1.1.1. B ($y_{over road} = 8 \text{ mm}$)	Figure G.6: Hydraulic Model Photograph – Test Run No.: 1.1.2. B ($y_{over road} = 8 \text{ mm}$)	Figure G.7: Hydraulic Model Photograph – Test Run No.: 1.2.1. B ($y_{over road} = 8 \text{ mm}$)
Figure G.8: Hydraulic Model Photograph – Test Run No.: 1.2.2. B ($y_{over road} = 8 \text{ mm}$)		

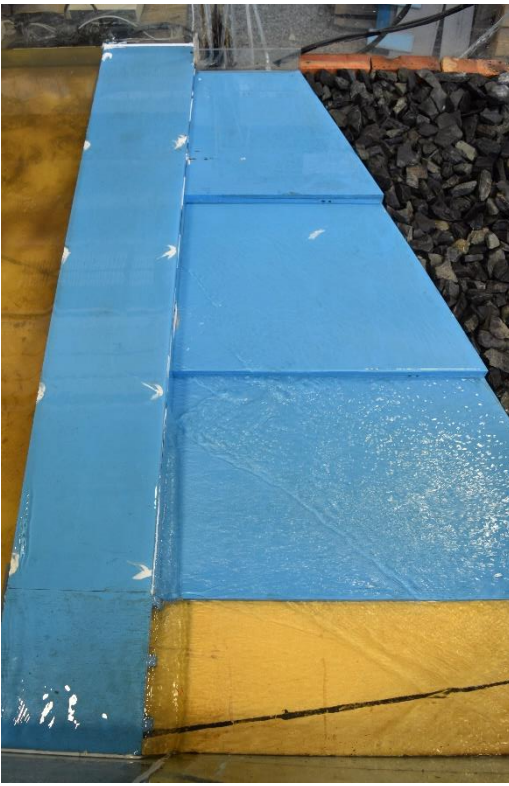
	Unvented Nappe	Vented Nappe
No Culvert Flow		
With Culvert Flow		
Figure G.9: Hydraulic Model Photograph – Test Run No.: 1.1.1. C ($y_{over road} = 12 \text{ mm}$)	Figure G.10: Hydraulic Model Photograph – Test Run No.: 1.1.2. C ($y_{over road} = 12 \text{ mm}$)	Figure G.11: Hydraulic Model Photograph – Test Run No.: 1.2.1. C ($y_{over road} = 12 \text{ mm}$)
Figure G.12: Hydraulic Model Photograph – Test Run No.: 1.2.2. C ($y_{over road} = 12 \text{ mm}$)		

	Unvented Nappe	Vented Nappe
No Culvert Flow		
With Culvert Flow		
Figure G.13: Hydraulic Model Photograph – Test Run No.: 1.1.1. D ($y_{over road} = 16 \text{ mm}$)	Figure G.14: Hydraulic Model Photograph – Test Run No.: 1.1.2. D ($y_{over road} = 16 \text{ mm}$)	Figure G.15: Hydraulic Model Photograph – Test Run No.: 1.2.1. D ($y_{over road} = 16 \text{ mm}$)
		Figure G.16: Hydraulic Model Photograph – Test Run No.: 1.2.2. D ($y_{over road} = 16 \text{ mm}$)

	Unvented Nappe	Vented Nappe
No Culvert Flow		
With Culvert Flow		
Figure G.17: Hydraulic Model Photograph – Test Run No.: 1.1.1. E ($y_{over road} = 20 \text{ mm}$)	Figure G.18: Hydraulic Model Photograph – Test Run No.: 1.1.2. E ($y_{over road} = 20 \text{ mm}$)	Figure G.19: Hydraulic Model Photograph – Test Run No.: 1.2.1. E ($y_{over road} = 20 \text{ mm}$)
		Figure G.20: Hydraulic Model Photograph – Test Run No.: 1.2.2. E ($y_{over road} = 20 \text{ mm}$)

	Unvented Nappe	Vented Nappe
No Culvert Flow		
With Culvert Flow		
Figure G.21: Hydraulic Model Photograph – Test Run No.: 2.1.1. A ($y_{over road} = 4 \text{ mm}$)		Figure G.22: Hydraulic Model Photograph – Test Run No.: 2.1.2. A ($y_{over road} = 4 \text{ mm}$)
Figure G.23: Hydraulic Model Photograph – Test Run No.: 2.2.1. A ($y_{over road} = 4 \text{ mm}$)		Figure G.24: Hydraulic Model Photograph – Test Run No.: 2.2.2. A ($y_{over road} = 4 \text{ mm}$)

		Unvented Nappe	Vented Nappe
No Culvert Flow			
With Culvert Flow			
	Figure G.25: Hydraulic Model Photograph – Test Run No.: 2.1.1. B ($y_{over road} = 8 \text{ mm}$)	Figure G.26: Hydraulic Model Photograph – Test Run No.: 2.1.2. B ($y_{over road} = 8 \text{ mm}$)	Figure G.27: Hydraulic Model Photograph – Test Run No.: 2.2.1. B ($y_{over road} = 8 \text{ mm}$)
			Figure G.28: Hydraulic Model Photograph – Test Run No.: 2.2.2. B ($y_{over road} = 8 \text{ mm}$)

	Unvented Nappe	Vented Nappe
No Culvert Flow		
With Culvert Flow		
Figure G.29: Hydraulic Model Photograph – Test Run No.: 2.1.1. C ($y_{over road} = 12 \text{ mm}$)	Figure G.30: Hydraulic Model Photograph – Test Run No.: 2.1.2. C ($y_{over road} = 12 \text{ mm}$)	Figure G.31: Hydraulic Model Photograph – Test Run No.: 2.2.1. C ($y_{over road} = 12 \text{ mm}$)
	2.2.1.	
Figure G.32: Hydraulic Model Photograph – Test Run No.: 2.2.2. C ($y_{over road} = 12 \text{ mm}$)		

	Unvented Nappe	Vented Nappe
No Culvert Flow		
With Culvert Flow		
Figure G.33: Hydraulic Model Photograph – Test Run No.: 2.1.1. D ($y_{over road} = 16 \text{ mm}$)	Figure G.34: Hydraulic Model Photograph – Test Run No.: 2.1.2. D ($y_{over road} = 16 \text{ mm}$)	Figure G.35: Hydraulic Model Photograph – Test Run No.: 2.2.1. D ($y_{over road} = 16 \text{ mm}$)
	2.2.2.	
		Figure G.36: Hydraulic Model Photograph – Test Run No.: 2.2.2. D ($y_{over road} = 16 \text{ mm}$)

	Unvented Nappe	Vented Nappe
No Culvert Flow	 A photograph of a hydraulic model showing a blue trapezoidal embankment on a yellow base. The water surface is flat and level across the entire width of the embankment. A vertical scale on the left indicates a height of 2.1.1.	 A photograph of a hydraulic model showing a blue trapezoidal embankment on a yellow base. The water surface is flat and level across the entire width of the embankment. A vertical scale on the left indicates a height of 2.2.2.
With Culvert Flow	 A photograph of a hydraulic model showing a blue trapezoidal embankment on a yellow base. The water surface is flat and level across the entire width of the embankment. A vertical scale on the left indicates a height of 2.1.1.	 A photograph of a hydraulic model showing a blue trapezoidal embankment on a yellow base. The water surface is flat and level across the entire width of the embankment. A vertical scale on the left indicates a height of 2.2.2.

Repeatability Tests: Unvented Nappe

No Culvert Flow

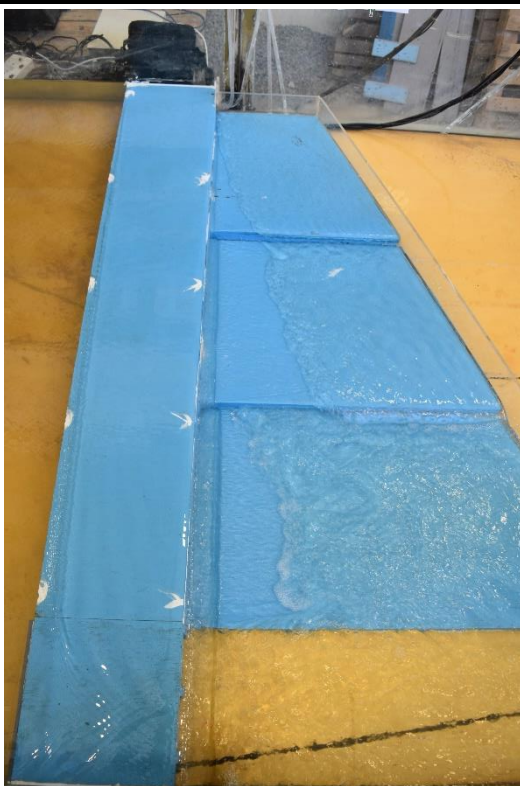


**Figure G.41: Hydraulic Model Photograph –
Test Run No.: 1.1.3. ($y_{over\ road} = 20\ mm$)**



**Figure G.42: Hydraulic Model Photograph –
Test Run No.: 1.2.3. ($y_{over\ road} = 20\ mm$)**



**Figure G.43: Hydraulic Model Photograph –
Test Run No.: 2.1.3. ($y_{over\ road} = 20\ mm$)**



**Figure G.44: Hydraulic Model Photograph –
Test Run No.: 2.2.3. ($y_{over\ road} = 20\ mm$)**